TRANSCRIPTOMIC AND EPIGENETIC RESPONSE TO CARDIAC INJURY

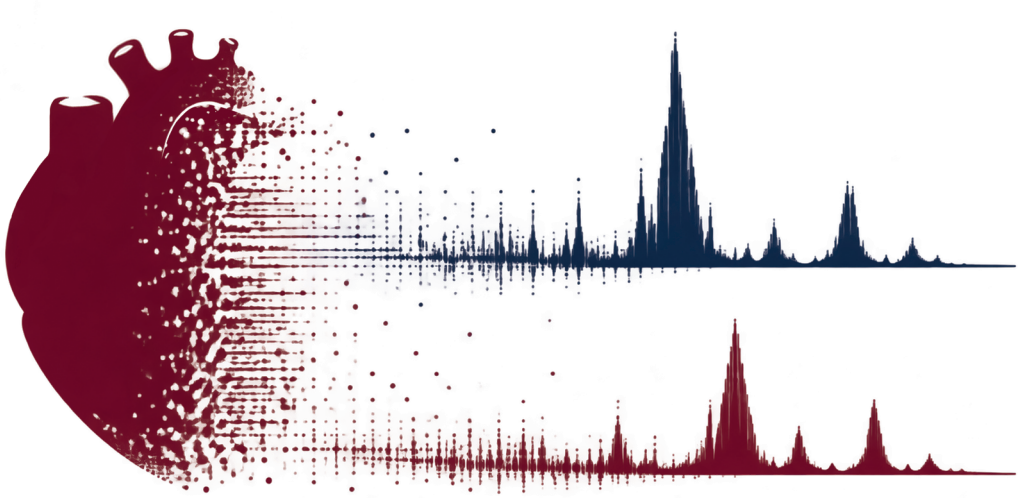

MARIE GÜNTHEL

Transcriptomic and epigenetic response to cardiac injury

Marie Günthel

Cover design: Koen Keijsers
Layout & print: ProefschriftMaken || www.proefschriftmaken.nl
ISBN: 978-94-6534-682-3

This research was funded by Netherlands Heart Foundation, grant number COBRA3 (NHS 2013T091).
Financial support by the Dutch Heart Foundation for the publication of this thesis is gratefully acknowledged.

Transcriptomic and epigenetic response to cardiac injury

ACADEMISCH PROEFSCHRIFT

ter verkrijging van de graad van doctor
aan de Universiteit van Amsterdam
op gezag van de Rector Magnificus
ten overstaan van een door het College voor Promoties ingestelde commissie,
in het openbaar te verdedigen in de Agnietenkapel
op woensdag 4 november 2026, te 13.00 uur

door Marie Günthel
geboren te Rostock

Promotiecommissie

Promotor:	prof. dr. V.M. Christoffels	AMC-UvA
Copromotor:	dr. P. Barnett	AMC-UvA
Overige leden:	prof. dr. C.J.M. de Vries	AMC-UvA
	dr. ir. C.J. Zuurbier	AMC-UvA
	prof. dr. P.L. Hordijk	Vrije Universiteit Amsterdam
	prof. dr. F. van Leeuwen	AMC-UvA
	dr. M.M. Gladka	AMC-UvA
	prof. dr. N.A. Blom	AMC-UvA

Faculteit der Geneeskunde

CONTENTS

Scope of the thesis		7
Chapter 1	Development, Proliferation and Growth of the Mammalian Heart	11
Chapter 2	Early Postnatal Cardiac Stress Does Not Influence Ventricular Cardiomyocyte Cell-Cycle Withdrawal	37
Chapter 3	Neuregulin-1 enhances cell-cycle activity, delays cardiac fibrosis and improves cardiac performance in rat pups with right ventricular pressure load	61
Chapter 4	Conserved NPPB+ Border Zone Switches From MEF2- to AP-1 Driven Gene Program	93
Chapter 5	Epigenetic State Changes Underlie Metabolic Switch in Mouse Post-Infarction Border Zone Cardiomyocytes	149
Chapter 6	General Discussion and Future Perspectives	179
Chapter 7	Summary	191
Chapter 8	Samenvatting	195
Appendix	PhD portfolio	200
	List of Contributing authors	203
	Author contributions	205
	Acknowledgements	207

SCOPE OF THE THESIS

The failure of the compromised or injured heart to regenerate often leads to functional insufficiency and the development of heart failure, a major cause of death[1]. Newborns with a congenital heart defect compromising physiological circulation will undergo surgical intervention to at least partially restore function. However, the remaining structural and functional deficit may cause heart failure years after birth. Heart injury as a consequence of myocardial infarction causes massive cardiomyocyte death, with the lost cardiomyocytes being replaced by fibrotic scar tissue instead. A major common factor in these two scenarios is that mammals lose the capacity to renew cardiomyocytes and to regenerate the heart soon after birth[2,3]. Hence, regeneration of human heart tissue has been and remains a major goal in cardiovascular research and medicine. Current research has shifted to the idea that proliferation can be re-induced in the muscle cells of the postnatal and adult mammalian heart, with new insights coming from highly regenerative species such as the zebrafish, and the regenerative capacity demonstrated in the heart of fetal and neonatal rodents, all of which regenerate cardiac tissue by proliferation of resident cardiomyocytes[4]. To be able to re-initiate cardiomyocyte proliferation in mammalian hearts, it is crucial to uncover the mechanisms that underlie cardiomyocyte adaption to injury and cardiac stress in the mammalian postnatal heart. Therefore, in this thesis, we aim to characterize the response of cardiomyocytes to early abnormal cardiac loading conditions, as found in patients with certain types of congenital heart defects, and after myocardial infarction.

In **Chapter 1** we provide an overview of the progress that has been made deciphering cardiomyocyte proliferation in the developing and postnatal mammalian (human) heart. Here we show that the proliferative capacity of cardiomyocytes is lost shortly after birth and that further growth of the heart is achieved by an increase in cardiomyocyte volume. Whereas fetal and neonatal hearts can still partially recover after injury, adult hearts fail to regenerate. Within this chapter, we also discuss potentially important studies that have identified small fractions of cardiomyocytes that have retained the proliferative capacity, and pathways that can evoke cardiomyocyte proliferation in the adult heart. In **Chapter 2**, we aim to investigate how early cardiac stress influences the postnatal cell-cycle activity in a genetic mouse model that develops left ventricular volume overload within the first two weeks after birth. We assess cell-cycle activity by assessing the cell-cycle marker Ki67 in cardiomyocytes. Using RNA-sequencing we compare transcriptomes in cardiomyocytes from healthy control mice and from mice with postnatal cardiac stress. In **Chapter 3** we aim to study the adaption to pressure overload of the right ventricle in juvenile rats, with and without the administration of the growth factor neuregulin-1. Neuregulin-1 has previously been reported to enhance cardiomyocyte proliferation. We induce pressure overload in rats on the day of weaning by pulmonary artery banding and study cardiac function using echocardiography and pressure-volume measurements. Using RNA-sequencing we compare transcriptional profiles of heart tissue at different time points after the induction of pressure

overload. In **Chapter 4**, we characterize cardiomyocytes originating from the border zone that surrounds the infarcted myocardium. Recently, these cardiomyocytes have been implicated in cardiac regeneration. Here, we identify their transcriptional properties using RNA-sequencing and epigenetic states using ATAC-sequencing, and validate new molecular markers, including *Nppb*, encoding B-type natriuretic peptide, in the mouse and human infarct border zone. In **Chapter 5**, we aim to further characterize the epigenetic landscape of border zone cardiomyocytes. The ATAC-seq data from Chapter 4 identified all accessible regulatory elements, irrespective of their function. Here, we aim to specifically distinguish active promoters and enhancers by performing CUT&RUN-sequencing for H3K27ac on isolated post infarction cardiomyocyte nuclei. In addition, we use RNA-sequencing on isolated cardiomyocyte nuclei to study their transcriptome. In **Chapter 6** the main findings and implications are being discussed in relation to current insights in the field.

REFERENCES

1. Mozaffarian, D. *et al.* Heart Disease and Stroke Statistics—2016 Update. *Circulation* (2016). doi:10.1161/cir.0000000000000350
2. Bergmann, O. *et al.* Evidence for cardiomyocyte renewal in humans. *Science* **324**, 98–102 (2009).
3. Alkass, K. *et al.* No evidence for cardiomyocyte number expansion in preadolescent mice. *Cell* **163**, 1026–1036 (2015).
4. Jopling, C. *et al.* Zebrafish heart regeneration occurs by cardiomyocyte dedifferentiation and proliferation. *Nature* **464**, 606–609 (2010).

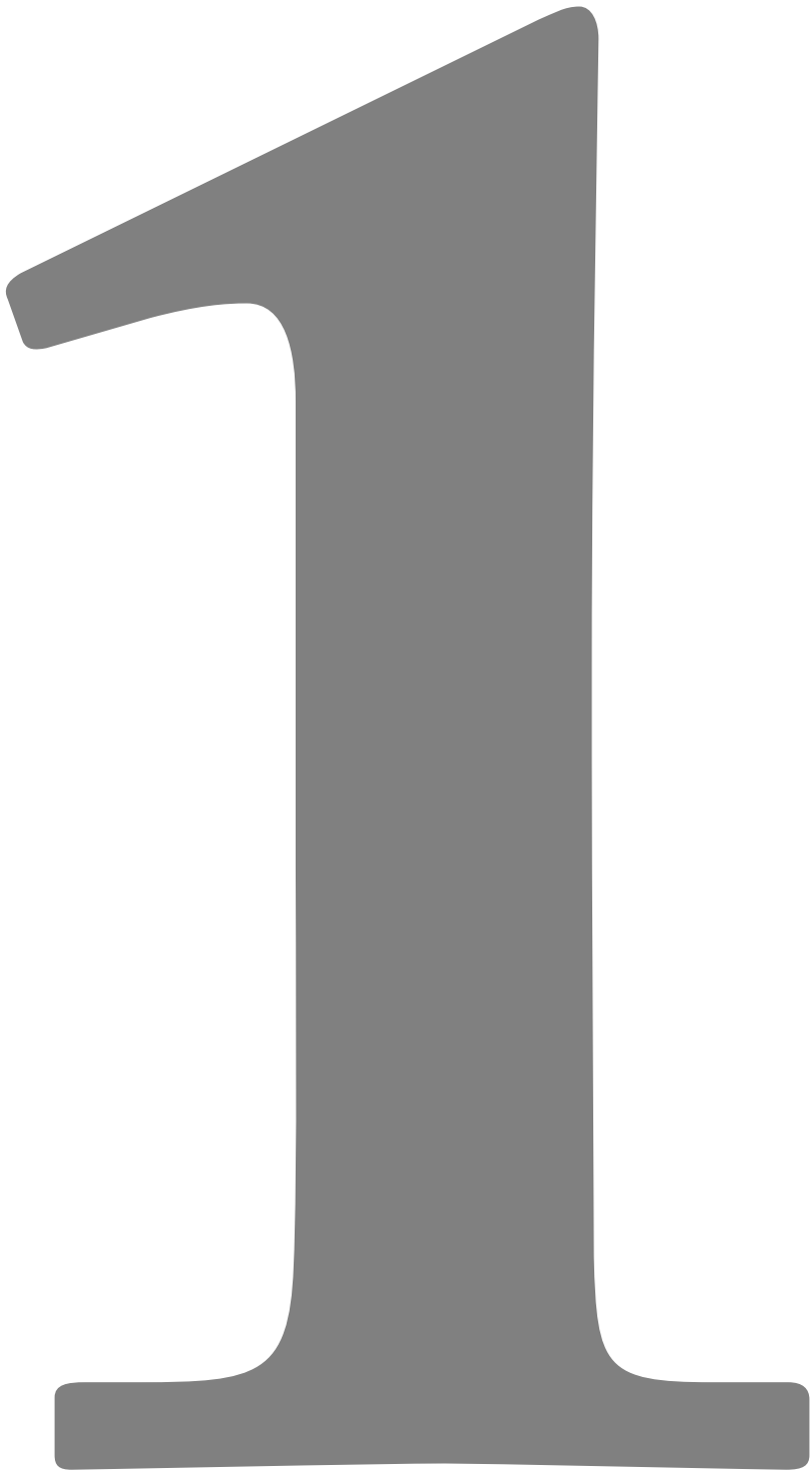

Chapter 1

Development, Proliferation and Growth of the Mammalian Heart

Marie Günthel, Phil Barnett, Vincent M. Christoffels

Molecular Therapy. Vol. 26, No 7, July 2018: 1599

ABSTRACT

During development, the embryonic heart grows by addition of cells from a highly proliferative progenitor pool and by subsequent precisely controlled waves of cardiomyocyte proliferation. In this period, the heart can compensate for cardiomyocyte loss by an increased proliferation rate of the remaining cardiomyocytes. This proliferative capacity is lost soon after birth, with heart growth continuing by an increase in cardiomyocyte volume. The failure of the injured adult heart to regenerate often leads to the development of heart failure, a major cause of death. With the recent observation of a small fraction of cardiomyocytes that appear to have retained the proliferative capacity within the adult heart, as well as the identification of developmental pathways such as the Hippo-signaling pathway that can invoke mature cardiomyocyte proliferation, more studies are taking a knowledge based mechanistic approach to heart regeneration. A key question being asked is if this knowledge can be used therapeutically to reinitiate cardiomyocyte proliferation after injury such as myocardial infarction? In this respect, uncovering and understanding the mechanisms and conditions that give rise to a fully functional and adaptive heart in the developing embryo, could provide us with the answers to many of the questions that are now being asked.

INTRODUCTION

Cardiomyocytes of the mature mammalian heart were considered to be essentially post-mitotic and not able to undergo postnatal cell division. However, during the last decade studies in human have revealed a limited, but significant rate of annual cardiomyocyte renewal.[1,2] Nevertheless, one can infer that this renewal rate would never be sufficient to replace the large numbers of cardiomyocytes that are lost after cardiac injuries such as myocardial infarction. Instead, the heart, upon injury, undergoes a quick patch-up repair. During a rapid inflammatory response, large numbers of fibroblasts infiltrate the damaged myocardium leading to the deposition of fibrotic scar tissue. As a consequence, cardiac function becomes compromised and heart failure, a leading cause of death, may soon ensue.[3] In light of this, regeneration of human heart tissue has been and remains a major goal in cardiovascular research. Over the last two decades research has mainly focused on tissue replacement approaches. Historically, the existence of cardiac endogenous stem cells and their ability to differentiate has been a topic of much discussion.[4] Alternative approaches focus on deriving cardiomyocytes from various stem cell sources including embryonic stem cells and induced pluripotent stem cells.[5,6] Stem-cell derived cardiomyocytes mature insufficiently under *in vitro* conditions and hence must adopt their fate after being transplanted into the host tissue.[6] Whereas studies administering stem-derived cardiomyocytes into rodents that underwent myocardial infarction have demonstrated the feasibility of this technique,[7–9] with remuscularization of the injured area, application in non-human primates has been fraught with difficulties including insufficient maturation of cardiomyocytes and sustained arrhythmias.[5,6]

New insights and in roads have come from highly regenerative species such as the zebrafish as well as the regenerative capacity demonstrated in the heart of fetal and neonatal rodents, all of which can regenerate cardiac tissue by proliferation of resident cardiomyocytes, a capacity that is then lost when mammals mature.[10–14] Current research has shifted to the idea that proliferation can be re-induced in adult cardiomyocytes. To achieve this, it is crucial to gain a deeper understanding of the switches and mechanisms of cardiomyocyte proliferation and differentiation from early embryonic development into adulthood.

Progenitor differentiation and cardiomyocyte proliferation underlie embryonic heart formation

During development the heart growths by differentiation of proliferating, multipotent cardiac progenitor cells into cardiomyocytes and controlled local proliferation of already differentiated cardiomyocytes.[15] This process requires the tight regulation of levels of extracellular growth factors as well the intracellular expression of transcription factors.

Most knowledge regarding heart development has been gained from studies of transgenic mouse embryos and histologic 3D reconstructions.[16,17] Other studies, however, have made use of magnetic resonance imaging and episcopic fluorescence image capture to compare

cardiac development in mice and humans. From these studies it could be demonstrated that the sequence of events in cardiac development are comparable in both species, thus establishing the mouse as a useful model for the extrapolation to the study of human heart development.[18]

The formation of the heart starts at week 3 of human embryonic development [16] corresponding to embryonic day 7.5 (E7.5) of mouse development.[17,19] At this stage the embryo consists of the three germ layers: the endoderm, mesoderm and ectoderm. Most of the cardiac tissue will originate from the mesoderm. During gastrulation, early cardiac progenitor cells reside at bilateral regions of the embryonic midline. When the embryo folds, these heart forming regions fuse across the midline forming what is commonly referred to as the cardiac crescent. The cells of the cardiac crescent display a cardiogenic gene expression profile, initiate calcium transients, and not long thereafter start to beat.[19]

In all vertebrates examined so far, two sets of precursor cells, based on temporal expression of various marker genes, can be distinguished during the early phases of cardiac development, the cells of the first heart field (FHF) and the second heart field (SHF; Figure 1).[15] The division in two populations is somewhat artificial, because different HF markers indicate different populations and borders between populations, and because the differentiation of the precursor cells and their addition to the heart tube is a continuous process.[20] Nevertheless, the FHF-derived differentiating cell populations from the cardiac crescent fuse at the midline and form the linear heart tube, enclosing the endocardial layer that is separated from the myocardial layer by the cardiac jelly, a layer of acellular matrix.[17] Upon forming the heart tube, the primitive cardiomyocytes stop proliferating (Figure 1). The heart tube grows by further addition of mesodermal SHF precursor cells, which migrate from the pericardial cavity dorsal and caudal of the heart tube.[21] SHF cells proliferate at high rates, mediated by canonical WNT/β-catenin signaling[22] and are added to the heart tube at the arterial and venous poles while they are undergoing differentiation.[21] During their addition to the heart tube, the SHF-derived cardiomyocytes also temporally cease proliferation.[21] In mammals, cells from the FHF contribute mainly, if not wholly to the definitive left ventricle and atrioventricular canal.[23] Cells from the SHF will contribute to the formation of the right ventricle, outflow tract and atria.[15]

Various cardiac transcription factors such as GATA4, NKX2-5, ISL1, TBX5, TBX1 and MEF2C determine the cardiogenic fate of the heart field precursors.[24,25] T-Box transcription factor family members that are regionally expressed in the heart, play a central role in defining the future characteristics of the cardiomyocytes such as their automaticity, conduction velocity and contractility.[26,27] Several families of microRNAs (miRNAs), single-stranded, non-coding RNAs, have been shown to target these transcription factors and thereby regulate the cardiac fate of progenitor cells.[28] In this respect, the actions of the families miR-1 and miR-133a have been well studied.[29,30]

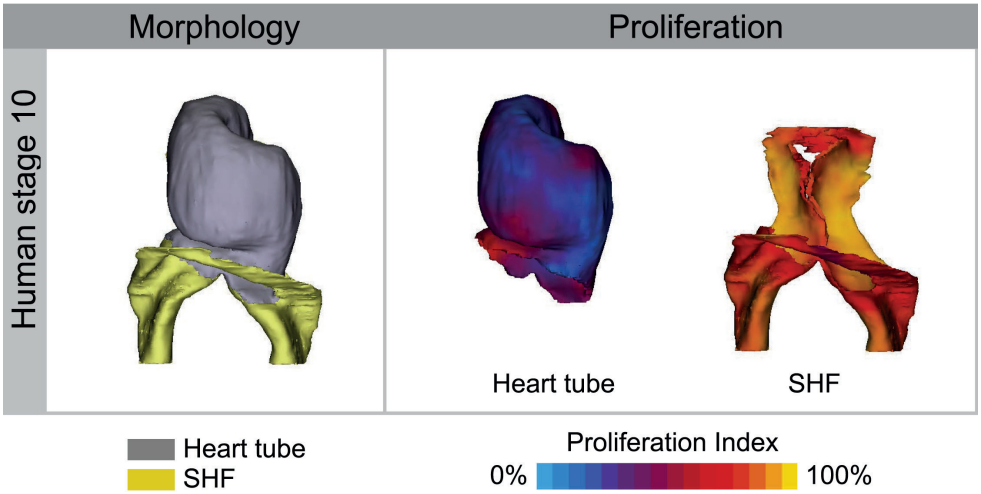

Figure 1. Formation and looping of the heart tube. Proliferation of the mesodermal precursor cells of the first heart field stop after differentiation into the cardiomyocytes of the heart tube, whereas the mesodermal precursor cells of the second heart field (SHF) remain highly proliferative. Proliferation is re-initiated after looping of the heart tube and the beginning of ventricular chamber formation at stage 10. The proliferation index indicates the percentage of Ki67 positive cells, as a marker for proliferation. Courtesy of Antoon Moorman.

Between Carnegie Stage (CS)10 – CS11, corresponding to E8.25[17] in the mouse, the heart tube loops.[16] During this process, cardiomyocytes at the outer curve of the tube display a distinct transcriptional program and start to re-enter the cell cycle and proliferate leading to the so-called "ballooning" of the ventricles (Figure 2).[16,31,32] Slightly later, the cardiomyocytes of the forming atria do likewise. The non-chamber regions, the atrioventricular canal, outflow tract and sinus venosus, however, express TBX2, TBX3, MSX2 and/or ID2, all of which function to suppress proliferation and chamber differentiation [17,21,23] The chambers grow considerably and the embryonic outflow tract gets taken up into the right ventricle. The atrioventricular canal will remain small in comparison to the chambers and give rise to the atrioventricular node[33], and the sinus node will form between from the sinus venosus.[34]

Further expansion of the embryonic heart occurs primarily through cell divisions in the ventricles and, to a lesser extent, the atrial chambers (Figure 2).[17] In the mouse embryo, the formation of the four chambers is visible from E9.5 onwards.[17] In human development the four chambers become visible at CS11.[16] At this stage cardiomyocyte proliferation rates differ locally within the developing heart.[16,17] In distal parts of the outflow tract proliferation rates decrease, whereas inflow tract and atria are formed by highly proliferating cardiomyocytes. During these stages, the highest proliferation rates can be observed in the ballooning ventricles (Figure 2). From E11 onwards, the proliferation rate and thereby the increase in cardiomyocyte number steadily declines during the further course of development (Figure 2).

Within the ventricles, the trabecules develop at the luminal site of the myocardium and become clearly visible by E9.5[35], corresponding to CS12.[16] Crucial signaling cues for the development of trabecules will come from the endocardial lining, located in the lumen of the chambers. Important molecular signals include the Notch signaling pathway, activating BMP10 and Neuregulin1 (NRG1).[36] NRG1 binds to the receptors ErbB3 and ErbB4, which will then dimerize with either ErbB3, ErbB4 or ErbB2.[37] They induce a high rate of proliferation in the less differentiated cardiomyocytes located at the base of the trabecules, where Notch signaling is strongest,[17,36,38] leading to trabecular elongation. Following this, the outer lining of the myocardium starts to compact and proliferation in the trabecules decreases.[16,17] Further myocardial cell divisions are now controlled by the epicardium that covers the outer surface of the myocardium and is derived from the pro-epicardium. It produces secreted factors that control the proliferative expansion of the compact sub-epicardial ventricular myocardium.[39] These factors include Fgf-signaling ligands (e.g. FGF9), Igf-signaling ligands (IGF2), Wnt-signaling ligands (e.g. WNT9B) and retinoic acid.[39–41] Epicardial cells are multipotent, and soon after covering the embryonic ventricular wall undergo epithelial-to-mesenchymal transformation and migrate into the myocardial wall. Here they differentiate into fibroblasts, coronary vascular smooth muscle cells and possibly endothelial cells.[42] Although there is a common consensus that cardiomyocytes comprise about 30% of the ventricular wall,[43] there have been varying reports about the content of fibroblasts and endothelial cells in the heart, probably due to a lack of suitable detection markers, varying isolation techniques and sampling bias.[2,43,44] A recent study reported that the murine and human heart contains 60% endothelial cells and less than 20% of fibroblasts.[43]

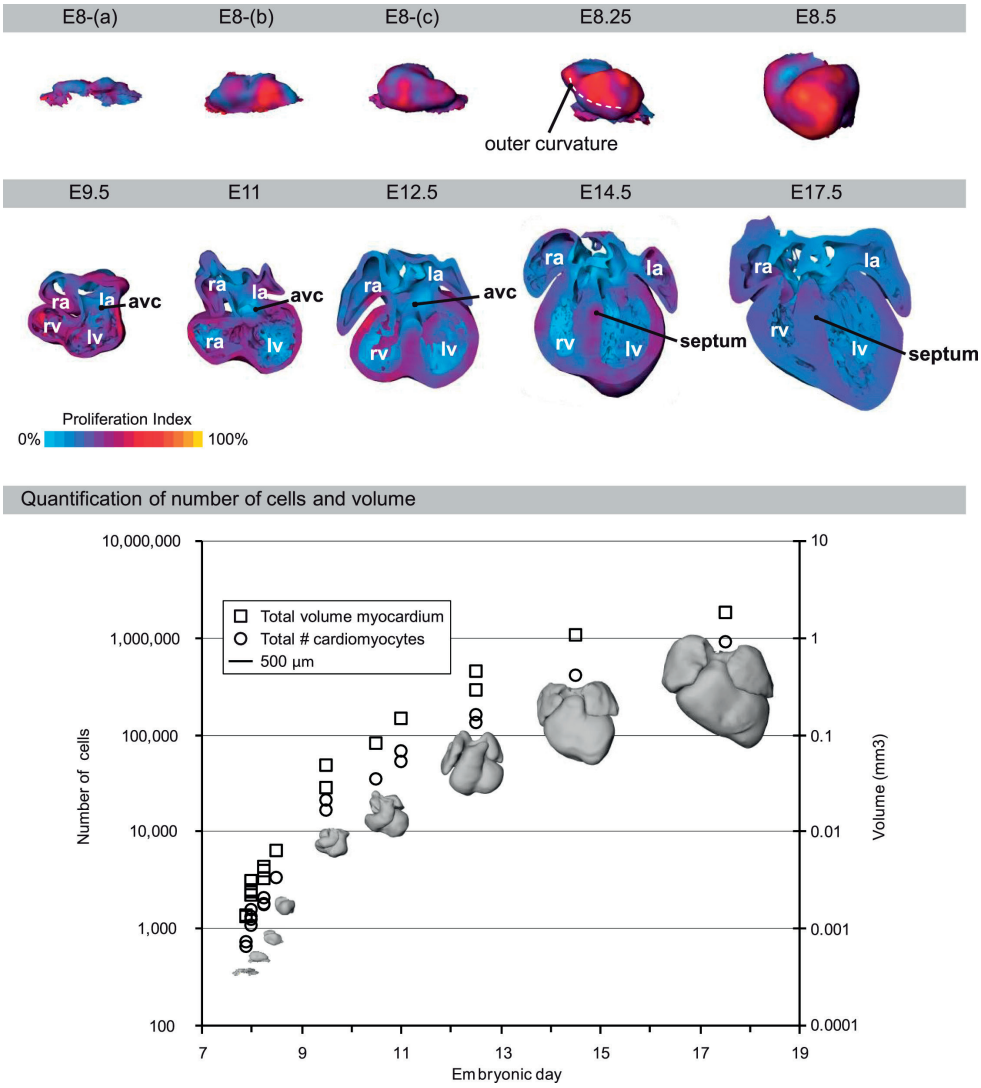

Figure 2. Ventral view of the proliferating myocardium during heart development in mouse E8-E17.5. The upper graph shows proliferation rates of cardiomyocytes within the developing heart. Initial formation of the heart tube takes place at E8(a) after which proliferation of the myocardium stops. Re-initiation of the proliferation starts at the left side of the heart tube at E8(b)-(c) and during looping of the heart tube at E8.25. The high proliferation at the outer curvature leads to ballooning of the future left ventricle at E8.5. At E9.5 the 4 chambers of the heart become visible. The non-chamber regions such as the outflow tract and the atrioventricular canal proliferate slowly (E11-E17.5). The highest proliferation rates are located at the base of the ventricular chambers and decrease from E11 onwards. The lower graph demonstrates that during heart development the heart rapidly grows by an increase in cell number. The proliferation index indicates the percentage of cells that had incorporated Bromodeoxy-Uridine (BrdU) during DNA synthesis. Courtesy of Antoon Moorman.

During cardiac development the myocardium increases in volume from about 0.003 mm^3 at CS9 (20 days of development) to around 2 mm^3 at CS16 (6 weeks of development) to around 15 mm^3 at CS23 (>8 weeks of development).[45] In mice, myocardium growths in volume from 0.0014 mm^3 at E8 to almost 2 mm^3 at E17.5. [17] During this time the volume of the cardiomyocytes stays constant whereas the number of cardiomyocytes within the heart increases exponentially and reaches almost one million (Figure 2).[17] A major regulator of the proliferation of differentiated cardiomyocytes during cardiac development is the Hippo pathway, an evolutionary conserved signaling pathway that controls organ size by regulating proliferation, apoptosis and stem cell-fate (Figure 3).[46] Suppression of this pathway underlies the high rates of cardiomyocyte proliferation during heart development.[47] When the Hippo pathway is active, the kinases mammalian sterile 20-like kinase 1 and 2 (MST1/2), which are homologous of the *Drosophila* Hippo kinase, form a complex with the scaffold protein Salvador (SAV), and in turn activate the large tumor suppressor homolog 1 and 2 (LATS1/2) kinases.[48,49] LATS1/2 and the Mps one binder kinase activator 1a/b (MOB1A/B) phosphorylate the downstream effector of the Hippo cascade, the Yes-associated protein (YAP).[50,51] Phosphorylation of YAP orchestrates its degradation or cytoplasmic retention by 14-3-3 binding.[52] Under the condition of an inactive Hippo pathway, YAP and its transcriptional co-activator with PDZ-binding motif (TAZ) translocate to the nucleus where they interact with various transcription factors. Interacting transcription factors include p73,[53–55] the runt-related transcription factor (RUNX)[56] and TBX5.[57,58] Interaction of YAP/TAZ with the TEA domain family members 1-4 (TEADs) has been shown to regulate the expression of target genes involved in the regulation of cell cycle progression.[59–61] Nuclear exclusion of YAP is also controlled via Hippo-independent ways, such as alpha-catenin that binds YAP under high cell density conditions.[62,63] The Hippo pathway's role during cardiac development was demonstrated by various studies in mouse models. Different conditional YAP knockout mice frequently showed reduced embryonic cardiomyocyte proliferation and embryonic or perinatal lethality.[64–66] The conditional deletion of the scaffolding protein SAV, upstream of YAP, also leads to a higher expression of various Wnt-target genes and accumulation of nuclear β-catenin which suggested an interaction between YAP and β-catenin.[47] Accordingly, overexpression of a constitutively active form of YAP during cardiac development was sufficient to cause elevated cardiomyocyte proliferation and increased heart size.[47,65,67]

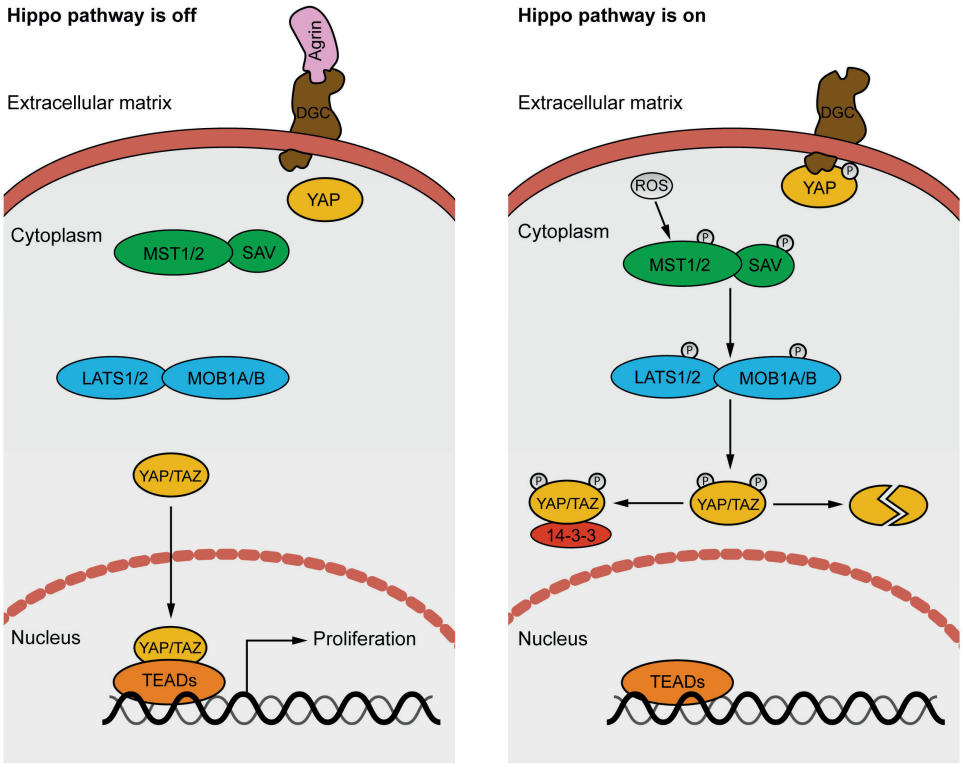

Figure 3. The Hippo pathway regulates cardiomyocyte proliferation. When the Hippo pathways is off, the Yes-associated protein (Yap) and its transcriptional co-activator with PDZ-binding motif (TAZ) translocate to the nucleus where they bind various transcription factors such as the TEA domain-containing sequence-specific transcription factors (TEADs). Expressed target genes promote cardiomyocyte proliferation. Postnatal activation of the Hippo pathway, for example by formed reactive oxygen species (ROS), leads to the formation of a complex between the mammalian sterile 20-like kinase 1/2 (Mst1/2) and Salvador (Sav). In turn, they activate the large tumor suppressor homolog 1/2 (Lats1/2) and the Mps one binder kinase activator 1a/b (Mob1a/b) [48,49] that phosphorylate Yap/TAZ, leading to their cytoplasmic retention by 14-3-3 binding or their degradation. [50,51] Next to the Hippo pathway, cytoplasmic retention of Yap is also caused by the Dystroglycan (DGC) complex which binds Yap with its intracellular domain, impeding its translocation to the nucleus. [94] High neonatal levels of Agrin in the extracellular matrix bind DGC leading to conformational changes, impeding the binding of Yap. [93]

The mammalian neonatal heart grows by hypertrophy and cardiomyocyte proliferation

Whereas cardiomyocytes actively proliferate before birth, the mammalian perinatal period is marked by a drop in cardiomyocyte proliferation. The subsequent increase in cardiac volume occurs almost exclusively by hypertrophy of cardiomyocytes.[68] In humans cardiomyocytes increase about 8.6-fold in their volume between the first 20 years of life.[69] The postnatal decrease of cardiomyocyte proliferation is accompanied by the occurrence of incomplete cell

cycles (Figure 4).[70] Within the first week after birth most cardiomyocytes complete their final cell division. In mice, a wave of karyokinesis without cytokinesis leading to binucleation as well as a wave of endoreplication, leading to polyploidization, account for most of the postnatal DNA synthesis up to 14 days of age.[70,71] This will eventually result in about 80-90% of all cardiomyocytes being binucleated.[70–72] It is relevant to note that mice are born one week after heart septation has completed at E14.5, whereas the human fetus will continue to grow for another several months.[18] This has led to the assumption that the heart of neonatal mice is less developed as compared to humans and some of the processes that occur during human fetal development still need to occur in mice during the postnatal period.[73] For example, whereas binucleation occurs during the first two weeks of murine postnatal development, in humans, about 25% of cardiomyocytes become binucleated already during a brief period before birth, a proportion that remains constant throughout life. [2,69,74] An increase in DNA content leading to polyploidization of cardiomyocytes takes place mainly during the second decade after birth.[2] Both binucleated and polyploid cardiomyocytes are generally believed to be terminally differentiated and unable to contribute to cardiomyocyte renewal during cardiac homeostasis and injury. In contrast, the small remaining population of diploid, mononucleated cardiomyocytes still has the capacity to proliferate.[75–77] Interestingly, a recent study showed that the frequency of these cells is highly variable within different mouse strains.[77] Mouse strains with a higher amount of mononucleated, diploid cardiomyocytes displayed an increased proliferation rate and a greater recovery after myocardial infarction as compared to mice carrying less of these fraction of cells. This shows that the genetic background may influence the regenerative process after injury and should be taken into account when comparing different studies. In contrast to mammals, zebrafish retain their regenerative capacity throughout adulthood.[78] Zebrafish cardiomyocytes stay mononucleated and diploid throughout their whole life and upon injury, lost cardiomyocytes are replaced by proliferation of resident cardiomyocytes.[10] When polyploidization was induced in zebrafish cardiomyocytes, the regenerative response was limited to the remaining fraction of dividing diploid cardiomyocytes and regenerative capacity was fully lost when the mononucleaeted fraction was reduced to 50% of all cardiomyocytes.[79] This indicates that indeed the proliferative capacity is restricted by the small number of the remaining mononucleated and diploid cardiomyocytes.

The time window and rate at which cardiomyocyte proliferation decreases after birth has been highly debated. In mice, a recent study reported a proliferative burst of cardiomyocytes at 14 days of postnatal age, already after the initial decline of cardiomyocyte proliferation.[80] However, this observation may have been the misinterpretation of endoreplication events and could be ruled out by studies showing that the rate of cardiomyocyte proliferation continuously decreases within the first two weeks after birth.[70,81] High cardiomyocyte proliferation rates in young humans were reported by a study combining stereological quantification and the analysis of mitotic events. [69] This group's findings suggested a strong increase in cardiomyocyte number within the first 20 years of human life. Conversely, the

application of ^{14}C birth-dating in combination with stereology, demonstrated no increase in cardiomyocyte cell number later than 1 month after birth with a final number of about 3.2×10^9 cardiomyocytes.[2] It could be shown that all events of subsequent cardiomyocyte proliferation account for cardiomyocyte replacement rather than number expansion, taking place majorly within the first 10 years of life.[2]

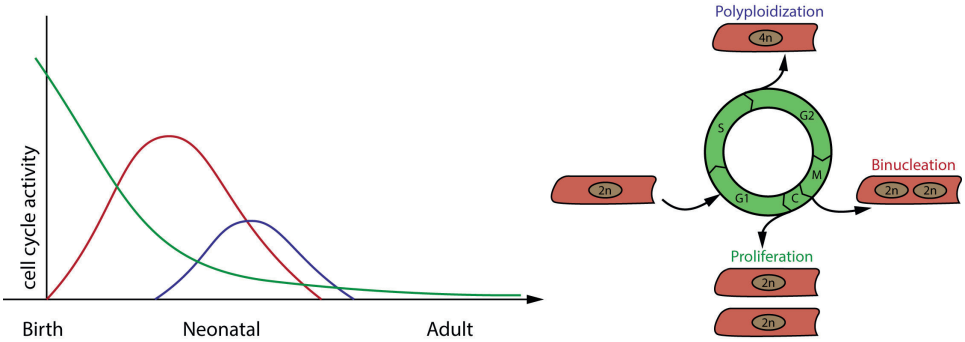

Figure 4. Schematic overview of the cardiomyocyte cell cycle activity during cardiac development and postnatal growth in mice. During cardiac development the heart grows by proliferation of cardiomyocytes (green line). Already before birth, cardiomyocyte proliferation decreases and incomplete cell cycles account for most of the neonatal cell cycle activity. Cardiomyocytes that undergo endoreplication exit the cell cycle after the S-phase and become polyploid. Karyokinesis without cytokinesis leads to binucleation of most of the cardiomyocytes. Both, polyploid and binucleated cardiomyocytes are unable to proliferate. After the neonatal period, annual cardiomyocyte proliferation is limited to less than 1%.

Numerous intrinsic and extrinsic factors that cause postnatal cardiomyocyte cell cycle exit leading to binucleation and polyploidization of cardiomyocytes have been identified. First of all, cardiomyocytes mature, leading to structural changes: during fetal cardiomyocyte proliferation, cardiomyocytes disassemble their sarcomeric apparatus before mitosis and re-assemble it during cell division, a process known as dedifferentiation. Likewise, the postnatal increase in sarcomeric content may interfere with the correct disassembly and re-assembly of these structures.[82] Cardiomyocytes withdraw from the cell cycle by a downregulation of positive cell cycle regulators such as cyclins and cyclin dependent kinases that maintain cardiomyocyte proliferation during heart development. At the same time levels of cell cycle inhibitors increase.[83] A change in the expression of transcription factors and miRNAs has been implicated in this process.[84,85] For example, increased postnatal expression of the transcription factor Meis homeobox 1 (*Meis 1*) was shown to activate the cell cycle dependent kinase (CDK) inhibitors p15, p16 and p21.[85] CDKs bind to their corresponding cyclins and thereby control progression through the different phases of the cell cycle. Accordingly, the inactivation of MEIS1 led to increased postnatal cardiomyocyte proliferation.[85] In adult mice, re-entry of cardiomyocyte proliferation could already be stimulated by overexpression cyclin D2, which decreased scar formation after myocardial infarction.[86]

Several miRNAs are involved in the drop of cardiomyocyte proliferation. Members of the miR-15 family are upregulated after birth and impede neonatal cardiomyocyte proliferation by the repression of cell cycle activators such as the checkpoint kinase 1, which regulates the progression of the cell cycle through mitosis.[84,87] An increased expression of miR-128 after birth was also implicated in the drop of postnatal cardiomyocyte proliferation. Overexpression of miR-128 reduced the time course of early neonatal cardiomyocyte proliferation and consequently cardiac hypertrophy.[88] Likewise, early neonatal heart regeneration was impeded in these mice. MiR-128 was shown to suppress the action of the positive cell-cycle regulators Cyclin E and CDK2. Levels of miR-128 stay high during adulthood and it could be demonstrated that deletion if miR-128 enhanced cardiac regeneration after myocardial infarction in adult mice. Also the delivery of exogenous miRNAs with viral vectors and intracardiac injections such as the human miRNAs hsa-miR-199a-3p and hsa-miR-590-3p stimulated proliferation of resident cardiomyocytes in neonatal rats and could induce cardiac regeneration in adult mice after myocardial infarction.[89,90] A safe delivery of miRNAs might be a promising way to stimulate cardiac regeneration in humans. Recently, miRNAs have also been suggested to be behind some of the beneficial effects observed after application of stem cells into the damaged cardiac tissue.[91] Extracellular vesicles released from these cells were shown to discharge paracrine factors that support cardiac repair processes when injected into infarcted myocardial tissue. Amongst other bioactive molecules, miRNAs released by the extracellular vesicles were proposed to stimulate proliferation and angiogenesis and may represent an attractive avenue of research to explore in detail if this can further be validated.

Whereas Yap is highly active before birth, the postnatal activation of the Hippo pathway causes restrained cardiomyocyte proliferation. Mechanical cues are an important upstream regulator of the Hippo pathway.[92] The extracellular matrix molecule Agrin and the dystrophin glycoprotein complex (DGC) were found to play an important role during postnatal cardiomyocyte proliferation (Figure 3). The transmembrane-complex DGC directly binds to YAP and thereby inhibits its translocation to the nucleus. High neonatal levels of Agrin bind to DGC and impede its interaction with YAP. Agrin levels are already markedly reduced after postnatal day 7, which may lead to increased YAP-DGC interaction and thus prevent YAP nuclear translocation.[93,94] When Agrin was administered after myocardial infarction consequent scar formation was reduced,[93] suggesting that this may be a promising therapeutic approach. In addition, adult mice deficient for the Hippo pathway due to the conditional knockout of *Sav* in cardiomyocytes, displayed a higher proliferation rate of cardiomyocytes after myocardial infarction and where enriched for nuclear localized YAP and sarcomere breakdown.[61,95]

Reactive oxygen species (ROS) are formed during the transition from the fetal hypoxic to the normoxic environment after birth have been shown to activate the Hippo pathway (Figure 3).[96] ROS develop when cardiomyocytes switch from anaerobic glycosylation to oxidative phosphorylation.[97] The DNA damage response that also becomes activated

in response to ROS, was shown to inhibit the cell cycle regulators Cyclin/CDKs.[98] In accordance with that, it was demonstrated that scavenging of the postnatal ROS extended the time window of cardiomyocyte proliferation after birth, confirmed by the smaller amount of hypertrophic cardiomyocytes and an increase in cardiomyocyte number. However, ROS scavenging only appeared to postpone but not impede the cardiomyocyte cell cycle arrest, suggesting that other intrinsic or extrinsic mechanisms play a role during the postnatal cell cycle exit.[98] In line with this, a small population of potentially proliferative mononucleated cardiomyocytes residing in an hypoxic niche within the adult heart, that supposedly is protected from oxidative damage, has been identified.[99] The oxygen-dependent degradation domain of the Hypoxia-inducible factor 1-alpha, which is stable in hypoxic cells but gets degraded in a normoxic environment, was fused to *Cre*, which was subsequently used to label the hypoxic cardiomyocytes followed by analysis of their fate.[99] The labelled cardiomyocytes increased in cell number throughout the whole heart with a calculated annual proliferation rate of 0.3%-1%, similar to results reported by other studies.[75]

Fetal and neonatal hearts can regenerate

Interestingly, whereas adult hearts are incapable of cardiomyocyte regeneration, fetal and neonatal hearts appear to retain this capacity for a short time window after birth.[11–14,87,100] In a study introducing mosaicism for depletion of the holocytochrome-c synthase, an enzyme necessary for myocardial energy generation at E12.5 of mouse development, it was observed that this depletion was met by an increased proliferation of the remaining cardiomyocytes, compensating for the impaired proliferation of about 50% of cardiomyocytes. Heart formation in these mice was partially impaired leading to cardiac abnormalities in almost half of the adult mice and postnatal mortality was mostly caused by dilated cardiomyopathy.[13] The response to direct cell loss earlier during development was studied in a genetic ablation model with the removal of up to 60% of cardiac progenitor cells and embryonic cardiomyocytes at E9.0. The depleted cardiomyocytes could be replaced by cardiac progenitor cells and, at least partly, by proliferating embryonic cardiomyocytes. In contrast to the previous study, cardiomyocyte depletion at E9.0 led to normal heart formation and fully functional hearts in adult mice.[14]

In neonatal mice the regenerative response to cardiac injury is strongly limited by the extent of injury and age.[11,12] For example, it was demonstrated that surgical resection of hearts of neonatal mice at postnatal day 1 led to complete cardiac regeneration (compensatory growth), whereas the same procedure at postnatal day 7 resulted in fibrosis and consequently scar formation. New cardiomyocytes were shown to originate from existing cardiomyocytes by proliferation and regeneration was accompanied by extensive angiogenesis.[11] Similar to what has been observed in fetal cardiomyocytes, neonatal cardiomyocytes displayed disorganized sarcomeres indicating their proliferative response.[11] Comparable results were obtained in studies with myocardial infarction leading to complete recovery after in mice of 1 day of age, whereas scarring occurred in 7 day old mice.[12] Regeneration in neonatal

mice seems to largely depend upon the formation of new vessels and the re-induction of perfusion after myocardial injury.[87,101] Major cues for neoangiogenisis might originate from the inflammatory response mediated by neonatal macrophages.[101] Whereas the adult inflammatory response after a myocardial infarction leads to fibrosis, the neonatal inflammatory response initiates angiogenesis and thereby facilitates regeneration of the injured cardiac tissue. Neonatal macrophages were demonstrated to be different in their transcriptional pattern and polarization as compared to adult macrophages.[101]

The brief period of time in which the neonatal heart can still recover from injury is termed the regenerative window, which in mice may be as short as 3 days, coinciding with the time frame in which at least a fraction of cardiomyocytes is still proliferating[11]. Interestingly, numerous studies have demonstrated that prolongation of the postnatal cardiomyocyte proliferative window can be achieved. For example, mice carrying a cardiomyocyte specific knockout of the Hippo component *Sav* displayed enhanced regeneration by proliferating cardiomyocytes after receiving cardiac apex resection at postnatal day 8.[102] Proliferation of neonatal cardiomyocytes was also increased when mice were compound deficient for SAV and DGC.[94] Sustained expression of the cardiac transcription factor GATA4, which is crucial for cardiac lineage specification during development, but decreases within the first neonatal week, enhanced myocardial regeneration after injury.[103] Also overexpression of *Tbx20*, increased cardiomyocyte proliferation and the regenerative response after myocardial infarction by repressing cell cycle inhibitor genes such as *Meis1* and *p21*.[104,105] Further, the expression of *ErbB2* that stimulates cardiomyocyte proliferation during fetal heart development is markedly downregulated within the first postnatal week. Accordingly, expression of constitutively active ErbB2 during the postnatal period as well as administration of NRG1 facilitated prolonged cardiomyocyte proliferation and enhanced regeneration after myocardial infarction.[76,106]

Perhaps a key question is if and for how long the regenerative window exists in humans? The higher rates of cardiomyocyte cell division detected in neonates[2] and young adults[69] could suggest the existence of a similar regenerative window. There is also some indication that hearts of children suffering from congenital heart defects, may respond better to cardiac surgery than adults due to a greater regenerative capacity.[107] In line with this is a reported case of myocardial infarction in a newborn child with coronary artery occlusion. Within weeks after the infarction the heart showed recovery and long term heart function and morphology was normal.[108] More studies are needed to assess the time span and extent of the regenerative window in humans, which might offer an important time window for therapeutic applications and corrective surgery in young patients born with a congenital heart defect.

Adult hearts fail to regenerate

After the neonatal period, humans and mice show a limited rate of annual cardiomyocyte turnover of about less than 1%.[1,75] Over the last 2 decades, a contribution of resident cardiac stem cells to cardiac homeostasis and regenerative response has also been suggested.[109] Perhaps the most striking of these stem cell populations comprised the c-kit+ resident stem cells, suggested to provide a significant contribution to the formation of new cardiomyocytes after cardiac injury.[110] In addition, in neonates, it was proposed that c-kit-expressing cardiac progenitor cells contribute to the generation of new myocardium after injury.[100] However, the contribution of c-kit+ cells to cardiac regeneration was lost in adults, c-kit+ cells adopting only a vascular fate instead.[100] Using lineage tracing another study demonstrated that c-kit+ cells mainly differentiate into endothelial cells and rarely to the cardiomyocyte population.[111] Misinterpretations could arise from the fact that also postnatal dedifferentiating cardiomyocytes,[112–114]and endocardial and epithelial cells[115] have been shown to express the surface marker c-kit, demonstrating the importance of accurate lineage tracing of progenitor cell populations before conclusions can be drawn. A recent study even suggested that c-kit+ cells might not be able to transdifferentiate in cardiomyocytes at all, as they demonstrated that c-kit+ cardiomyocytes originated from fusion with leukocytes.[116] The present consensus is that in adult mammals, resident cardiac progenitor cells contribute only a very minor fraction (<0.01% per annum) to new cardiomyocytes during homeostasis and after injury.[111,117,118] Similarly, extracardiac progenitor cell sources such as bone marrow derived stem cells contribute only marginally to homeostasis via fusion and transdifferentiation into cardiomyocytes.[118,119] These rates are therefore too low to replace the large numbers of cardiomyocytes that are lost after myocardial infarction and it can be concluded that they do not significantly contribute to regeneration.

Future perspectives: turning on cardiomyocyte proliferation?

Currently, the consensus view is that cardiomyocyte proliferation occurs at extremely low rates in the homeostatic adult mammalian heart, and that stem cell contribution to the heart muscle is rare. After cardiomyocyte loss during myocardial infarction the remaining cardiomyocytes fail to proliferate leading to heart failure and death. Causes of the postnatal cell cycle withdrawal are complex and involve intrinsic as well as extrinsic signaling pathways. Fully unraveling these pathways may be necessary to achieve cardiac regeneration in adult hearts. The lessons learned from proliferation control during mammalian heart development and in fish heart regeneration may help us find ways to therapeutically induce cardiac regeneration in adults. Manipulating the activity of pathways that are active during cardiac development such as the ErbB signaling pathway and the Hippo pathway are currently among the most promising that may be harnessed for this purpose. However, YAP signaling is also a key component in the development and progression of cancer and oncogenic risks might hinder translation to the clinic. The role of miRNAs in cardiomyocyte proliferation might be of translational value. However, as for other therapeutic molecules, specificity and side effects need to be assessed and safe and efficient delivery methods established before these can safely

be applied in the clinic. Moreover, it will be necessary to further identify and characterize the target population of potentially proliferative cardiomyocytes within the human heart that may differ between patients. Alternative approaches such as direct reprogramming of cardiac fibroblasts into cardiomyocytes and other cell types to increase functional muscle mass is also being explored. [120,121]. Precise understanding of the developmental differentiation and epigenetic mechanisms will help to improve reprogramming efficiency and increase its clinical potential. New technologies such as precise genome editing using CRISPR and single-cell RNA sequencing provide promising tools to identify the molecular cues that would illicit a controlled and sufficient rate of cell-division, and to investigate whether the newly formed cardiomyocytes are and remain fully functional. Furthermore, it remains to be established whether and to what extent we need to control the cell-type composition, including the endothelial cells and fibroblasts, and coronary vasculature, after successfully restoring the muscle cell mass.

ACKNOWLEDGEMENTS

VMC is supported by Netherlands Heart Foundation grant COBRA^3 (2012T091).

REFERENCES

1. Bergmann, O, Bhardwaj, RD, Bernard, S, Zdunek, S, Walsh, S, Zupicich, J, *et al.* (2009). Evidence for cardiomyocyte renewal in humans. *Science (80-.).* **324**: 98–102.
2. Bergmann, O, Zdunek, S, Felker, A, Salehpour, M, Alkass, K, Bernard, S, *et al.* (2015). Dynamics of cell generation and turnover in the human heart. *Cell* **161**: 1566–1575.
3. Lozano, R, Naghavi, M, Foreman, K, Lim, S, Shibuya, K, Aboyans, V, *et al.* (2012). Global and regional mortality from 235 causes of death for 20 age groups in 1990 and 2010: A systematic analysis for the Global Burden of Disease Study 2010. *Lancet* **380**: 2095–2128.
4. Van Berlo, JH and Molkentin, JD (2014). An emerging consensus on cardiac regeneration. *Nat Med* **20**: 1386–1393.
5. Chong, JJH, Yang, X, Don, CW, Minami, E, Liu, YW, Weyers, JJ, *et al.* (2014). Human embryonic-stem-cell-derived cardiomyocytes regenerate non-human primate hearts. *Nature* **510**: 273–277.
6. Shiba, Y, Gomibuchi, T, Seto, T, Wada, Y, Ichimura, H, Tanaka, Y, *et al.* (2016). Allogeneic transplantation of iPS cell-derived cardiomyocytes regenerates primate hearts. *Nature* **538**: 388–391.
7. Caspi, O, Huber, I, Kehat, I, Habib, M, Arbel, G, Gepstein, A, *et al.* (2007). Transplantation of Human Embryonic Stem Cell-Derived Cardiomyocytes Improves Myocardial Performance in Infarcted Rat Hearts. *J. Am. Coll. Cardiol.* **50**: 1884–1893.
8. van Laake, LW, Passier, R, Monshouwer-Kloots, J, Verkleij, AJ, Lips, DJ, Freund, C, *et al.* (2007). Human embryonic stem cell-derived cardiomyocytes survive and mature in the mouse heart and transiently improve function after myocardial infarction. *Stem Cell Res* **1**: 9–24.
9. Laflamme, MA, Gold, J, Xu, C, Hassanipour, M, Rosler, E, Police, S, *et al.* (2005). Formation of Human Myocardium in the Rat Heart from Human Embryonic Stem Cells. *Am. J. Pathol.* **167**: 663–671.
10. Jopling, C, Sleep, E, Raya, M, Martí, M, Raya, A and Belmonte, JCII (2010). Zebrafish heart regeneration occurs by cardiomyocyte dedifferentiation and proliferation. *Nature* **464**: 606–609.
11. Porrello, ER, Mahmoud, AI, Simpson, E, Hill, JA, Richardson, JA, Olson, EN, *et al.* (2011). Transient regenerative potential of the neonatal mouse heart. *Science* **331**: 1078–80.
12. Haubner, BJ, Adamowicz-Brice, M, Khadayate, S, Tiefenthaler, V, Metzler, B, Aitman, T, *et al.* (2012). Complete cardiac regeneration in a mouse model of myocardial infarction. *Aging (Albany NY)* **4**: 966–977.
13. Drenckhahn, JD, Schwarz, QP, Gray, S, Laskowski, A, Kiriazis, H, Ming, Z, *et al.* (2008). Compensatory Growth of Healthy Cardiac Cells in the Presence of Diseased Cells Restores Tissue Homeostasis during Heart Development. *Dev Cell* **15**: 521–533.
14. Sturzu, AC, Rajarajan, K, Passer, D, Plonowska, K, Riley, A, Tan, TC, *et al.* (2015). Fetal mammalian heart generates a robust compensatory response to cell loss. *Circulation* **132**: 109–121.
15. Kelly, RG, Buckingham, ME and Moorman, AF (2014). Heart fields and cardiac morphogenesis. *Cold Spring Harb Perspect Med* **4**: 1–10.
16. Sizarov, A, Ya, J, De Boer, BA, Lamers, WH, Christoffels, VM and Moorman, AFM (2011). Formation of the building plan of the human heart: Morphogenesis, growth, and differentiation. *Circulation* **123**: 1125–1135.

17. de Boer, BA, van den Berg, G, de Boer, PAJJ, Moorman, AFMM and Ruijter, JM (2012). Growth of the developing mouse heart: An interactive qualitative and quantitative 3D atlas. *Dev. Biol.* **368**: 203–213.
18. Krishnan, A, Samtani, R, Dhanantwari, P, Lee, E, Yamada, S, Shiota, K, *et al.* (2014). A detailed comparison of mouse and human cardiac development. *Pediatr Res* **76**: 500–507.
19. Tyser, RCV, Miranda, AMA, Chen, CM, Davidson, SM, Srinivas, S and Riley, PR (2016). Calcium handling precedes cardiac differentiation to initiate the first heartbeat. *Elife* **5**: 1–25.
20. Moorman, AF., Christoffels, VM, Anderson, RH and van den Hoff, MJ. (2007). The heart-forming fields: one or multiple? *Philos. Trans. R. Soc. B Biol. Sci.* **362**: 1257–1265.
21. van den Berg, G, Abu-Issa, R, De Boer, BA, Hutson, MR, De Boer, PAJ, Soufan, AT, *et al.* (2009). A caudal proliferating growth center contributes to both poles of the forming heart tube. *Circ Res* **104**: 179–188.
22. Kwon, C, Arnold, J, Hsiao, EC, Taketo, MM, Conklin, BR and Srivastava, D (2007). Canonical Wnt signaling is a positive regulator of mammalian cardiac progenitors. *Proc Natl Acad Sci* **104**: 10894–10899.
23. Aanhaanen, WTJ, Brons, JF, Domínguez, JN, Rana, MS, Norden, J, Airik, R, *et al.* (2009). The Tbx2+ primary myocardium of the atrioventricular canal forms the atrioventricular node and the base of the left ventricle. *Circ. Res.* **104**: 1267–1274.
24. Devine, WP, Wythe, JD, George, M, Koshiba-Takeuchi, K and Bruneau, BG (2014). Early patterning and specification of cardiac progenitors in gastrulating mesoderm. *Elife* **3**: 1–23.
25. Van Vliet, P, Wu, SM, Zaffran, S and Pucéat, M (2012). Early cardiac development: A view from stem cells to embryos. *Cardiovasc. Res.* **96**: 352–362.
26. Greulich, F, Rudat, C and Kispert, A (2011). Mechanisms of T-box gene function in the developing heart. *Cardiovasc. Res.* **91**: 212–222.
27. Christoffels, VM, Smits, GJ, Kispert, A and Moorman, AFM (2010). Development of the pacemaker tissues of the heart. *Circ. Res.* **106**: 240–254.
28. Katz, MG, Fargnoli, AS, Kendle, AP, Hajjar, RJ and Bridges, CR (2016). The role of microRNAs in cardiac development and regenerative capacity. *Am. J. Physiol. Heart Circ. Physiol.* **310**: H528-41.
29. Chen, JF, Mandel, EM, Thomson, JM, Wu, Q, Callis, TE, Hammond, SM, *et al.* (2006). The role of microRNA-1 and microRNA-133 in skeletal muscle proliferation and differentiation. *Nat. Genet.* **38**: 228–233.
30. Wystub, K, Besser, J, Bachmann, A, Boettger, T and Braun, T (2013). miR-1/133a Clusters Cooperatively Specify the Cardiomyogenic Lineage by Adjustment of Myocardin Levels during Embryonic Heart Development. *PLoS Genet.* **9**.
31. Christoffels, VM, Habets, PEMH, Franco, D, Campione, M, de Jong, F, Lamers, WH, *et al.* (2000). Chamber Formation and Morphogenesis in the Developing Mammalian Heart. *Dev. Biol.* **223**: 266–278.
32. Soufan, AT, Van Den Berg, G, Ruijter, JM, De Boer, PAJ, Van Den Hoff, MJB and Moorman, AFM (2006). Regionalized sequence of myocardial cell growth and proliferation characterizes early chamber formation. *Circ. Res.* **99**: 545–552.
33. Aanhaanen, WTJ, Boukens, BJD, Sizarov, A, Wakker, V, De Gier-De Vries, C, Van Ginneken, AC, *et al.* (2011). Defective Tbx2-dependent patterning of the atrioventricular canal myocardium causes accessory pathway formation in mice. *J. Clin. Invest.* **121**: 534–544.

34. Bakker, ML, Moorman, AFM and Christoffels, VM (2010). The atrioventricular node: origin, development, and genetic program. *Trends Cardiovasc. Med.* **20**: 164–171.
35. Captur, G, Wilson, R, Bennett, MF, Luxán, G, Nasis, A, de la Pompa, JL, *et al.* (2016). Morphogenesis of myocardial trabeculae in the mouse embryo. *J. Anat.* **229**: 314–325.
36. Luxán, G, D'Amato, G, MacGrogan, D and De La Pompa, JL (2016). Endocardial Notch signaling in cardiac development and disease. *Circ. Res.* **118**: e1–e18.
37. Jones, JT, Akita, RW and Sliwkowski, MX (1999). Binding specificities and affinities of egf domains for ErbB receptors. *FEBS Lett.* **447**: 227–231.
38. D'Amato, G, Luxán, G, Del Monte-Nieto, G, Martínez-Poveda, B, Torroja, C, Walter, W, *et al.* (2016). Sequential Notch activation regulates ventricular chamber development. *Nat. Cell Biol.* **18**: 7–20.
39. Sucov, HM, Gu, Y, Thomas, S, Li, P and Pashmforoush, M (2009). Epicardial control of myocardial proliferation and morphogenesis. *Pediatr. Cardiol.* **30**: pp 617–625.
40. Shen, H, Cavallero, S, Estrada, KD, Sandovici, I, Kumar, SR, Makita, T, *et al.* (2015). Extracardiac control of embryonic cardiomyocyte proliferation and ventricular wall expansion. *Cardiovasc. Res.* **105**: 271–278.
41. Li, P, Cavallero, S, Gu, Y, Chen, THP, Hughes, J, Hassan, AB, *et al.* (2011). IGF signaling directs ventricular cardiomyocyte proliferation during embryonic heart development. *Development* **138**: 1795–1805.
42. Riley, PR (2012). An epicardial floor plan for building and rebuilding the mammalian heart. *Curr. Top. Dev. Biol.* **100**: 233–251.
43. Pinto, AR, Ilinykh, A, Ivey, MJ, Kuwabara, JT, D'antoni, ML, Debuque, R, *et al.* (2016). Revisiting cardiac cellular composition. *Circ. Res.* **118**: 400–409.
44. Banerjee, I, Fuseler, JW, Price, RL, Borg, TK and Baudino, TA (2007). Determination of cell types and numbers during cardiac development in the neonatal and adult rat and mouse. *Am. J. Physiol. Heart Circ. Physiol.* **293**: H1883-91.
45. De Bakker, BS, De Jong, KH, Hagoort, J, De Bree, K, Besselink, CT, De Kanter, FEC, *et al.* (2016). An interactive three-dimensional digital atlas and quantitative database of human development. *Science (80-.).* **354**.
46. Dong, J, Feldmann, G, Huang, J, Wu, S, Zhang, N, Comerford, SA, *et al.* (2007). Elucidation of a universal size-control mechanism in drosophila and mammals. *Cell* **130**: 1120–1133.
47. Heallen, T, Zhang, M, Wang, J, Bonilla-claudio, M, Klysik, E, Randy, L, *et al.* (2012). Hippo pathway inhibits Wnt signaling to restrain cardiomyocyte proliferation and heart size. *Science (80-.).* **332**: 458–461.
48. Callus, BA, Verhagen, AM and Vaux, DL (2006). Association of mammalian sterile twenty kinases, Mst1 and Mst2, with hSalvador via C-terminal coiled-coil domains, leads to its stabilization and phosphorylation. *FEBS J* **273**: 4264–4276.
49. Chan, EHY, Nousiainen, M, Chalamalasetty, RB, Schäfer, A, Nigg, EA and Sillje, HHW (2005). The Ste20-like kinase Mst2 activates the human large tumor suppressor kinase Lats1. *Oncogene* **24**: 2076–2086.
50. Hao, Y, Chun, A, Cheung, K, Rashidi, B and Yang, X (2008). Tumor suppressor LATS1 is a negative regulator of oncogene YAP. *J Biol Chem* **283**: 5496–5509.
51. Oka, T, Mazack, V and Sudol, M (2008). Mst2 and Lats kinases regulate apoptotic function of Yes kinase-associated protein (YAP). *J Biol Chem* **283**: 27534–27546.

52. Huang, J, Wu, S, Barrera, J, Matthews, K and Pan, D (2005). The Hippo signaling pathway coordinately regulates cell proliferation and apoptosis by inactivating Yorkie, the Drosophila homolog of YAP. *Cell* **122**: 421–434.
53. Strano, S, Munarriz, E, Rossi, M, Castagnoli, L, Shaul, Y, Sacchi, A, *et al.* (2001). Physical interaction with Yes-associated protein enhances p73 transcriptional activity. *J Biol Chem* **276**: 15164–15173.
54. Lapi, E, Di Agostino, S, Donzelli, S, Gal, H, Domany, E, Rechavi, G, *et al.* (2008). PML, YAP, and p73 are components of a proapoptotic autoregulatory feedback loop. *Mol Cell* **32**: 803–814.
55. Okazaki, T, Kageji, T, Kuwayama, K, Kitazato, KT, Mure, H, Hara, K, *et al.* (2012). Up-regulation of endogenous PML induced by a combination of interferon-beta and temozolomide enhances p73/YAP-mediated apoptosis in glioblastoma. *Cancer Lett* **323**: 199–207.
56. Zaidi, SK, Sullivan, AJ, Medina, R, Ito, Y, Van Wijnen, AJ, Stein, JL, *et al.* (2004). Tyrosine phosphorylation controls Runx2-mediated subnuclear targeting of YAP to repress transcription. *EMBO J* **23**: 790–799.
57. Murakami, M, Nakagawa, M, Olson, EN and Nakagawa, O (2005). A WW domain protein TAZ is a critical coactivator for TBX5, a transcription factor implicated in Holt-Oram syndrome. *Proc Natl Acad Sci U S A* **102**: 18034–18039.
58. Rosenbluh, J, Nijhawan, D, Cox, AG, Li, X, Neal, JT, Schafer, EJ, *et al.* (2012). β-Catenin-driven cancers require a YAP1 transcriptional complex for survival and tumorigenesis. *Cell* **151**: 1457–1473.
59. Zhao, B, Ye, X, Yu, JJ, Li, L, Li, W, Li, S, *et al.* (2008). TEAD mediates YAP-dependent gene induction and growth control TEAD mediate. *Genes Dev*: 1962–1971doi:10.1101/gad.1664408.
60. Zanconato, F, Forcato, M, Battilana, G, Azzolin, L, Quaranta, E, Bodega, B, *et al.* (2015). Genome-wide association between YAP/TAZ/TEAD and AP-1 at enhancers drives oncogenic growth. *Nat Cell Biol* **17**: 1218–1227.
61. Morikawa, Y, Zhang, M, Heallen, T, Leach, J, Tao, G, Xiao, Y, *et al.* (2015). Actin cytoskeletal remodeling with protrusion formation is essential for heart regeneration in Hippo-deficient mice **8**.
62. Li, J, Gao, E, Vite, A, Yi, R, Gomez, L, Goossens, S, *et al.* (2015). Alpha-catenins control cardiomyocyte proliferation by regulating yap activity. *Circ Res* **116**: 70–79.
63. Schlegelmilch, K, Mohseni, M, Kirak, O, Pruszak, J, Rodriguez, JR, Zhou, D, *et al.* (2011). Yap1 acts downstream of β-catenin to control epidermal proliferation. *Cell* **144**: 782–795.
64. Xin, M, Kim, Y, Sutherland, LB, Qi, X, Mcanally, J, Robert, J, *et al.* (2011). Regulation of Insulin-like growth factor signaling by Yap governs cardiomyocyte proliferation and embryonic heart size. *Sci. Signal.* **4**: ra70.
65. von Gise, A, Lin, Z, Schlegelmilch, K, Honor, LB, Pan, GM, Buck, JN, *et al.* (2012). YAP1, the nuclear target of Hippo signaling, stimulates heart growth through cardiomyocyte proliferation but not hypertrophy. *Proc Natl Acad Sci U S A* **109**: 2394–9.
66. Wang, Y, Hu, G, Liu, F, Wang, X, Wu, M, Schwarz, JJ, *et al.* (2014). Deletion of yes-associated protein (YAP) specifically in cardiac and vascular smooth muscle cells reveals a crucial role for YAP in mouse cardiovascular development. *Circ Res* **114**: 957–965.
67. Xin, M, Kim, Y, Sutherland, LB, Murakami, M, Qi, X, McAnally, J, *et al.* (2013). Hippo pathway effector Yap promotes cardiac regeneration. *Proc Natl Acad Sci U S A* **110**: 13839–13844.

68. Li, F, Wang, X, Capasso, JM and Gerdes, AM (1996). Rapid transition of cardiac myocytes from hyperplasia to hypertrophy during postnatal development. *J. Mol. Cell. Cardiol.* **28**: 1737–1746.
69. Mollova, M, Bersell, K, Walsh, S, Savla, J, Das, LT, Park, S-Y, *et al.* (2013). Cardiomyocyte proliferation contributes to heart growth in young humans. *Proc. Natl. Acad. Sci. U. S. A.* **110**: 1446–51.
70. Alkass, K, Panula, J, Westman, M, Wu, T-D Di, Guerquin-Kern, J-LL and Bergmann, O (2015). No evidence for cardiomyocyte number expansion in preadolescent mice. *Cell* **163**: 1026–1036.
71. Soonpaa, MH, Kim, KK, Pajak, L, Franklin, M and Field, LJ (1996). Cardiomyocyte DNA synthesis and binucleation during murine development. *Am. J. Physiol.* **271**: H2183–H2189.
72. Walsh, S, Pontén, A, Fleischmann, BK and Jovinge, S (2010). Cardiomyocyte cell cycle control and growth estimation in vivo-An analysis based on cardiomyocyte nuclei. *Cardiovasc. Res.* **86**: 365–373.
73. Wessels, A and Sedmera, D (2003). Developmental anatomy of the heart: a tale of mice and man. *Physiol. Genomics* **15**: 165–176.
74. Olivetti, G, Cigola, E, Maestri, R, Corradi, D, Lagrasta, C, Gambert, SR, *et al.* (1996). Aging, cardiac hypertrophy and ischemic cardiomyopathy do not affect the proportion of mononucleated and multinucleated myocytes in the human heart. *J Mol Cell Cardiol* **28**: 1463–1477.
75. Senyo, SE, Steinhauser, ML, Pizzimenti, CL, Yang, VK, Cai, L, Wang, M, *et al.* (2013). Mammalian heart renewel by preexisting cardiomyocytes. *Nature* **493**: 433–436.
76. Bersell, K, Arab, S, Haring, B and Kühn, B (2009). Neuregulin1/ErbB4 signaling induces cardiomyocyte proliferation and repair of heart injury. *Cell* **138**: 257–270.
77. Patterson, M, Barske, L, Van Handel, B, Rau, CD, Gan, P, Sharma, A, *et al.* (2017). Frequency of mononuclear diploid cardiomyocytes underlies natural variation in heart regeneration. *Nat. Genet.* doi:10.1038/ng.3929.
78. Poss, KD, Wilson, LG and Keating, MT (2002). Heart regeneration in zebrafish. *Science (80-.).* **298**: 2188–2190.
79. González-Rosa, JM, Sharpe, M, Field, D, Soonpaa, MH, Field, LJ, Burns, CE, *et al.* (2018). Myocardial Polyploidization Creates a Barrier to Heart Regeneration in Zebrafish. *Dev. Cell* **44**: 433–446.e7.
80. Naqvi, N, Li, M, Calvert, JW, Tejada, T, Lambert, JP, Wu, J, *et al.* (2014). A proliferative burst during preadolescence establishes the final cardiomyocyte number. *Cell* **157**: 795–807.
81. Soonpaa, MHH, Zebrowski, DCC, Platt, C, Rosenzweig, A, Engel, FBB and Field, LJJ (2015). Cardiomyocyte cell-cycle activity during preadolescence. *Cell* **163**: 781–2.
82. Ahuja, P (2004). Sequential myofibrillar breakdown accompanies mitotic division of mammalian cardiomyocytes. *J. Cell Sci.* **117**: 3295–3306.
83. Ikenishi, A, Okayama, H, Iwamoto, N, Yoshitome, S, Tane, S, Nakamura, K, *et al.* (2012). Cell cycle regulation in mouse heart during embryonic and postnatal stages. *Dev Growth Differ* **54**: 731–738.
84. Porrello, ER, Johnson, BA, Aurora, AB, Simpson, E, Nam, YJ, Matkovich, SJ, *et al.* (2011). MiR-15 family regulates postnatal mitotic arrest of cardiomyocytes. *Circ Res* **109**: 670–679.
85. Mahmoud, AI, Kocabas, F, Muralidhar, SA, Kimura, W, Koura, A, Thet, S, *et al.* (2013). Meis1 regulates postnatal cardiomyocyte cell cycle arrest. *Nature* **497**: 249–253.

86. Pasumarthi, KBS, Nakajima, HHO, Nakajima, HHO, Soonpaa, MH and Field, LJ (2005). Targeted expression of cyclin D2 results in cardiomyocyte DNA synthesis and infarct regression in transgenic mice. *Circ Res* **96**: 110–118.
87. Porrello, ER, Mahmoud, AI, Simpson, E, Johnson, BA, Grinsfelder, D, Canseco, D, *et al.* (2013). Regulation of neonatal and adult mammalian heart regeneration by the miR-15 family. *Proc Natl Acad Sci U S A* **110**: 187–92.
88. Huang, W, Feng, Y, Liang, J, Yu, H, Wang, C, Wang, B, *et al.* (2018). Loss of microRNA-128 promotes cardiomyocyte proliferation and heart regeneration. *Nat. Commun.* **9**.
89. Eulalio, A, Mano, M, Ferro, MD, Zentilin, L, Sinagra, G, Zacchigna, S, *et al.* (2012). Functional screening identifies miRNAs inducing cardiac regeneration. *Nature* **492**: 376–381.
90. Lesizza, P, Prosdocimo, G, Martinelli, V, Sinagra, G, Zacchigna, S and Giacca, M (2017). Integrative Physiology Single-Dose Intracardiac Injection of Pro-Regenerative MicroRNAs Improves Cardiac Function After Myocardial Infarction. *Circ Res* **120**: 1298–1304.
91. El Harane, N, Kervadec, A, Bellamy, V, Pidial, L, Neametalla, HJ, Perier, M-C, *et al.* (2018). Acellular therapeutic approach for heart failure: in vitro production of extracellular vesicles from human cardiovascular progenitors. *Eur. Heart J.*: 1–13doi:10.1093/eurheartj/ehy012.
92. Dupont, S, Morsut, L, Aragona, M, Enzo, E, Giulitti, S, Cordenonsi, M, *et al.* (2011). Role of YAP/TAZ in mechanotransduction. *Nature* **474**: 179–184.
93. Bassat, E, Mutlak, YE, Genzelinakh, A, Shadrin, IY, Baruch Umansky, K, Yifa, O, *et al.* (2017). The extracellular matrix protein agrin promotes heart regeneration in mice. *Nature* **547**: 179–184.
94. Morikawa, Y, Heallen, T, Leach, J, Xiao, Y and Martin, JF (2017). Dystrophin-glycoprotein complex sequesters Yap to inhibit cardiomyocyte proliferation. *Nature* **547**: 227–231.
95. Leach, JP, Heallen, T, Zhang, M, Rahmani, M, Morikawa, Y, Hill, MC, *et al.* (2017). Hippo pathway deficiency reverses systolic heart failure after infarction. *Nature*doi:10.1038/nature24045.
96. Lehtinen, MK, Yuan, Z, Boag, PR, Yang, Y, Villén, J, Becker, EBE, *et al.* (2006). A Conserved MST-FOXO Signaling Pathway Mediates Oxidative-Stress Responses and Extends Life Span. *Cell* **125**: 987–1001.
97. Lopaschuk, GD and Jaswal, JS (2010). Energy metabolic phenotype of the cardiomyocyte during development, differentiation, and postnatal maturation. *J Cardiovasc Pharmacol* **56**: pp 130–140.
98. Puente, BN, Kimura, W, Muralidhar, SA, Moon, J, Amatruda, JF, Phelps, KL, *et al.* (2014). The oxygen-rich postnatal environment induces cardiomyocyte cell-cycle arrest through DNA damage response. *Cell* **157**: 565–79.
99. Kimura, W, Xiao, F, Canseco, DC, Muralidhar, S, Thet, S, Zhang, HM, *et al.* (2015). Hypoxia fate mapping identifies cycling cardiomyocytes in the adult heart. *Nature* **523**: 226–230.
100. Jesty, SA, Steffey, MA, Lee, FK, Breitbach, M, Hesse, M, Reining, S, *et al.* (2012). c-kit+ precursors support postinfarction myogenesis in the neonatal, but not adult, heart. *Proc Natl Acad Sci U S A* **109**: 13380–13385.
101. Aurora, AB, Porrello, ER, Tan, W, Mahmoud, AI, Hill, JA, Bassel-Duby, R, *et al.* (2014). Macrophages are required for neonatal heart regeneration. *J. Clin. Invest.* **124**: 1382–1392.
102. Heallen, T, Morikawa, Y, Leach, J, Tao, G, Willerson, JT, Johnson, RL, *et al.* (2013). Hippo signaling impedes adult heart regeneration. *Development* **140**: 4683–4690.

103. Malek Mohammadi, M, Kattih, B, Grund, A, Froese, N, Korf-Klingebiel, M, Gigina, A, *et al.* (2017). The transcription factor GATA4 promotes myocardial regeneration in neonatal mice. *EMBO Mol Med* **9**: 265–279.
104. Xiang, FL, Guo, M and Yutzey, KE (2016). Overexpression of Tbx20 in adult cardiomyocytes promotes proliferation and improves cardiac function after myocardial infarction. *Circulation* **133**: 1081–1092.
105. Chakraborty, S, Sengupta, A and Yutzey, KE (2013). Tbx20 promotes cardiomyocyte proliferation and persistence of fetal characteristics in adult mouse hearts. *J. Mol. Cell. Cardiol.* **62**: 203–213.
106. D'Uva, G, Aharonov, A, Lauriola, M, Kain, D, Yahalom-Ronen, Y, Carvalho, S, *et al.* (2015). ERBB2 triggers mammalian heart regeneration by promoting cardiomyocyte dedifferentiation and proliferation. *Nat Cell Biol* **17**: 627–638.
107. Fratz, S, Hager, A, Schreiber, C, Schwaiger, M, Hess, J and Stern, HC (2011). Long-term myocardial scarring after operation for anomalous left coronary artery from the pulmonary artery. *Ann Thorac Surg* **92**: 1761–1765.
108. Haubner, BJ, Schneider, J, Schweigmann, U, Schuetz, T, Dichtl, W, Velik-Salchner, C, *et al.* (2016). Functional Recovery of a Human Neonatal Heart after Severe Myocardial Infarction. *Circ Res* **118**: 216–221.
109. Sturzu, AC and Wu, SM (2011). Developmental and regenerative biology of multipotent cardiovascular progenitor cells. *Circ Res* **108**: 353–364.
110. Beltrami, AP, Barlucchi, L, Torella, D, Baker, M, Limana, F, Chimenti, S, *et al.* (2003). Adult cardiac stem cells are multipotent and support myocardial regeneration. *Cell* **114**: 763–776.
111. van Berlo, JH, Kanisicak, O, Maillet, M, Vagnozzi, RJ, Karch, J, Lin, S-CJ, *et al.* (2014). C-Kit+ Cells Minimally Contribute Cardiomyocytes To the Heart. *Nature* **509**: 337–41.
112. Kubin, T, Pöling, J, Kostin, S, Gajawada, P, Hein, S, Rees, W, *et al.* (2011). Oncostatin M is a major mediator of cardiomyocyte dedifferentiation and remodeling. *Cell Stem Cell* **9**: 420–432.
113. Li, M, Naqvi, N, Yahiro, E, Liu, K, Powell, PC, Bradley, WE, *et al.* (2008). c-kit is required for cardiomyocyte terminal differentiation. *Circ Res* **102**: 677–685.
114. Zhang, Y, Li, TS, Lee, ST, Wawrowsky, KA, Cheng, K, Galang, G, *et al.* (2010). Dedifferentiation and proliferation of mammalian cardiomyocytes. *PLoS One* **5**: 1–13.
115. Tallini, YN, Greene, KS, Craven, M, Spealman, A, Breitbach, M, Smith, J, *et al.* (2009). c-kit expression identifies cardiovascular precursors in the neonatal heart. *Proc Natl Acad Sci U S A* **106**: 1808–13.
116. Bryan D. Maliken, Onur Kanisicak, Jason Karch, Hadi Khalil, Xing Fu, Justin G. Boyer, Vikram Prasad, Yi Zheng, JDM (2018). Gata4-Dependent Differentiation of c-Kit + Derived Endothelial Cells Underlies Artefactual Cardiomyocyte Regeneration in the Heart. *Circulation* **137**.
117. Sultana, N, Zhang, L, Yan, J, Chen, J, Cai, W, Razzaque, S, *et al.* (2015). Resident c-kit + cells in the heart are not cardiac stem cells. *Nat Commun* **6**: 1–10.
118. Eschenhagen, T, Bolli, R, Braun, T, Field, LJ, Fleischmann, BK, Frisén, J, *et al.* (2017). Cardiomyocyte Regeneration: A Consensus Statement. *Circulation*: 680–686doi:10.1161/CIRCULATIONAHA.117.029343.
119. Wu, JMF, Hsueh, YC, Ch'ang, HJ, Luo, CY, Wu, LW, Nakauchi, H, *et al.* (2015). Circulating cells contribute to cardiomyocyte regeneration after injury. *Circ Res* **116**: 633–641.
120. Kojima, H and Ieda, M (2017). Discovery and progress of direct cardiac reprogramming. *Cell. Mol. Life Sci.* **74**: 2203–2215.

121. Liu, Z, Wang, L, Welch, JD, Ma, H, Zhou, Y, Vaseghi, HR, *et al.* (2017). Single-cell transcriptomics reconstructs fate conversion from fibroblast to cardiomyocyte. *Nature* **551**: 100–104.

2

Chapter 2

Early Postnatal Cardiac Stress Does Not Influence Ventricular Cardiomyocyte Cell-Cycle Withdrawal

Marie Günthel, Karel van Duijvenboden, Jorn Jeremiasse, Maurice J. B. van den Hoff, Vincent M. Christoffels

Journal of Cardiovascular Development and Disease. Vol. 8, April 2021: 38

ABSTRACT

Congenital heart disease (CHD) is the most common birth defect. After birth, patients with CHD may suffer from cardiac stress resulting from abnormal loading conditions. However, it is not known how this cardiac burden influences the postnatal development and adaptation of the ventricles. To study the transcriptional and cell-cycle response of neonatal cardiomyocytes to cardiac stress, we used a genetic mouse model that develops left ventricular volume overload within 2 weeks after birth. The increased volume load caused upregulation of the cardiac stress marker *Nppa* in the left ventricle and interventricular septum as early as 12 days after birth. Transcriptome analysis revealed that cardiac stress induced the expression of cell-cycle genes. This did not influence postnatal cell-cycle withdrawal of cardiomyocytes and other cell types in the ventricles as measured by Ki-67 immunostaining.

Keywords: neonatal heart, volume overload, congenital heart defect, cardiomyocyte cell-cycle

INTRODUCTION

Congenital heart disease (CHD) is the most common birth defect with an incidence of 0.8% of all live births [1]. Right after birth, patients with CHD often suffer from cardiac loading abnormalities such as volume or pressure overload [2]. Whereas small muscular ventricular septal defects may close spontaneously, complex CHDs will require surgical correction [2]. Although nowadays childhood survival is excellent and 90% of the children born with a CHD reach adulthood, pediatric patients are still at risk to develop heart failure during their first year of life [3,4]. In addition, the majority of adult patients develops cardiac complications such as arrhythmias and heart failure, leading to an increased re-hospitalization and the need for re-interventions [5]. Little is known on how cardiomyocytes adapt to cardiac loading abnormalities in CHD patients during early postnatal development of the heart, or how this influences the development of cardiac complications such as heart failure.

The transition from the fetal to the postnatal heart is marked by an increase in oxygen and changed hemodynamics. Cardiomyocytes adapt to these changes by switching from glycolytic to fatty acid metabolism [6]. This metabolic transition is accompanied by a change in cardiomyocyte cell-cycle activity. Before birth, the heart grows by proliferation of small cardiomyocytes. After birth, the proliferation rate drops and the heart grows by hypertrophy of the existing cardiomyocytes [7]. In mice, cardiomyocyte proliferation is completed 7 days after birth [8]. After that, cardiomyocytes will undergo incomplete cell-cycles leading to polyploidization and multinucleation. Most of the postnatal DNA synthesis is finished at 14 days after birth [8]. In humans, the final number of cardiomyocytes is reached already 1 month after birth and afterwards cardiomyocyte cell-cycle activity mainly accounts for polyploidization [9]. The postnatal metabolic switch and cell-cycle withdrawal of cardiomyocytes are suggested to be highly susceptible to perturbations [10,11]. Therefore, we reasoned that early postnatal cardiac stress could alter cardiomyocyte proliferation and metabolic maturation.

Thus far, there is a lack of animal models investigating adaptation of cardiomyocytes to neonatal cardiac stress due to ventricular volume overload. In this study we used a mouse model which develops severe cardiac abnormalities early after birth [12]. In *Fstl1*$^{KO/fl}$*;Tie2-Cre* mice, Fstl1 was ablated from the endocardial/endothelial cell-lineage under the control of *Tie2-Cre* [12]. After birth, *Fstl1*$^{KO/fl}$*;Tie2-Cre* (cKO) mice develop progressive malformation of the mitral valves, but do not show echocardiographic abnormalities at postnatal day (P) 7. From P10 onwards, the first cKO pups show valvular insufficiency, causing mitral regurgitation and volume overload of the left ventricle. The malformation of the mitral valves develops progressively and the left ventricle of cKO mice increases in mass and internal diameter. The first cKO mice start dying at P14. At P21, more than 70% of the mice have died from heart failure with preserved ejection fraction [12].

We performed RNA-sequencing of PCM-1+ cardiomyocyte nuclei of P12 cKO and healthy control mice to investigate the molecular mechanisms that influence cardiomyocyte development during early ventricular volume overload. Heart to body weight ratios (HW/BW) and the expression of the atrial natriuretic peptide (*Nppa*) were used as markers to score for cardiac disease state in these mice. Transcriptional profiles of cardiomyocytes from cKO without cardiac stress and control mice showed almost no differences. cKO mice with induced *Nppa* expression and a significantly higher HW/BW expressed genes involved in cell-cycle regulation. However, PCM-1/Ki-67 double staining showed that the increased expression of cell–cycle genes did not translate into cell-cycle activity of cardiomyocytes and non-cardiomyocytes in cKO mice at P12 and P19.

MATERIALS AND METHODS

Ethical statement

All animal experiments were performed according to the directive 2010/63/EU of the European Parliament. The protocol was approved by the Animal Experimental Commit-tee of the Amsterdam University Medical Center and was carried out according the guide-lines of the Dutch government. Experiments were performed under DAE285.

Animals and tissues

The *Fstl1*$^{KO/fl}$*;Tie2-Cre* mice were generated as previously described [12]. Both, male and female *Fstl1*$^{KO/fl}$*;Tie2-Cre* mice were used for this study. Control mice used for assessment of cell-cycle activity had the genotype: *Fstl*$^{WT/fl}$, *Fstl1*$^{KO/fl}$ or *Fstl1*$^{WT/fl}$*;Tie2Cre*. Control mice used for RNA-seq had the genotype: *Fstl*$^{WT/fl}$. Mice were sacrificed by CO2 and cervical dislocation. Hearts were removed and weighed to assess the heart weight to body weight ratio. For RNA-sequencing experiments hearts were immediately snap frozen in liquid nitrogen. For histological analysis hearts were flushed with PBS and fixed in 4% paraformaldehyde overnight. Subsequently, hearts were transferred to 70% ethanol. Tissues were processed in an automated tissue processor through a graded series of ethanol, embedded in paraffin and sectioned at 7 um in 4-chamber view.

Immunohistochemistry

For immunohistochemistry 1/20 sections were deparaffinised in xylene, rehydrated through a graded series of ethanol and boiled for 5 min in unmasking solution (H3300, Vector) using a pressure cooker. Sections were stained with antibodies against PCM-1 (di-luted 1:400, HPA023370, Atlas Antibodies) and Ki-67 (diluted 1:200, 556003, BD Pharmingen). SYTOX Green was used (diluted 1:40.000, Thermo Fisher) as a nuclear stain. The antibodies were visualized with the secondary antibodies Alexa647 (diluted 1:250, A-31571, Thermo Fisher) and Alexa555 (diluted 1:250, A-31572, Thermo Fisher). Sections were mounted in PBS:Glycerol (*v/v*).

Quantification of cardiomyocyte cell-cycle activity

Pictures were taken with the Leica TCS SPE confocal microscope at 40x magnification. For each heart, ca. 3000 total SYTOX Green positive nuclei and ca. 700 PCM-1+ nuclei were scored for co-staining with Ki-67. Double stained nuclei were manually counted using ImageJ.

In situ hybridization

In situ hybridization was performed as described previously [13]. Briefly, sections were de-paraffinized and rehydrated to MilliQ. Sections were treated with Proteinase K (25530031, Invitrogen) and were pre-hybridized in hybridization buffer (50% formamide, 20X SSC, blocking reagent, 0.5 M EDTA, 10% CHAPS, heparine solution and 10 mg/ml yeast RNA) at 70 °C. Hybridization was performed overnight with dioxigenin (DIG) labeled probe against *Nppa* (forward: 5'gggcagagacagcaaacatc 3', reverse: 5' cacagtggcaatgtgaccaa 3'). Probes were visualized using alkaline phosphatase-conjugated anti-DIG Fab fragments (10932740, Roche) and NBT/BCIP staining reagent (1681451, Roche). Sections were dehydrated and following mounted in Entellan (107961, Merck). Images were acquired with the Leica DM5000 microscope.

Picrosiriusred staining

For Picrosirus red staining sections were deparaffinised in xylene, rehydrated through a graded series of ethanol and stained for 1h in Picrosirus red. Sections were washed in acidified water twice for 1 min and dehydrated with a series of graded ethanol up to xylene. Sections were mounted in Entellan (107961, Merck). Images were acquired with the Leica DM5000 microscope.

Cardiomyocyte nuclei isolation and ploidy analysis

Snap frozen samples of the left ventricle were used for nuclei isolation. Nuclei isolation was performed as described previously [14]. All steps were performed on ice. Samples were homogenized with an Ultra-Turrax homogenizer (IKA) in 3 ml lysis buffer (10mM Tris-HCl (pH8.0), 5 mM CaCl2, 2 mM EDTA, 0.5 mM EGTA, 1 mM DTT, 3 mM MgAc). 3 ml of lysis buffer containing 0.4% triton-X was added and the suspension was dounced 10 times using a large and small pestle (Wheaton). The solution was filtered through a 100 μm and 30 μm filter (Sysmex). The filters were washed with 2 ml lysis buffer containing 0.2% triton-X. The solution was centrifuged at 1000g for 5 min at 4°C. The pellet was re-suspended in 500 μl staining buffer (2.5% BSA in PBS pH8.0 and 0.2% Igepal CA-630). The solution was incubated with rabbit anti-PCM-1 (diluted 1:1000, HPA023370, Atlas Antibodies) and Alexa 647 (diluted 1:500, A-31573, Thermo Fisher) for 1h in total. DAPI was added (0.001 mg/ml, Sigmar-Aldrich, D9542) to stain all nuclei. Sorting of PCM-1 positive nuclei was done on the BD Influx cell sorter (BD Bioscience). Nuclei were sorted into lysis buffer of the RNeasy plus micro kit (74034, Quiagen) for subsequent RNA isolation. Ploidy analysis of

sorted nuclei was performed in Flowjo v10.7.1 based on the intensity of DAPI incorporation into on average 20.000 PCM-1 positive nuclei.

RNA-sequencing

RNA-sequencing from cardiac nuclei was performed as described previously [14]. 500 pg of RNA was used for cDNA preparation with the Ovation RNA-seq V2 kit (7102-08, Tecan). Libraries were prepared with the UltraLow V2 kit (0344NB-08, Tecan) and sequencing was performed on the HiSeq4000 system (Illumnia) with 50 bp single-end reads.

Analysis of RNA-seq data

Reads were mapped to the mm10 build of the mouse transcriptome using STAR [15]. Differential expression between groups was determined using the DESeq2 package based on using the negative binominal distribution [16]. P-values were corrected for multiple testing by using the false discovery rate of Benjamini- Hochberg. Values of $P<0.05$ were considered statistically significant. Principal component analysis was performed with the DESeq2 package, using default parameters.

Using DAVID v6.8 (https://david.ncifcrf.gov/) gene ontology (GO) Term analysis was performed. P-values indicated for GO-terms were corrected for multiple testing using Benjamini-Hochberg correction [17,18].

Statistics

Significant differences in heart to body weight between genotypes were analyzed by the unpaired Student's t test using Graphpad Prism version 9. $P< 0.05$ was considered to be significant.

RESULTS

Fstl1$^{KO/fl}$;Tie2-Cre mice develop cardiac stress soon after birth

We studied *Fstl1$^{KO/fl}$;Tie2-Cre* (cKO) mice to determine the influence of early postnatal cardiac stress on cardiomyocyte gene expression. The phenotype of cKO mice is characterized by the development of malformed mitral valves visible at postnatal day (P) 12 (Figure 1A). The mitral valves become incompetent, causing mitral regurgitation and volume overload of the left ventricle. As a secondary phenotype, the left ventricle of cKO mice di-lates and the heart increases in size [12]. At P12, when compared to control (*Fstl$^{WT/fl}$*, *Fstl1$^{KO/fl}$* or *Fstl1$^{WT/fl}$;Tie2Cre*) mice, cKO mice displayed a significant increase in their heart weight to body weight ratio (HW/BW) due to heart weight increase, as their bodyweight was not decreased (Figure 1B, Supplemental Figure S1). At P20, hearts of cKO were visibly enlarged (Figure 1C).

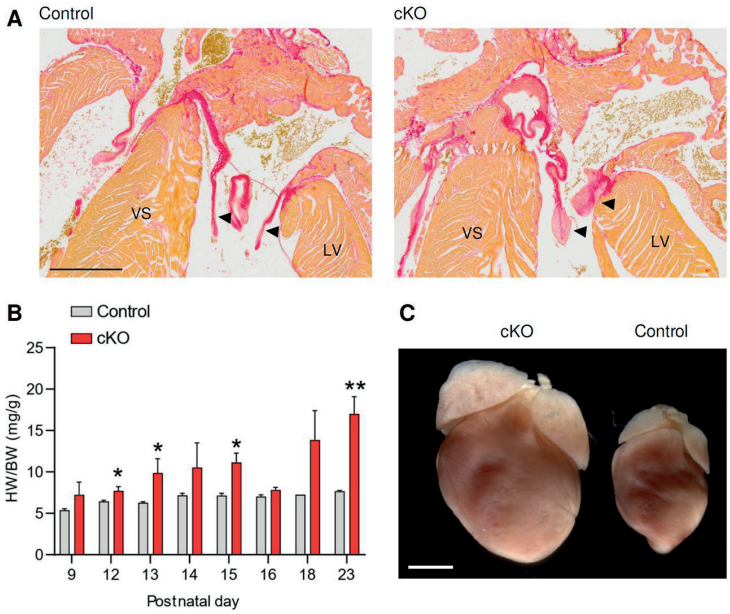

Figure 1. (**A**) Picrosirius red staining shows mitral valves of hearts from control and cKO mice at postnatal day (P) 12. Scale bar indicates 0.5 mm. VS: Ventricular septum, LV: Left ventricle. Arrowheads indicates mitral valves. (**B**) Hearts of cKO mice at P20 are enlarged. Scale bar indicates 2 mm. (**C**) Heart weight to body weight ratio (HW/BW) of control and cKO mice at different postnatal stages. * $p<0.05$, ** $p<0.001$ (unpaired Student's *t* test).

We used *in situ* hybridization to assess the expression pattern of *Nppa* in the hearts of cKO and control mice at P12 and P19 (Fig 2A). *Nppa* encodes the hormone atrial natriuretic factor and is broadly used as a cardiac stress marker, induced in ventricles of postnatal hearts undergoing injury or hypertrophy and heart failure [19]. According to the pattern of *Nppa* expression, cardiac stress was scored (Figure 2B, Supplemental Figure S2, Supplemental Figure S3). A score of *Nppa*=0 indicated that Nppa expression was comparable to that of control mice. *Nppa* expression in these hearts is restricted to the atria and the base of the heart. Mice with a score of *Nppa*=1 showed upregulation of *Nppa* in the left ventricle and at the luminar side of the interventricular septum. HW/BW increased from about 6 mg/g in control hearts and hearts with *Nppa*=0, to more than 8 mg/g in hearts with a score of *Nppa*=1.

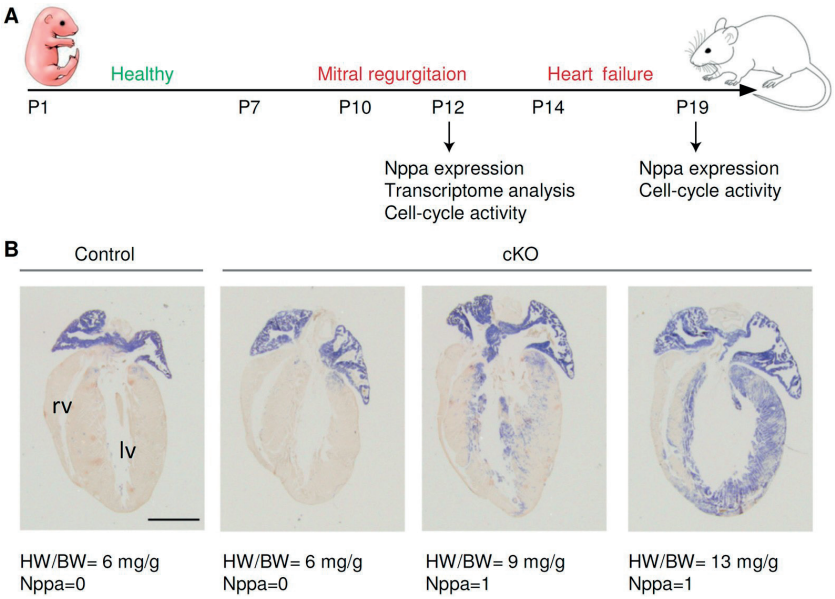

Figure 2. (**A**) Schematic overview of the performed experiments. Starting from postnatal day (P) 10, cKO mice develop mitral regurgitation and heart failure. The transcriptome and *Nppa* expression of cardiomyocytes was analyzed at P12. Cardiomyocyte cell-cycle activity was studied by staining with anti-Ki-67 at P12 and P19. (**B**) *In situ* hybridization shows expression of *Nppa* in control and cKO hearts at P12. Mice that express *Nppa* in the left ventricle have higher heart weight to body weight ratios (HW/BW). According to the expression pattern of *Nppa* hearts received a *Nppa* score of 0 (*Nppa* not expressed in the left ventricle, or only expressed at the base of the in the left ventricle) and *Nppa*=1 (*Nppa* expression in the left ventricle and luminal side of the interventricular septum). Scale bar indicates 1 mm. lv. Left ventricle; rv, right ventricle.

Cardiac stress in pre-weaning mice does not affect cell-cycle activity and ploidy

To investigate the response of postnatal cell-cycle activity to stress, we determined cell-cycle activity of cardiomyocytes of the left ventricle of cKO and control mice by performing immunostaining for Ki-67 (Figure 2A, Figure 3A). We chose time points P12, at which the first mice will have started to develop mitral regurgitation and cardiac stress (Figure 2A) and P19. Ki-67 is expressed throughout all phases of the cell-cycle except G0 [20]. Cardiomyocytes that were in cell-cycle were identified by co-staining for PCM-1, specifically staining the nuclear membrane of cardiomyocytes [8]. In addition, we identified all nuclei that were in cell-cycle, but negative for PCM-1 (mostly endothelial cells and fibroblasts) by co-staining with SYTOX Green. According to their pattern of *Nppa* expression, samples were given an *Nppa* score of 0 or 1 (Figure 3B, Supplemental Figure S2, Supplemental Figure S3). At P12, cell-cycle activity was not significantly altered between cKO (n=4) and control (n=9) samples. The fraction of Ki-67 positive non-cardiomyocyte nuclei varied between 7-16%. At P19 only 1-6% of cells of cKO (n=5) and control (n=3) samples were in cell-cycle. The percentage of cycling cardiomyocytes was much lower with

on average 0.78% of cardiomyocytes being in cell-cycle at P12 (Figure 3B). At P19 we could not identify any cardiomyocyte nuclei that were positively stained for Ki-67 (Figure 3C). Starting around the second postnatal week, cardiomyocytes will undergo polyploidization, increasing their DNA content from diploid (2n) to tetraploid (4n) [8]. We therefore assessed the degree of polyploidization, of cardiomyocyte nuclei isolated at P12 according to their intensity in DAPI signal measured during flow cytometry (Figure 3D, E; Supplemental Figure S4). The percentage of diploid and tetraploid cardiomyocyte nuclei was comparable between control mice (n=3), unstressed cKO mice (n=3) and cKO mice with a stress score of 1 (n=3). At P12 approximately 75% of cardiomyocyte nuclei were diploid and 25% were tetraploid (Figure 3E).

Neonatal cardiac stress induces cell-cycle gene expression

To study the response of neonatal cardiomyocytes to cardiac stress we performed RNA-seq on isolated PCM-1 positive cardiomyocyte nuclei from the left ventricle of P12 mice (Figure 2A, Supplemental Figure S4C). Three control ($Fstl^{WT/ff}$) mice and five cKO mice were selected for RNA-seq analysis (Figure 4A). The HW/BW of control mice ranged from 4.5-7.6 mg/g. The cKO mice were assigned a cardiac stress score dependent on their HW/BW, as we did not investigate the *Nppa* pattern in these hearts. Three cKO mice had a HW/BW of less than 8 mg/g (6.3-7.0 mg/g) and were assumed to be unstressed (score of 0). The remaining three cKO mice displayed a HW/BW > 8mg/g, ranging from 8.1-11.5 mg/g, and were given a cardiac stress score of 1.

Unsupervised principal component (PC) analysis showed grouping of the healthy control samples, as well as samples from the unstressed cKO mice (Figure 4B). The first PC discriminated between the different genotypes of mice whereas the second PC seems to reflect the stress phenotype. Samples originating from cardiomyocytes of ventricles with a stress score of 1 did not cluster together, showing that gene expression in these samples was more heterogeneous. To study the impact of the genotype on the cardiomyocyte transcriptome in mice without cardiac stress we compared the gene expression between control mice and the three unstressed cKO mice. We found that only 6 genes were significantly differentially expressed between these two groups (Figure 4C). The 4 most significantly higher expressed genes by cKO mice (*Kdm5d*, *Uty*, *Eif2s3y*, and *Ddx3y*) (-log10 padj >40) are located on the Y-chromosome, consistent with the sex of the cKO mice (male) versus control mice (female). The lack of further significantly differentially expressed genes indicate that neither the absence of Fstl1 from endocardium-derived cells in unstressed hearts nor the sex difference greatly impact on the transcriptome of cardiomyocytes.

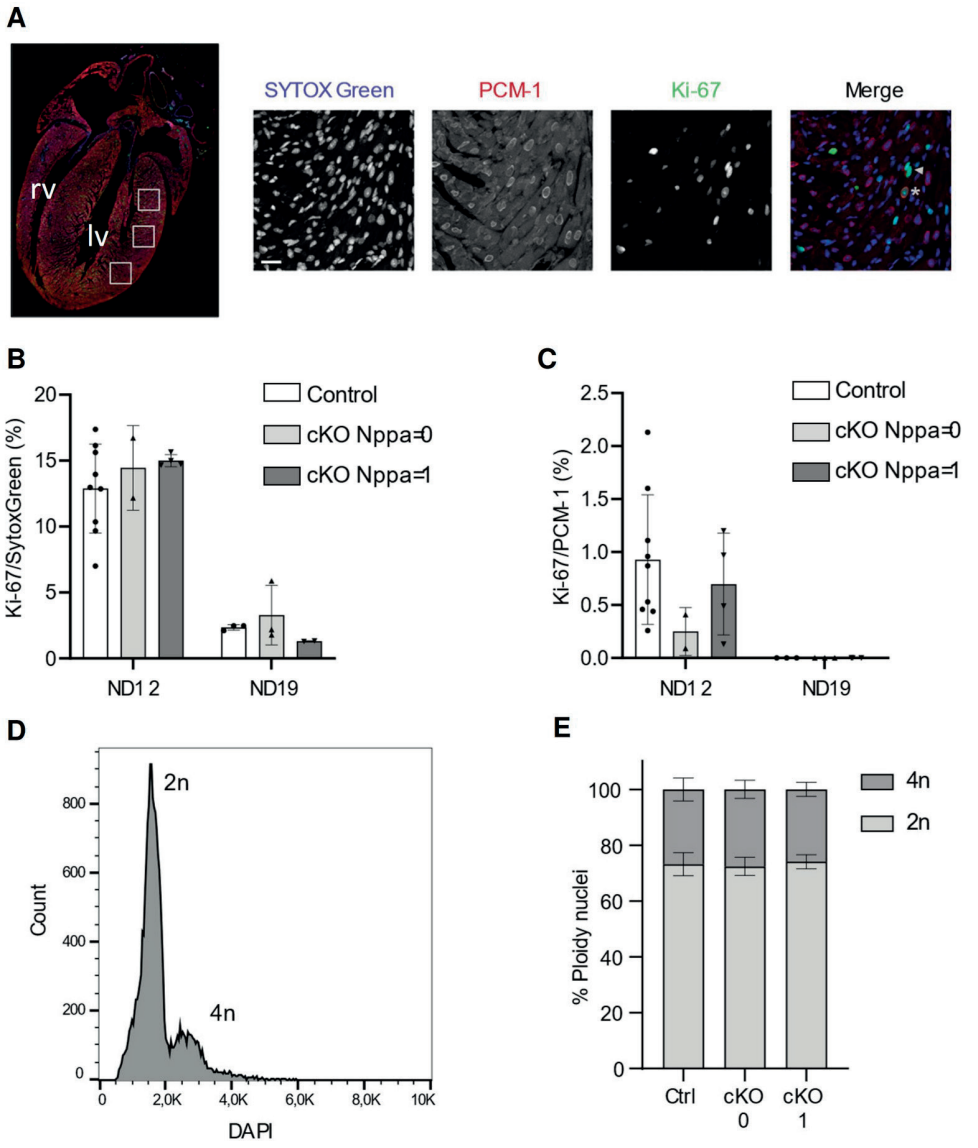

Figure 3. (**A**) Overview of regions within the left ventricle in which cell-cycle activity was determined. (**B**) Immunohistochemical staining of SYTOX Green as nuclear stain, pericentriolar material 1 (PCM-1), and Ki-67 of a part of the left ventricle at postnatal day (P) 12. The arrow-head indicates an example of a Ki-67 positive nucleus. * indicates a Ki-67 and PCM-1 double positive nucleus. Scale bar indicates 10 µm. (**C**) Ratios of Ki-67 positive nuclei (PCM-1 negative) and Ki-67/PCM-1 positive nuclei in left ventricles of P12 and P19 mice (P12: N_{Nppa}=9, $N_{Nppa=0}$= 2, $N_{Nppa=1}$=4, P19: $N_{control}$=3, $N_{Nppa=1}$=4). (**D**) DNA (DAPI intensity) histogram of cardiomyocyte nuclei. **(E)** Percentage of PCM-1 positive nuclei with a diploid (2n) and tetraploid (4n) DNA content of control and cKO mice based on the stress score according their heart weight to bodyweight ratios (HW/BW) ($N_{control}$=3, $N_{cKO\ 0}$=3, $N_{cKO\ 1}$=3). lv. Left ventricle; rv, right ventricle.

To assess the effect of cardiac stress, we compared expression profiles between cKO mice with a stress score of 1 and control samples. 30 genes were significantly higher expressed in the cKO samples (Figure 4D). These include genes involved in the regulation of the cell-cycle and apoptosis such as the proto-oncogene *Myc* as well as *Anln* and *Bcl2*, and genes known to be upregulated in response to cardiac hypertrophy such as *Acta1*. cKO samples showed a significant downregulation of the pro-apoptotic factor *Egln3*. Similar genes were significantly differentially expressed when comparing cKO mice with a stress score of 1 to control mice and unstressed cKO mice (Supplemental Figure S5). cKO mice expressed 16 genes significantly lower than controls and 42 genes significantly higher, including *Myc*, *Anln, Bcl2* and *Cdkn1a*. We performed cluster analysis of the most differentially expressed genes between control samples and cKO samples with a stress score of 1 (Figure 4E). Gene ontology (GO) analysis revealed that genes expressed at lower levels are involved in mitochondrial processes and chaperone activity. Higher expressed genes are involved in transcription regulation, cell organization (cell adhesion, SH3 domain) and transcriptional organization.

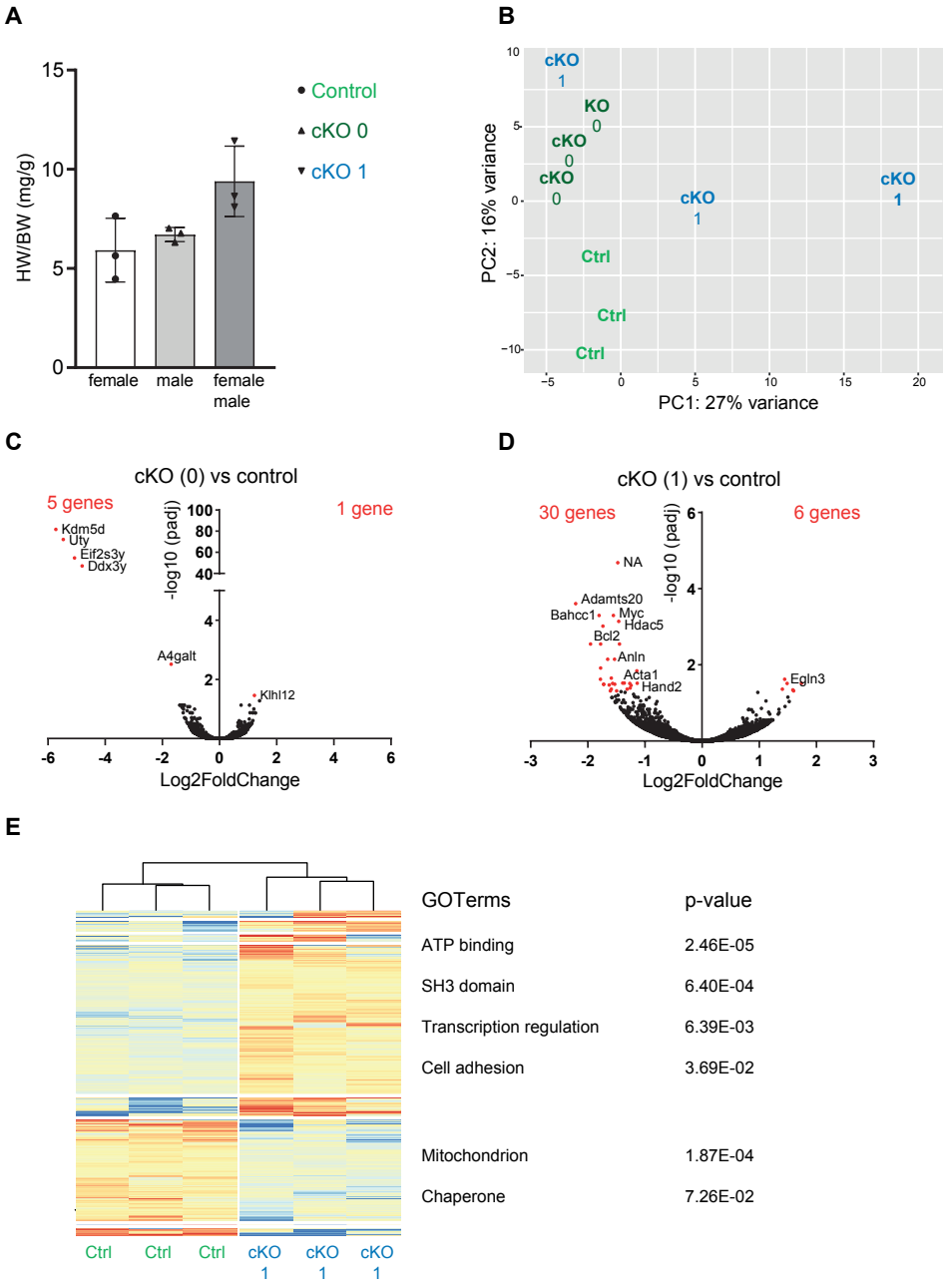

Figure 4. (**A**) Heart weight to body weight ratio (HW/BW) of mice used for sequencing (control: n=3, cKO: n=5). cKO mice with a HW/BW < 8 mg/g received a stress score of 0. cKO mice with HW/BW > 8 mg/g received a stress score of 1. (**B**) Principal component analysis shows clustering of the control samples and samples with a score of 0. Control samples and samples with different HW/BW scores are marked by different colors. (**C**) Volcano plot shows differential gene expression between control and cKO with a score of 0 samples. Significantly differentially expressed genes (p- adjusted for

multiple testing, false discovery rate <0.05) are marked in red. (**D**) Volcano plot shows differential gene expression be-tween samples of control and cKO with a score of 1. Significantly differentially expressed genes (p- adjusted for multiple testing, false discovery rate <0.05) are marked in red. (**E**) Functional annotation heat map based on hierarchical clustering on the most differential expressed genes between control and cKO score= 1 (p-value < 0.05) and GO–terms of groups of differentially expressed genes. The p-value of GO-terms is corrected for multiple testing (Benjamini).

DISCUSSION

In this study, we aimed to assess how cardiac stress of the growing heart after birth influences the transcriptome of cardiomyocytes. This will help us to gain a better understanding of cardiomyocyte adaptation in pediatric patients with CHD. Therefore, we have used a mouse model for early abnormal cardiac loading conditions and consequent pediatric heart failure. cKO mice develop cardiac stress resulting from left ventricular volume overload caused by mitral regurgitation starting at P10, and heart failure from P14 onwards [12]. Thus far, only a limited number of studies describes the cardiac response to volume overload and its impact on the cardiomyocyte transcriptome and cell-cycle activity in neonatal mice [21]. Studies have mainly focused on understanding cardiomyocyte renewal after injury, such as apical resection [22,23] and myocardial infarction [24-27]. Both methods cause massive damage and a high degree of cardiomyocyte apoptosis and infiltration of immune cells [28], a condition that may differ from cardiac stress observed in young patients with abnormal loading due to CHD.

To assess the degree of cardiac stress in cKO mice, we determined the expression pattern of *Nppa*. By using in situ hybridization we observed expression of *Nppa* in the left ventricle and luminal site of the interventricular septum in cKO mice at P12, demonstrating that cardiac tissue in these regions was exposed to cardiac stress [14,19]. In cKO mice expressing *Nppa* in the ventricles, the HW/BW increased to more than 8 mg/g. In the healthy control mice and mice without ventricular *Nppa* expression, the HW/BW was about 6 mg/g. This indicates that *Nppa* can be a useful cardiac disease state marker in neonatal mice.

In order to study the transcriptional response of cardiomyocytes to cardiac stress we performed RNA-seq of PCM-1 positive nuclei. We selected hearts of control and cKO mice according to their HW/BW and gave them a stress score of 0 or 1. Interestingly, the transcriptome between control mice and cKO mice with a stress score of 0 did essentially not differ, apart from the expression of Y-chromosome linked genes highly expressed by the group of male cKO mice. This indicates that the lack of Fstl1 expression in endothelial cells did not affect cardiomyocyte gene expression in mice without cardiac stress. Furthermore, this also suggests that the impact of sex on the transcriptome of cardiomyocytes at this stage is limited. The transcriptional changes between cKO mice that experienced cardiac stress and control mice

revealed higher expression of genes important in the regulation of cell-cycle progression and apoptosis such as *Anln*, *Myc* and *Bcl2*. Anllin (*Anln*) is known to be important for completion of the final part of cytokinesis, and a defect in localization of Anillin at the cleavage furrow was associated with binucleation in cardiomyocytes [29]. The proto-oncogene *Myc* drives proliferation in various tissues and is upregulated in many tumors [30]. However, although Myc was observed to bind its responsive elements in the heart, it fails to initiate proliferation due to the lack of its transcriptional co-factor P-TEFb [31]. Blc2 plays an important role in the regulation of cell-survival, and overexpression of Bcl2 was shown to increase the number of cycling cardiomyocytes [32]. We also observed an upregulation of the cyclin-depenent kinase (CDK) inhibitor gene *Cdkn1a*. The negative cell-cycle regulator *Cdkn1a* becomes highly expressed during postnatal development, preventing cardiomyocyte proliferation [33]. Next to cell-cycle genes, also genes involved in cardiac hypertrophy such as *Acta1* and *Hdac5* were higher expressed in cKO mice. The histone deacytelase 5 (HDAC5) is highly expressed in the heart and regulates transcription of genes by influencing chromatin state and together with HDAC9 it suppresses hypertrophic growth under cardiac stress [34]. Our results are similar to a study of early pressure overload in neonatal rats [10]. Here the authors used bulk RNA-sequencing of right ventricular tissue and found that pressure overload caused an upregulation of genes involved in the hypertrophy response as well as cell-cycle regulation. In contrast to our results, they also identified large sets of differentially expressed genes involved in cardiomyocyte maturation. We did not detect significantly differential expression of genes involved in metabolic maturation such as oxidative phosphorylation or glycolysis. However, when comparing the most differentially expressed genes between control and cKO mice, lower expressed genes were involved in mitochondrial processes. The differences of the models (pressure overload versus volume overload) and use of whole right ventricular tissue RNA-seq [10] versus cardiomyocyte-specific nuclear RNA-seq (this study) may account for the differences observed.

Based on the differential expression of cell-cycle genes, we hypothesized that cardiac stress influenced the timing of cell-cycle arrest in cKO mice after birth. We have used Ki-67 as marker for cell-cycle activity, as Ki-67 is expressed during all phases of the cell-cycle [20]. It should be noted that Ki67 does not allow us to distinguish between proliferation and events of incomplete cell-cycles such as multinucleation or polyploidization [35]. Studies in postnatal mice have identified that the final number of cardiomyocytes is reached 11 days after birth [8]. Accordingly, less than 2% of cardiomyocytes showed Ki-67 positive cardiomyocyte nuclei between postnatal day 14 and 16 [8]. At P12 we could detect only a low percentage of cycling cardiomyocytes (on average only 0.78%) and found no differences between control and cKO mice. At weaning, cardiomyocyte cell-cell cycle activity is completed [8,36], which explains why we could not detect any cycling cardiomyocytes in ventricles of P19 mice. If early postnatal volume overload were to interfere with cardiomyocyte cell-cycle activity, it is likely that the onset of mitral regurgitation in our model occurs too late during postnatal development as mitral valves start being malformed from P10 onward when almost the final

number of cardiomyocytes is reached [8,12]. Accordingly, studies using cardiac injury models have shown that the capacity of the heart to react to injury by proliferation is limited to two-three days after birth [24]. In a mouse model of pressure overload by neonatal transverse aortic constriction (TAC) it could be shown that TAC induced at P7 caused myocardial fibrosis and hypertrophy of cardiomyocytes [21]. However, when TAC was performed at P1 the number of cardiomyocytes positive for the mitosis marker phospho-Histone3 increased significantly when compared to sham mice. In addition, we did also not detect changes in ploidy levels between control and cKO mice. An increase in cardiomyocyte ploidy mainly occurs between the second and third week after birth with a peak at postnatal day 14 [8]. Hence, it is possible that the volume overload could influence cardiomyocyte ploidy levels after P12. Studies in a rat model of neonatal pressure overload demonstrated that polyploidization and multinucleation were increased upon cardiac stress [10].

Our results show that the murine neonatal heart responds to volume overload with only minor changes in the transcriptome of cardiomyocytes. Although the expression of cell-cycle genes was affected in mice experiencing cardiac stress, cardiomyocyte cell-cycle activity was unchanged. It remains challenging to translate this study to the human situation. In CHD patients, abnormal loading conditions usually occur from birth onward and cardiac maturation events such as the transition to cell-cycle arrest may be influenced by gestation time, age at weaning as well as the intrauterine environment [37]. For example, in humans the increase in cardiomyocyte ploidy levels persist till the end of the second decade after birth [9] whereas in mice this process is completed three weeks after birth [8]. However, our study provides insights into the adaption of neonatal cardiomyocytes to cardiac stress and it will be interesting to investigate if similar transcriptional changes occur in pediatric patients with cardiac volume overload and early heart failure.

Funding: This research was funded by Netherlands Heart Foundation COBRA3 to VMC.

Institutional Review Board Statement: All animal experiments were performed according to the directive 2010/63/EU of the European Parliament. The protocol was approved by the Animal Experimental Committee of the Amsterdam University Medical Center and was carried out according the guidelines of the Dutch government. Experiments were performed under DAE285.

Data Availability Statement: The RNA-seq data has been deposited at the Gene Expression Omnibus under the following accession number: GSE165134. An excel file is available of the RNA sequencing data, containing normalized tag counts and differential expression analysis.

Conflicts of Interest: The authors declare no conflict of interest.

REFERENCES

1. Dolk, H. EUROCAT: 25 years of European surveillance of congenital anomalies. Arch Dis Child Fetal Neonatal Ed 2005, 90, F355-358, doi:10.1136/adc.2004.062810.
2. Schwerzmann, M.; Schwitz, F.; Thomet, C.; Kadner, A.; Pfammatter, J.P.; Wustmann, K. Challenges of congenital heart disease in grown-up patients. Swiss Med Wkly 2017, 147, w14495, doi:10.4414/smw.2017.14495.
3. Hinton, R.B.; Ware, S.M. Heart Failure in Pediatric Patients With Congenital Heart Disease. Circ Res 2017, 120, 978-994, doi:10.1161/CIRCRESAHA.116.308996.
4. Moons, P.; Bovijn, L.; Budts, W.; Belmans, A.; Gewillig, M. Temporal Trends in Survival to Adulthood Among Pa-tients Born With Congenital Heart Disease From 1970 to 1992 in Belgium. Circulation 2010, 122, 2264-2272, doi:10.1161/Circulationaha.110.946343.
5. Warnes, C.A. Adult congenital heart disease: the challenges of a lifetime. European Heart Journal 2017, 38, 2041-2047, doi:10.1093/eurheartj/ehw529.
6. Puente, B.N.; Kimura, W.; Muralidhar, S.A.; Moon, J.; Amatruda, J.F.; Phelps, K.L.; Grinsfelder, D.; Rothermel, B.A.; Chen, R.; Garcia, J.A.; et al. The Oxygen-Rich Postnatal Environment Induces Cardiomyocyte Cell-Cycle Arrest through DNA Damage Response. Cell 2014, 157, 565-579, doi:10.1016/j.cell.2014.03.032.
7. Li, F.; Wang, X.; Capasso, J.M.; Gerdes, A.M. Rapid transition of cardiac myocytes from hyperplasia to hypertrophy during postnatal development. J Mol Cell Cardiol 1996, 28, 1737-1746, doi:10.1006/jmcc.1996.0163.
8. Alkass, K.; Panula, J.; Westman, M.; Wu, T.D.; Guerquin-Kern, J.L.; Bergmann, O. No Evidence for Cardiomyocyte Number Expansion in Preadolescent Mice. Cell 2015, 163, 1026-1036, doi:10.1016/j.cell.2015.10.035.
9. Bergmann, O.; Zdunek, S.; Felker, A.; Salehpour, M.; Alkass, K.; Bernard, S.; Sjostrom, S.L.; Szewczykowska, M.; Jackowska, T.; Dos Remedios, C.; et al. Dynamics of Cell Generation and Turnover in the Human Heart. Cell 2015, 161, 1566-1575, doi:10.1016/j.cell.2015.05.026.
10. Ding, X.; Wang, S.; Wang, Y.; Yang, J.; Bao, N.; Liu, J.; Zhang, Z. Neonatal Heart Responds to Pressure Overload With Differential Alterations in Various Cardiomyocyte Maturation Programs That Accommodate Simultaneous Hypertrophy and Hyperplasia. Front Cell Dev Biol 2020, 8, 596960, doi:10.3389/fcell.2020.596960.
11. Kannan, S.; Kwon, C. Regulation of cardiomyocyte maturation during critical perinatal window. J Physiol 2020, 598, 2941-2956, doi:10.1113/JP276754.
12. Prakash, S.; Borreguero, L.J.J.; Sylva, M.; Flores Ruiz, L.; Rezai, F.; Gunst, Q.D.; de la Pompa, J.L.; Ruijter, J.M.; van den Hoff, M.J.B. Deletion of Fstl1 (Follistatin-Like 1) From the Endocardial/Endothelial Lineage Causes Mitral Valve Dis-ease. Arterioscler Thromb Vasc Biol 2017, 116-130, doi:10.1161/ATVBAHA.117.309089.
13. Moorman, A.F.M.; Houweling, A.C.; de Boer, P.A.J.; Christoffels, V.M. Sensitive nonradioactive detection of mRNA in tissue sections: novel application of the whole-mount in situ hybridization protocol. J.Histochem.Cytochem. 2001, 49, 1-8, doi:10.1177/002215540104900101.

14. van Duijvenboden, K.; de Bakker, D.E.M.; Man, J.C.K.; Janssen, R.; Gunthel, M.; Hill, M.C.; Hooijkaas, I.B.; van der Made, I.; van der Kraak, P.H.; Vink, A.; et al. Conserved NPPB+ Border Zone Switches from MEF2 to AP-1 Driven Gene Program. Circulation 2019, doi:10.1161/CIRCULATIONAHA.118.038944.
15. Dobin, A.; Davis, C.A.; Schlesinger, F.; Drenkow, J.; Zaleski, C.; Jha, S.; Batut, P.; Chaisson, M.; Gingeras, T.R. STAR: ultrafast universal RNA-seq aligner. Bioinformatics 2013, 29, 15-21, doi:10.1093/bioinformatics/bts635.
16. Love, M.I.; Huber, W.; Anders, S. Moderated estimation of fold change and dispersion for RNA-seq data with DESeq2. Genome biology 2014, 15, 550, doi:10.1186/s13059-014-0550-8.
17. Huang, d.W.; Sherman, B.T.; Lempicki, R.A. Bioinformatics enrichment tools: paths toward the comprehensive functional analysis of large gene lists. Nucleic Acids Res. 2009, 37, 1-13, doi:gkn923 [pii];10.1093/nar/gkn923 [doi].
18. Huang, d.W.; Sherman, B.T.; Lempicki, R.A. Systematic and integrative analysis of large gene lists using DAVID bioinformatics resources. Nat.Protoc. 2009, 4, 44-57, doi:nprot.2008.211 [pii];10.1038/nprot.2008.211 [doi].
19. Sergeeva, I.A.; Hooijkaas, I.B.; van der Made, I.; Jong, W.M.; Creemers, E.E.; Christoffels, V.M. A transgenic mouse model for the simultaneous monitoring of ANF and BNP gene activity during heart development and disease. Cardiovasc.Res. 2014, 78-86, doi:cvt228 [pii];10.1093/cvr/cvt228 [doi].
20. Scholzen, T.; Gerdes, J. The Ki-67 protein: from the known and the unknown. J Cell Physiol 2000, 182, 311-322, doi:10.1002/(SICI)1097-4652(200003)182:3<311::AID-JCP1>3.0.CO;2-9.
21. Malek Mohammadi, M.; Abouissa, A.; Azizah, I.; Xie, Y.; Cordero, J.; Shirvani, A.; Gigina, A.; Engelhardt, M.; Trogisch, F.A.; Geffers, R.; et al. Induction of cardiomyocyte proliferation and angiogenesis protects neonatal mice from pressure overload-associated maladaptation. JCI Insight 2019, 5, 1-20, doi:10.1172/jci.insight.128336.
22. Porrello, E.R.; Mahmoud, A.I.; Simpson, E.; Hill, J.A.; Richardson, J.A.; Olson, E.N.; Sadek, H.A. Transient regenerative potential of the neonatal mouse heart. Science 2011, 331, 1078-1080, doi:331/6020/1078 [pii];10.1126/science.1200708 [doi].
23. Zebrowski, D.C.; Jensen, C.H.; Becker, R.; Ferrazzi, F.; Baun, C.; Hvidsten, S.; Sheikh, S.P.; Polizzotti, B.D.; Andersen, D.C.; Engel, F.B. Cardiac injury of the newborn mammalian heart accelerates cardiomyocyte terminal differentiation. Scientific reports 2017, 7, 8362, doi:10.1038/s41598-017-08947-2.
24. Lam, N.T.; Sadek, H.A. Neonatal Heart Regeneration: Comprehensive Literature Review. Circulation 2018, 138, 412-423, doi:10.1161/CIRCULATIONAHA.118.033648.
25. Quaife-Ryan, G.A.; Sim, C.B.; Ziemann, M.; Kaspi, A.; Rafehi, H.; Ramialison, M.; El-Osta, A.; Hudson, J.E.; Porrello, E.R. Multicellular Transcriptional Analysis of Mammalian Heart Regeneration. Circulation 2017, 136, 1123-1139, doi:10.1161/CIRCULATIONAHA.117.028252.
26. Porrello, E.R.; Mahmoud, A.I.; Simpson, E.; Johnson, B.A.; Grinsfelder, D.; Canseco, D.; Mammen, P.P.; Rothermel, B.A.; Olson, E.N.; Sadek, H.A. Regulation of neonatal and adult mammalian heart regeneration by the miR-15 family. Proc Natl Acad Sci U S A 2013, 110, 187-192, doi:10.1073/pnas.1208863110.

27. Vivien, C.J.; Hudson, J.E.; Porrello, E.R. Evolution, comparative biology and ontogeny of vertebrate heart regeneration. NPJ Regen Med 2016, 1, 16012, doi:10.1038/npjregenmed.2016.12.
28. Aurora, A.B.; Porrello, E.R.; Tan, W.; Mahmoud, A.I.; Hill, J.A.; Bassel-Duby, R.; Sadek, H.A.; Olson, E.N. Macrophages are required for neonatal heart regeneration. J Clin Invest 2014, 124, 1382-1392, doi:10.1172/JCI72181.
29. Engel, F.B.; Schebesta, M.; Keating, M.T. Anillin localization defect in cardiomyocyte binucleation. J Mol Cell Cardiol 2006, 41, 601-612, doi:10.1016/j.yjmcc.2006.06.012.
30. Sodir, N.M.; Swigart, L.B.; Karnezis, A.N.; Hanahan, D.; Evan, G.I.; Soucek, L. Endogenous Myc maintains the tumor microenvironment. Genes Dev 2011, 25, 907-916, doi:10.1101/gad.2038411.
31. Bywater, M.J.; Burkhart, D.L.; Straube, J.; Sabo, A.; Pendino, V.; Hudson, J.E.; Quaife-Ryan, G.A.; Porrello, E.R.; Rae, J.; Parton, R.G.; et al. Reactivation of Myc transcription in the mouse heart unlocks its proliferative capacity. Nature communications 2020, 11, 1827, doi:10.1038/s41467-020-15552-x.
32. Limana, F.; Urbanek, K.; Chimenti, S.; Quaini, F.; Leri, A.; Kajstura, J.; Nadal-Ginard, B.; Izumo, S.; Anversa, P. bcl-2 overexpression promotes myocyte proliferation. Proc Natl Acad Sci U S A 2002, 99, 6257-6262, doi:10.1073/pnas.092672899.
33. Foglia, M.J.; Poss, K.D. Building and re-building the heart by cardiomyocyte proliferation. Development 2016, 143, 729-740, doi:10.1242/dev.132910.
34. Chang, S.; McKinsey, T.A.; Zhang, C.L.; Richardson, J.A.; Hill, J.A.; Olson, E.N. Histone deacetylases 5 and 9 govern responsiveness of the heart to a subset of stress signals and play redundant roles in heart development. Mol Cell Biol 2004, 24, 8467-8476, doi:10.1128/MCB.24.19.8467-8476.2004.
35. Leone, M.; Magadum, A.; Engel, F.B. Cardiomyocyte proliferation in cardiac development and regeneration: a guide to methodologies and interpretations. Am J Physiol Heart Circ Physiol 2015, 309, H1237-1250, doi:10.1152/ajpheart.00559.2015.
36. Soonpaa, M.H.; Zebrowski, D.C.; Platt, C.; Rosenzweig, A.; Engel, F.B.; Field, L.J. Cardiomyocyte Cell-Cycle Activity during Preadolescence. Cell 2015, 163, 781-782, doi:10.1016/j.cell.2015.10.037.
37. Velayutham, N.; Agnew, E.J.; Yutzey, K.E. Postnatal Cardiac Development and Regenerative Potential in Large Mammals. Pediatr Cardiol 2019, 40, 1345-1358, doi:10.1007/s00246-019-02163-7.

SUPPLEMENTAL MATERIAL

Supplemental Figure 1

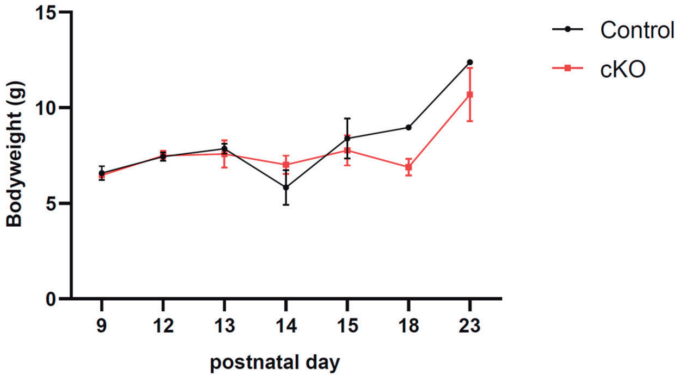

Figure S1. Bodyweight (g) of control and cKO mice during postnatal development.

Supplemental Figure 2

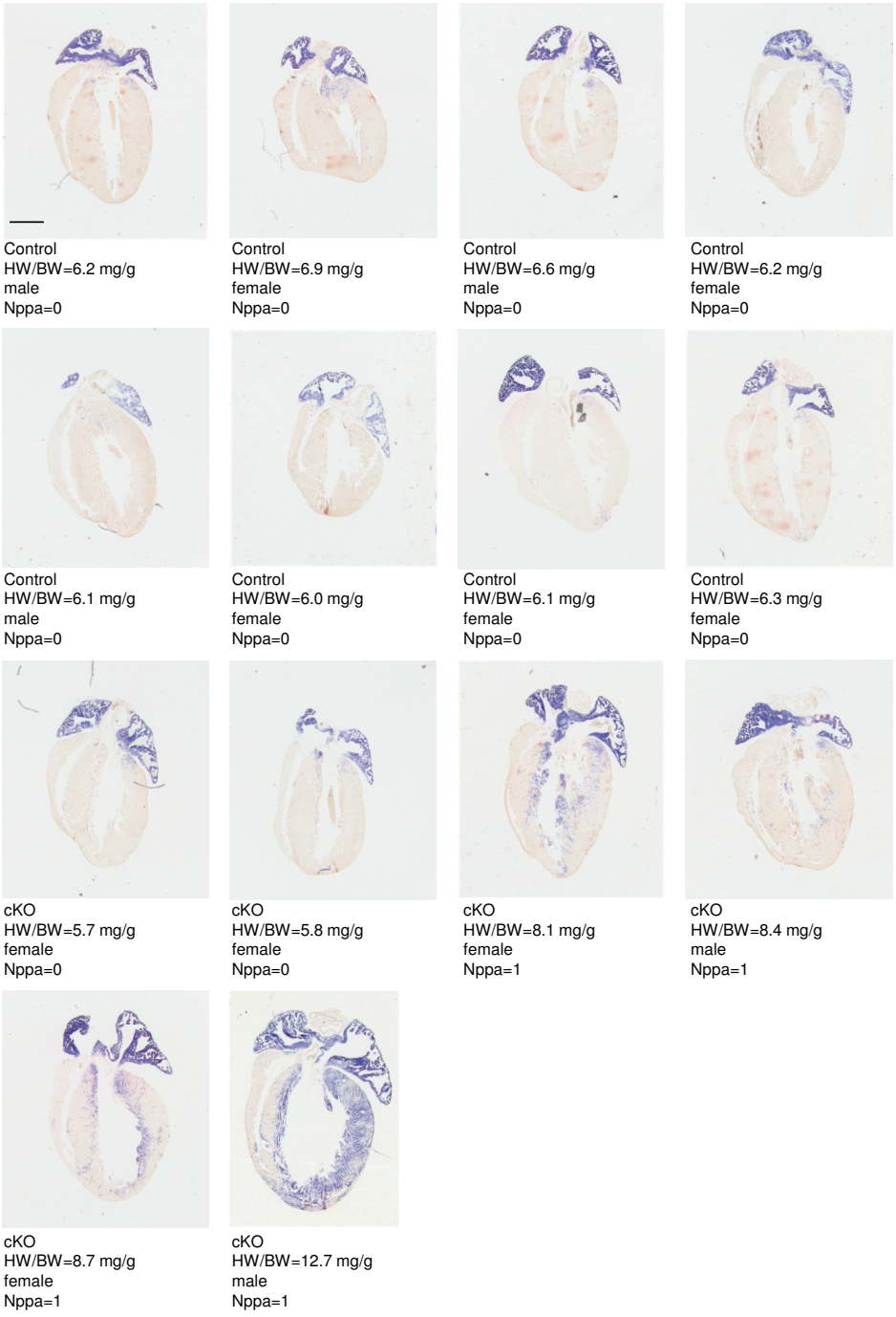

Figure S2. *Nppa* expression in control and cKO mice at postnatal day (P)12.

Supplemental Figure 3

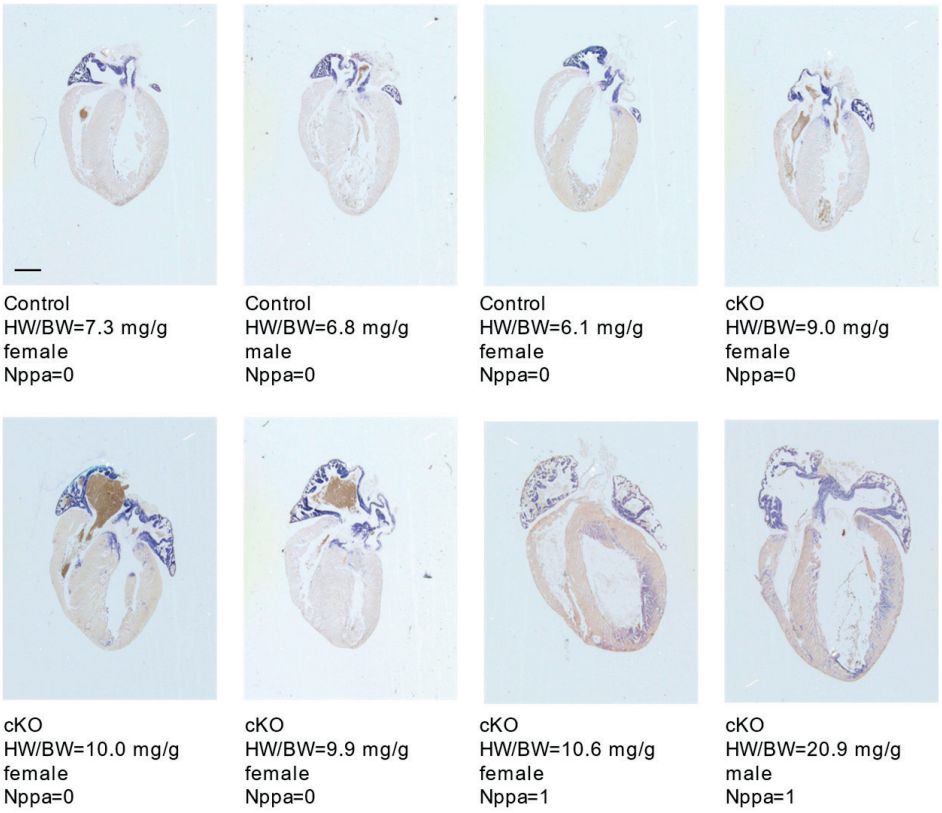

Figure S3. *Nppa* expression in control and cKO mice at postnatal day (P)19.

Supplemental Figure 4

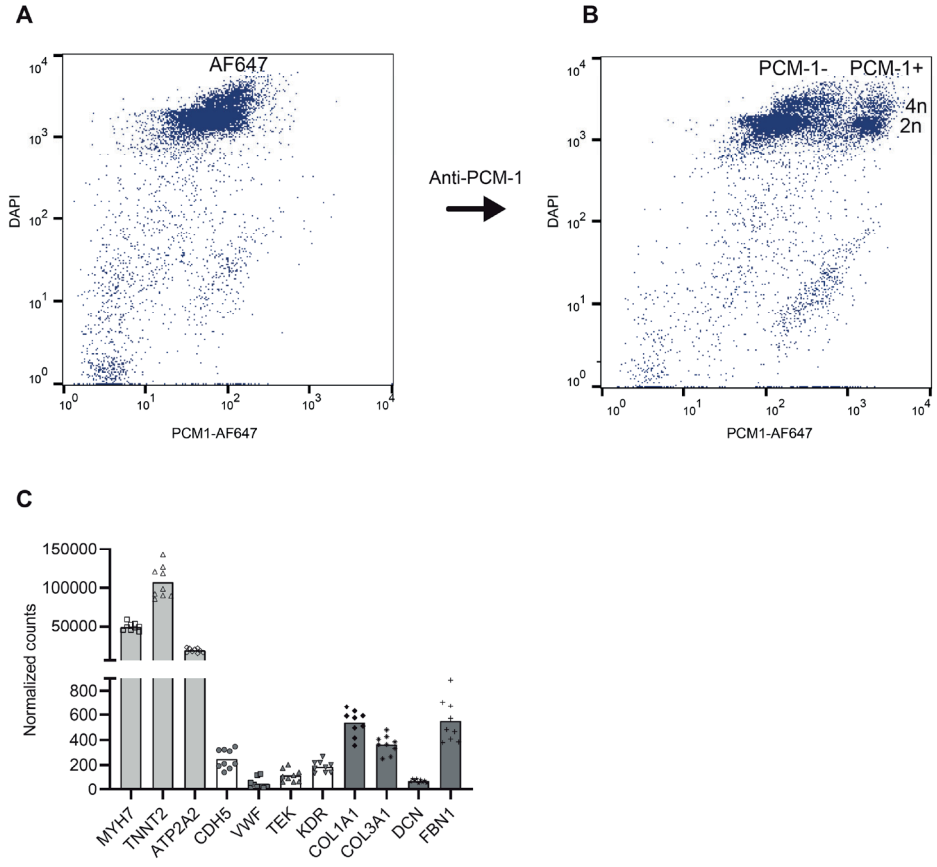

Figure S4. FACS purification of cardiomyocyte nuclei.

Supplemental Figure 5

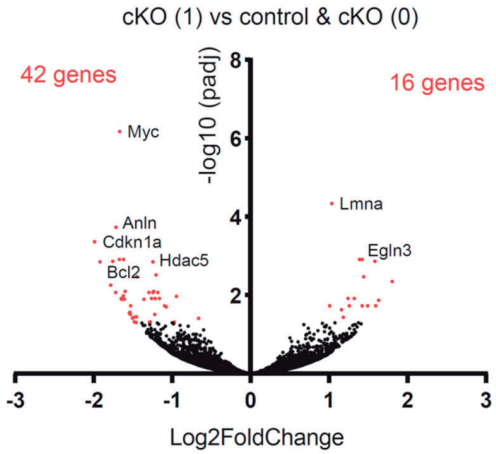

Figure S5. Vulcano plot shows differential gene expression between control and cKO with a score of 1 samples and control and cKO samples with a score of 0.



Chapter 3

Neuregulin-1 enhances cell-cycle activity, delays cardiac fibrosis, and improves cardiac performance in rat pups with right ventricular pressure load

Guido P. L. Bossers, Marie Günthel, Diederik E. van der Feen, Quint A. J. Hagdorn, Anne-Marie C. Koop, Karel van Duijvenboden, Phil Barnett, Marinus A. J. Borgdorff, Vincent M. Christoffels, Herman H. W. Sillje, Rolf M. F. Berger, and Beatrijs Bartelds

The Journal of Thoracic and Cardiovascular Surgery. Vol. 164, Issue 6, December 2022: E493-E510

ABSTRACT

Objectives: Right ventricular (RV) failure is a leading cause of death in patients with congenital heart disease. RV failure is kept at bay during childhood. Limited proliferation of cardiomyocytes is present in the postnatal heart. We propose that cardiomyocyte proliferation improves RV adaptation to pressure load (PL). We studied adaptation in response to increased RV PL and the role of increased cardiomyocyte cell cycle activity (CCA) in rat pups growing into adulthood.

Methods: We induced RV PL at day of weaning in rats (3 weeks; 30-40 g) by pulmonary artery banding and followed rats into adulthood (300 g). We performed histological analyses and RNA sequencing analysis. To study the effects of increased cardiomyocyte cell cycle activity, we administered neuregulin-1 (NRG1), a growth factor involved in cardiac development.

Results: PL induced an increase in CCA, with subsequent decline of CCA (sham/PL at 4 weeks: 0.14%/0.83%; P = .04 and 8 weeks: 0.00%/0.00%; P = .484) and cardiac function (cardiac index: control/PL 4 weeks: 4.41/3.29; P = .468 and 8 weeks: 3.57/1.44; P = .024). RNA sequencing analysis revealed delayed maturation and increased CCA pathways. NRG1 stimulated CCA (PL vehicle/NRG1 at 2 weeks: 0.62%/2.28%; P = .003), improved cardiac function (cardiac index control vs vehicle/NRG1 at 2 weeks: 4.21 vs 3.07/4.17; P = .009/.705) and postponed fibrosis (control vs vehicle/NRG1 at 4 weeks: 1.66 vs 4.82%/2.97%; P = .009/.078) in RV PL rats during childhood.

Conclusions: RV PL during growth induces a transient CCA increase. Further CCA stimulation improves cardiac function and delays fibrosis. This proof-of-concept study shows that stimulation of CCA can improve RV adaptation to PL in the post- natal developing heart and might provide a new approach to preserve RV function in patients with congenital heart disease.

Central Message: Neuregulin-1 stimulated cell cycle activity, postponed fibrosis, and improved cardiac function and outcome during childhood, suggesting a new approach to preserve the RV in patients with congenital heart disease.

Perspective: Right ventricular (RV) function and failure are key determinants of morbidity and mortality in congenital heart disease and pulmonary hypertension. No treatment options are available for these patients. Interestingly, RV failure due to chronic pressure overload commences mainly after adulthood is reached. Putatively, processes of adaptation may prevent the RV from failing during childhood.

Keywords: right ventricle, proliferation, heart failure, pressure load, Neuregulin-1

INTRODUCTION

Right ventricular (RV) dysfunction is a leading cause of heart failure and death in patients with congenital heart disease (CHD), heart failure with preserved ejection fraction, and pulmonary arterial hypertension.[1] Increased pressure load (PL) is an important determinant in the development of RV failure in CHD (eg, pulmonary hyper- tension, hypoplastic left heart syndrome).[2] The detection and treatment of RV failure recently has been issued as one of the 3 major research focuses by the National Heart, Lung, and Blood Institute and the Adult Congenital Heart Association working group.[3]

The adaptation of a normal morphological RV to chronic PL has been studied extensively in adult patients with pulmonary hypertension and experimental models mimicking PL induced mainly in adult animals.[4] These studies have shown that the development of RV failure is characterized by progressive diastolic dysfunction, RV- pulmonary arterial uncoupling, myocardial fibrosis, and metabolic dysregulation.[5,6] Unfortunately, treatment options for the failing right ventricle have proven to be disappointing.[4,7]

In patients with severe CHD, RV failure typically develops in the second or third decade.[8] It is yet unknown what protective mechanisms help children with CHD to sustain increased PL throughout growth and development.

The cardiomyocyte has a high proliferative potential before birth, which, in the period (mouse: days; human: years) after birth virtually disappears.[9,10] It is yet unknown how this residual proliferative potential after birth affects the adaptive response to CHD-associated RV PL. Various pathways have been identified that can stimulate cardio- myocyte cell cycle activity (CCA). Exploration of these pathways might help identify new therapeutic strategies.11 Neuregulin-1 (NRG1) is a growth factor that acts through the v-erb-b2 erythroblastic leukemia viral oncogene homolog signaling pathway. NRG1-mediated signaling is involved in cardiac development and can increase CCA.[12] It is unknown whether stimulation of CCA in the postnatal growing and developing myocardium under stress is cardioprotective and might be able to postpone the development of heart failure.

The aim of the present study was to assess the adaptation to PL of the right ventricle in the postnatal devel- oping heart growth and development and to test the effects of therapeutic stimulation with NRG1 on cardiac function. For that purpose, we have developed a model of chronic PL of the right ventricle in rat pups, starting at the age of weaning toward young adulthood (body weight from 30 g to approximately 300 g), and studied RV hemodynamic adaptation and remodeling. Young adulthood in humans correlates with 9-12 weeks after birth in rats.[13] In this model, we tested *in vivo* the effects of NRG1 administration on CCA and cardiac performance.

METHODS

Animal care and experiments were conducted according to the Dutch Animal Experimental Act and conform to the Guide for the Care and Use of Laboratory Animals published by the US National Institutes of Health (publication 85-23, revised 1996). The Animal Experiments Committee of the University of Groningen in the Netherlands approved the experimental protocol (permit number: AVD10500201515134; date of approval: July 29, 2015).

Animal Model

Figure 1A shows the schematic outline of the experiment. Wistar rat pups (male; Charles River) were randomized after weaning (third week of life; 30-40 g) into 2 groups: sham-operated rats (control, n = 13) and rats with a pulmonary artery banding (PL, n = 22). One animal died during PL surgery and was excluded from the study. Pulmonary artery banding was applied with the animals under general anesthesia with ventilation (isoflurane/air mixture, 5% induction; 2%-3% maintenance; analgesia with carprofen 5 mg/kg subcutaneous) via a left thoracotomy as described previously.[5] After a 22-gauge needle was placed in line with the pulmonary artery, a suture around the pulmonary artery and the 22-gauge needle was tightened to standardize the degree of stenosis. A video of the surgical procedure is included as Video1. Control rats underwent the same surgical procedure, without application of the pulmonary artery banding. Clinical signs (e.g. dyspnea, weight loss, ruffled fur), were monitored in all animals. One PL rat showed severe unexpected cachexia immediately post-surgery and was therefore excluded from the study. Rats were humanely killed at 4 weeks (control: n = 5; PL: n = 7) or 8 weeks (control: n = 8; PL: n = 10) after surgery (Figure 1A). Four rats were humanely killed between 3 and 8 weeks after application of PL because of clinical RV failure (humane end point) and could not be analyzed.

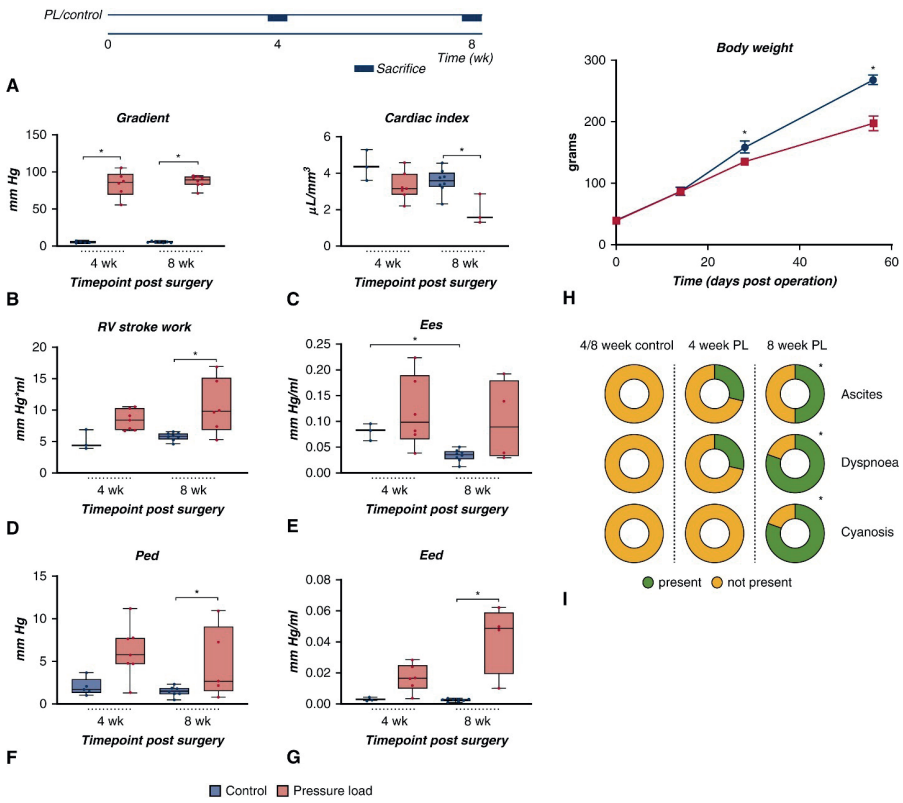

Figure 1. A) Schematic overview of experimental design. Surgery in both groups consisted of pulmonary artery banding (PL) or sham surgery (control). Rats were humanely killed 4 or 8 weeks after surgery. **B**) PL gradient was increased in all groups compared with control. *P* values: 4/8 week control versus PL:<.001/<.001; control/PL 4 weeks versus 8 weeks: 1.000/.918. **C**) Decreased cardiac index in PL. *P* values: 4/8 week control versus PL: .468/.032; control/PL 4 weeks versus 8 weeks: .776/.096. **D**) Right ventricle (*RV*)-PL increased RV stroke work after 8 weeks, measured according to echocardiographic stroke volume and pressure measurements with an RV pressure-volume catheter. *P* values: 4/8 week control versus PL: .268/.045; control/PL 4 at weeks versus 8 weeks: 1.000/1.000. **E**) Large variation in RV contractility measured with end-systolic elastance in the PL rats. *P* values: 4/8 weeks control versus PL: 1.000/.340; control/PL at 4 weeks versus 8 weeks: .048/.905. **F**) **G**) Indices of diastolic dysfunction progressively worsen in PL rats. *P* values: 4/8 weeks control versus PL: .120/.004; control/PL at 4 weeks versus 8 weeks: 1.000/.628. *P* values: 4/8 weeks control versus PL: .192/.048; control/PL 4 weeks versus 8 weeks: .921/.096. H, RV-PL impaired body weight growth, starting at 4 weeks. *P* values: 2/4/8 weeks control versus PL: 1.000/.003/<.001. I, Progressive increase in signs of clinical RV failure over time in PL rats. Control rats did not show signs of RV failure. The *circles* indicate the total number of rats with PL surgery. Ascites: $P = .045$, dyspnoea: $P = .038$, pleural effusion: $P = .001$. In some groups, numbers are lower than mentioned in methods because of failed analyses. *Red bars* represent PL rats, *blue bars* represent control rats. The *lower and upper borders of the box* are the lower and upper quartiles. The *middle horizontal line* represents the median. The *whiskers* are the minimum and maximum values. *Dots* in the box-and-whisker dot plots represent individual measurements. Statistical analysis for B-H: Kruskal–Wallis with correction for multiple testing; I: c^2 test. *PL*, Pressure load; *Ees*, end-systolic elastance; *Ped*, end diastolic pressure; *Eed*, end-diastolic elastance. *P <.05.

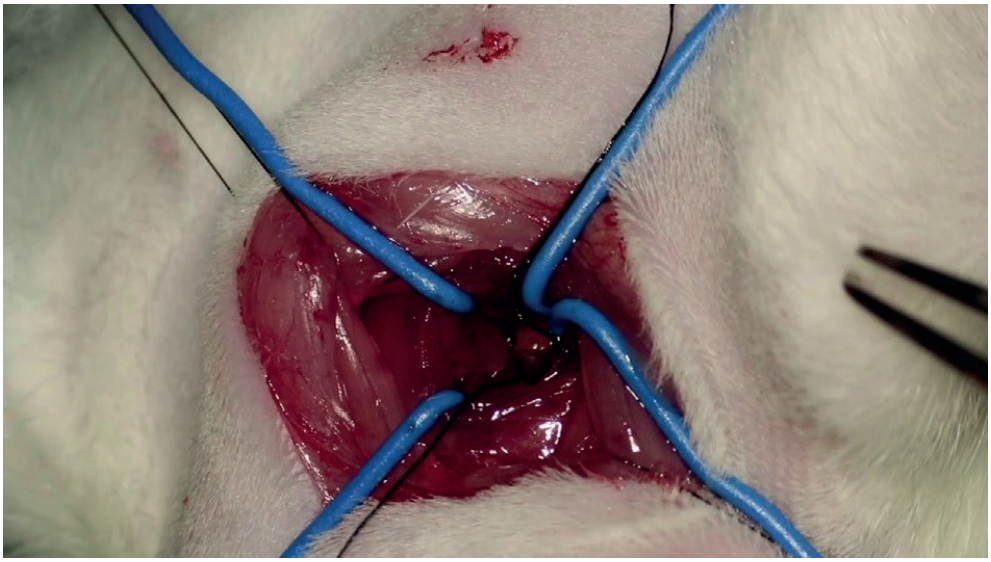

Video 1. Presentation of the surgical procedure of pulmonary artery banding in rats. Because of ethical restrictions, the experimental animal in this video is an adult rat. The procedure is identical in 3-week-old rat pups. The size of the needle in the video is 19G (22G in rat pups). Video available at: https://www.jtcvs.org/article/S0022-5223(21)01520-8/ fulltext.

NRG1 Administration

Figure 2A shows the schematic outline of the experiment. Wistar rat pups underwent weaning and randomization as described previously (PL: n = 68; control: n = 29). Subsequently, both groups were randomized into treatment (NRG1) and placebo (vehicle). Ten pups died because of the PL surgery and were therefore excluded (total surgery mortality PL rats: 12.9%). rhNRG1 (Peprotech; 60 mg/kg/d, dissolved in 0.1% Bovine Serum Albumin/Milli-Q water) or vehicle (0.1% Bovine Serum Albumin/Milli-W water) was administered daily to rats through intraperitoneal injection from time (t) = 3 until t = 14 days. Animals were randomized into different groups depending on planned time of humane killing (planned humane killing at time point 2 weeks [vehicle: control, n = 6; PL, n = 9; NRG1: control, n = 5; PL, n = 10], 4 weeks [vehicle: control, n = 6; PL, n = 7; NRG1: PL, n = 10], or 8 weeks after surgery [vehicle: control n = 6, PL n = 11. NRG1: control n = 6, PL n = 11]). Clinical signs (e.g. dyspnea, weight loss, ruffled fur), were monitored in all animals.

Echocardiography and Pressure-Volume Measurements

We assessed PL according to maximum flow velocity over the pulmonary artery banding with echocardiography in all animals at 2, 4, and 8 weeks after surgery and assessed cardiac function before humane killing (Vivid Dimension 7; 10S-transducer [GE Healthcare]) as described previously.[5] Rats were anesthetized with isoflurane (induction 5%; 2%-3% maintenance) and warmed at 37 C.

Maximum flow velocity over the pulmonary artery banding, left ventricular cardiac output, left ventricular stroke volume, end-systolic eccentricity index, and tricuspid annular plane systolic excursion were derived using the parasternal long axis, short axis (at aortic and midpapillary level), apical 4- chamber, and 5-chamber view. Cardiac output was calculated as follows: (aortic diameter)^2 x 3.14 x velocity-time integral x heart rate. Beat-to- beat variation was accounted for by averaging measurements from 6 to 12 consecutive beats. Cardiac index was calculated using tibia length as described previously.[14]

Before humane killing, open chest pressure-volume measurements were performed in anesthetized and intubated rats using a pressure-admittance catheter (1.9-French, 6-mm spacing; Transonic), as described previously.[5] After bilateral thoracotomy and pericardiotomy, the catheter was introduced in the apex of the right ventricle toward the outflow tract. The pressure signal was recorded in Chartlab 5 with an ADVantage PV system (ADV500) processor (Transonic).

Analysis of the obtained signals was performed using custom-made software (Circlab 2012, P. Steendijk) to derive RV end-diastolic pressure, RV peak pressure, and RV maximum and minimum delta pressure and delta time. Stroke volume measured using echocardiography was used to calibrate the conductance-derived stroke volume. Steady-state pressure-volume loops were used for the calculation of all parameters. End-systolic and end-diastolic elastance were determined using the single-beat method as described previously.[5]

Organ Weights and Histological Analyses

After catheterization, the rats were euthanized by blood withdrawal. After flushing the heart with NaCL 0.9%, the heart and organs were removed. The right ventricle, ventricular septum, left ventricle, and both atria were dissected and weighed. After fixation of the right ventricle (formalin), cardiomyocyte cross-sectional area (wheat germ agglutinin), fibrosis (Masson Trichrome), and capillary density (Lectin) were assessed in the RV free wall as described previously.[5]

Immunohistochemistry

To analyze CCA, 4-mm paraffin-embedded RV free wall sections were stained using the following primary antibodies: Ki-67 (1:200, BD Pharmingen) and histone-3-phosphate ([H3P] 1:100; Sigma). To analyze cardiomyocyte-specific CCA, pericentriolar material 1 ([PCM-1] 1:400, Atlas Antibodies) in combination with Ki-76 was used. For PCM-1 counting, Alexa 647 and Alexa 555 were used (1:250) as secondary antibodies.

Pictures were taken with a Leica DM600 microscope, 10x magnification. Pictures of H3P staining were taken with a Hamamatsu scanner, 20x magnification. Nuclei were counted with ImageJ. Per sample, 1500 nuclei were counted.

Gene Expression

Changes in gene expression in the RV myocardium were analyzed using whole transcriptome expression profiling (RNAseq) as described in Appendix E1. Raw read files are submitted to the National Center for Biotechnology Information Gene Expression Omnibus online database (Gene Expression Omnibus submission, GSE143745; National Center for Biotechnology Information tracking system 20583856).

Quantitative real-time polymerase chain reaction was performed as previously described.[5] The primer sequences used are included in Table E1. Expression data were corrected for the expression of the reference gene, glyceraldehyde 3-phosphate dehydrogenase.

Statistical Analyses

The Kruskal–Wallis test was used to analyze differences between more than 2 independent groups. In case of significance, Mann–Whitney *U*, corrected for multiple testing, was used with Bonferroni post hoc analysis to evaluate the specific differences between groups (SPSS statistics, version 23, 2015). The c^2 test was used for comparisons of categorical variables between independent groups. The assumption of expected cell counts was validated of observing at least 5 counts per cell. NRG1 administration did not affect any of the parameters assessed in rats without PL (tested with Mann–Whitney *U*). Therefore, for statistical analyses, data for control animals with and without NRG1 treatment were pooled at each time point and presented as 1 group. Mortality was defined as unplanned humane killing when the humane end point was reached or death.

RESULTS

Characterization

The PL of the right ventricle in the banded pups increased progressively over time as shown by increased Doppler maximal flow velocity over the pulmonary trunk compared with control rats (Figure 1B). PL rats had reduced cardiac index at 8 weeks after banding compared with control rats (Figure 1C). PL led to increased RV stroke work at 8 weeks (Figure 1D). RV end-systolic elastance showed a large variation and as a group. No increase in end-systolic elastance was shown at 4 or 8 weeks of PL (Figure 1E). PL worsened RV end-diastolic elastance and progressively increased RV diastolic pressure (Figure 1F and G). PL decreased tricuspid annular plane systolic excursion and increased eccentricity index, both echocardiographic parameters of RV dysfunction (Table 1).

Four weeks after banding, weight gain was lower compared with control rats (Figure 1H). At 8 weeks, PL rats showed clinical signs of RV dysfunction (i.e. dyspnoea, ruffled fur, ascites, and pleural effusion; Figure 1I).

Table 1. Characteristics of the experimental rat groups

	4 Weeks			8 Weeks		
	Control	PL	P 1	Control	PL	P 2/3/4
Number of rats	**5**	**7**		**8**	**9**	
Weight, g						
LV þ IVS	0.35 (0.04)	0.55 (0.05)	.418	0.58 (0.08)	0.59 (0.15)	1.000/1.000/.608
RV/(LV þ IVS)	0.35 (0.04)	0.55 (0.06)*	.012	0.30 (0.06)	0.68 (0.21)*	<.001/1.000/1.000
RA	0.04 (0.04)	0.16 (0.5)*	.012	0.11 (0.14)	0.17 (0.12)*	.260/.508/1.000
Echocardiographic parameters						
Eccentricity index diastolic	0.9 (0.4)	1.6 (0.3)	.068	0.9 (0.3)	1.6 (0.3)	.120/.497/1.000
TAPSE, mm	2.9 (0.7)	2.2 (0.5)	.468	3.0 (0.6)	2.9 (1.2)	.464/.776/1.000
Cardiac output, mL/min	108.8 (5,6)	66.0 (13,8)	.068	110.6 (23.2)	68.2 (29.4)*	<.001/.096/.805
Histology						
RV Ki-67 positive nuclei, %	5.78 (1,54)	8.33 (1,56)	.09	2.54 (0.45)t	4.40 (1.98) t	.004/.012/.036
RV histone-3-phosphate nuclei, %	0.14 (0.09)	0.20 (0.05)	.639	0.19 (0.06)	0.22 (0.48)	1.000/.684/1.000
Capillary-myocyte ratio	0.81 (0.20)	0.95 (0.18)*	.040	0.69 (0.20)	1.16 (0.30)*	<.001/1.000/.204

Data are presented as mean (SEM), except where otherwise noted. *PL*, Pressure load; *P1*, *P* value control versus pressure load at 4 weeks; *P2*, value control versus pressure load at 8 weeks; *P3*, *P* value control at 4 weeks versus control at 8 weeks; *P4*, *P* value pressure load at 4 weeks versus pressure load at 8 weeks; *LV*, left ventricle; *IVS*, interventricular septum; *RV*, right ventricle; *RA*, right atrium; *TAPSE*, tricuspid annular plane systolic excursion. *P <.05 control versus PL at same time point. t P <.05 same intervention at different time points.

PL induced RV hypertrophy, measured as RV weight and cardiomyocyte cross-sectional area (Table 1, Figure 3A). PL increased RV fibrosis at 8 weeks (Figure 3B). PL increased capillary:myocyte ratio at 4 and 8 weeks (Table 1).

Immunohistochemistry revealed decreasing cell cycle activity from 4 to 8 weeks in RV tissue of control and PL rats, on the basis of the assessment of Ki-67 staining, which is expressed during all phases of the cell cycle, except the G0 phase (resting phase).[15] PL tended to increase the number of cells positive for Ki-67 staining (Table 1). To assess whether this cell cycle activity was also present in cardio- myocytes, we used double-staining with PCM-1, a cardiomyocyte-specific nuclear marker.[16] PL increased the amount of Ki-67/PCM-1 double-positive cells in the right ventricle of PL rats compared with control rats after 4 weeks. This increase declined significantly over time (Figure 3C). To further assess cell cycle activity in cardiac tissue we stained for H3P (Table 1), but no important differences were observed for PL and control rats. Markers of cardiac stress, natriuretic pro-peptide A/B, and myosin heavy chain isoform switch, increased at 4 and 8 weeks of PL. Similarly, heme oxygenase 1, a marker of oxidative stress and metallopeptidase inhibitor 1, a metallopeptidase inhibitor and pro-fibrotic marker, were increased (Figure 3D).

To dissect pathways associated with maturation and adaptation to PL, we performed RNA sequencing analyses using RV tissue 4 and 8 weeks after surgery. Principle component analysis showed differential clustering around control versus PL (Figure E1, *A*). Within the groups PL and control, principal component analysis showed clustering around time after surgery (4 vs 8 weeks). At a cutoff of >1 log2-fold change, 5 clusters of genes were differentially expressed. These clusters involved a wide range of processes (Figure 4A). Within the control and PL groups, we found maturational differences. Gene ontology analysis indicated that genes with higher expression in control rats at 4 weeks versus 8 weeks were mainly related to cell cycle, whereas genes with higher expression in control rats after 8 weeks versus 4 weeks were mainly related to metabolism (mitochondrion, fatty acid metabolism, peroxisome, tricarboxylic acid cycle; Figure 4B).

Within the group of PL rats, we identified maturational differences between 4 and 8 weeks (i.e., changes in transcriptional profiles related to change from "fetal program" toward "mature cardiomyocytes.") To assess the effect of PL on this development from fetal to adult programs, we specifically selected genes that were differentially expressed in PL rats versus control rats at 4 weeks and 8 weeks (Figure E1, *B*). The genes with increased expression after 4 weeks of PL are involved in cell division in mitosis, similar to the differences at 4 and 8 weeks in control rats. The genes that were increased only at 8 weeks of PL are mostly involved in immunity.

PL also induced a time-independent up-regulation of many known candidates affected in hypertrophy. A comparison of PL rats with control rats revealed up-regulated genes belonging to the processes of, among others, stress response and cell division, whereas down-regulated genes were those belonging to processes of metabolism. These changes were largely similar after 4 and 8 weeks of PL. Several changes in gene expression were confirmed with quantitative polymerase chain reaction (natriuretic pro-peptide B, myosin heavy chain 7 [*Myh7*], myosin heavy chain 6 [*Myh6*]; Figure 4C).

Treatment With NRG1

The results of the study show no differences for NRG1 control and vehicle control groups at time points 2 and 8 weeks. In light of reduction of experimental animals, we therefore made the assumption that no differences would be found among the control groups at time point 4 weeks. The applied pulmonary banding induced equal RV PL in vehicle- and NRG1-treated rats, measured according to increased Doppler maximal flow velocity (Figures 2B, and E2). NRG1 treatment after surgery restored cardiac index in PL rats, to values comparable with rats without PL (Figure 2C). NRG1 treatment also increased RV stroke work in PL rats, but did not affect RV end-systolic elastance (Figure 2D and E). We believe NRG1 treatment tends to improve diastolic function because end-diastolic elastance was lower at 2 weeks, although the statistical analysis used did not support this finding (Figure 2G). This effect weaned at 4 and 8 weeks. NRG1 did not affect other echocardiographic indices of RV function (Tables 2-4).

Between 4 and 8 weeks, 13 rats with PL developed severe clinical RV failure or death and were humanely killed (vehicle: 7 rats; NRG1: 6 rats). Treatment with NRG1 in PL rats postponed the age of death (time after surgery) and/or development of severe RV failure (Figure 2H). NRG1 treatment did not affect weight gain in the PL rats.

NRG1 treatment decreased the progression of fibrosis development in RV PL rats at 4 and 8 weeks. Other markers of RV remodeling, hypertrophy and capillary:myocyte ratio, were not affected by NRG1 treatment (Figure 5A and B, Tables 2-4).

NRG1 treatment increased cardiomyocyte-specific Ki-67. The increase in fraction of Ki-67 cardiomyocytes was most prominent after 2 weeks but still present after 4 and 8 weeks, albeit at a lower size (Figure 5C). Quantitative polymerase chain reaction did not show differences be- tween vehicle and NRG1 treatment in fetal gene switch (*Myh7*:*Myh6* ratio; Tables 2-4), genes associated with cardiomyocyte proliferation (runt-related transcription factor 1, Disabled adaptor protein 2) or metabolism (medium-chain acyl-CoA dehydrogenase, glucose trans- porter 1). Metallopeptidase inhibitor 1, involved in fibrosis, tended to be lower in the NRG1 treatment group ($P = .051$; Figure 5D).

Table 2. Values at 2 weeks

	Control	n	PL veh	n	P 1	PL NRG1	n	P 2/3
Body weight, g	82.4 (9.5)	28	73.3 (7.5)	25	.393	70.1 (9.5)	31	.297/.780
Tibia length, mm	23.6 (0.7)	11	22.9 (1.2)	9	.456	22.9 (1.3)	10	.519/.968
Organ weights, g								
RV	0.08 (0.03)	11	0.18* (0.03)	9	<.001	0.15*, † (0.03)	10	<.001/.009
LV þ IVS	0.27 (0.03)	11	0.29 (0.03)	9	.525	0.28 (0.06)	10	1.000/1.000
RV/(LV þ IVS)	0.29 (0.03)	11	0.64* (0.12)	9	<.001	0.53* (0.06)	10	<.001/.129
RA	0.024 (0.013)	11	0.075* (0.033)	9	<.001	0.045* (0.015)	9	.012/.189
Echocardiographic parameters								
Cardiac output, mL/min	55.3 (12.3)	11	37.2* (13.2)	9	.018	49.8 (13.0)	10	.753/.066
TAPSE, mm	2.1 (0.3)	11	1.5* (0.3)	8	<.001	1.5* (0.3)	10	<.001/.829
Eccentricity index diastolic	1.00 (0.07)	11	1.64* (0.05)	6	<.001	1.59* (0.32)	9	<.001/.388
Histology								
Capillary:myocyte ratio	0.65 (0.10)	11	0.87* (0.14)	8	.012	0.96* (0.16)	10	<.001/.519
qPCR								
Myh7/6	0.99 (0.40)	10	102.0* (89.91)	9	<.001	44.24* (38.9)	10	<.001/.129

Data are presented as mean (SD), except where otherwise noted. *PL*, Pressure load; *veh*, vehicle; *P 1*, *P* value control versus pressure load vehicle; *NRG1*, neuregulin-1; *P 2*, *P* value control versus pressure load neuregulin-1; *P 3*, *P* value pressure vehicle versus pressure load neuregulin-1; *RV*, right ventricle; *LV*, left ventricle; *IVS*, interventricular septum; *RA*, right atrium; *TAPSE*, tricuspid annular plane systolic excursion; *qPCR*, quantitative polymerase chain reaction; *Myh7/6*, myosin heavy chain 7/6. *$P<.05$ control versus PL. † $P<.05$ PL vehicle versus PL NRG1.

Table 3. Values at 4 weeks

	Control	n	PL veh	n	*P*	PL NRG1	n	*P*
Body weight, g	149.8 (12.4)	16	127.4* (4.9)	16	.015	120.2* (18.3)	21	<.001/1.000
Tibia length, mm	27.6 (0.7)	6	26.3* (0.1)	7	.024	26.1* (0.3)	10	.009/.945
Organ weights, g								
RV	0.10 (0.02)	5	0.25* (0.01)	7	.009	0.23* (0.03)	10	.003/1.000
LV þ IVS	0.40 (0.02)	5	0.39 (0.02)	7	1.000	0.48 (0.06)	10	.618/.579
RV/(LV þ IVS)	0.10 (0.02)	5	0.65* (0.06)	7	.009	0.52* (0.13)	10	.003/.264
RA	0.037 (0.017)	5	0.147* (0.010)	7	.009	0.147* (0.025)	10	.003/1.000
Echocardiographic parameters								
Cardiac output, mL/min	107.4 (19.0)	4	38.7* (2.0)	7	.012	60.0* (17.1)	10	.006/.129
TAPSE (mm)	3.9 (0.8)	4	1.4* (0.1)	6	.006	1.7* (0.32)	10	<.001/.354
Eccentricity index diastolic	0.94 (0.09)	5	1.83* (0.13)	7	.009	1.87 (0.62)	8	.090/1.000
Histology								
Capillary:myocyte ratio	0.74 (0.17)	6	1.05* (0.06)	7	.024	1.06* (0.19)	10	.021/1.000
qPCR								
Myh7/6	1.12 (0.51)	5	154.9* (63.72)	7	.009	154.7* (62.9)	10	.003/.690

Data are presented as mean (SD), except where otherwise noted. *PL*, Pressure load; *veh*, vehicle; *NRG1*, neuregulin-1; *RV*, right ventricle; *LV*, left ventricle; *IVS*, interventricular septum; *RA*, right atrium; *TAPSE*, tricuspid annular plane systolic excursion; *qPCR*, quantitative polymerase chain reaction; *Myh7/6*, myosin heavy chain 7/6. *P<.05 control versus PL.

Table 4. Values at 8 weeks

	Control	n	PL veh	n	*P*	PL NRG1	n	*P*
Body weight, g	274.3 (19.4)	12	206.5* (18,6)	4	.012	214.4* (20.8)	5	.003/.730
Tibia length, mm	34.5 (0.3)	11	32.3* (1.2)	4	.012	32.4* (1.1)	5	.006/.730
Organ weights, g								
RV	0.16 (0.03)	12	0.31* (0.21)	3	.012	0.32* (0.07)	5	<.001/1.000
LV þ IVS	0.60 (0.03)	12	0.57 (0.07)	3	.885	0.59 (0.11)	5	1.000/.786
RV/(LV þ IVS)	0.27 (0.03)	12	0.54* (0.14)	3	.012	0.56* (0.16)	5	<.001/1.000
RA	0.041 (0.014)	12	0.225* (0.007)	3	.012	0.241* (0.022)	5	<.001/1.000
Echocardiographic parameters								
Cardiac output, mL/min	118.1 (23.9)	12	50.5* (21.2)	4	.006	75.1* (13,9)	5	.012/.333
TAPSE, mm	3.1 (0.3)	12	2.55 (1.2)	4	.599	2.0* (0.45)	5	<.001/.730
Eccentricity index diastolic	1.00* (0.03)	11	1.46* (0.21)	3	.025	1.21* (0.45)	5	<.001/.571
Histology								
Capillary:myocyte ratio	0.99 (0.14)	12	1.53* (0.20)	6	.003	1.34* (0.04)	4	.003/.171
qPCR								
Myh7/6	0.97 (0.27)	11	17.67 (11.2)	3	.078	19.97 (2.27)	3	.078/1.000

Data are presented as mean (SD), except where otherwise noted. *PL*, Pressure load; *veh*, vehicle; *NRG1*, neuregulin-1; *RV*, right ventricle; *LV*, left ventricle; *IVS*, interventricular septum; *RA*, right atrium; *TAPSE*, tricuspid annular plane systolic excursion; *qPCR*, quantitative polymerase chain reaction; *Myh7/6*, myosin heavy chain 7/6. *P <.05 control versus PL.

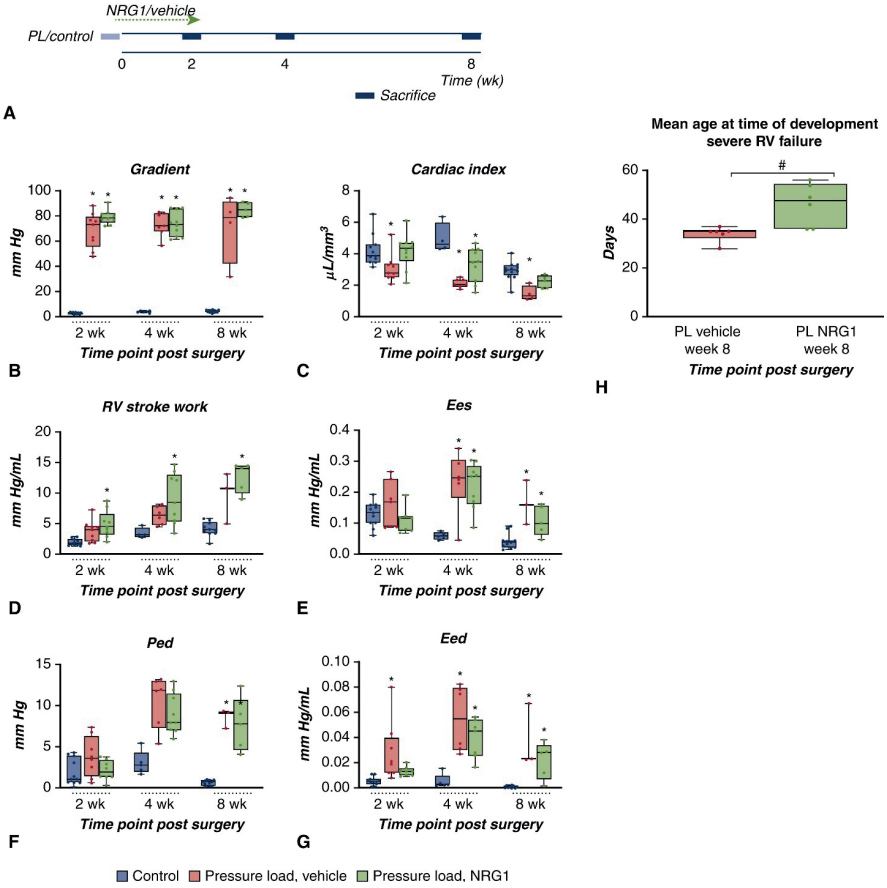

Figure 2. A) Schematic overview of experimental design. Surgery in both groups consisted of pulmonary artery banding (PL) or sham surgery (control). Rats received daily neuregulin-1 (*NRG1*) or vehicle from day 3 to day 14 post surgery. Rats were humanely killed after 2 weeks, 4 weeks, or 8 weeks. **B**) PL gradient was increased in all groups compared with control *P* values: 2/4/8 weeks control versus PL vehicle:<.001/.003/.003; control vs PL NRG1:<.001/<.001/<.001 ; 2/4/8 weeks PL vehicle versus PL NRG1: .231/.030/1.000. **C**) No decreased cardiac index at time point 2 weeks in NRG1-treated PL rats. *P* values: 2/4/8 weeks control versus PL vehicle: .009/.024/.006; control versus PL NRG1: .705/.024/.042; 2/4/8 weeks PL vehicle versus PL NRG1: .105/.165/.189. **D**) NRG1 increased right ventricular (RV) stroke work after 4 weeks, measured according to echocardiographic stroke volume and pressure measurements with a RV pressure-volume catheter. *P* values: 2/4/8 weeks control versus PL vehicle: .012/.057/.147; control versus PL NRG1:<.001/.024/.003; 2/4/ 8 weeks PL vehicle versus PL NRG1: .666/.684/.750. **E**) NRG1- and vehicle-treated PL rats show increased RV contractility 4 and 8 weeks after surgery. *P* values: 2/4/8 weeks control versus PL vehicle: .714/.012/.015; control versus PL NRG1: .387/.003/.015; 2/4/8 weeks PL vehicle versus PL NRG1: .195/.816/1.000. **F**) and **G**) NRG1 tends to improve diastolic function in RV-PL; end diastolic pressure (*P* values: 2/4/8 weeks control vs PL vehicle: .387/.012/.015; control vs PL NRG1: 1.000/.003/<.001; 2/4/8 weeks PL vehicle vs PL NRG1: .585/1.000/1.000), and end diastolic elastance (*P* values: 2/4/8 weeks control vs PL vehicle:<.001/.012/.015; control vs PL NRG1: .003/.009/.006; 2/4/8 weeks PL vehicle vs PL NRG1: .585/.885/1.000). H, NRG1 postpones the development of clinical RV failure due to chronic RV PL in the week 8 cohort; *P* value: 8 weeks PL vehicle versus PL NRG1: .002. *Red bars* represent PL vehicle

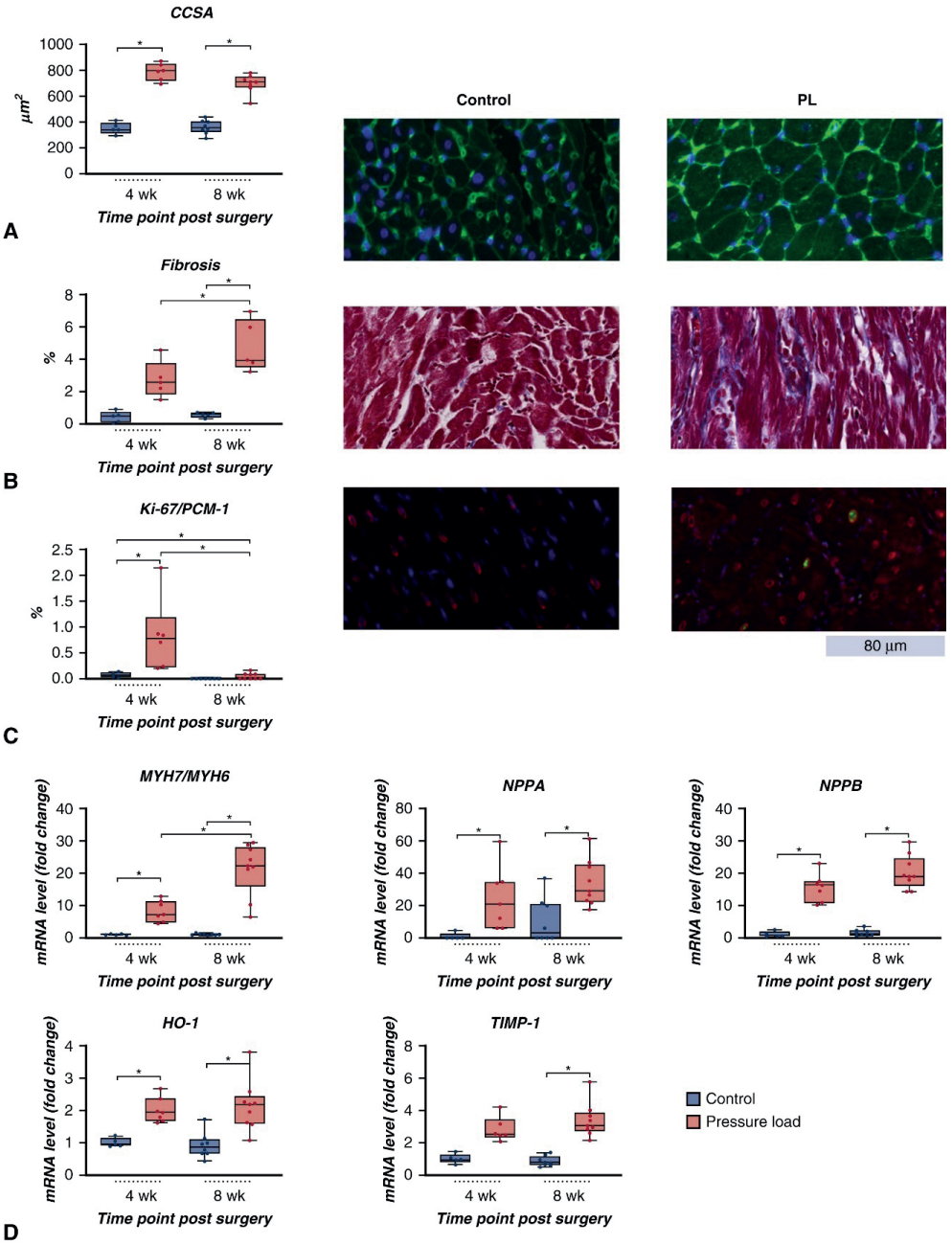

Figure 3. Histology and gene expression. **A**) Pulmonary artery banding (PL) increased right ventricular (RV) hypertrophy expressed by cardiomyocyte cross-sectional area (*CCSA*; first row are representative images of wheat germ agglutinin-stained RVs 4 weeks after surgery). *P* values: 4/8 weeks control versus PL: .016/<.001; control/PL at 4 weeks versus 8 weeks: 1.000/.140. **B**) fibrosis increased in PL rats at 8 weeks (second row images are representative images of Masson-Trichrome–stained RVs 8 weeks after surgery). *P* values: 4/8 weeks control versus PL: .468/<.001; control/PL at 4 weeks versus 8 weeks: .096/.008. **C**) RV-PL increased cardiomyocyte specific cell-cycle activity and decreases over time

in control and PL rats. Representative slides of DAPI (*blue*)/Ki-67 (*green*)/pericentriolar material 1 (*PCM-1*, *red*) staining in the RV at 4 weeks of control and PL right ventricles. Colors were enhanced for analysis and presentation. *P* values: 4/8 weeks control versus PL: .040/.484; control/PL at 4 weeks versus 8 weeks: .024/.004. **D**) mRNA expression of genes from left to right related to fetal gene switch, stress markers, and fibrosis (control 4 weeks = 1). b/a-Myosin heavy chain switch (*MYH7/6*) *P* values: 4/ 8 weeks control versus PL: .012/<.001; control/PL at 4 weeks versus 8 weeks: 1.000/.032. Natriuretic pro-peptides type A (*NPPA*) *P* values: 4/8 weeks control versus PL: .012/.024; control/PL at 4 weeks versus 8 weeks: 1.000/.840. Natriuretic pro-peptides type B (*NPPB*) *P* values: 4/8 weeks control versus PL: .012/<.001; control/PL at 4 weeks versus 8 weeks: .888/.364. Heme oxygenase (*HO-1*) *P* values: 4/8 weeks control versus PL: .012/.004; control/PL at 4 weeks versus 8 weeks: 1.000/1.000. Metallopeptidase inhibitor 1 (*TIMP-1*) *P* values: 4/8 weeks control versus PL: .192/<.001; control/PL at 4 weeks versus 8 weeks: 1.000/.465. *Red bars* represent PL rats, *blue bars* represent control rats. The *circles* indicate the total number of rats with PL surgery. In some groups, numbers are lower than mentioned in methods because of failed analyses. The *lower and upper borders of the box* are the lower and upper quartiles. The *middle horizontal line* represents the median. The *whiskers* are the minimum and maximum values. *Dots* in the box-and-whisker dot plots represent individual measurements. Statistical analysis: Kruskal–Wallis with correction for multiple testing. **P* <.05

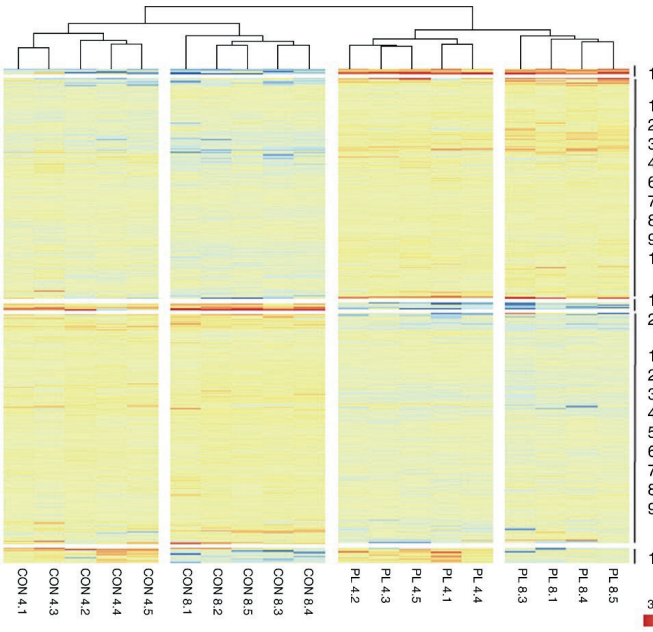

	GO Term	*P* value
1.	Extracellular matrix	$1.7e^{-2}$
1.	Cell-cell adherens junctions	$4.6e^{-16}$
2.	Innate immune response	$5.7e^{-7}$
3.	Pleckstrin homology domain	$1.6e^{-8}$
4.	Nucleotide binding	$1.4e^{-17}$
6.	Microtubule	$8.8e^{-6}$
7.	EGF-like domain	$7.2e^{-6}$
8.	GTP-binding	$3.9e^{-6}$
9.	Glycoprotein	$1.1e^{-14}$
10.	Cell cycle	$1.7e^{-7}$
1.	Glycoprotein	$4.1e^{-3}$
2.	Ion channel	$1.8e^{-4}$
1.	Mitochondrion	$4.6e^{-86}$
2.	Oxidative phosphorylation	$1.5e^{-15}$
3.	Citrate cycle (TCA cycle)	$3.2e^{-11}$
4.	Fatty acid metabolism	$3.8e^{-11}$
5.	Peroxisome	$3.5e^{-11}$
6.	Zinc-finger	$3.4e^{-6}$
7.	Respiratory chain	$1.6e^{-6}$
8.	Nucleotide binding	$9.7e^{-7}$
9.	Lipid biosynthesis	$1.1e^{-7}$
1.	Cell division	$2.9e^{-16}$

A

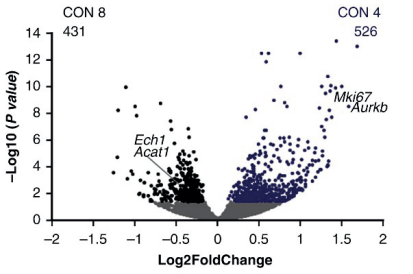

1. Mitochondrion	$2.7e^{-25}$	1. Cell cycle	$1.2e^{-11}$
2. Fatty acid beta-oxidation	$6.9e^{-14}$	2. Actin-binding	$4.0e^{-11}$
3. Lipid metabolism	$2.9e^{-5}$	3. Collagen	$1.2e^{-9}$
4. Peroxisome	$1.1e^{-6}$	4. Focal adhesion	$2.5e^{-8}$
5. NADP	$3.7e^{-6}$	5. Microtubule	$6.6e^{-7}$

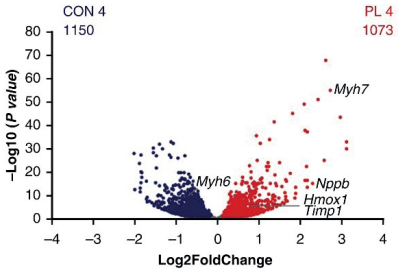

1. Mitochondrion	$4.6e^{-36}$	1. Cell-cell adherens junctions	$1.5e^{-8}$
2. Fatty acid beta-oxidation	$8.1e^{-10}$	2. Nucleotide-binding	$3.7e^{-8}$
3. Oxidative phosphorylation	$4.4e^{-6}$	3. Cell division	$1.1e^{-4}$
4. Flavoprotein	$4.3e^{-5}$	4. Stress response	$1.2e^{-2}$
5. Peroxisome	$1.3e^{-4}$	5. GTPase activity	$1.5e^{-3}$

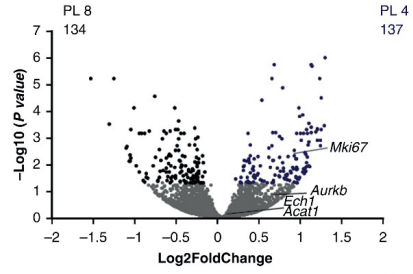

1. Hemoglobin complex	$5.4e^{-6}$	1. Cell cycle	$8.9e^{-9}$
2. Immunity	$6.3e^{-4}$	2. Methylation	$2.2e^{-4}$
		3. Chromosome	$1.9e^{-13}$
		4. Mitosis	$8.0e^{-8}$
		5. Cell cycle	$2.5e^{-8}$

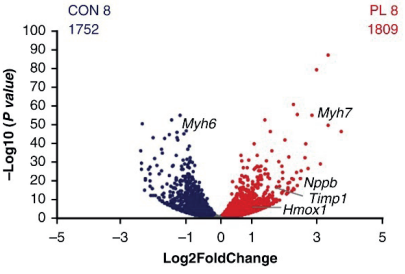

1. Mitochondrion	$3.6e^{-97}$	1. Cell-cell adherens junctions	$2.1e^{-12}$
2. Oxidative phosphorylation	$1.9e^{-20}$	2. Innate immune response	$3.6e^{-9}$
3. Citrate cycle (TCA cycle)	$1.0e^{-12}$	3. Glycoprotein	$1.6e^{-24}$
4. Respiratory chain	$6.6e^{-8}$	4. EGF-like domain	$1.8e^{-8}$
5. Fatty acid metabolism	$1.2e^{-10}$	5. Pleckstrin homology-like domain	$1.2e^{-7}$

B

Figure 4. RNA sequencing identifies delayed silencing of fetal pathways. **A**) Functional annotated heat map of pulmonary artery banding (PL) versus control (*CON*) at 2 time points (4 weeks and 8 weeks). Gene ontology analysis was performed on each cluster. **B**) Volcano plot showing cardiac transcripts differentially expressed between 4 and 8 weeks in control (top left), PL (bottom left) and between control and PL at 4 weeks (top right) and 8 weeks (bottom right). *Colored dots* indicate significantly differentially expressed genes (*P* adjusted for multiple testing; false discovery rate<.05). *PL*, Pressure load; *GO*, gene ontology; *EGF*, epidermal growth factor; *GTP, guanosine 5'-triphosphate*; *TCA*, tricarboxylic acid cycle.

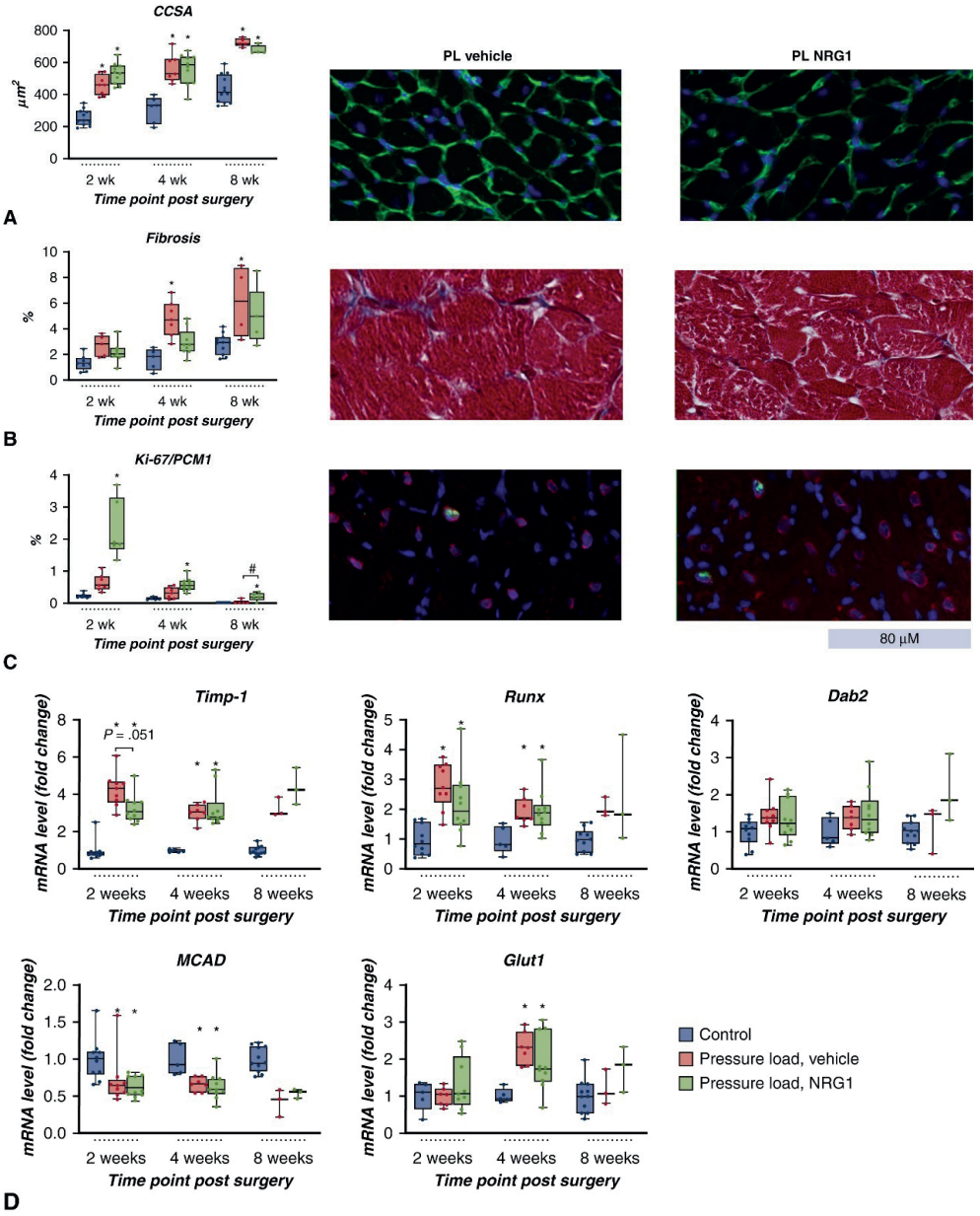

Figure 5. Histology and gene expression. **A**) No differences in right ventricular (RV) hypertrophy expressed in cardiomyocyte cross-sectional area (*CCSA*) for neuregulin-1 (*NRG1*)- and vehicle-treated pressure load (*PL*) rats (first row are representative images of wheat germ agglutinin-stained RVs 4 weeks after surgery). *P* values: 2/4/8 weeks control versus PL vehicle: .012/.003/.003; control versus PL NRG1:<.001/<.001/.003; 2/4/8 weeks PL vehicle versus PL NRG1: 1.000/1.000/.600. **B**) fibrosis is less pronounced in NRG1-treated PL rats (second row images are representative images of Masson-Tri- chrome–stained RVs 4 weeks after surgery). *P* values: 2/4/8 weeks control versus PL vehicle: .018/.000/.054; control versus PL NRG1: .162/.087/.114; 2/4/ 8 weeks PL vehicle versus PL

NRG1: 1.000/.036/1.000. **C**) NRG1 increased cardiomyocyte specific cell cycle activity in PL rats (third row: representative slides of DAPI [*blue*]/Ki-67 (*green*)/pericentriolar material 1 [*PCM-1*], *red*) staining in the right ventricle at 2 weeks of control and PL right ventricle. *P* values: 2/4/8 weeks control versus PL vehicle: .003/.219/1.000; control versus PL NRG1: .003/.039/.027; 2/4/8 weeks PL vehicle versus PL NRG1: .003/.327/.189. **D**) mRNA expression of genes from left to right related to fibrosis, dedifferentiation/cell cycle activity, and metabolism. *P* values: 2/4/8 weeks control versus PL vehicle: <.001/.009/.078; control versus PL NRG1: <.001/.003/.078; 2/4/8 weeks PL vehicle versus PL NRG1: .051/1.000/1.000. *P* values: 2/4/8 weeks control versus PL vehicle: <.001/.015/.090; control versus PL NRG1: .012/.024/.819; 2/4/8 weeks PL vehicle versus PL NRG1: .399/1.000/1.000. *P* values: 2/4/8 weeks control versus PL vehicle: .066/.318/1.000; control versus PL NRG1: .840/.387/.309; 2/4/8 weeks PL vehicle versus PL NRG1: 1.000/1.000/1.000. *P* values: 2/4/8 weeks control versus PL vehicle: .024/.009/.078; control versus PL NRG1: .003/.015/.078; 2/4/8 weeks PL vehicle versus PL NRG1: 1.000/1.000/.999. *P* values: 2/4/8 weeks control versus PL vehicle: 1.000/.009/1.000; control versus PL NRG1: 1.000/.039/1.000; 2/4/8 weeks PL vehicle versus PL NRG1: 1.000/.483/.999. *Red bars* represent PL vehicle rats, *green bars* represent PL NRG1 rats, *blue bars* represent control rats. In some groups, numbers are lower than mentioned in methods because of failed analyses. The *lower and upper borders of the box* are the lower and upper quartiles. The *middle horizontal line* represents the median. The *whiskers* are the minimum and maximum values. *Dots* in the box-and-whisker dot plots represent individual measurements. Statistical analysis: Kruskal–Wallis with correction for multiple testing. *Timp-1*, Metallopeptidase inhibitor 1; *Runx*, runt-related transcription factor 1; *Dab2*, disabled adaptor protein 2; *MCAD*, medium-chain acyl-CoA dehydrogenase; *Glut1*, glucose transporter 1. **P* <.05 compared with control. #*P* <.05 PL vehicle compared with NRG1.

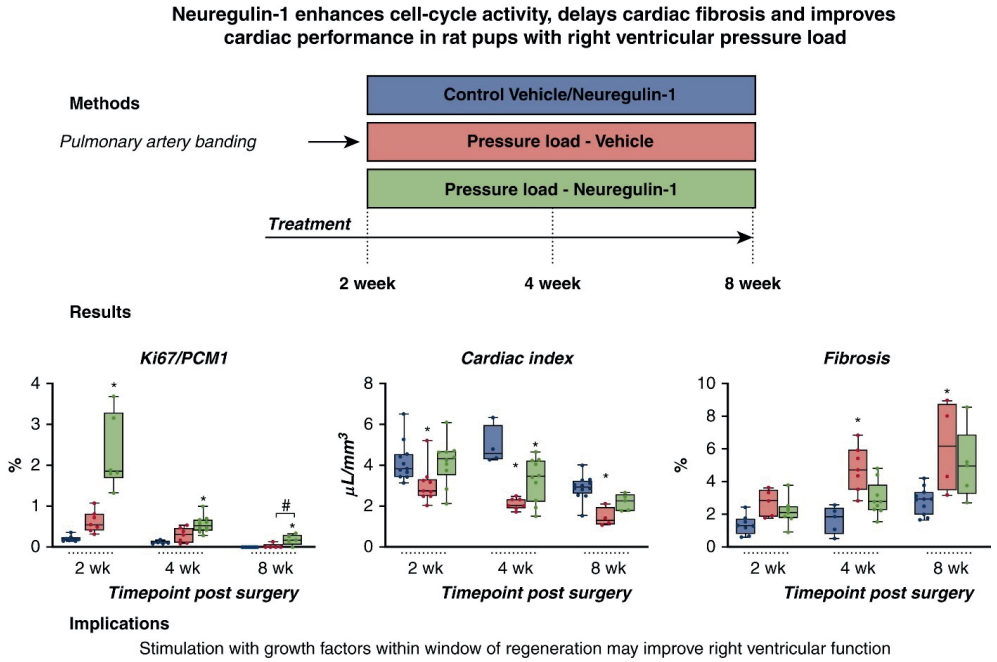

Figure 6. Summary of the experiment. *Red bars* represent pressure load (PL) vehicle rats, *green bars* represent PL neuregulin-1 (NRG1) rats, *blue bars* represent control rats. Results: Ki-67/pericentriolar material 1 (PCM-1) *P* values: 2/4/8 weeks control versus PL vehicle: .003/.219/1.000; control versus PL NRG1: .003/.039/.027; 2/4/8 weeks PL vehicle versus PL NRG1: .003/.327/.189. Cardiac index *P* values: 2/4/8 weeks control versus PL vehicle: .018/.000/.054; control versus PL NRG1: .162/.087/.114; 2/4/8 weeks PL vehicle versus PL NRG1: 1.000/.036/1.000. Fibrosis *P* values: 2/4/8 weeks control versus PL vehicle: .018/.000/.054; control versus PL NRG1: .162/.087/.114; 2/4/8 weeks PL vehicle versus PL NRG1: 1.000/.036/1.000. The *lower and upper borders of the box* are the lower and upper quartiles. The *middle horizontal line* represents the median. The *whiskers* are the minimum and maximum values. *Dots* in the box-and-whisker dot plots represent individual measurements. **P* <.05 versus control. #*P* <.05 NRG1 versus vehicle.

DISCUSSION

In this study, we used a rat pup model for chronic, increased RV PL from immaturity into adulthood to mimic cardiac adaptation in patients with CHD. RV PL in rat pups induced cell cycle activity and delayed transcriptional maturation. After 4 weeks of initial adaptation, progressive failure to thrive, RV dysfunction, and RV fibrosis developed. Increased cell cycle activity via exogenous administration of the growth fac- tor, NRG1, improved cardiac function, and delayed the onset of RV fibrosis and failure. This proof-of-concept study suggests that stimulation of cell cycle activity during growth enhances RV adaptation to PL and might provide a new approach to preserve RV function in CHD.

In this study we modeled adaptation to PL during growth and development from "early childhood" into "adulthood." This new approach has been developed in rats and pigs.[17,18] The use of such models is especially relevant for CHD, where the heart has to adapt to PL conditions during physical maturation. Throughout this study, the body mass increased from 30 g to 300 g, a growth rate comparable with humans during childhood.[13] Our study extends recently described observations from PL in newborn rat pups,[18] in which a gradient of 8 mm Hg was applied, compared with 80 mm Hg in the present study. In that study, the initial adaptation to the mild PL applied on postnatal day 1 was RV hypertrophy without fibrosis. The age and weight of the newborn rats precluded further cardiac performance measurements as performed in this study. Other rat models, in which PL was applied at an older age (e.g., body weight of 80-100 g) yielded different age-dependent responses.[17] Chronic PL applied at an older age eventually induces RV dysfunction, fibrosis, and remodeling, which has been previously characterized.[5] These signals have also been identified in children with RV PL (eg, tetralogy of Fallot) in tissues obtained at primary surgery.[19] These experimental models of chronic RV PL during growth and development show similarities to children with CHD, and might create a window of opportunity to search for potential therapies during childhood. In accordance with patients with severe CHD, this model of RV PL induced failure to thrive and signs of clinical RV failure after a relative incident-free youth.[20] This model underscores that diastolic dysfunction is a leading cause for the development of clinical right heart failure.[17,21] Known markers of RV failure in adult PL models (e.g., natriuretic pro-peptide A/B levels and *Myh7*:*Myh6* ratio) also increase in young PL rats.[4] In patients with tetralogy of Fallot, increased stiffness and PL are accompanied by increased signaling involved in muscle tissue development, ventricle contractility, and calcium signaling.[19] These signals also arose in the expression pro- files of RV PL tissue.

A major finding in the present study was the delay in transcriptional maturation and increase in cell cycle activity observed during growth and development in the pups with PL. Since the initial description of postnatal cardiomyocyte proliferation,[22,23] many investigators have studied this phenomenon.[23,24] In the study applying increased PL to 1-day-old rat pups a similar profile of delay in maturation and activation of proliferation signals was measured.[18] Several postnatal processes might be involved in the loss of proliferative potential with age, (e.g., increase in oxygen saturation).[25] The functional consequences of these transcriptional changes for RV adaptation are still elusive. We introduced a growth factor, NRG1, to further study the con- sequences of increased CCA on chronic PL in the postnatal developing heart.

Since the first observation of that NRG1 might enhance CCA *in vitro*,[26] few studies have assessed the effects of NRG1 in vivo in acute stress models.[27] This study extends the observation that in vivo administration of NRG1 in rat pups with chronic PL increases CCA and improves RV cardiac performance. These findings implicate first that the transcriptional changes involved in cell cycle activity observed in rat pups with PL are positive coping mechanisms. Further stimulation of CCA via NRG1 improves cardiac adaptation to PL.

Another finding is the delayed onset of cardiac fibrosis in NRG1-treated PL rats. It is known that NRG1 treatment might also induce paracrine effects via cardiac fibroblasts *in vivo*[28] and increase phosphorylation of phospholamban.[29] *In vitro*, NRG1 decreases RV fibrosis in adult PL rats.[30] However, this did not result in improvement of cardiac function. It should be noted that RV fibrosis is part of the adaptive as well as maladaptive response to increased RV afterload. Previous studies in adult mice and rats suggested that RV dysfunction is not directly related to RV fibrosis, yet fibrosis might be interpreted as a sign of maladaption.[5,31] Potentially, NRG1 can induce side effects on other organs. This has not been the case. Administration of NRG1 during growth and development has not been shown to induce effects on other organs.[32] These findings underline the therapeutic potential of NRG1 administration in the RV PL during growth and development.

Several approaches have been taken to improve RV adaptation to stress in patients with CHD.[33] Multiple studies inject either stem cells or cardiospheres into the myocardium or into the coronary artery. None of these studies have shown actual CCA, but some show improvements in ejection fraction and reduction in fibrosis. The approach in the present study yields a noninvasive therapeutic strategy with few side effects and might offer new treatment opportunities, and shows that RV failure might be amenable for therapy focusing on processes involved in cardiac regeneration. NRG1 administration has been tested in adult experimental models and has been tested safe and well- tolerated in 2 phase II trials in adult heart failure patients.[34] Further experiments are needed to study the effects of repetitive long-term administration during the first months of life to evaluate the durability of NRG1 in the preservation of RV function in children with CHD.

The most accurate way to assess the proliferation of cardiomyocytes is a matter of ongoing debate.[15] We assessed Ki-67, a marker of cell cycle activity, which, during post- natal development, can be coupled to polyploidization in cardiomyocytes rather than cell division, as described in the proliferation consensus statement.[11] In contrast to many other studies, we combined the staining with PCM-1, in the heart a specific marker for cardiomyocyte nuclei,[9] to assess CCA. In addition, we used H3P, a marker of mitosis, to confirm this signal. Yet, H3P represents actual nucleus division, which is known to be present in low amounts.[9,15] In line with this knowledge, the number of events appeared too low to detect differences. Also, our study did not find increased gene activity known to play a role in the pathways that stimulate cardiomyocyte proliferation through NRG1.[35] Combined, these findings indicate cell cycle activation without progression to actual mitosis.

Limitation

The RNA expression profile was obtained in whole cardiac tissue, which is constituted of different cell types including endothelial cells, epicardial cells, macrophages, cardiomyocytes, and fibroblasts. Cell lineage tracing are not feasible in the rat at present, but development of single-cell sequencing might be used in further studies. The PL we applied in the present

study was more progressive than that applied previously in adult rats.[5] This is because of the growth of the rats with a fixed banding. This could be viewed as a strength of the study because we studied adaptation throughout growth and development.

CONCLUSIONS

RV PL applied in rats during postnatal growth and development transiently increased CCA. Stimulation of CCA via exogenous administration of NRG1 improved cardiac function, decreased fibrosis, and improved clinical outcome (Figure 6). The results of this proof-of-concept study imply that stimulation of CCA might provide a new approach to preserve RV function in patients with CHD.

CONFLICT OF INTEREST STATEMENT

The authors reported no conflicts of interest. The *Journal* policy requires editors and reviewers to disclose conflicts of interest and to decline handling or re- viewing manuscripts for which they may have a conflict of interest. The editors and reviewers of this article have no conflicts of interest.

REFERENCES

1. Stout KK, Broberg CS, Book WM, Cecchin F, Chen J, Dimopoulos K, et al. Chronic heart failure in congenital heart disease. *Circulation*. 2016;133:770-801.
2. Triedman JK, Newburger JW. Trends in congenital heart disease. *Circulation*. 2016;133:2716-33.
3. Kuehl KS, Landzberg MJ, Mahle WT, Mann D, Marelli A, Newburger J, et al. Emerging research directions in adult congenital heart disease: a report from an NHLBI/ACHA working group. *J Am Coll Cardiol*. 2016; 67:1956-64.
4. Borgdorff MAJ, Dickinson MG, Berger RMF, Bartelds B. Right ventricular failure due to chronic pressure load: what have we learned in animal models since the NIH working group statement? *Heart Fail Rev*. 2015;20:475-91.
5. Borgdorff MAJ, Koop AMC, Bloks VW, Dickinson MG, Steendijk P, Sillje HHW, et al. Clinical symptoms of right ventricular failure in experimental chronic pressure load are associated with progressive diastolic dysfunction. *J Mol Cell Cardiol*. 2015;79:244-53.
6. van de Veerdonk MC, Bogaard HJ, Voelkel NF. The right ventricle and pulmonary hypertension. *Heart Fail Rev*. 2016;21:259-71.
7. Konstam MA, Kiernan MS, Bernstein D, Bozkurt B, Jacob M, Kapur NK, et al. Evaluation and management of right-sided heart failure: a scientific statement from the American Heart Association. *Circulation*. 2018;137:e578-622.
8. Khairy P, Ionescu-Ittu R, MacKie AS, Abrahamowicz M, Pilote L, Marelli AJ. Changing mortality in congenital heart disease. *J Am Coll Cardiol*. 2010;56: 1149-57.
9. Bergmann O, Zdunek S, Felker A, Salehpour M, Alkass K, Bernard S, et al. Dynamics of cell generation and turnover in the human heart. *Cell*. 2015;161: 1566-75.
10. Mollova M, Bersell K, Walsh S, Savla J, Das LT, Park S, et al. Cardiomyocyte proliferation contributes to heart growth in young humans. *Proc Natl Acad Sci U S A*. 2013;110:1446-51.
11. Eschenhagen T, Bolli R, Braun T, Field L, Fleischmann BK, Fris en J, et al. Car diomyocyte regeneration: a consensus statement. *Circulation*. 2017;8:680-6.
12. Wadugu B, Kuhn B. The role of neuregulin/ErbB2/ErbB4 signaling in the heart with special focus on effects on cardiomyocyte proliferation. *Am J Physiol Heart Circ Physiol*. 2012;302:H2139-47.
13. Sengupta P. The laboratory rat: relating its age with human's. *Int J Prev Med*. 2013;4:624-30.
14. Hagdorn QAJ, Bossers GPL, Koop AMC, Piek A, Eijgenraam TR, van der Feen DE, et al. A novel method optimizing the normalization of cardiac pa- rameters in small animal models: the importance of dimensional indexing. *Am J Physiol Heart Circ Physiol*. 2019;316:H1552-7.
15. Leone M, Magadum A, Engel FB. Cardiomyocyte proliferation in cardiac development and regeneration: a guide to methodologies and interpretations. *Am J Physiol Heart Circ Physiol*. 2015;309:H1237-50.
16. Bergmann O, Zdunek S, Alkass K, Druid H, Bernard S, Fris en J. Identification of cardiomyocyte nuclei and assessment of ploidy for the analysis of cell turnover. *Exp Cell Res*. 2011;317:188-94.
17. Ko JH, Eom GH, Cho HJ, Nam K, Ma JS, Kook H, et al. Right ventricular myocardial performance index is decreased with severe pressure-overload cardiac hypertrophy in young rats. *Pediatr Cardiol*. 2013;34:1556-66.
18. Ye L, Wang S, Xiao Y, Jiang C, Huang Y, Chen H, et al. Pressure overload greatly promotes neonatal right ventricular cardiomyocyte proliferation: a new model for the study of heart regeneration. *J Am Heart Assoc*. 2020;9:e015574.

19. Bond AR, Iacobazzi D, Abdul-Ghani S, Ghorbel M, Heesom K, Wilson M, et al. Changes in contractile protein expression are linked to ventricular stiffness in in- fants with pulmonary hypertension or right ventricular hypertrophy due to congenital heart disease. *Open Heart*. 2018;5:1-14.
20. Zomer AC, Vaartjes I, Van Der Velde ET, De Jong HMY, Konings TC, Wagenaar LJ, et al. Heart failure admissions in adults with congenital heart dis- ease; risk factors and prognosis. *Int J Cardiol*. 2013;168:2487-93.
21. Hillgaard TK, Andersen A, Andersen S, Vildbrad MD, Ringgaard S, Nielsen JM, et al. Levosimendan prevents pressure-overload-induced right ventricular failure. *J Cardiovasc Pharmacol*. 2016;67:275-82.
22. Porrello ER, Mahmoud AI, Simpson E, Hill JA, Richardson JA, Olson EN, et al. Transient regenerative potential of the neonatal mouse heart. *Science*. 2011;331: 1078-81.
23. Pasumarthi KBS, Nakajima H, Nakajima HO, Soonpaa MH, Field LJ. Targeted expression of cyclin D2 results in cardiomyocyte DNA synthesis and infarct regression in transgenic mice. *Circ Res*. 2005;96:110-8.
24. Tian Y, Liu Y, Wang T, Zhou N, Kong J, Chen L, et al. A microRNA-Hippo pathway that promotes cardiomyocyte proliferation and cardiac regeneration in mice. *Sci Transl Med*. 2015;7:279ra38.
25. Nakada Y, Canseco DC, Thet S, Abdisalaam S, Asaithamby A, Santos CX, et al. Hypoxia induces heart regeneration in adult mice. *Nature*. 2017;541:222-7.
26. Bersell K, Arab S, Haring B, Ku€hn B. Neuregulin1/ErbB4 signaling induces car- diomyocyte proliferation and repair of heart injury. *Cell*. 2009;138:257-70.
27. Polizzotti BD, Ganapathy B, Walsh S, Choudhury S, Ammanamanchi N, Bennett DG, et al. Neuregulin stimulation of cardiomyocyte regeneration in mice and human myocardium reveals a therapeutic window. *Sci Transl Med*. 2015;7:281ra45.
28. Kirabo A, Ryzhov S, Gupte M, Sengsayadeth S, Gumina RJ, Sawyer DB, et al. Neuregulin-1b induces proliferation, survival and paracrine signaling in normal human cardiac ventricular fibroblasts. *J Mol Cell Cardiol*. 2017;105:59-69.
29. Ad~ao R, Mendes-Ferreira P, Maia-Rocha C, Santos-Ribeiro D, Rodrigues SG, Vi- dal-Meireles A, et al. Neuregulin-1 attenuates right ventricular diastolic stiffness in experimental pulmonary hypertension. *Clin Exp Pharmacol Physiol*. 2019;46: 255-65.
30. Mendes-Ferreira P, Maia-Rocha C, Ad~ao R, Mendes MJ, Santos-Ribeiro D, Alves BS, et al. Neuregulin-1 improves right ventricular function and attenuates experimental pulmonary arterial hypertension. *Cardiovasc Res*. 2016;109:44-54.
31. Crnkovic S, Egemnazarov B, Damico R, Marsh LM, Nagy BM, Douschan P, et al. Disconnect between fibrotic response and right ventricular dysfunction. *Am J Re- spir Crit Care Med*. 2019;199:1550-60.
32. Ganapathy B, Nandhagopal N, Polizzotti BD, Bennett D, Asan A, Wu Y, et al. Neuregulin-1 administration protocols sufficient for stimulating cardiac regeneration in young mice do not induce somatic, organ, or neoplastic growth. *PLoS One*. 2016;11:1-20.
33. Haller C, Friedberg MK, Laflamme MA. The role of regenerative therapy in the treatment of right ventricular failure: a literature review. *Stem Cell Res Ther*. 2020;11:1-9.
34. Mendes-Ferreira P, De Keulenaer GW, Leite-Moreira AF, Br as-Silva C. Thera- peutic potential of neuregulin-1 in cardiovascular disease. *Drug Discov Today*. 2013;18:836-42.

35. D'Uva G, Aharonov A, Lauriola M, Kain D, Yahalom-Ronen Y, Carvalho S, et al. ERBB2 triggers mammalian heart regeneration by promoting cardiomyocyte dedifferentiation and proliferation. *Nat Cell Biol*. 2015;17:627-38.

SUPPLEMENTAL DATA

APPENDIX E1. METHODS

RNA Sequencing

For RNA sequencing analysis, samples were used of rats that were analyzed for the characterization study (time point 4 and 8 weeks after surgery). RNA was extracted from the right ventricular free wall, in 3 biological replicates of 800 ng each. After quality control, the RNAseq library was prepared using the TruSeq Ribo Gold kit (Illumina). The library was sequenced on 2 HiSeq4000 lanes (Illu-mina). Adapter and polyA sequences and low-quality nucleotides were removed using BB Tools Decontamination Using Kmers (BBDuk). Trimmed reads were mapped against the Rnor_6.0 rat genome using Spliced Transcripts Alignment to a Reference (STAR), and high-throughput sequence analysis count (htseq-count) was used to deter- mine read counts. After quality control with fast quality control (FastQC), biological replicates were averaged, followed by differential expression analysis using the DE- Seq2 package (PMID: 25516281). Differentially expressed genes were included at cutoffs of >1 log2-fold change and false discovery rate (FDR)-adjusted *P* value < .05. Kyoto Encyclopedia of Genes and Genomes (KEGG) pathway and gene ontology analyses were conducted using Database for Annotation, Visualization, and Integrated Discovery (DAVID).

Principal component analysis was performed on rlog-normalized RNAseq data using the DESeq2 package. The first 2 principle components (PCs), PC1 and PC2, are reported in the graph on x- and y-axes, respectively (Figure E1*A*).

Differential expression analysis was performed using the DESeq2 package. *P* values were corrected for multiple testing using the FDR method of Benjamini–Hochberg (FDR< 0.05).

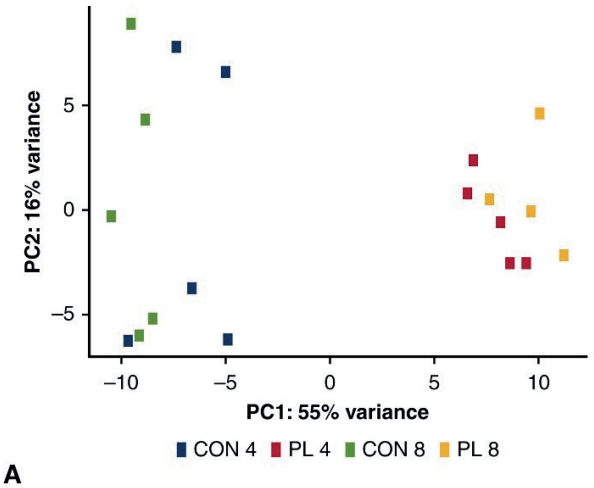

A

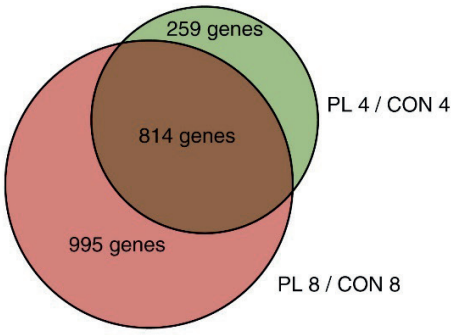

GO Term	*P* value
1. Cell division	$7.80e^{-04}$
3. Endosome	$7.70e^{-03}$
1. Cell-cell adhesion	$2.80e^{-07}$
2. Stress response	$1.00e^{-02}$
3. Nucleotide-binding	$9.00e^{-07}$
4. EGF-like domain	$1.70e^{-04}$
1. Immunity	$9.20e^{-11}$
2. Response to virus	$3.70e^{-05}$
3. Pleckstrin homology-like domain	$2.50e^{-05}$
4. cell-cell adherens junction	$6.20e^{-04}$
5. Glycoportein	$6.70e^{-09}$

B

Figure E1. A) Principal component (*PC*) analysis clustered the right ventricle (RV) by pressure load (*PL*). **B**) Comparison of differentially expressed genes in PL versus control (*CON*) between 4 and 8 weeks identified genes involved in cell division to be involved at 4 weeks. Statistical analysis: see para- graph "RNA Sequencing" in Appendix E1. *GO*, Gene ontology; *EGF*, epidermal growth factor.

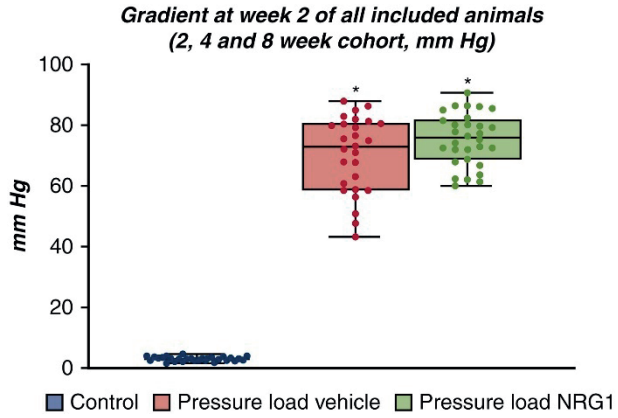

Figure E2. Gradient at week 2 of all included animals. *Red bars* represent pressure load (PL) vehicle rats, *green bars* represent PL neuregulin-1 (*NRG1*) rats, *blue bars* represent control rats. *P* values: week control versus PL vehicle: <.001; control versus PL NRG1:<.001; PL vehicle versus PL NRG1: .468. The *lower and upper borders of the box* are the lower and up- per quartiles. The *middle horizontal line* represents the median. The *whiskers* are the minimum and maximum values. *Dots* in the box-and-whisker dot plots represent individual measurements. **P* < .05 compared with control.

Table E1. Sequence of primers used for quantitative real-time polymerase chain reaction

	Sequence forward primer	Sequence reverse primer
GADPH	TCTCTGCTCCTCCCTGTTCTA	TACGGCCAAATCCGTTCACA
Nppa	ATGGGCTCCTTCTCCATCAC	TCTACCGGCATCTTCTCCTC
Nppb	CTCCTATCCTCTGGGAAGTC	CCGATCCGGTCTATCTTGTG
Timp-1	AGAGCCTCTGTGGATATGTC	CTCAGATTATGCCAGGGAAC
HO-1	CAGAGGGTGACAGAAGAGGCTAA	CTGGTCTTTGTGTTCCTCTGTCAG
MCAD	CCGTTCCCTCTCATCAAAAG	ACACCCATACGCCAACTCTT
Glut1	GCTTTGGCAGGCGGAACT	AGCACGGCAGACACAAAGG
Runx1	AACCCTCAGCCTCAAAGTCA	GGGTGCACAGAAGAGGTGAT
Dab2	CTCAGCGCATGACTCCATAG	CTGAAGACTTAGCGGTCCTC
Myh7	ATCCTCATCACCGGAGAATC	CCCAATGGCAGCAATAACAG
Myh6	GCGTGTCATCCAGTACTTTG	GGTGCCCTTGTTTGCATTAG

GADPH, Glyceraldehyde-3-phosphate dehydrogenase; *Npp*, natriuretic pro-peptide; *Timp-1*, metallopeptidase inhibitor 1; *HO-1*, heme oxygenase; medium-chain acyl-CoA de- hydrogenase; *Glut1*, glucose transporter 1; *Runx1*, runt-related transcription factor 1; *Dab2*, disabled adaptor protein 2; *Myh*, myosin heavy chain.



Chapter 4

Conserved *NPPB*+ Border Zone Switches From MEF2- to AP-1–Driven Gene Program

Karel van Duijvenboden*, Dennis E.M. de Bakker*, Joyce C.K. Man*, Rob Janssen*, Marie Günthel*, Matthew C. Hill, Ingeborg B. Hooijkaas, Ingeborg van der Made, Petra H. van der Kraak, Aryan Vink, Esther E. Creemers, James F. Martin, Phil Barnett, Jeroen Bakkers, Vincent M. Christoffels

*these authors contributed equally.

Circulation. 2019; Sep 9, 140(10):864–879.

ABSTRACT

Background: Surviving cells in the post-infarction border zone are subjected to intense fluctuations of their microenvironment. Recently, border zone cardiomyocytes have been specifically implicated in cardiac regeneration. Here, we defined their unique transcriptional and regulatory properties, and comprehensively validated new molecular markers, including *Nppb*, encoding B-type natriuretic peptide, after infarction.

Methods: Transgenic reporter mice were used to identify the *Nppb*-positive border zone after myocardial infarction. Transcriptome analysis of remote, border and infarct zones and of purified cardiomyocyte nuclei was performed using RNA-sequencing. Top candidate genes displaying border zone spatial specificity were histologically validated in ischemic human hearts. Mice in which *Nppb* was deleted by genome editing were subjected to myocardial infarction. Chromatin accessibility landscapes of border zone and control cardiomyocyte nuclei were assessed using ATAC-sequencing.

Results: We identified the border zone as a spatially confined region transcriptionally distinct from the remote myocardium. The transcriptional response of the border zone was much stronger than that of the remote ventricular wall, involving acute downregulation of mitochondrial oxidative phosphorylation, fatty acid metabolism, calcium handling and sarcomere function, and the activation of a stress response program. Analysis of infarcted human hearts revealed that the transcriptionally discrete border zone is conserved in humans, and led to the identification of novel conserved border zone markers including *NPPB*, *ANKRD1*, *DES*, *UCHL1, JUN* and *FOXP1*. Homozygous *Nppb* mutant mice developed acute and lethal heart failure after myocardial infarction, indicating B-type natriuretic peptide is required to preserve post-infarct heart function. ATAC-seq revealed thousands of cardiomyocyte lineage-specific MEF2-occupied regulatory elements that lost accessibility in the border zone. Putative injury-responsive enhancers that gained accessibility were highly associated with AP-1 binding sites. Nuclear c-Jun, a component of AP-1, was observed specifically in border zone cardiomyocytes.

Conclusion: Cardiomyocytes in a discrete zone bordering the infarct switch from a MEF2-driven homeostatic lineage-specific to an AP-1-driven injury-induced gene expression program. This program is conserved between mouse and human, and includes *Nppb* expression, which is required to prevent acute heart failure after infarction.

Clinical Perspective

What is new?

- Mouse myocardial infarctions are surrounded by an *Nppb*-positive border zone, which contains cardiomyocytes that are transcriptionally and epigenetically distinct from remote myocardium.
- Infarcted human hearts contain similar border zone cardiomyocytes that share expression of novel border zone markers including *NPPB*, *JUN*, *DES* and *ANKRD1*, and are mainly located at the sub-endocardium adjacent to the infarction.
- *Nppb* knock-out mice are unable to recover from an ischemic injury, illustrating the importance of processes that occur in the border zone.
- *Nppb*-positive border zone cardiomyocytes undergo a profound transcriptional and epigenetic reprogramming, switching from a MEF2 to an AP-1-responsive gene program.

What are the clinical implications?

- Using *Nppb* knock-out mouse we illustrate that processes activated in the border zone are required for recovery after myocardial infarction, which may be applicable to patients that suffered an ischemic injury.
- Here, we present novel border zone markers that can be used in clinical research and are candidate biomarkers for assessing infarction severity and state.
- Since border zone cardiomyocytes have recently been implicated as a source for cardiomyocyte regeneration, the identification of the human sub-endocardial border zone might lead to novel strategies focussing on stimulating these cardiomyocytes to regenerate the injured heart.

Keywords: Myocardial infarction, border zone, remote myocardium, epigenetics, ATAC-seq, RNA-seq

INTRODUCTION

After acute myocardial infarction (MI), the compromised ischemic muscle is lost and replaced by scar tissue, impairing heart function. The mammalian heart is considered to be an essentially post mitotic organ with negligible regenerative capacity,[1] with cardiomyocyte (CM) hypertrophy serving as the principle adaptive response to injury. The infarct zone is usually highly irregular in shape, infiltrating the adjacent spared myocardium,[2] which is comprised of a mixture of viable, though severely affected CMs.[3] The increase in CM cell size and reduction in capillary density is greater in the region bordering the infarct zone than in the remote area. CMs closer to the injury show hallmarks of dedifferentiation, sarcomere depletion and decrease in mitochondrial volume compared to remote CMs.[4, 5] Molecular analyses of samples taken from different locations of the infarcted wall have consistently shown the existence of transcriptional differences between myocardium proximal and distal to the infarct.[6-9]

Pragmatically, the proximal-distal axis of the infarcted ventricular wall has been divided in an infarct zone (IZ), an infarct boundary zone or border zone (BZ; perfused but hypocontractile), and a remote zone (RM; perfused).[10] The BZ remodels electrophysiologically and can be the origin of ventricular tachycardia, which are a common cause of sudden cardiac arrest in patients after MI, which originate from the BZ.[11-13] Furthermore, the BZ may be more susceptible to additional ischemic episodes, and its hypocontractile property seemingly expands after MI to involve contiguous myocardium that progressively loses contractile function as the heart remodels.[10] Recently, the BZ myocardium received renewed attention with respect to its potential role in post-injury cardiac regeneration. Zebrafish efficiently regenerates the heart after injury, replacing the infarcted tissue by proliferating CMs, which are mainly located in the zone bordering the injury.[14] Furthermore, in transgenic mouse models of enhanced regeneration, CM proliferation is primarily seen in the region proximal to the infarct, i.e. the putative BZ.[15-18] Here, we identified and characterized a transcriptionally distinctive *NPPB*-expressing BZ conserved in mouse and human, and observed a role for *Nppb* in the survival after MI. Our findings indicate a CM lineage-specific MEF2-driven regulatory program is replaced by an AP-1-driven stress-responsive program in BZ CMs.

METHODS

An expanded methods section is available in the Supplemental Material. The data, analytic methods, and study materials will be made available by the authors to other researchers for purposes of reproducing the results or replicating the procedure.

Mice

Animal care and experiments conform to the Directive 2010/63/EU of the European Parliament. All animal work was approved by the Animal Experimental Committee of the Academic Medical Center, Amsterdam, and was carried out in compliance with the Dutch government guidelines.

BAC-Nppb-Katushka,[19] *Myh6-MerCreMer*[20] and *nTnG* (JAX stock #023035) mice were bred on the FVB/N background. Tamoxifen (20 mg/kg) was administrated i.p. one week prior to t=0 and repeated the two following days. Myocardial infarction was performed. Two independent *Nppb*-deficient mouse lines were generated by CRISPR/Cas9-mediated genome editing in FVB oocytes.

Human material

Paraffin embedded infarcted human heart tissue from 3 individuals that had died due to myocardial infarction were retrieved from the pathology archive of the University Medical Center Utrecht. Material was handled in a coded manner that met the criteria of the Code of Conduct used in the Netherlands for the responsible use of human tissue in medical research (www.federa.org/codes-conduct). Collection of the archive material was approved by the local biobank review committee (protocol 15–252).

Statistical analysis

Differential expression analysis was performed using the DESeq2 package. [21] P-values were corrected for multiple testing using the false discovery rate (FDR) method of Benjamini-Hochberg ($p<0.05$).

To compare the survival distributions between $Nppb^{-/-}$ mice and wildtype littermates after MI we used a log-rank test ($p<0.05$).

Motifs detected with HOMER were considered enriched when $p<1^{-10}$ was reached, as recommended by the authors (http://homer.ucsd.edu/homer/).[22]

To determine whether ATAC-seq peak categories were differentially bound by TFs, we counted the number of ChIP-seq tags present per peak. To test for differences between groups a one-way ANOVA was performed, using a multi comparison procedure post hoc Games-Howell test ($p<0.05$). We performed a log-transformation on the ChIP-seq count data when the counts were not normally distributed.

Data Availability

All RNA-seq and ATAC-seq data have been deposited at the Gene Expression Omnibus under the accession number (GSE110209); as well as PCM-1 (GSE128034) and *Nppb*$^{-/-}$ (GSE128196) RNA-seq data. An Excel file has been made available in the online-only Data Supplement that contains tables with candidate BZ genes using various criteria.

RESULTS

Identification of three transcriptionally distinct zones in the injured ventricular wall

To assess the spatial distribution of the transcriptome in the injured heart, we permanently ligated the left anterior descending coronary artery (LAD) in 10-12 week old mice. *Col1a1* and *Tnni3* expression patterns typically marked the infarct zone (IZ) and myocardium, respectively. *Nppa* expression, marking a border zone (BZ) region[19] was evident in the area adjacent the infarcted area and overlapping the spared myocardium (Figure 1A, B). The *Nppa*-negative myocardium was considered to be the remote myocardium (RM). The spatial analysis of the Katushka and *Nppa/Nppb* patterns in *BAC-Nppb-Katushka* mice 7 days post infarction (dpi) revealed that the transition of expression between the BZ and RM was relatively sharp rather than gradual, indicating the BZ is a discrete region adjacent to the infarct. Moreover, the size of the BZ was relatively constant across varying infarct sizes (Figure 1C). The thickness (from IZ to RM) of the *Nppa/Nppb*-positive zone was between 0.2 and 0.7 mm (Figure 1B, C and data not shown). The discreteness and sizes of the zones made it possible to isolate each zone by microdissection for characterization by RNA-seq analysis. Three independent samples of RM, BZ and IZ of 3, 7, and 14 dpi hearts were microdissected and the *Nppa* expression level in the microdissected tissues was compared to sham-operated left ventricular tissue to confirm correct dissection and isolation of the respective zones (Figure 1D). Using unsupervised principal component analysis, segregation between samples by time-points and zones was observed. Based on overall expression patterns, all sham samples clustered together, followed by RM, BZ and IZ. Interestingly, samples harvested three days after LAD were separated from both other time points, which were more similar to each other (Figure 1E).

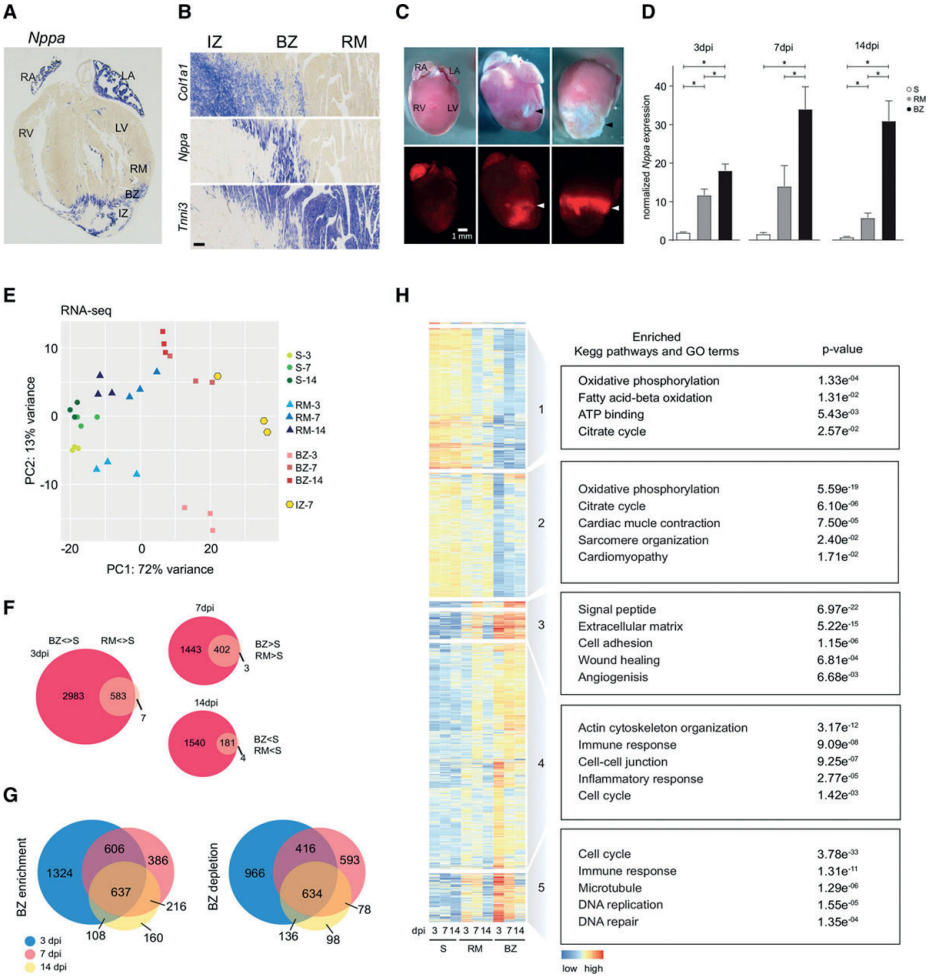

Figure 1. RNA-sequencing identifies the border zone based on a distinct expression profile on microdissected LV tissue. (**A**) *In situ* hybridization analysis showing the expression pattern of *Nppa* in the 7 dpi heart. (**B**) Spatial expression patterns and corresponding *in situ* hybridization of three references genes *Col1a1*, *Nppa*, and *Tnni3* at 7 dpi. *Nppa* expression highlights the BZ. (**C**) Light (upper row) and fluorescent microscopic pictures (lower row) of hearts of 7 dpi BAC-Nppb::Katushka mice, revealing the relatively sharply defined BZ (white arrowheads) around both a small and large infarct area (black arrowheads). (**D**) Following microdissection of the BZ and RM, *Nppa* expression was assessed by qPCR and compared to control sham hearts. Values are means ± SEM; * $p<0.05$. (**E**) Principal component analysis (PCA) clustered the microdissected LV tissue by zone and time post-injury. Samples from different zones and time-points are designated by colors. (**F**) Comparison of differentially expressed genes of BZ (n=3) and RM (n=3) to sham (n=3) at 7 dpi showed that majority of differentially expressed genes originate from the BZ. (**G**) The set of differentially expressed genes of BZ tissue was cross-referenced with data obtained from infarcted LV tissue to highlight those differentially expressed genes that potentially play a part in the cardiomyocyte response to injury. (**H**) Functional annotation heatmap of sham, RM, and BZ at different time-points (n=3 per time-point per tissue) based on differentially expressed genes sham vs BZ. RA = right atrium; LA = left atrium; RV = right ventricle; LV = left ventricle; RM = remote zone; BZ = border zone; IZ = infarct zone.

Characterization of the transcriptional response of the BZ

Comparison of the transcriptomes of the BZ and RM at different time points to those of sham tissue showed that the majority of differentially expressed genes (3563) originated from the BZ (2983 genes), whereas the contribution of differentially expressed genes solely in the remote ventricular wall was minor (Figure 1F Supplemental Figure 1). The direction of change of differentially expressed genes in RM and BZ was the same, i.e. either up in both zones or down in both zones, indicating that the injury response of the BZ and RM are comparable, but much more extensive in the BZ (Supplemental Figure 1). The early response involved the highest number of genes and stabilized thereafter as shown by increased gene overlap (Figure 1G). Analysis of changes in KEGG pathways and GO terms between different time points and zones was concordant with the course of pathology, for example at three days post-injury a dominant inflammatory response was noted (Figure 1H, clusters 3-5). In the BZ downregulated genes were enriched for CM-specific genes (sarcomere, calcium handling), whereas upregulated genes were enriched for those known to be expressed in non-CMs, compatible with the invasion of immune cells and activation of fibroblasts after injury.[12, 23, 24] Moreover, a strong cell-cycle activation response, probably derived from activated fibroblasts and immune cells, was observed at 3 dpi, (Figure 1H, cluster 5).

Cluster analysis revealed a set of 165 transcription factor encoding genes induced in the BZ (Supplemental Figure 2 and Excel-file table 1 in the online-only Data Supplement). These include *Jun* and *Fosl2*, encoding components of the activator protein 1 (AP-1) complex that regulates a wide range of cellular processes, including cell proliferation, death, survival and differentiation.[25-27] Furthermore, a number of genes (587) encoding excreted proteins were induced in the BZ that are candidate biomarkers (*e.g. Clu*, *Gpx3*; Excel-file table 2 in the online-only Data Supplement).

The (post-MI) ventricular wall is composed of many different cell-types.[9, 12, 23, 24, 28] To gain insight into the CM-specific response to injury, we purified CM nuclei from the BZ and RM using PCM-1-mediated purification (Figure 2 and Supplemental Figure 3A, B). Compared to whole tissue samples, PCM-1 sorted samples were enriched for cardiac genes and showed a low expression of genes specifically expressed by fibroblasts, endothelial cells and leukocyctes (Supplemental Figure 3C). As also seen for the RNA-seq of whole tissue, the majority of significantly differentially expressed genes originates from cells of the BZ (Figure 2A). Genes upregulated in BZ CMs include the known markers *Nppa* and *Nppb*.

We compared the BZ and RM PCM-1+ nuclear RNA-seq data with those obtained from adult CMs from uninjured hearts[29] using unsupervised hierarchical clustering (Figure 2C). Samples from the RM clustered together with CMs from uninjured heart, whereas the BZ samples clusters alone. GO term analysis of each gene cluster revealed that CMs in the BZ downregulate genes involved in processes like oxidative phosphorylation, citrate cycle and lipid metabolism, while they upregulate genes involved in regulating transcriptional

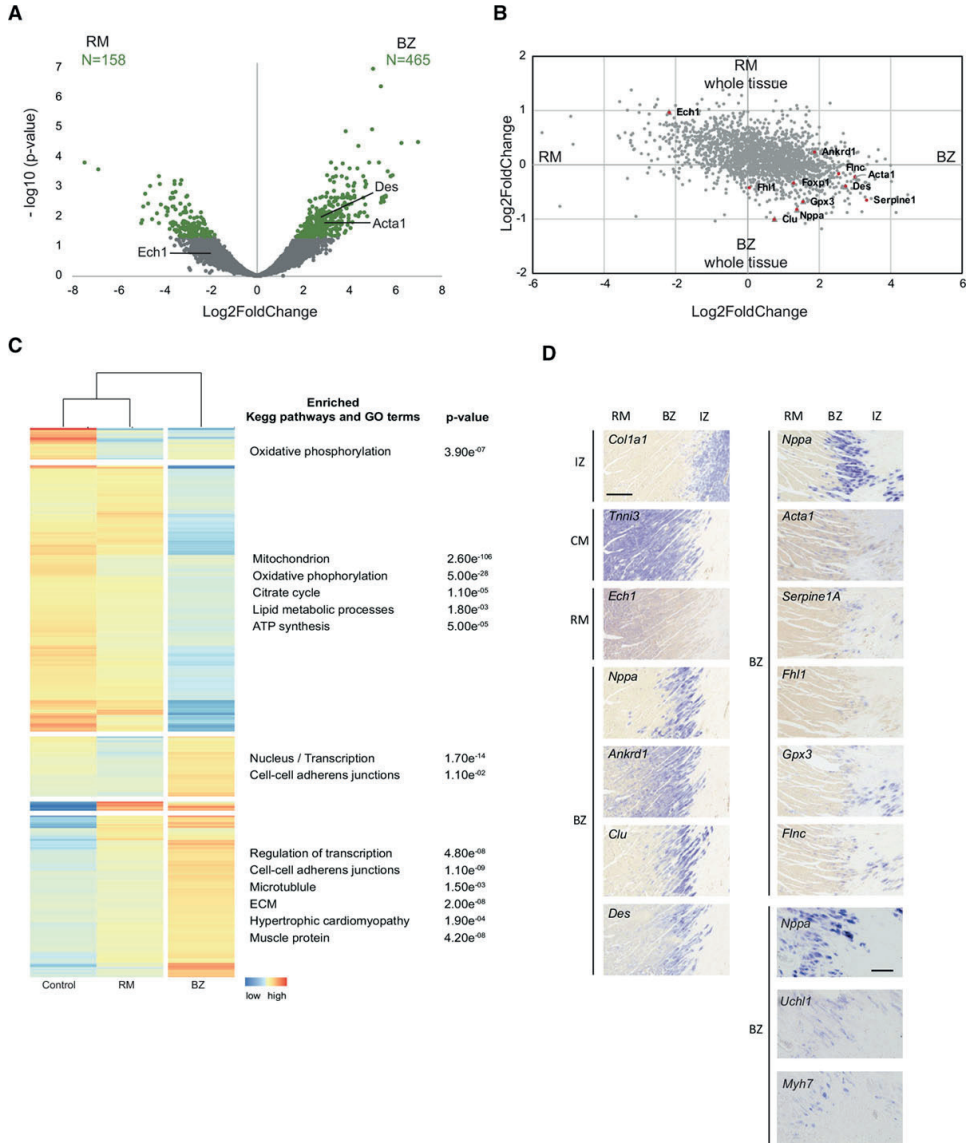

Figure 2. Gene expression in border zone cardiomyocytes. (**A**) Vulcano plot showing cardiomyocyte nuclear transcripts differentially expressed between remote myocardium (RM; n=2) and border zone (BZ; n=3) tissues. Green dots indicate significantly differentially expressed genes (p-adjusted for multiple testing: FDR< 0.05). (**B**) Scatter plot of differentially expressed genes (Log2FoldChange) between the RM and BZ samples. (**C**) Unsupervised functional annotation heatmap of control[29], RM and BZ samples. Gene ontology analysis was performed on each cluster. (D) *In situ* hybridization shows the three reference genes *Col1a1* for the infarct zone (IZ), *Tnni3* for cardiomyocytes and *Ech1* for remote myocardium (RM). *Nppa* marks the border zone (BZ). New markers of the BZ resemble the expression pattern of *Nppa*. Scale bar indicates 0.5 mm and 0.1 mm (right, lower panel). CM indicates cardiomyocyte; and ECM, extracellular matrix.

regulation, cell-cell adherens junctions and hypertrophy. Cross-analysis with dissected BZ and PCM-1 sorted BZ samples indicated that *Clu*, *Gpx3, Flnc, Des, Fhl1, Serpine1, Synpo2l* and *Ankrd1* are bona fide BZ markers confirmed in both experiments (Figure 2B). Using *in situ* hybridization (ISH), the BZ CM-specific induction of several markers at 7 dpi was validated (Figure 2D). Information regarding their function is provided in the online-only Data Supplement. Taken together, we present a rich dataset analysis which can be used as a starting point for future studies on BZ restricted processes.

BZ CMs partially revert to a neonatal CM state

To gain insight into the state of differentiation of the BZ and RM, we compared our tissue and PCM1+ CM RNA-seq data sets with those from isolated neonatal and adult CMs.[29] The BZ profiles clustered with those of neonatal CMs (Supplemental Figure 4A). The RM and sham profiles clustered with those of adult CMs, indicating that RM does not dedifferentiate significantly after injury, in keeping with previous observations.[30] Scatter plot and GoTerm analysis (Supplemental Figure 4B) revealed that genes expressed at lower levels in neonatal as well as BZ CMs are involved in oxidation-reduction processes and lipid metabolism. Genes expressed at higher levels in neonatal CMs and BZ CMs control transcription and cell-cell adherent junctions. However, many genes expressed at higher levels in neonatal CMs were not upregulated in BZ CMs, including genes involved in cell cycle regulation. Taken together, BZ CMs partially revert to the immature state of neonatal CMs.

Identification of the BZ in human infarcted hearts

Next, we addressed whether a conserved transcriptional BZ could be identified in the ischemic human heart. Histological analysis of human cardiac tissue samples from individuals that suffered from MI (n=3) identified areas of coagulation necrosis of CMs, compatible with MI of 1-3 days post coronary artery occlusion, and collagen rich areas, compatible with MI scars of ≥ 2 months old (Figure 3A). The infarcted areas of selected samples were located in the sub-endocardial region of the left ventricle or intraventricular septum. These locations were confirmed by immunostaining against C4d, an excreted complement factor that is specific to necrotic CMs[31] (Figure 3B). Most of the surviving myocardium was found in the compact myocardium, away from the infarcted area, or in oxygenated peri-vascular and sub-endocardial regions (Figure 3A, orange). Areas of surviving myocardium towards the epicardial layer were considered to be RM.

A number of genes with region-specific expression in the murine heart were selected for spatial expression analysis. Most tested BZ-induced genes (*e.g. NPPA, NPPB, ANKRD1, DES, UCHL1, JUN, MYH7, FOXP1*) showed similar expression patterns in the infarcted human hearts, with consistent but low expression in-between the IZ and the RM (Figure 3C, arrows) and around blood vessels with presumed residual blood flow (Figure 3C, stars). Interestingly, strongest expression of the examined genes was observed in the *NPPA*-positive BZ CMs located in-between the IZ and the endocardium (Figure 3C, D and

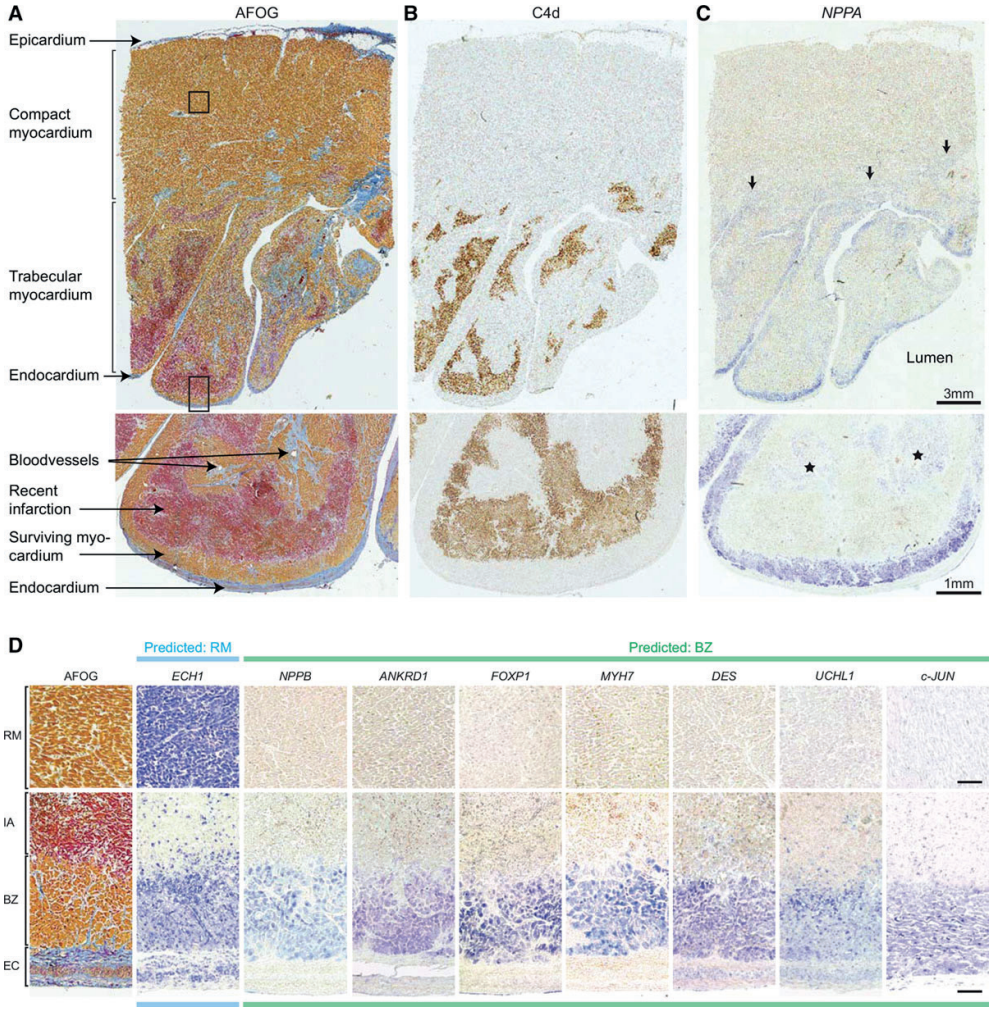

Figure 3. Human ischemic hearts show most pronounced expression of border zone markers in the sub-endocardium. (**A**) Acid fuchsin orange G (AFOG) staining on human heart tissue showing a with a large myocardial infarction. AFOG marks cytoplasm (orange), elastic fibrin (red) and collagen fibrils (blue). Elastic fibrin is indicative of coagulation necrosis, thus revealing a non-transmural recent infarction (red). In addition, collagen depositions suggest previous cardiac insults (blue). Black boxes indicate zoom locations for figure (**D**). (**B**) Anti-C4d antibody staining on a consecutive section marking necrotic cardiomyocytes overlying with the fibrin rich region. (**C**) *In situ* hybridization against *NPPA* on a consecutive section. *NPPA* expression was observed in regions adjacent to the fibrin, including light staining in regions in the compact muscle layer (marked by arrows) and around blood vessels (marked by stars). Most pronounced staining is found at the surviving cells of the sub-endocardium. (**D**) Zoom of the remote myocardium (RM) and the sub-endocardial region, including the injury area (IA), border zone (BZ) and endocardium (EC). *In situ* hybridization on consecutive sections confirmed expression of *ECH1* in RM. Predicted border zone genes showed specific expression in sub-endocardial myocardium. Scale bars, 100 μm.

Supplemental Figure 5A). This strong sub-endocardial expression was observed in all three ischemic heart samples that were investigated (Supplemental Figure 5B-D). The size of the sub-endocardial BZ was consistently around 0.4 mm, similar to the BZ size in murine hearts. The RM-specific, sarcomeric genes *ECH1* and *TCAP*, showed strong expression in the RM and weak expression in the *NPPA*-positive sub-endocardial BZ region (Figure 3D and Supplemental Figure5A).

The histological analysis identified regions that experienced a recent MI (1-3 days old, C4d and fibrin-positive) and regions with older fibrotic scars (collagen positive, C4d negative). A consistently higher expression of BZ genes was observed in CMs in close proximity to recent infarcted areas (fibrin positive) compared to their expression levels in CMs close to older collagen rich scars within the same heart (Supplemental Figure 6), indicating that expression of BZ genes in human MI hearts is temporally regulated. We conclude that in the ischemic injured human heart, a distinct BZ is formed that is most pronounced at the sub-endocardial location, comprised of CMs with high expression of BZ markers involved in processes such as the stress response (*JUN*, *JUNB*, *ANKRD1*), development and proliferation (*NPPA*, *NPPB, FOXP1*) and muscle structure (*MYH7*, *DES*), and reduced expression of metabolic and sarcomeric genes (*ECH1*, *TCAP*). Based on the similar presence of these marker genes in the injured murine heart, we conclude that these injury responsive processes are evolutionarily conserved.

Nppb is required during recovery from myocardial infarction

To gain insight into the role of the BZ-induced transcriptional program, we investigated the role of the conserved BZ gene *Nppb* after MI. We generated two independent *Nppb* knockout mouse lines using CRISPR/Cas9 genome editing technology (Figure 4A and Supplemental Figure 7). To assess to what extent our *Nppb* knockout model is affected we performed RNA-sequencing of adult left ventricles of wildtype (n=4) and $Nppb^{-/-}$ mice (n=4). Consistent with previous findings,[32] *Nppa* was significantly upregulated (Figure 4B). Surprisingly, only 27 additional genes were mildly differentially expressed in $Nppb^{-/-}$ mice (Figure 4C). We could not identify any fibrosis markers among the differentially expressed genes in $Nppb^{-/-}$ mice, did not observe fibrotic lesions (Supplemental Figure 8C, D) and did not observe differences in left ventricular systolic and diastolic function between genotypes (Figure 4D, E and Supplemental Figure 8E-L).

To assess the function of *Nppb* after injury, we subjected $Nppb^{-/-}$ mice and wildtype littermates to MI surgeries. $Nppb^{-/-}$ mice of both independent transgenic lines died more frequently shortly after MI due to acute heart failure (Figure 4F and Supplemental Figure 7A). $Nppb^{-/-}$ mice that did not die of rupture presented shortness of breath, excess fluid in chest cavity and fluid leakage from the nose, blood coagulation in the left atrium (Figure 4H) and white spots were found locally on the lungs (Figure 4I), in line with the occurrence of acute heart failure. These heart failure symptoms were not observed in wildtype mice after MI. No differences

between genotypes were observed in relative heart weight, left ventricular function, or left atrial dimensions at 1 dpi between the two genotypes (Figure 4D, E and Supplemental Figure 8B, E-J). Left ventricular diastolic parameters at 3 dpi showed a significant decrease in left ventricular internal diameter (LVID) and left ventricular volume in *Nppb*$^{-/-}$ mice in diastole compared to wildtype (Supplemental Figure 8K, L).

Both before and after MI, we did not find differences between genotypes in ventricular expression levels of myocardial hypertrophy markers (*Myh7* and *Atp2a2* (SERCA2A)) or fibrosis markers (*Col1a1* and *Pstn)* (Figure 4J). A more detailed description of the data is provided in the in the Supplemental Material. Together, these findings suggest that *Nppb*$^{-/-}$ mice do not show a baseline phenotype but die 1-3 days after MI due to acute heart failure, indicating the requirement of induced *Nppb* expression to survive acute cardiac injury. This illustrates the importance of BZ-induced gene program after MI.

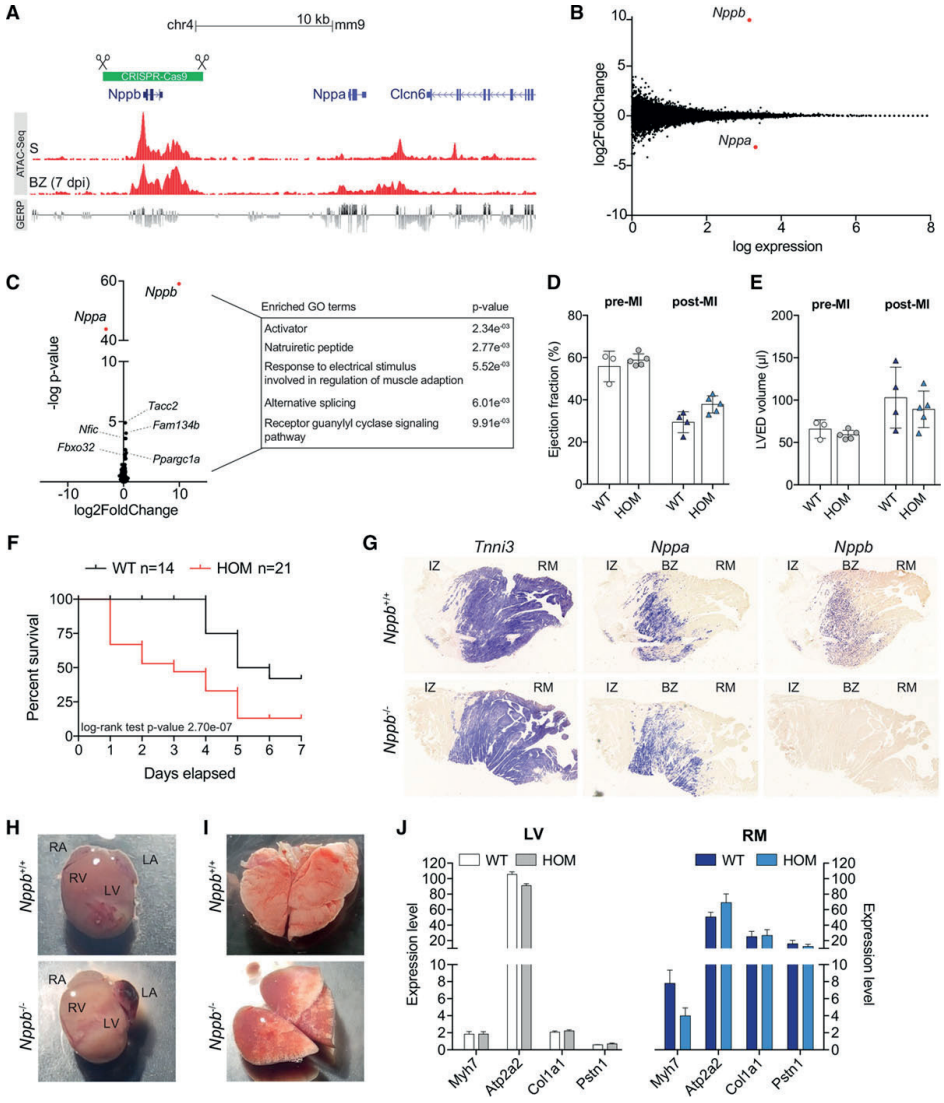

Figure 4. ***Nppb*** **is required during recovery of myocardial infarction.** (**A**) Using CRISPR/Cas9 genome editing technology *Nppb* was targeted. (**B**) MA plot showing approximately 15.000 transcripts detected in wildtype (WT) LV (n=4) and *Nppb*$^{-/-}$ (HOM) LV (n=4). *Nppa* is significantly upregulated in HOM LV. (**C**) Vulcano plot showing significantly differentially expressed genes in HOM LV (p-adjusted for multiple testing: FDR<0.05). Included gene ontology analysis of several genes shown in the vulcano plot (**D, E**) Echocardiographic parameters showing ventricular function: ejection fraction (EF) and left ventricular end diastolic volume (LVED) pre- (WT n=3; HOM n=5) and post-MI (WT n=4; HOM n=5) at 7 dpi. (**F**) Kaplan-Meier survival curve of HOM mice (n=21) and wildtype littermates (n=14) showed significant difference in survival (log-rank test p=2.70e-07). (**G**) *In situ* hybridization analysis showing the expression pattern of *Tnni3*, *Nppa* and *Nppb* in HOM mouse and wildtype at 7 dpi. (**H, I**) Whole heart and lung of a HOM mouse presenting acute heart failure and a wildtype. (**J**) Following microdissection of RM (WT n=6; HOM n=6), expression of hypertrophy markers (*Myh7* and *Atp2a2* (SERCA2A)) and fibrosis markers (*Col1a1* and *Pstn*) were assessed by qPCR and compared to left

ventricular tissue (WT n=6; HOM n=6). Values are means ± SEM. ATAC-seq indicates assay for transposase-accessible chromatin using sequencing; BZ, border zone; dpi, days postinfarction; GERP, Genomic Evolutionary Rate Profiling; IZ, infarct zone; LA, left atrium; LV, left ventricle; MA plot, Bland-Altman plot; MI, myocardial infarction; RA, right atrium; RM, remote zone; and RV, right ventricle.

Dynamic epigenetic landscape in the border zone cardiomyocytes

Chromatin accessibility patterns reveal positions in the genome of actively engaged regulatory DNA elements, *i.e.* promoters, enhancers, repressors and insulators. We assessed how open chromatin states differ across homeostatic (sham) and 4, 7 and 14 dpi BZ CMs *in vivo* using ATAC-seq,[33] a technique sufficiently sensitive to detect these states in the limited number (50,000) of CM nuclei that were isolated from the BZ (Figure 5A). Analysis of the distribution of accessible sites revealed that the majority mapped to intra- and intergenic regions and on average 15,000 to promoters (Figure 5B). In sham-operated mice, promoter accessibility at three different time points overlapped for 86% (Figure 5C), indicating that the experiments performed on these tissues were reproducible and peak calling consistent between samples. Inspection of loci likely to be accessible in CMs confirmed accessible promoters originating from CMs (Figure 5D, E).

To determine the correlation between promoter accessibility and gene expression, we integrated the ATAC-seq data with BZ whole-tissue RNA-seq data. Because of the observed correlation between accessibility of promoters and expression levels of their respective genes (Figure 5F), we analyzed the dynamic temporal changes in promoter accessibility 4, 7 and 14 dpi. A large number of promoters gained or lost accessibility after injury (Figure 5G), which correlated well with the induction (*e.g. Nppa*, *Nppb*) and reduction (*e.g. Ryr2*, *Pln*), respectively, of gene expression in the BZ (Supplemental Figure 9). In contrast, promoters of cell cycle genes and of Hippo-, NRG-, BMP-, and Wnt-signaling, implicated in CM renewal and regeneration, did not show consistent changes in accessibility. Cluster analysis of differentially accessible promoters between the BZ and sham CMs indicated at least 5 temporal patterns of changed accessibility (Figure 5H). A large number of promoters of cardiac lineage-specific genes involved in contraction, sarcoplasmic reticulum, ion handling, calcium signaling became less accessible in the BZ CMs. Promoters of genes involved in angiogenesis and hypoxia response showed an early response but normalized thereafter, whereas other promoters for genes involved in the immune response, wound healing and extracellular matrix became accessible (Figure 5H).

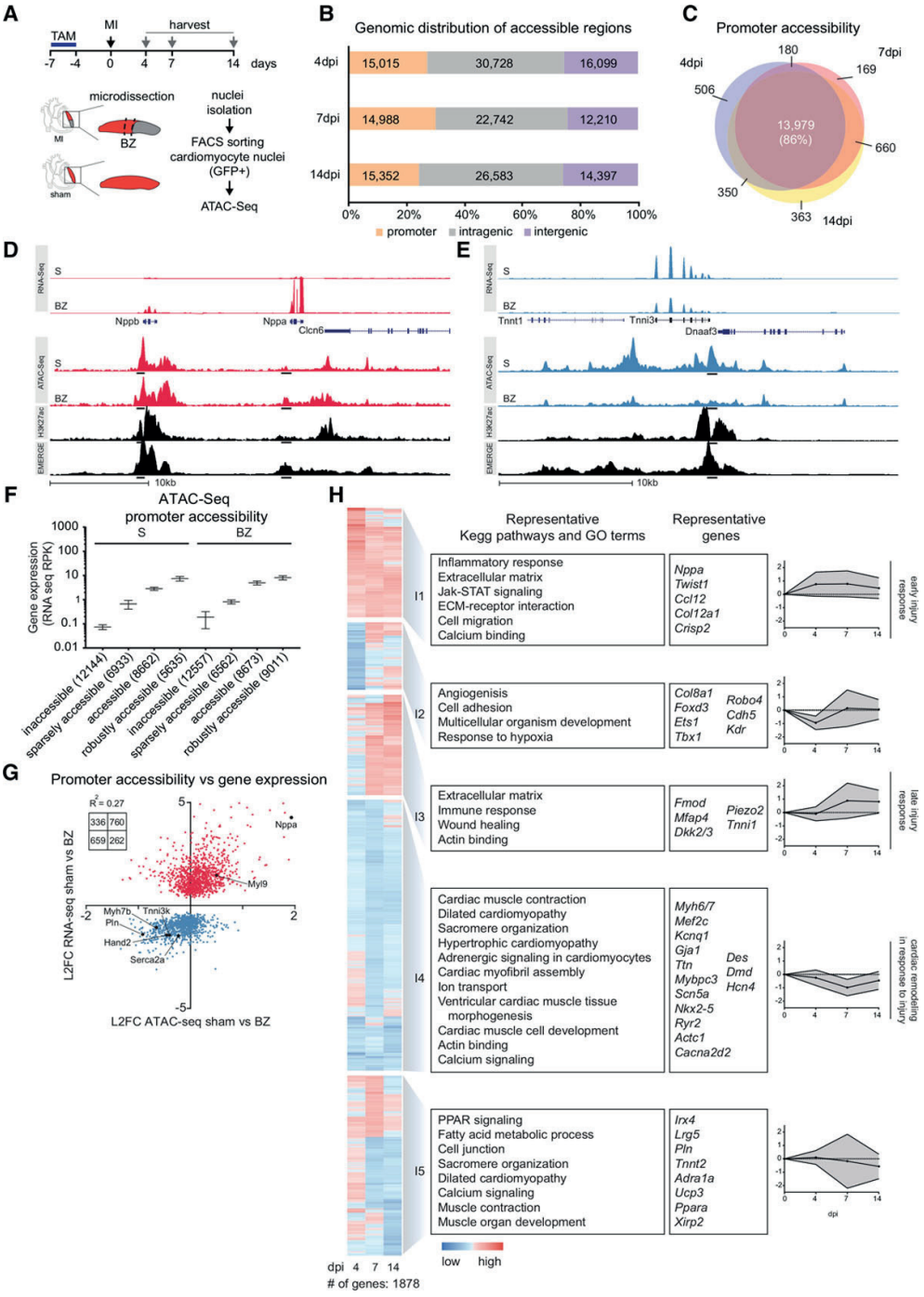

Figure 5. Epigenetic profiling of BZ cardiomyocyte response to injury. (**A**) Schematic of GFP+ nuclei sorting for ATAC-sequencing. (**B**) Analysis of the distribution of accessible sites intra-, intergenic regions, and promoters at different time-points. (**C**) Overlapping promoter accessibility at three time-points in sham operated mice (86%) indicated that performed experiments were reproducible. (**D, E**)

Representative loci containing accessible promoters originating from cardiomyocytes. (**F**) Dotplot plotting average gene expression levels (RNA-seq RPK) as a function of promoter accessibility (as determined by ATAC-seq). (**G**) Scatterplot showing the relation between BZ differential expression (RNA-seq) and BZ differential accessibility of promoters (ATAC-seq) All significantly DE genes (p-value adjusted for multiple testing: FDR<0.05) between sham and BZ at 7 dpi (RNA-seq) were included. Correlation coefficient and number of genes per quadrant are given. (**H**) Functional annotation heatmap showing dynamics of chromatin accessibility of promoters between sham and BZ (n=3 per tissue per time-point). ATAC-seq indicates assay for transposase-accessible chromatin using sequencing; BZ, border zone; DE, differentialexpression; dpi, days postinfarction; GFP, green fluorescent protein; MI, myocardial infarction; RNA-seq, RNA sequencing; RPK, read per kilobase; and TAM, Tamoxifen

In addition to promotor accessibility studies, we investigated accessibility patterns of putative regulatory elements (*e.g.* enhancers). Although the majority of signals remained stable between sham and BZ CMs, we identified thousands of sites that either gain or lose accessibility, indicative of profound changes in gene regulation (Figure 6B). Unchanging accessible sites were enriched for CM-specific H3K27ac signatures, indicating that these represent regulatory elements active in both sham and BZ CMs (Figure 6C). Sites displaying decreasing accessibility were enriched for H3K27ac marks, suggesting that regulatory elements active under homeostatic conditions lose activity after injury. In contrast, emerging sites and sites with increasing accessibility were much less frequently marked by H3K27ac, suggesting that these regulatory elements are not typically active in CMs during normal homeostasis (Figure 6C).

To determine which transcription factors may interact with the accessibility-enriched or -depleted sites at the three time points after MI, we used HOMER to identify enriched sequence motifs potentially recognized by specific transcriptional regulators (Figure 6D, E). Both disappearing sites and sites with decreasing accessibility were highly enriched for motifs recognized by members of the Mef2 transcription factor family, and to a lesser extent by members of the T-box, Meis and Smad (TGFbeta/BMP-signaling) transcription factor families. Members of each of these families are involved in cardiogenesis and CM lineage-specific gene regulation.[34] In contrast, both sites with increasing and emerging accessibility were strikingly enriched for motifs recognized by Jun and Fos family members (Figure 6D, E).[25] In addition, Runx, Erg, Smad, E-box (MyoD), and TEAD recognition sites were enriched.

To gain insight into the temporal pattern of accessibility, we identified 933 chromatin sites differentially accessible at least one time point (Figure 6F and Supplemental Figure 10). We observed that depleted sites, enriched in recognition sites for Mef2 family members, are less accessible during the onset of pathology, whereas at a later stage (14 dpi) partially restored their accessibility. In contrast, sites in clusters 5 and 6, highly enriched in AP-1 recognition sites (Jun/Fos), became more accessible after MI and sustained accessibility until at least 14 dpi.

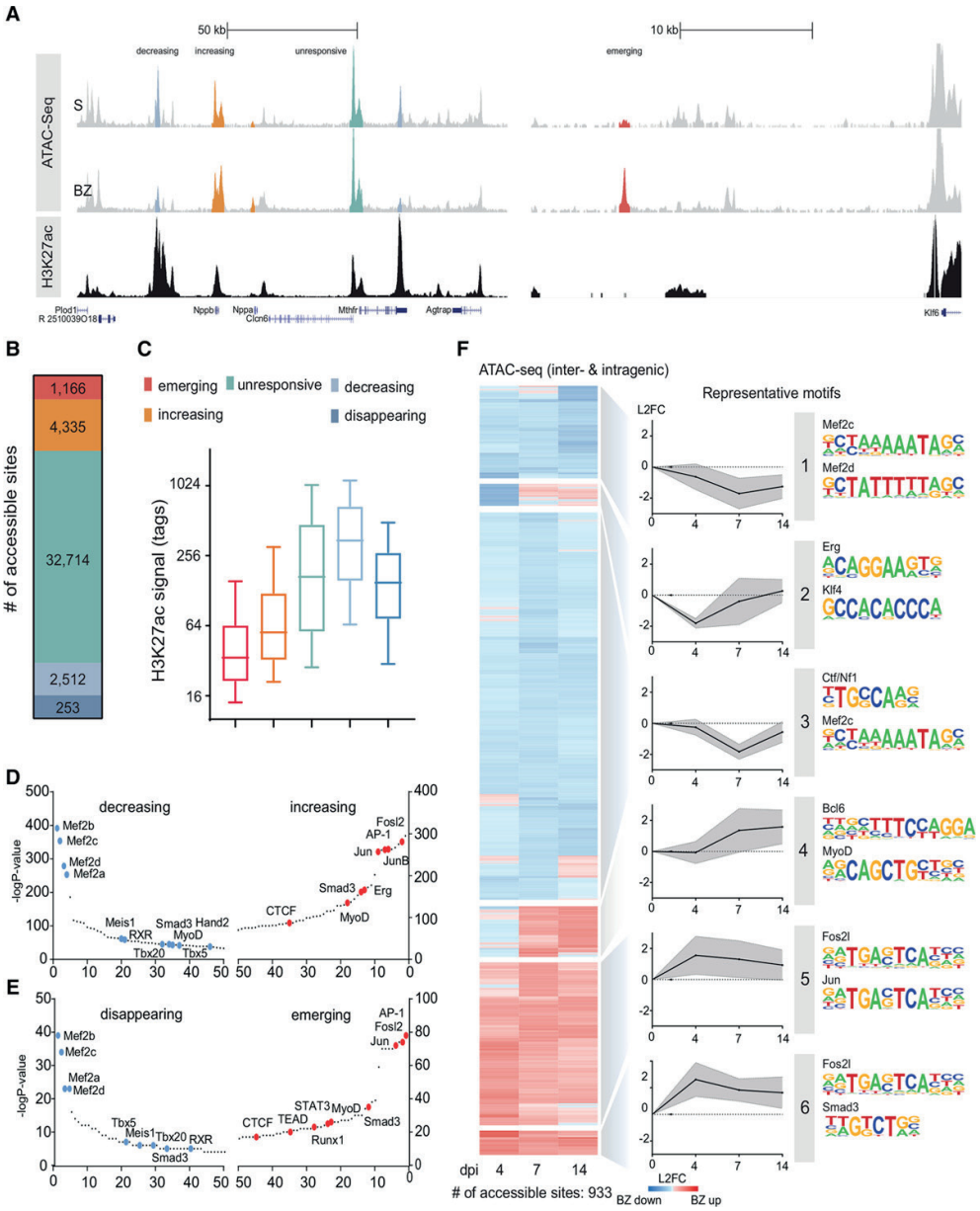

Figure 6. Identification of enriched motifs in BZ cardiomyocytes. (**A**) Representative inter- and intragenic accessibility patterns, reflecting changes in activity of enhancers and other types of regulatory elements in the BZ. (**B**) Distribution of distal accessibility regions across the five classes of dynamic peaks. (**C**) Box plots showing the intensity of ACM H3K27ac signal (total tags) per dynamic peak class. Enriched transcription factor binding motifs in decreasing and increasing (**D**) and disappearing and emerging (**E**) ATAC-seq peaks, as determined by HOMER, were ranked based on their p-value. Motifs involved in maintaining the CM lineage homeostasis such as Mef2c, were no longer accessible, whereas AP-1 binding sites gained accessibility. (**F**) Hierarchical clustering heatmap of distal accessible regions detectable at all time points (n=3 per tissue per time-point) and differentially affected at least 1 time

point. The highest enriched motifs per cluster (as calculated by HOMER) are given. AP-1 indicates activator protein 1; ATAC-seq, assay for transposase-accessible chromatin using sequencing; BZ, border zone; CTCF, CCCTC-binding factor; and dpi, days postinfarction.

To test whether the motif enrichment results correspond to increased binding, we cross-referenced our different ATAC-seq signal classes (increased, maintained, decreased) with available adult cardiac MEF2[35] and myoblast c-Jun[36] ChIP-seq data. We plotted heart MEF2 ChIP-seq tag abundance per ATAC-seq peak group (Figure 7A, B), which shows that regions that become accessible in the BZ have markedly less MEF2 binding. Reduced MEF2 binding could not be attributed to lower expression of *Mef2a*, the main postnatal cardiac isoform,[37] *Mef2c or Mef2d,* as BZ CMs readily expressed these genes (Figure 7E and Supplemental Figure 11E and Excel-file table 3 in the online-only Data Supplement). Likewise, we plotted c-Jun (AP-1 component) ChIP-seq tag abundance (Figure 7C), and find that the BZ-enriched peaks show stronger c-Jun binding activity at all measured timepoints (Figure 7C, D). The expression of AP-1 component genes *Jun*, *Junb*, *Jund*, *Fosl1* and *Fosl2* was increased in BZ CM nuclei compared to RM nuclei (Figure 7E and Supplemental Figure 11E and Excel-file table 3, 4 in the online-only Data Supplement). Furthermore, we detected c-Jun in BZ CM nuclei at 7 and at 14 dpi, but not in CM of RM or of sham operated mice (Figure 7G and Figure 12 in the online-only Data Supplement), and we validated the dependency of several of the stress-response enhancer fragments to c-Jun, (Supplemental Figure 11B-D). These data corroborate the motif enrichment findings, and indicate that the CM specific BZ response is, in part, driven by activated c-Jun.

Taken together, these data suggest that the CM lineage specific program is downregulated after injury in BZ CMs, involving reduced MEF2 interaction with target regulatory sequences, whereas a stress program is induced by, amongst others, induced c-Jun (AP-1) activity in the BZ CM nuclei (Figure 7F).

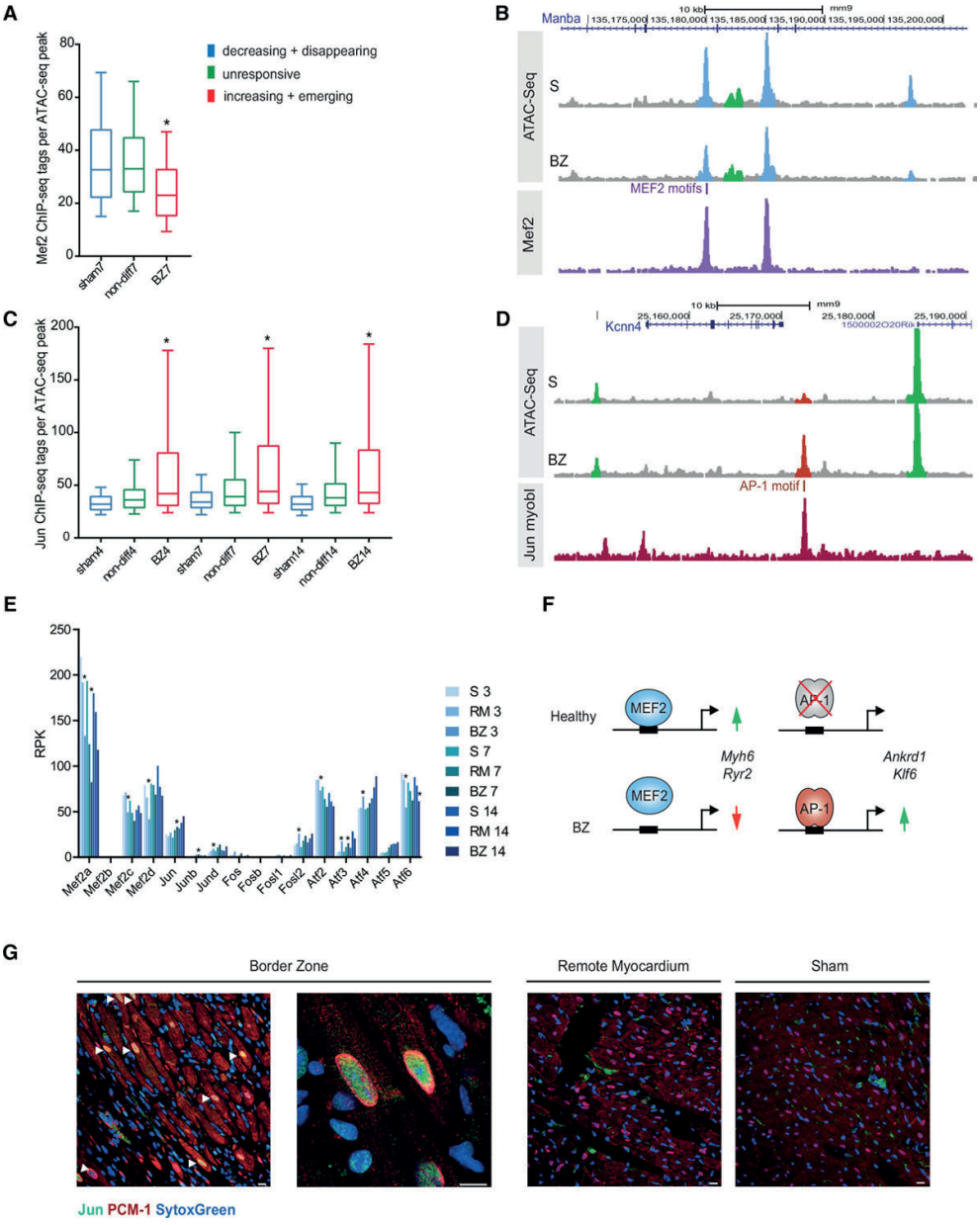

Figure 7. BZ cardiomyocytes are enriched for AP-1 binding motifs. (**A**) Box plots showing the intensity of MEF2 ChIP-seq signal (total tags) per dynamic peak class at 7 dpi. (**B**) Example UCSC browser view of BZ decreasing accessibility regions that overlap with MEF2 ChIP-seq peaks. A MEF2 consensus motif was found and noted for one of the peaks. (**C**) Box plots showing the intensity of Jun ChIP-seq signal (total tags) per dynamic peak class across all measured time points. (**D**) Example UCSC browser view of a BZ emerging accessibility region that overlaps with a Jun ChIP-seq peak, containing a consensus AP-1 motif. (**E**) Average RPK values obtained from whole tissue RNA-seq (n=3 per tissue per time-point) for the members of the AP-1 family of transcription factors and the

Mef2 family of transcription factors (**F**) Cardiac lineage specific transcription binding sites, such as Mef2, whereas accessibility of non-CM lineage typical promoters /genes and enhancers with binding motifs for AP-1 and other stress responsive transcription factors increases. (**G**) Immunohistochemical staining of pericentriolar material 1 (PCM-1), c-Jun, and Sytox Green of BZ, RM, and sham at 7 dpi. Arrowheads indicate c-Jun–positive cardiomyocyte nuclei. Scale bar, 10 μm. *P<0.05 in a 1-way ANOVA. AP-1 indicates activator protein 1; ATAC-seq, assay for transposase-accessible chromatin using sequencing; BZ, border zone; ChIP-seq, chromatin immunoprecipitation sequencing; dpi, days postinfarction; RM, remote myocardium; RPK, read per kilobase; and S, sham.

DISCUSSION

In this study we identified the BZ of the ischemically injured ventricular wall as a transcriptionally discrete compartment distinct from the RM. The observed expression patterns of many novel BZ markers including *Gpx3*, *Clu* and *Ankrd1* closely matched those of *Nppa*, indicating a generalized transcriptional BZ compartment forms around the infarct in the mouse heart. In the BZ and to a much lesser extent in the RM, we observed a striking and immediate downregulation of genes implicated in cardiac muscle contraction, oxidative phosphorylation, mitochondrial activity and fatty acid beta oxidation, all of which are specifically highly active in the mature CM lineage. This genome wide-assessment is in agreement with previous studies in which CMs close to the infarct were found to activate *Nppa* (ANF), *Acta2* (aSMA), and *Runx1*, amongst others, and to show accumulation of lipid droplets, perinuclear sarcomere depletion and glycogen accumulation.[4, 5, 13] These changes, however, may also result from stress mechanisms instead of dedifferentiation in the strict developmental sense. For example, the induction of *Nppa, Nppb* and presumably other genes in adult cardiac stress, often referred to as the activation of the "fetal gene program" is achieved through adult stress regulatory DNA sequences that are different from those that activate *Nppa* and *Nppb* during development.[38]

Adult post MI CMs were reported to not revert back to the neonatal stage.[30] We note, however, that in these studies CMs were isolated from whole heart, which mainly comprises RM CMs, as the BZ is but a small fraction of the total cell population. Both our ATAC-seq data and the PCM-1+ CM nuclear expression profiling data revealed a striking absence of induction of cell cycle and glycolysis genes (Figure 5 and Supplemental Figure 9), which were expected to be induced if BZ CMs would revert to the neonatal stage. Indeed, CM cell cycle activity in the BZ after MI is negligible[15]. Furthermore, promoters of genes for signaling pathway components associated with CM proliferation and cardiac regeneration[14-18] were not induced in BZ CMs. Thus, the BZ CMs downregulate mature CM lineage-specific genes but fail to induce neonatal programs for proliferation and metabolic switching to glycolysis. Interestingly, transgenic mice in which the CM cell cycle is stimulated show CM proliferation after MI preferentially in the BZ,[15-18] suggesting that the dedifferentiated (or

stressed) state the BZ CMs acquire after MI is involved but not sufficient for CM renewal after injury.

B-type natriuretic peptide (BNP), encoded by *NPPB*, is a widely used biomarker for diagnosis and prognosis in patients with acute or chronic heart failure.[39] While *Nppb*$^{-/-}$ mice do not show elevated blood pressure or hypertrophy, they were reported to develop cardiac fibrosis from 15 weeks of age onwards, which was exaggerated in response to pressure overload.[32, 40] Infusion of BNP in mice lead to arrhythmia and calcium handling alterations in the heart.[41] In contrast, local BNP treatment by viral delivery to the heart restored calcium homeostasis in CMs and restored contractility.[42] However, in our mutants we did not observe changed expression of any of the genes implicated in these processes both before and after MI, indicating they are not predisposed to develop heart failure or fibrosis in response to MI. Further analysis will be required to gain insight into the underlying mechanism and possibly secondary effects such as pulmonary vascular remodeling.[43] The acute development of heart failure and death of *Nppb*$^{-/-}$ mice after MI illustrates the importance of a proper injury response by the BZ after MI. We expect many other vital processes to occur in this region and the RNA-seq and ATAC-seq data presented here might form the starting point for their discovery. Furthermore, it may be interesting to assess the relation between BNP levels and vulnerability to develop complications after MI.

ATAC-seq analysis of CM nuclei revealed that sites losing accessibility after MI were marked by CM-specific acetylated H3K27, a marker for active transcription regulatory sequences (*i.e.* enhancers), and were enriched in motifs for binding of MEF2, though to a lesser extent, TBX and MEIS families of transcription factors. The Mef2 family of transcription factors plays an important role during cardiac development and cardiac hypertrophy.[44, 45] *Mef2a* maintains CM differentiation and mitochondrial activity.[37] The reduced accessibility of MEF2-enriched elements in BZ CMs indicates the Mef2-driven program is downregulated, which is in line with the observed reduction of mature state and mitochondrial activity of the BZ CMs. In heart failure-induced enhancers (H3K27ac signals), the MEF2 motif is enriched,[46] compatible with the activation of Mef2 function in hypertrophy.[44, 45] This suggests that BZ CMs respond opposite to stress in heart failure and after MI, and indicate CM lineage-specific enhancers are being inactivated after MI.

Sites that gained accessibility, in contrast, were much less frequently marked by CM-specific H3K27ac, suggesting they were activated *de novo* in response to MI. These sites were highly enriched in motifs for members of the Jun and Fos families of transcription factors.[25] *Jun* and *Fosl2* were found to be required for heart development.[26, 27] A recent study found that in skin wound repair, cells lose homeostatic lineage-specific properties when injury-induced stress-responsive enhancers are activated by factors such as AP-1 that override homeostatic regulatory elements governing lineage specificity.[47] Our data indicate such a mechanism occurs in BZ CMs as well. We observe a massive reduction of accessibility of

CM lineage-specific promoters/genes and enhancers with CM lineage-specific transcription factor binding motifs, whereas accessibility of non-CM lineage typical promoters/genes and enhancers with binding motifs for AP-1, TEAD and other stress-responsive transcription factors increased (Figure 6D-F). The MEF2 and AP-1 motif enrichment results were supported by overlap analysis with available ChIP-seq data and the selective BZ CM nuclear localization of c-Jun (Figure 7).

When the cell cycle is stimulated through cardiac overexpression of for example cyclin D2, Tbx20 or YAP, CM cycling is observed predominantly in the BZ, suggesting that the phenotype of the BZ CMs is favorable for the stimulation of proliferation.[15, 17, 18] In mice, direct or indirect activation of nuclear YAP leads to proliferation of both healthy and post-injury CMs.[16, 46] YAP interacts with TEAD, a DNA-binding transcription factor, to regulate downstream gene expression.[48] ChIP-seq and ATAC-seq data revealed that YAP-TEAD binding sites are enriched for AP-1 binding sites.[46, 49, 50] In breast cancer cells, YAP-TEAD was found to associate with AP-1/JUN/FOS at enhancers controlling proliferation.[50] We speculate that the emergence of AP-1 motif enhancers in BZ CMs associated with activation of a stress-responsive gene program creates a favorable state poised for proliferation to occur when YAP-TEAD signaling is activated experimentally in post-injury CMs (Supplemental Figure 13).

For future targeted therapy it is relevant to identify and characterize the BZ CMs in the ischemic human heart. In this study, we show that the BZ is transcriptionally conserved between mouse and human and identified novel BZ marker genes. CMs adjacent to both the IZ and endocardium showed strongest expression of these BZ markers. Likely, these cells survive the MI by oxygen and nutrients supplied directly from the ventricular lumen. This region of activated myocardium is important since the CMs in this rim might be most responsive to proliferative stimuli like YAP-TEAD. Furthermore, our data suggests that this responsiveness might be restricted to a temporal window, since the expression of marker genes subsides with the maturation of the scar. For therapeutic purposes, techniques could be developed to target this sub-endocardial rim of surviving and activated CMs with stimuli to promote regeneration of the human heart.

ACKNOWLEDGEMENTS

We thank Corrie de Gier-de Vries for help with the *in situ* hybridizations.

SOURCES OF FUNDING

This study was supported by Netherlands Heart Foundation COBRA3 and CVON HUSTCARE to VMC and JB, an ERA-CVD CARDIOPRO grant to JB and by a Leducq Foundation grant (14CVD01) to VMC.

REFERENCES

1. Bergmann O, Zdunek S, Felker A, Salehpour M, Alkass K, Bernard S, Sjostrom SL, Szewczykowska M, Jackowska T, Dos Remedios C, Malm T, Andra M, Jashari R, Nyengaard JR, Possnert G, Jovinge S, Druid H and Frisen J. Dynamics of Cell Generation and Turnover in the Human Heart. *Cell*. 2015;161:1566-75.
2. Factor SM, Sonnenblick EH and Kirk ES. The histologic border zone of acute myocardial infarction--islands or peninsulas? *Am J Pathol*. 1978;92:111-24.
3. Driesen RB, Verheyen FK, Dijkstra P, Thone F, Cleutjens JP, Lenders MH, Ramaekers FC and Borgers M. Structural remodelling of cardiomyocytes in the border zone of infarcted rabbit heart. *Mol Cell Biochem*. 2007;302:225-32.
4. Sharov VG, Sabbah HN, Ali AS, Shimoyama H, Lesch M and Goldstein S. Abnormalities of cardiocytes in regions bordering fibrous scars of dogs with heart failure. *Int J Cardiol*. 1997;60:273-9.
5. Dispersyn GD, Mesotten L, Meuris B, Maes A, Mortelmans L, Flameng W, Ramaekers F and Borgers M. Dissociation of cardiomyocyte apoptosis and dedifferentiation in infarct border zones. *Eur Heart J*. 2002;23:849-57.
6. Ounzain S, Micheletti R, Beckmann T, Schroen B, Alexanian M, Pezzuto I, Crippa S, Nemir M, Sarre A, Johnson R, Dauvillier J, Burdet F, Ibberson M, Guigo R, Xenarios I, Heymans S and Pedrazzini T. Genome-wide profiling of the cardiac transcriptome after myocardial infarction identifies novel heart-specific long non-coding RNAs. *Eur Heart J*. 2015;36:353-68a.
7. Kaikkonen MU, Halonen P, Liu OH, Turunen TA, Pajula J, Moreau P, Selvarajan I, Tuomainen T, Aavik E, Tavi P and Yla-Herttuala S. Genome-Wide Dynamics of Nascent Noncoding RNA Transcription in Porcine Heart After Myocardial Infarction. *Circulation Cardiovascular genetics*. 2017;10.
8. Lacraz GPA, Junker JP, Gladka MM, Molenaar B, Scholman KT, Vigil-Garcia M, Versteeg D, de Ruiter H, Vermunt MW, Creyghton MP, Huibers MMH, de Jonge N, van Oudenaarden A and van Rooij E. Tomo-Seq Identifies SOX9 as a Key Regulator of Cardiac Fibrosis During Ischemic Injury. *Circulation*. 2017;136:1396-1409.
9. Gladka MM, Molenaar B, de Ruiter H, van der Elst S, Tsui H, Versteeg D, Lacraz GPA, Huibers MMH, van Oudenaarden A and van Rooij E. Single-Cell Sequencing of the Healthy and Diseased Heart Reveals Ckap4 as a New Modulator of Fibroblasts Activation. *Circulation*. 2018.
10. Jackson BM, Gorman JH, Moainie SL, Guy TS, Narula N, Narula J, John-Sutton MG, Edmunds LH, Jr. and Gorman RC. Extension of borderzone myocardium in postinfarction dilated cardiomyopathy. *Journal of the American College of Cardiology*. 2002;40:1160-7; discussion 1168-71.
11. de Bakker JM, van Capelle FJ, Janse MJ, Wilde AA, Coronel R, Becker AE, Dingemans KP, van Hemel NM and Hauer RN. Reentry as a cause of ventricular tachycardia in patients with chronic ischemic heart disease: electrophysiologic and anatomic correlation. *Circulation*. 1988;77:589-606.
12. Francis Stuart SD, De Jesus NM, Lindsey ML and Ripplinger CM. The crossroads of inflammation, fibrosis, and arrhythmia following myocardial infarction. *J Mol Cell Cardiol*. 2016;91:114-22.

13. Ursell PC, Gardner PI, Albala A, Fenoglio JJ, Jr. and Wit AL. Structural and electrophysiological changes in the epicardial border zone of canine myocardial infarcts during infarct healing. *Circ Res*. 1985;56:436-51.
14. Wu CC, Kruse F, Vasudevarao MD, Junker JP, Zebrowski DC, Fischer K, Noel ES, Grun D, Berezikov E, Engel FB, van Oudenaarden A, Weidinger G and Bakkers J. Spatially Resolved Genome-wide Transcriptional Profiling Identifies BMP Signaling as Essential Regulator of Zebrafish Cardiomyocyte Regeneration. *Dev Cell*. 2016;36:36-49.
15. Pasumarthi KB, Nakajima H, Nakajima HO, Soonpaa MH and Field LJ. Targeted expression of cyclin D2 results in cardiomyocyte DNA synthesis and infarct regression in transgenic mice. *Circ Res*. 2005;96:110-8.
16. Leach JP, Heallen T, Zhang M, Rahmani M, Morikawa Y, Hill MC, Segura A, Willerson JT and Martin JF. Hippo pathway deficiency reverses systolic heart failure after infarction. *Nature*. 2017;550:260-264.
17. Xiang FL, Guo M and Yutzey KE. Overexpression of Tbx20 in Adult Cardiomyocytes Promotes Proliferation and Improves Cardiac Function After Myocardial Infarction. *Circulation*. 2016;133:1081-92.
18. Lin Z, von Gise A, Zhou P, Gu F, Ma Q, Jiang J, Yau AL, Buck JN, Gouin KA, van Gorp PR, Zhou B, Chen J, Seidman JG, Wang DZ and Pu WT. Cardiac-specific YAP activation improves cardiac function and survival in an experimental murine MI model. *Circ Res*. 2014;115:354-63.
19. Sergeeva IA, Hooijkaas IB, van der Made I, Jong WM, Creemers EE and Christoffels VM. A transgenic mouse model for the simultaneous monitoring of ANF and BNP gene activity during heart development and disease. *CardiovascRes*. 2014:78-86.
20. Sohal DS, Nghiem M, Crackower MA, Witt SA, Kimball TR, Tymitz KM, Penninger JM and Molkentin JD. Temporally regulated and tissue-specific gene manipulations in the adult and embryonic heart using a tamoxifen-inducible Cre protein. *CircRes*. 2001;89:20-25.
21. Love MI, Huber W and Anders S. Moderated estimation of fold change and dispersion for RNA-seq data with DESeq2. *Genome biology*. 2014;15:550.
22. Heinz S, Benner C, Spann N, Bertolino E, Lin YC, Laslo P, Cheng JX, Murre C, Singh H and Glass CK. Simple combinations of lineage-determining transcription factors prime cis-regulatory elements required for macrophage and B cell identities. *Mol Cell*. 2010;38:576-89.
23. Frangogiannis NG. The inflammatory response in myocardial injury, repair, and remodelling. *Nat Rev Cardiol*. 2014;11:255-65.
24. Fu X, Khalil H, Kanisicak O, Boyer JG, Vagnozzi RJ, Maliken BD, Sargent MA, Prasad V, Valiente-Alandi I, Blaxall BC and Molkentin JD. Specialized fibroblast differentiated states underlie scar formation in the infarcted mouse heart. *J Clin Invest*. 2018;128:2127-2143.
25. Hess J, Angel P and Schorpp-Kistner M. AP-1 subunits: quarrel and harmony among siblings. *J Cell Sci*. 2004;117:5965-73.
26. Eferl R, Sibilia M, Hilberg F, Fuchsbichler A, Kufferath I, Guertl B, Zenz R, Wagner EF and Zatloukal K. Functions of c-Jun in liver and heart development. *J Cell Biol*. 1999;145:1049-1061.
27. Jahangiri L, Sharpe M, Novikov N, Gonzalez-Rosa JM, Borikova A, Nevis K, Paffett-Lugassy N, Zhao L, Adams M, Guner-Ataman B, Burns CE and Burns CG. The AP-1 transcription factor component Fosl2 potentiates the rate of myocardial differentiation from the zebrafish second heart field. *Development*. 2016;143:113-122.

28. Pinto AR, Ilinykh A, Ivey MJ, Kuwabara JT, D'Antoni ML, Debuque R, Chandran A, Wang L, Arora K, Rosenthal NA and Tallquist MD. Revisiting Cardiac Cellular Composition. *Circ Res*. 2016;118:400-9.
29. Preissl S, Schwaderer M, Raulf A, Hesse M, Gruning BA, Kobele C, Backofen R, Fleischmann BK, Hein L and Gilsbach R. Deciphering the Epigenetic Code of Cardiac Myocyte Transcription. *Circ Res*. 2015;117:413-23.
30. Quaife-Ryan GA, Sim CB, Ziemann M, Kaspi A, Rafehi H, Ramialison M, El-Osta A, Hudson JE and Porrello ER. Multicellular Transcriptional Analysis of Mammalian Heart Regeneration. *Circulation*. 2017;136:1123-1139.
31. Jenkins CP, Cardona DM, Bowers JN, Oliai BR, Allan RW and Normann SJ. The utility of C4d, C9, and troponin T immunohistochemistry in acute myocardial infarction. *Arch Pathol Lab Med*. 2010;134:256-63.
32. Tamura N, Ogawa Y, Chusho H, Nakamura K, Nakao K, Suda M, Kasahara M, Hashimoto R, Katsuura G, Mukoyama M, Itoh H, Saito Y, Tanaka I, Otani H and Katsuki M. Cardiac fibrosis in mice lacking brain natriuretic peptide. *Proc Natl Acad Sci U S A*. 2000;97:4239-44.
33. Buenrostro JD, Giresi PG, Zaba LC, Chang HY and Greenleaf WJ. Transposition of native chromatin for fast and sensitive epigenomic profiling of open chromatin, DNA-binding proteins and nucleosome position. *Nature methods*. 2013;10:1213-8.
34. Liu Q, Jiang C, Xu J, Zhao MT, Van Bortle K, Cheng X, Wang G, Chang HY, Wu JC and Snyder MP. Genome-Wide Temporal Profiling of Transcriptome and Open Chromatin of Early Cardiomyocyte Differentiation Derived From hiPSCs and hESCs. *Circ Res*. 2017;121:376-391.
35. Guo A, Wang Y, Chen B, Wang Y, Yuan J, Zhang L, Hall D, Wu J, Shi Y, Zhu Q, Chen C, Thiel WH, Zhan X, Weiss RM, Zhan F, Musselman CA, Pufall M, Zhu W, Au KF, Hong J, Anderson ME, Grueter CE and Song LS. E-C coupling structural protein junctophilin-2 encodes a stress-adaptive transcription regulator. *Science*. 2018;362.
36. Umansky KB, Feldmesser E and Groner Y. Genomic-wide transcriptional profiling in primary myoblasts reveals Runx1-regulated genes in muscle regeneration. *Genom Data*. 2015;6:120-2.
37. Naya FJ, Black BL, Wu H, Bassel-Duby R, Richardson JA, Hill JA and Olson EN. Mitochondrial deficiency and cardiac sudden death in mice lacking the MEF2A transcription factor. *Nat Med*. 2002;8:1303-9.
38. Sergeeva IA, Hooijkaas IB, Ruijter JM, van der Made I, de Groot NE, van de Werken HJ, Creemers EE and Christoffels VM. Identification of a regulatory domain controlling the Nppa-Nppb gene cluster during heart development and stress. *Development*. 2016.
39. Ponikowski P, Voors AA, Anker SD, Bueno H, Cleland JGF, Coats AJS, Falk V, Gonzalez-Juanatey JR, Harjola VP, Jankowska EA, Jessup M, Linde C, Nihoyannopoulos P, Parissis JT, Pieske B, Riley JP, Rosano GMC, Ruilope LM, Ruschitzka F, Rutten FH, van der Meer P and Group ESCSD. 2016 ESC Guidelines for the diagnosis and treatment of acute and chronic heart failure: The Task Force for the diagnosis and treatment of acute and chronic heart failure of the European Society of Cardiology (ESC) Developed with the special contribution of the Heart Failure Association (HFA) of the ESC. *Eur Heart J*. 2016;37:2129-2200.

40. Holditch SJ, Schreiber CA, Nini R, Tonne JM, Peng KW, Geurts A, Jacob HJ, Burnett JC, Cataliotti A and Ikeda Y. B-Type Natriuretic Peptide Deletion Leads to Progressive Hypertension, Associated Organ Damage, and Reduced Survival: Novel Model for Human Hypertension. *Hypertension*. 2015;66:199-210.
41. Thireau J, Karam S, Fauconnier J, Roberge S, Cassan C, Cazorla O, Aimond F, Lacampagne A, Babuty D and Richard S. Functional evidence for an active role of B-type natriuretic peptide in cardiac remodelling and pro-arrhythmogenicity. *Cardiovasc Res*. 2012;95:59-68.
42. Moilanen AM, Rysa J, Mustonen E, Serpi R, Aro J, Tokola H, Leskinen H, Manninen A, Levijoki J, Vuolteenaho O and Ruskoaho H. Intramyocardial BNP gene delivery improves cardiac function through distinct context-dependent mechanisms. *Circ Heart Fail*. 2011;4:483-95.
43. Casserly B and Klinger JR. Brain natriuretic peptide in pulmonary arterial hypertension: biomarker and potential therapeutic agent. *Drug Des Devel Ther*. 2009;3:269-87.
44. Desjardins CA and Naya FJ. The Function of the MEF2 Family of Transcription Factors in Cardiac Development, Cardiogenomics, and Direct Reprogramming. *J Cardiovasc Dev Dis*. 2016;3.
45. Wei J, Joshi S, Speransky S, Crowley C, Jayathilaka N, Lei X, Wu Y, Gai D, Jain S, Hoosien M, Gao Y, Chen L and Bishopric NH. Reversal of pathological cardiac hypertrophy via the MEF2-coregulator interface. *JCI Insight*. 2017;2.
46. Monroe TO, Hill MC, Morikawa Y, Leach JP, Heallen T, Cao S, Krijger PHL, de Laat W, Wehrens XHT, Rodney GG and Martin JF. YAP Partially Reprograms Chromatin Accessibility to Directly Induce Adult Cardiogenesis In Vivo. *Dev Cell*. 2019.
47. Ge Y, Gomez NC, Adam RC, Nikolova M, Yang H, Verma A, Lu CP, Polak L, Yuan S, Elemento O and Fuchs E. Stem Cell Lineage Infidelity Drives Wound Repair and Cancer. *Cell*. 2017;169:636-650 e14.
48. Piccolo S, Dupont S and Cordenonsi M. The biology of YAP/TAZ: hippo signaling and beyond. *Physiol Rev*. 2014;94:1287-312.
49. Stein C, Bardet AF, Roma G, Bergling S, Clay I, Ruchti A, Agarinis C, Schmelzle T, Bouwmeester T, Schubeler D and Bauer A. YAP1 Exerts Its Transcriptional Control via TEAD-Mediated Activation of Enhancers. *PLoS Genet*. 2015;11:e1005465.
50. Zanconato F, Forcato M, Battilana G, Azzolin L, Quaranta E, Bodega B, Rosato A, Bicciato S, Cordenonsi M and Piccolo S. Genome-wide association between YAP/TAZ/TEAD and AP-1 at enhancers drives oncogenic growth. *Nat Cell Biol*. 2015;17:1218-27.

SUPPLEMENTAL MATERIAL

Extended Results

Function of BZ marker genes

Clu is thought to play a protective role by acting as an antioxidant during oxidative stress.[1] Similar to *Nppa*, in the postnatal heart *Clu* is expressed in the atria and re-activated upon myocardial stress. It was shown to inhibit cell apoptosis by acting on the NF-κB signaling pathway and Bax/Bcl-xL expression.[2] In a rat model of myocardial infarction, *Clu*, as an inflammatory modulator, could reduce infarct size and improve survival, while increasing macrophage infiltration at the infarcted area.[3] Recently, plasma CLU levels have been associated with left ventricular remodeling after MI.[4]

Gpx3 encodes a member of the glutathione peroxidase family, which catalyze the reduction of organic hydroperoxides and hydrogen peroxide by glutathione, and thereby protect cells against oxidative damage. Although reduced *Gpx3* activity has been associated with increased risk of cardiovascular events[5, 6], still little is known about its role in cardiovascular disease.

Ankrd1 encodes cardiac ankyrin repeat protein (CARP).[7-9] Ventricular *Ankrd1* upregulation was observed in models of pressure overload or clinical heart failure due to dilated and arrhythmogenic RV cardiomyopathy.[10-12] Moreover, mutations in *Ankrd1* were found to be associated with dilated and hypertrophic cardiomyopathy.[13, 14] Functionally, myocardial *Ankrd1* acts as an anti-apoptotic survival factor after ischemia-reperfusion injury and hypoxia.[15, 16]

Foxp1 is a member of the forkhead box family of transcription factors that is required for heart development in mouse and human. It coordinates the balance of CM proliferation and differentiation during development and postnatally represses hypertrophy-associated gene expression.[17-19]

Nppb is required during recovery from myocardial infarction

NPPB is induced in the BZ from fish [20, 21] to human (our study) and serves as a paradigm for cardiac injury responsive gene expression. Previous reports have revealed that loss of *Nppb* leads to increased age-related progression of fibrosis under both baseline and pathological conditions.[22] Furthermore, it has been demonstrated in animal studies that exogenous administration of BNP exerts an anti-fibrotic effect by limiting the infarct size after MI, which is regulated by endogenous NOS/NO component and opening of KATP channels [23, 24]. RNA-seq analysis detected transcripts of approximately 15.000 genes in the left ventricle of *Nppb*$^{-/-}$ mice under baseline conditions. However, we could not identify any fibrosis markers among the differentially expressed genes in *Nppb*$^{-/-}$ mice, and GO term annotation analysis did not reveal pathological processes of fibrosis (Figure 4C). We stained

microdissected left ventricular tissue of 12 wks and 20 wks old *Nppb*$^{-/-}$ mice with Picosirius Red, and did not observe fibrotic lesions (Supplemental Figure 7C, D in the Supplemental Material).

Of the 21 *Nppb*$^{-/-}$ mice subjected to MI surgeries with an infarct size β30%, 9 mice (42%) died between 1-3 days after MI. During the course of 7 days, additional *Nppb*$^{-/-}$ mice died (n=13), only 2 of which had infarct rupture (n=2) (Figure 7A and Supplemental Figure 8B in the Supplemental Material). In contrast, wildtype littermates with infarct size of 40-50% (n=5) survived7 days post-MI or died as a result of infarct rupture (n=7) or discomfort (n=1) (Figure 4F and Supplemental Figure 7A in the Supplemental Material). Note, the FVB genetic background used has an infarct rupture frequency of approximately 1 in 3.[25]

Using *in situ* hybridization, we validated the absence of *Nppb* expression and induction of *Nppa* in the BZ of wildtype and *Nppb*$^{-/-}$ mice (Figure 4G and Supplemental Figure 8F in the Supplemental Material). We assessed the transcript levels of myocardial hypertrophy markers (*Myh7* and *Atp2a2* (SERCA2A)), a two fibrosis markers (*Col1a1* and *Pstn)* in healthy myocardium and (WT n=6; HOM n=6) and 7 dpi RM (WT n=6; HOM n=6). Neither the healthy hearts nor the RM after MI showed any differences in expression of the indicated marker genes between *Nppb*$^{-/-}$ and wildtypes (Figure 4J)

Supplemental Methods

Animals

Animal care and experiments conform to the Directive 2010/63/EU of the European Parliament. All animal work was approved by the Animal Experimental Committee of the Academic Medical Center, Amsterdam, and was carried out in compliance with the Dutch government guidelines. Myh6-MerCreMer[1], nTnG (JAX stock #023035) and Gt(ROSA)26Sortm5(CAG-Sun1/sfGFP)Nat/J (JAX stock #021039) mice were bred on the FVB/N background. Tamoxifen (20 mg/kg) was administrated i.p. one week prior to t=0 and repeated the two following days.

Myocardial infarction

Mice were analgesized subcutaneously with buprenorfine (0.075 mg/kg). Anesthesia was induced with 4% Isoflurane in 1L/min O_2. Mice were shaved, intubated and locally analgesized subcutaneously with Lidocaine (2 mg/kg) and Bupivacaine (3 mg/kg) at the site of incision. Mice were placed on a heating mat to maintain body temperature. Anesthesia was maintained via ventilation by a Minivent Mouse Ventilator (Hugo Sachs Electronic, Harvard Apparatus) with 2% Isoflurane in 1L/min O_2 . Left thoracotomy was performed at the fourth intercostal space. Infarction was created by permanent ligation of the left anterior descending coronary artery (LAD) by surpassing a BV130-5 6.5mm taper point needle with a 8-0 Nylon wire (Ethilon, Ethicon, Johnson&Johnson) under the LAD, tied with a triple

knot. The thoracotomy and skin were closed with a C-1 12mm cutting needle with a 6-0 silicone coated brained silk wire (SOFSILK, Covidien). Analgesia was maintained up till 2 days after MI using buprenorphine (0.075 mg/kg) or Meloxicam (0.02 mg/kg).

Echocardiographic measurements in mice

Mice were anesthetized using isoflurane inhalation (4% induction, 1-1.5% in 700 ml O2/ minute for maintenance) and echocardiographic measurements were recorded as previously described.[2]

Histological analysis

Microdissected left ventricle were fixed overnight in 4% paraformaldehyde, transferred to 70% ethanol, dehydrated, and embedded using standard techniques. Sections of 7 μm were stained with Picosirius Red for fibrosis.

In situ hybridization was performed as described previously.[3] Briefly, hearts or microdissected tissue were fixed in 4% formaldehyde, embedded in paraplast and sectioned at 10 μm. The cDNA probes were designed against mouse tissue were *Nppa*, *Nppb*, *Col1a2*, *Ech1*, *Ankrd1*, *Clu*, *Des*, *Acta1*, *Serpine1A*, *Fhl1*, *Gpx3*, *Flnc* and *Tnni3*. For human tissue, cDNA probes used were *AFOG*, *Cd4*, *NPPA*, *NPPB*, *ECH1*, *ANKRD1*, *FOXP1*, *MYH7*, *DES*, *UCHL1*, *TMSB4X*, *CCR9*, *SERPINE1*, *JUNB* and *TCAP*. Images were acquired with Leica DM3000 microscope.

Immunohistochemistry

Immunohistochemistry was performed as described previously.[4] Briefly, sections of 7 μm were deparaffinized and dehydrated by a series of ethanol. For antigen retrieval, sections were boiled in unmasking solution (H3300, Vector) and blocked in 4% BSA. Sections were incubated with rabbit anti-PCM-1 (1:400, Atlas Antibodies, HPA023370), mouse anti-Jun (1:400, BD Bioscience, 610327), rabbit anti-Dystrophin (1:200, Abcam, ab15277). SytoxGreen (1:40,000, Thermo Fischer Scientific, S7020) was used as a nuclear stain. Fluorescence was visualized with the Leica TCS SP8 confocal microscope and the LasX software (Leica microsystems).

CRISPR/Cas9 genome editing

Three single guide RNAs (sgRNAs) (sgRNA 1: GGGTGATCTGCCATGTAGTC; sgRNA 2: GGGGCTTATGGCGTGACTCA; sgRNA 3: GGGAATGCCTCAGCTACTGT) were designed using the online tool ZiFiT Targeter[5,6] to target the *Nppb* gene. The sgRNAs (DR274) and Cas9 (MLM3613)[7] were *in vitro* transcribed according to manufacturer's instructions (ThermoFisher Scientific). The sgRNAs (10 ng/μl per sgRNA) and Cas9 mRNA (25 ng/μl) were micro-injected into the cytoplasm of once-cell embryo's for generation of founder mouse lines on FVB/N background. Myocardial infarction was performed as described previously.[8]

RNA isolation and quantitative real-time PCR (qPCR)

Total RNA was extracted from the border zone, remote zone, and the left ventricle of sham-operated mice at 3, 7, and 14 dpi and from the remote zone at 7 dpi and the left ventricle of *Nppb*-deficient mice using RNAzol according to manufacturer's instructions (Sigma-Aldrich). Prior to cDNA synthesis, total RNA samples were treated with RNase-free DNase I according to manufacturer's instructions (Invitrogen). The cDNA synthesis was carried out on 500 ng DNase-treated RNA using oligo-dT following the Superscript II system protocol (Invitrogen). Expression levels were assayed by quantitative real-time PCR using the LightCycler 480 system. Relative start concentrations were calculated as previously described.[9] Values were normalized to the geomean of *Hprt* and *Eef1e1* expression levels.

Isolation of nuclei from cardiomyocytes

Nuclear isolation was performed as described previously.[10] Briefly, all steps were carried out on ice. Snap frozen samples from the border zone and remote myocardium were blended and homogenized in 3ml lysis buffer (10mM Tris-HCL (pH8.0), 5mM $CaCl_2$, 2mM EDTA, 0.5mM EGTA, 1mM DTT, 3mM MgAc) using the Ultra-Turrax homogenizer (IKA). The suspension was dounced 10 times with a large pestle and 10 time with a tight pestle (Wheaton) in lysis buffer added with 0.4% triton-X. The solution was filtered through 100 µm and 30 µm filters (Sysmex) and subsequently centrifuged for 5 min at 1000 g at 4˚C. The nuclear pellet was resuspended in 500 µl staining buffer (PBS (pH8.0) with 5% BSA and 0.2% Igepal CA-630). Cardiomyocyte nuclei were incubated with rabbit-anti PCM-1 antibody (Atlas antibodies, 1:1000, HPA023370) and a secondary antibody Alexa-647 (1:500, Invitrogen) for 1h. DAPI (1:1000, Sigmar-Aldrich, D9542) was used as a nuclear stain. Sorting was performed on the BD Influx cell sorter (BD Bioscience). RNA was isolated using the RNeasy plus micro Kit (Quiagen).

RNA sequencing

For RNA isolated from cardiac nuclei, 500pg was used for library generation with the Ovation RNA-seq v2 kit (NuGEN) kit. Libraries were prepared with the UltraLow V2 (NuGen) kit and sequenced on the HiSeq4000 system (Illumnia) with 50 bp single-end reads.

For RNA-seq libraries from whole tissue, 40 ng DNase-treated total RNA was amplified and converted to cDNA using the Ovation RNA-seq v2 kit (NuGEN). Amplified cDNA was sheared to an average fragment length of 200-400 bp and used with the SOLiD system (Life Technologies) to generate index-tagged sequencing libraries. Library quality and size distribution were determined with TapeStation (Agilent Technologies). Pooled libraries sequenced on a HiSeq 2500 system (Illumina) with 125 bp single-end reads. Data was cross-referenced to available PCM1-sorted RNA-seq data.[10]

Nppb$^{-/-}$ left ventricle RNA-seq liberary was prepared with the Truseq Stranded Total RNA Library PreparationKit (Illumina, Part# 15031048 Rev. E). Total RNA (1 μg) was purified and sheared into small fragments followed by cDNA synthesis and ligation of the adapter. The quality and size distribution of the cDNA library templates were validated with Agilent DNA 1000 on 2100 Bioanalyzer (Agilent Technologies). cDNA samples were pooled per lane of single-end 50 bp sequencing on an Illumina HiSeq 2500 system (Illumina).

Differential expression analysis

Reads were mapped to mm10 build of the mouse transcriptome using STAR.[11] Differential expression analysis was performed using the DESeq2 package based on a model using the negative binomial distribution.[12] Unsupervised hierarchical clustering was performed on genes differentially expressed between BZ and sham using the R package pheatmap, version 1.0.8. (http://cran.r-project.org/web/packages/pheatmap/index.html).

Besides DAVID[13], ClueGO[14] was used to find overrepresented gene ontology (GO) terms and Kegg pathways in the categories 'biological process' and 'molecular function'. P-values were corrected for multiple testing using the false discovery rate (FDR) method of Benjamini-Hochberg. We have used 0.05 as FDR control level. Significantly enriched terms were functionally grouped and visualized. The highest significant term of the group was displayed as leading term.

Differentially expressed genes were also cross-referenced with a list of published transcription factors.[15]

ATAC sequencing

Nuclei isolation was performed on BZ tissue and the left ventricle of Tamoxifen-treated, sham-operated Myh6-MerCreMer (JAX stock #005657);nTnG (JAX stock #023035) mice at 7 and 14 dpi or PCM-1 (SIGMA stock #HPA023370) mice 4 dpi. Subsequently, isolated nuclei were sorted on a SH800 flow cytometer (Sony). Samples were gated in such a way that debris, nuclei clumps, and nuclei with no cardiomyocyte origin were excluded. A total of 50.000 nuclei per sample was collected and successively washed with PBS and used as input for ATAC-seq. Prior to sequencing, a quality check was performed to assure cardiomyocyte-specific open chromatin. Illumina sequencing libraries were generated and sequenced using the NextSeq platform.

Differential accessibility analysis

Reads were mapped to mm9 build of the mouse genome using BWA[16]; the default settings were used. The numbers of aligned reads from each sample are shown in Suppl. data files, Table 3. The BEDTools suite[17] was used to distribute the genome wide signal into bins of 500bp. For promoter accessibility analysis the ATAC-seq signal was distributed into promoter bins defined as 1500bp upstream and 500bp of the canonical TSS (BioMart, mm9

build). To allow for differential peak calling between datasets, quantile normalization was applied using the deepTools2 suite[18]. Unsupervised hierarchical clustering was performed using the R package pheatmap, version 1.0.8. ((http://cran.r-project.org/web/packages/pheatmap/index.html) on promoters and putative enhancers determined to be differentially accessible between BZ and sham. Motif enrichment analysis was performed on the 200bp summits of clustered putative enhancers using HOMER (http://homer.ucsd.edu/homer/).[19]

Overlap with H3K27ac, MEF2 and c-Jun ChIP-seq

ATAC-seq peaks were cross-referenced with ChIP-seq data from PCM1-sorted H3K27ac[10], MEF2 from whole heart tissue[20] and c-Jun from myoblasts (GSE56077).[21] Raw ChIP-seq reads were extracted from the Sequence Read Archives (GSM851290) and mapped to the mouse genome (mm9) using BWA.[16] Peaks were called and subsequently overlapped with different categories of ATAC-seq peaks using the BEDTools suite.[17]

Luciferase assays

Putative regulatory elements cloned into pGL2-basic upstream of a minimal SV40 promoter. This vector, without cloned element, also served as control. Transfections were performed in duplicate to COS7 cells using polyethyleneimine (Brunschwick). Standard 24 well scale transfections used 1 ug of reporter plasmid cotransfected with 6 ng pHRG-TK Renilla for normalization. Luminescence was measured using a Promega Explorer luminometer. Mutations in regulatory elements were made using the Quickchange mutageneis kit (Agilent), after which mutated regulatory elements were digested recloned to the pGL2-SV40 min reporter vector.

Supplemental Figure 1

Venn diagrams: overlapping BZ & RM differential gene expression versus sham (RNA-seq)

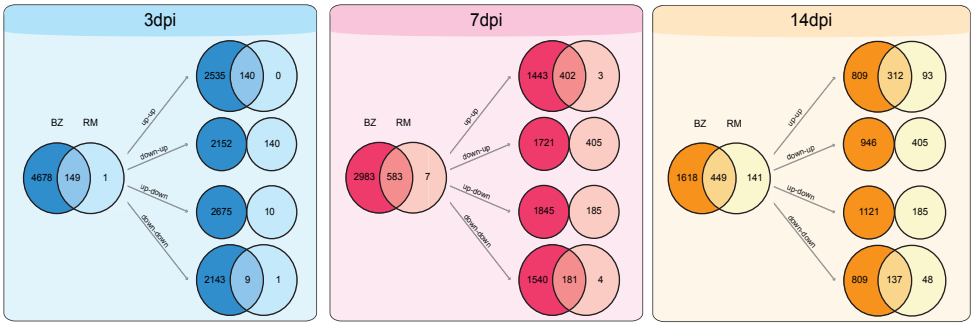

Supplemental Figure 1. Venn diagrams: overlapping border zone (BZ) & remote myocardium (RM) differential gene expression versus sham (RNA-seq).

Supplemental Figure 2

Hierarchical clustering heatmaps of all BZ differentially expressed transcription factors

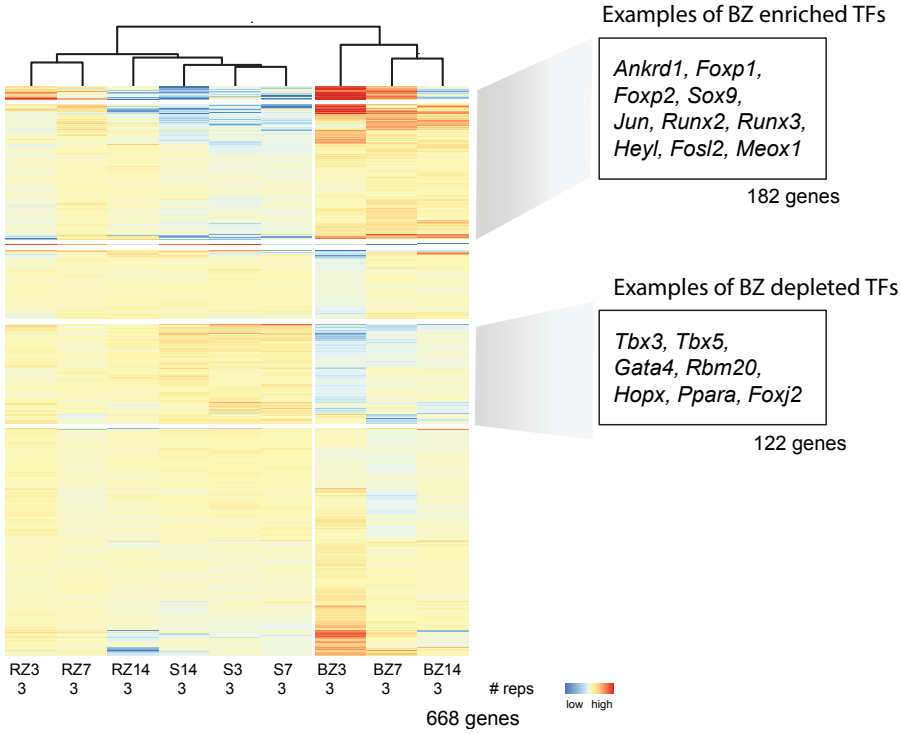

Supplemental Figure 2. Hierarchical clustering heatmaps of all border zone (BZ) differentially expressed transcription factors.

Supplemental Figure 3

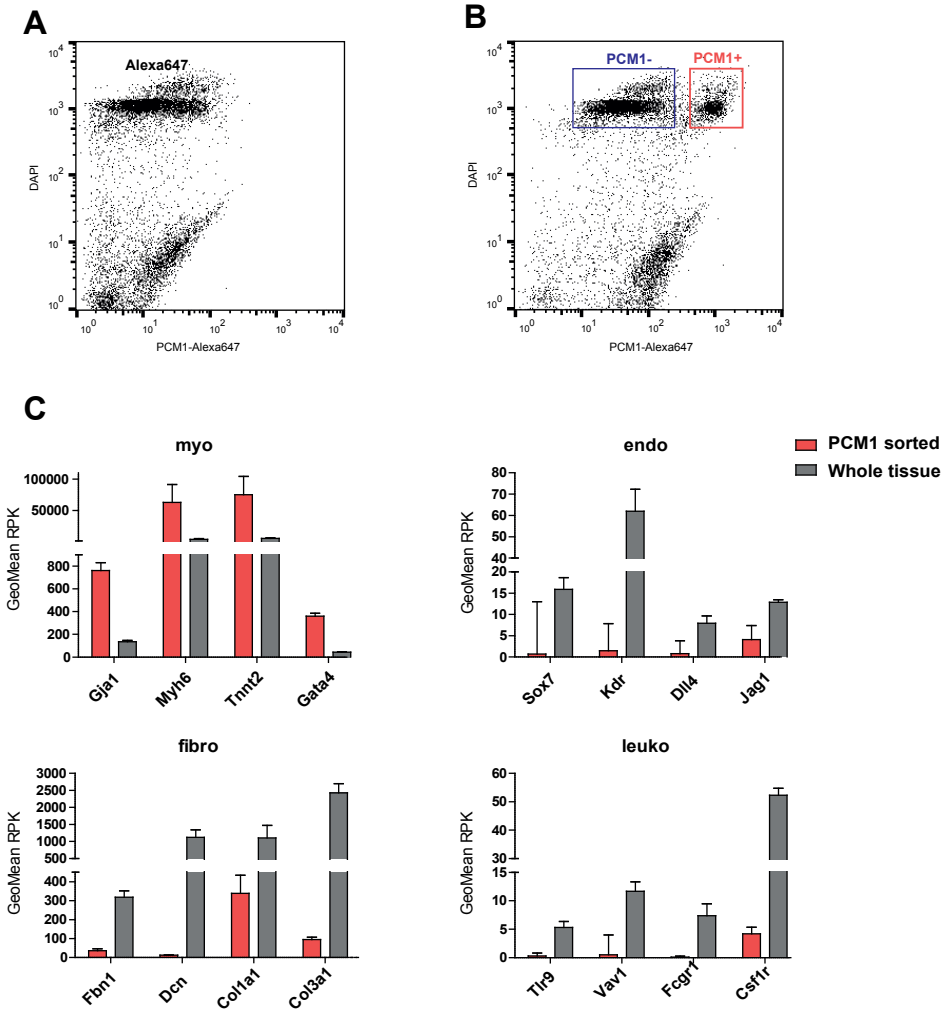

Supplemental Figure 3. Flow cytometry analysis of cardiomyocyte nuclei by pericentriolar material 1 (PCM-1) staining validation of enrichment for cardiomyocytes. **(A)** Flow cytometry dot plot showing nuclei isolated from border zone tissue stained with DAPI and a secondary AB (Alexa647). **(B)** Cardiomyocyte nuclei were identified by staining with anti-PCM-1 antibody bound by the secondary antibody Alexa-647. **(C)** GeoMean RPK values for selected genes expressed by cardiomyocytes (myo), fibroblasts (fibro), leukocytes (leuko) and endothelial cells (endo) shows enrichment of the PCM-1 sorted RNAseq dataset for cardiomyocytes when compared to RNAseq data obtained from whole tissue.

Supplemental Figure 4

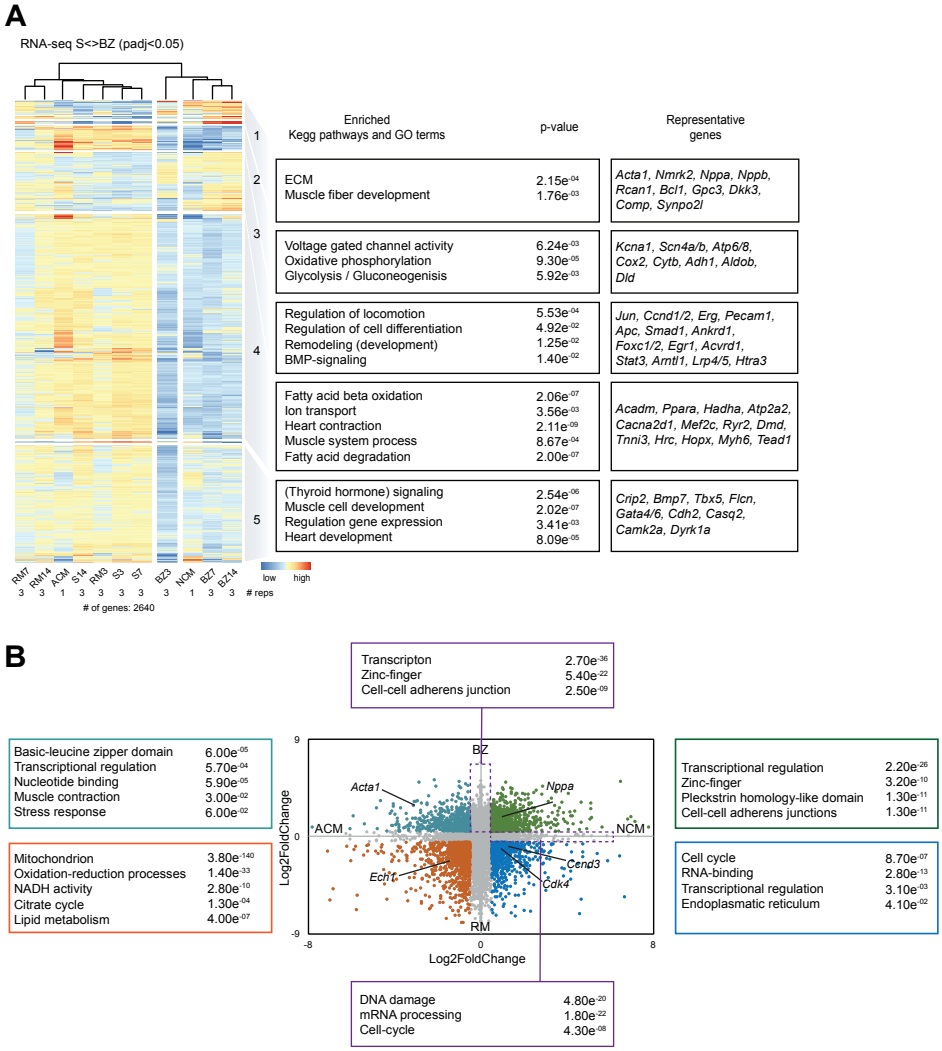

Supplemental Figure 4. Cardiomyocytes originating from the BZ partially revert to an immature state. **(A)** Unsupervised functional annotation heatmap of sham, RM, and BZ at different time points based on differentially expressed genes sham vs BZ compared to RNA-seq data from isolated neonatal cardiomyocytes (NCM) and adult CMs (ACM). Samples from RMs and sham cluster with ACM, whereas BZ 7 and 14 dpi clustered with NCMs. Only genes expressed at sufficient levels (RPK >240 in NCM or ACM) and at lower levels than in infarct zone samples were included. **(B)** Scatter plot of cardiomyocytes specific differentially expressed genes (Log2FoldChange) between RM and BZ and ACM and NCM. Gene ontology analysis was performed on each quadrant.

Supplemental Figure 5

Expression of border zone markers in human ischemic hearts

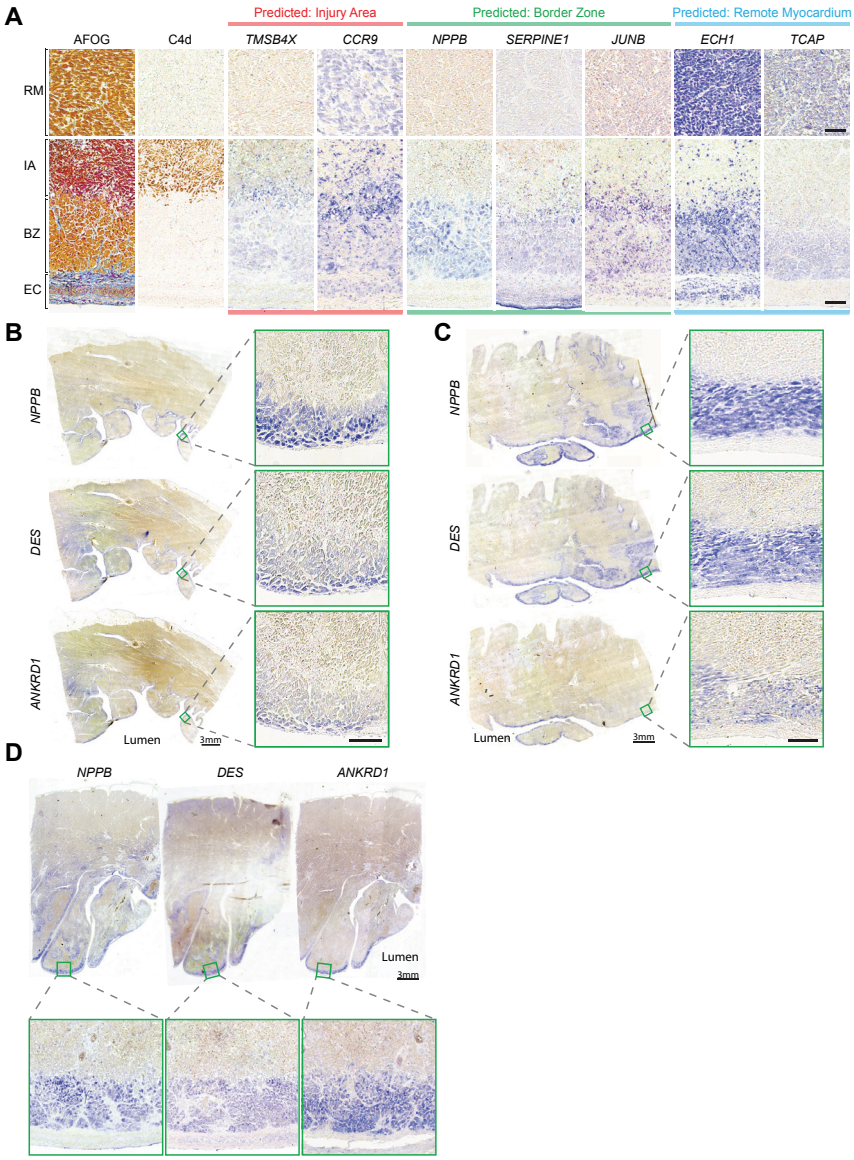

Supplemental Figure 5. Identified zone-specific marker genes for the ischemic human heart. (**A**) *In situ* hybridization of predicted marker genes on ischemic human heart tissues. Scale bars represent 100μm (**B-D**) *In situ* hybridization on left ventricular trans-mural samples (**B, D**) and intraventricular septum (**C**) of three different individuals. *NPPB*, *DES* and *ANKRD1* were expressed in a sub-endocardial region in all 3 samples. The tissue sample in (**D**) was from the same individual as the samples shown in (**A**). Scale bars represent 200 μm unless indicated otherwise.

Supplemental Figure 6

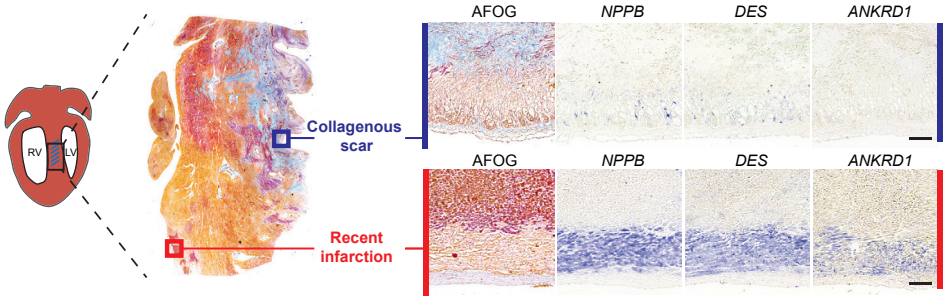

Supplemental Figure 6. Expression of border zone markers is temporally restricted. Human interventricular septum was analysed in AFOG, marking cytoplasm (orange), elastic fibrin (red) and collagen fibrils (blue), identifying recent infarcts (red) and matured scars (blue). *In situ* hybridization for BZ marker genes was performed on consecutive sections, showing strong signal adjacent to recent infarcts but not matured scars. Scale bars represent 200 μm.

Supplemental Figure 7

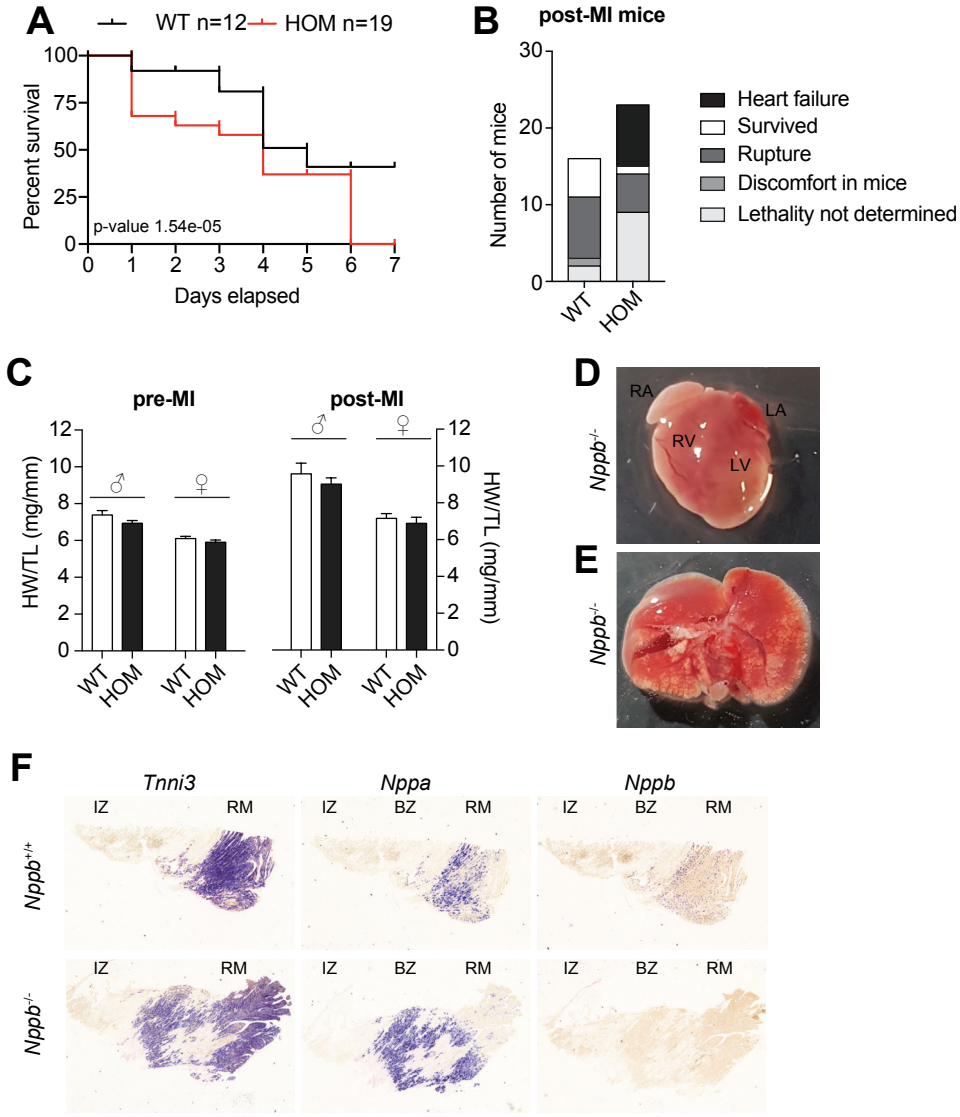

Supplemental Figure 7. Analysis of second independent *Nppb* knockout mouse line. (**A**) Kaplan-Meier curve of *Nppb*$^{-/-}$ mice (n=19) and wildtype littermates (n=12) showed significant difference in survival (p=1.54e-05). (**B**) The causes of death in the post-MI *Nppb*$^{-/-}$ mice and wildtype littermates. (**C**) Heart weight-to-tibia length ratio of male and female *Nppb*$^{-/-}$ mice and wildtype pre- (males, WT n=6; HOM n=4 and females, WT n=5; HOM n=4) and post-MI, 7 dpi (males, WT n=8; HOM n=15 and females, WT n=5; HOM n=2). (**D, E**) Whole heart and lungs of a *Nppb*$^{-/-}$ mouse presenting acute heart failure. (**F**) *In situ* hybridization analysis showing the expression pattern of *Tnni3*, *Nppa* and *Nppb* in *Nppb*$^{-/-}$ mouse and wildtype at 3 dpi. RA = right atrium; LA = left atrium; RV = right ventricle; LV = left ventricle; RM = remote zone; BZ = border zone; IZ = infarct zone.

Supplemental Figure 8

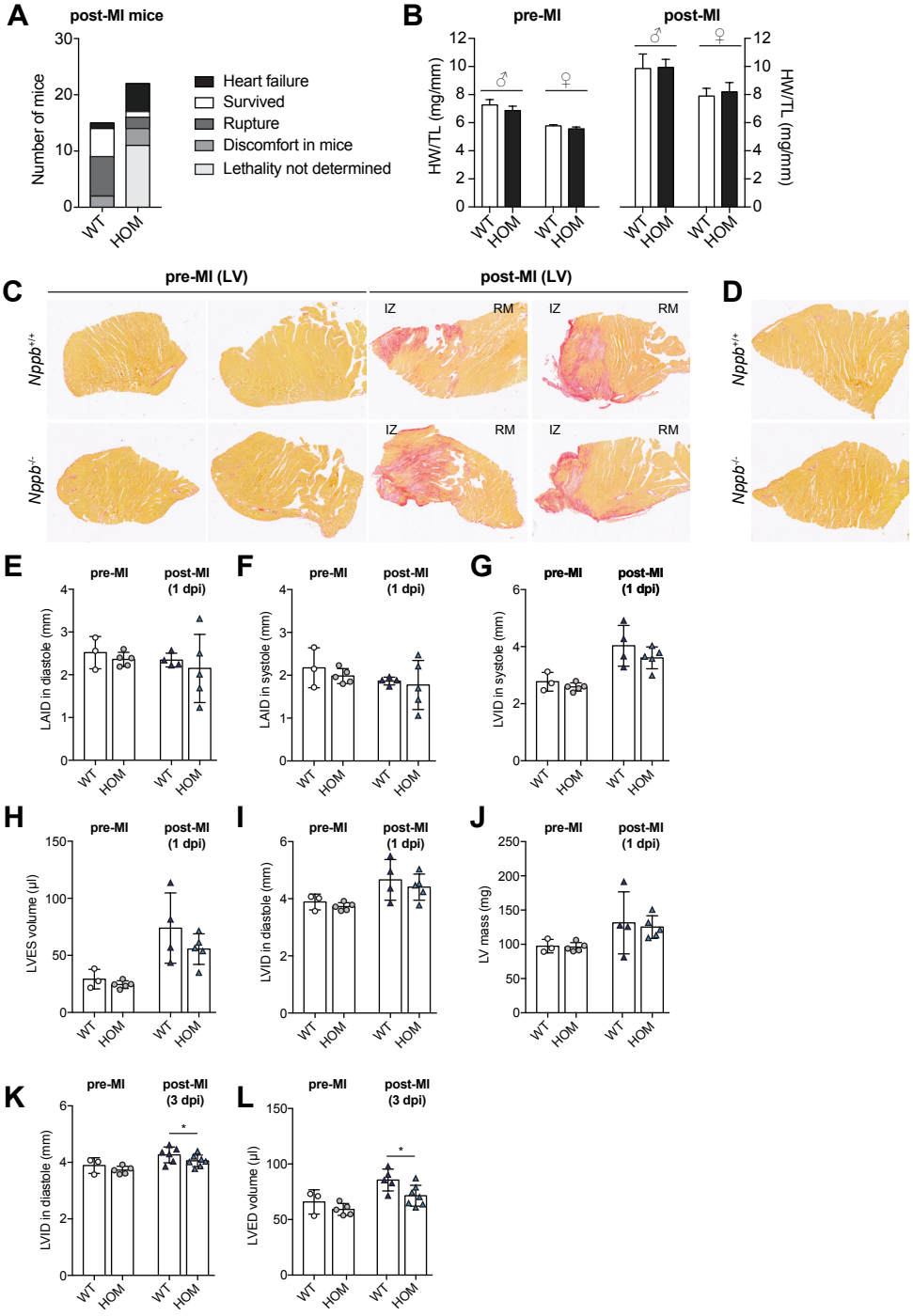

Supplemental Figure 8. Histological and echocardiographic analysis of primary *Nppb* knock mouse line. (**A**) The causes of death in the post-MI *Nppb*$^{-/-}$ mice and wildtype littermates. (**B**) Heart weight-to-tibia length ratio of male and female *Nppb*$^{-/-}$ mice and wildtype pre- and post-MI. (**C**) Picosirius Red staining of microdissected left ventricle of *Nppb*$^{-/-}$ hearts, 12 wks pre- (males, WT n=4; HOM n=5 and females, WT n=4; HOM n=8) and post-MI, 7 dpi (males, WT n=3; HOM n=8 and females, WT n=6; HOM n=8). (**D**) Picosirius Red staining of microdissected left ventricle of *Nppb*$^{-/-}$ hearts, 20 wks under baseline conditions. Echocardiographic parameters showing left atrial and ventricular function pre- and post-MI (1 dpi): (**E**) LA internal diameter in diastole. (**F**) LA internal diameter in systole. (**G**) LV internal diameter in systole. (**H**) left ventricular endsystolic volume. (**I**) LV internal diameter in diastole. (**J**) LV mass. Echocardiographic parameters showing (**K**) LV internal diameter in diastole (* p=0.02) and (**L**) LV enddiastolic volume (* p=0.02) pre- (WT n=3; HOM n=5) and post-MI, 3 dpi (WT n=4; HOM n=5). LV = left ventricle, LA = left atrium.

Supplemental Figure 9

ATAC-seq signals on gene promoters compared between sham- and BZ- derived cardiomyocyte nuclei. The selected promoters represent pathways or processes.

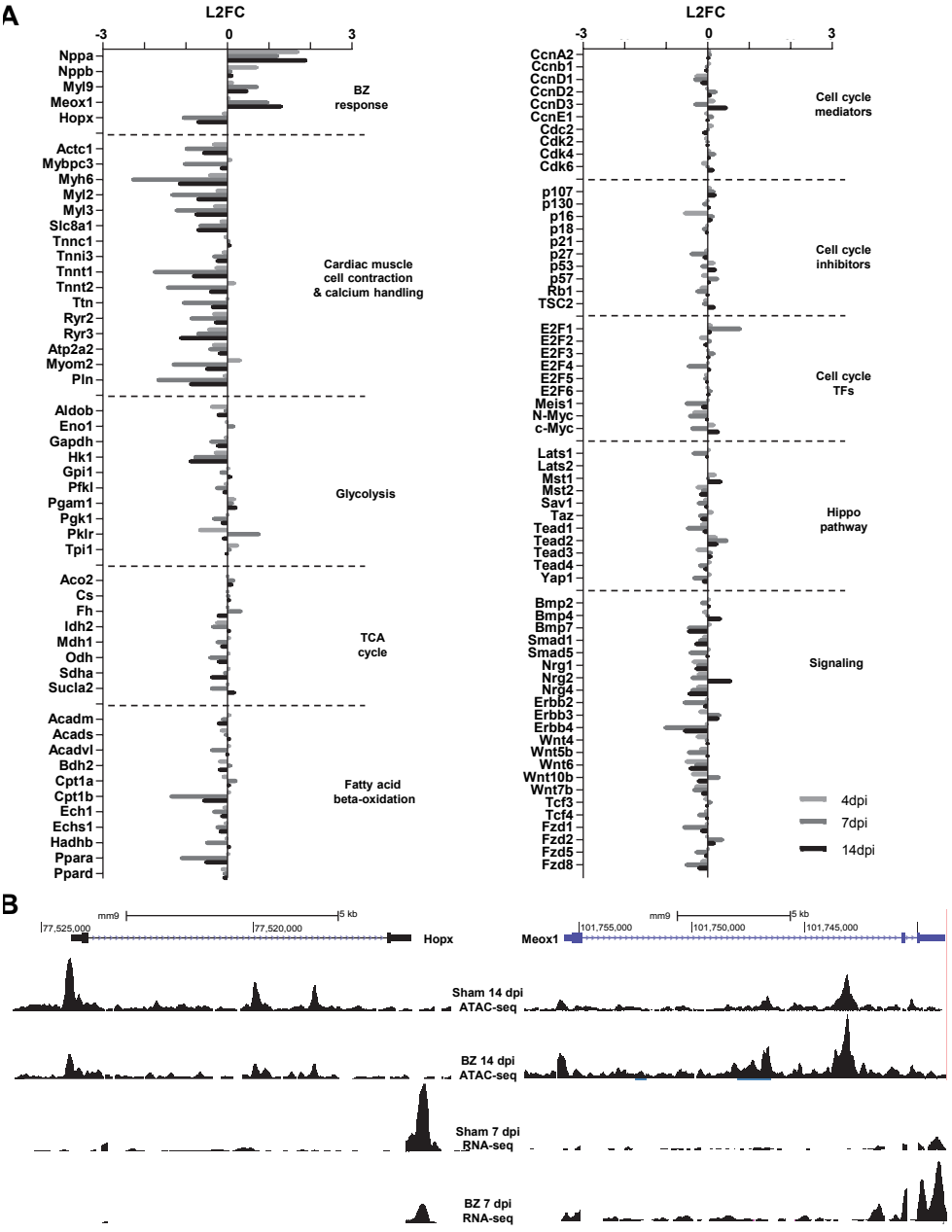

Supplemental Figure 9. Dynamic changes in promoter accessibility in sham and border zone (BZ) cardiomyocytes. The ATAC-seq signals on promoters of genes (-1.5 kbp to 0.5 kbp relative to transcription start sites) were compared between sham- and BZ-derived cardiomyocyte nuclei (**A**). The selected gene promoters represent indicated pathways or processes. The promoters of BZ-induced genes were more accessible in BZ cardiomyocyte nuclei compared to sham cardiomyocyte nuclei, whereas the promoters of sarcomere genes and calcium handling genes were less accessible. UCSC browser views of representative examples (**B**).

Supplemental Figure 10

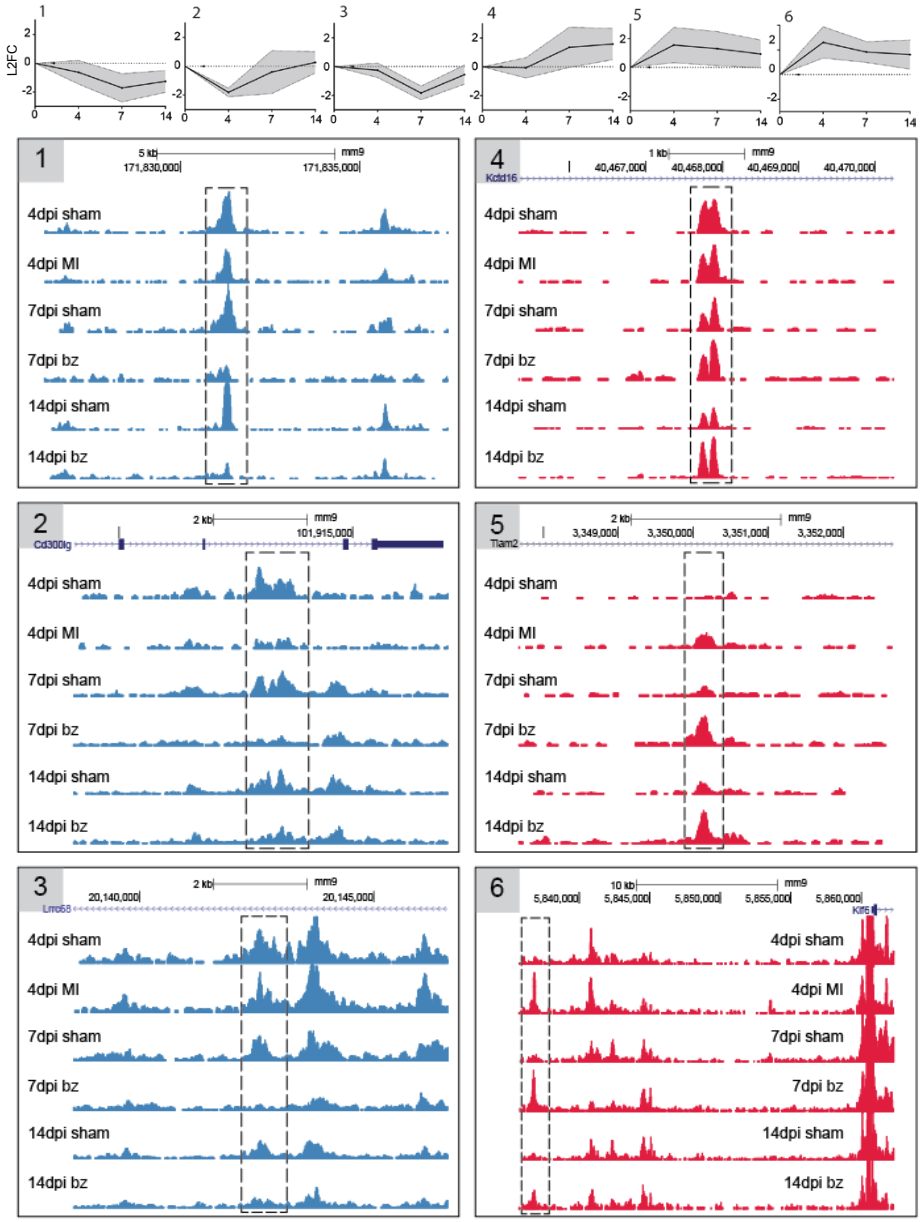

Supplemental Figure 10. UCSC browser views of representative examples of each of the six different temporal accessibility profiles of distal elements (ATAC-seq)

Supplemental Figure 11

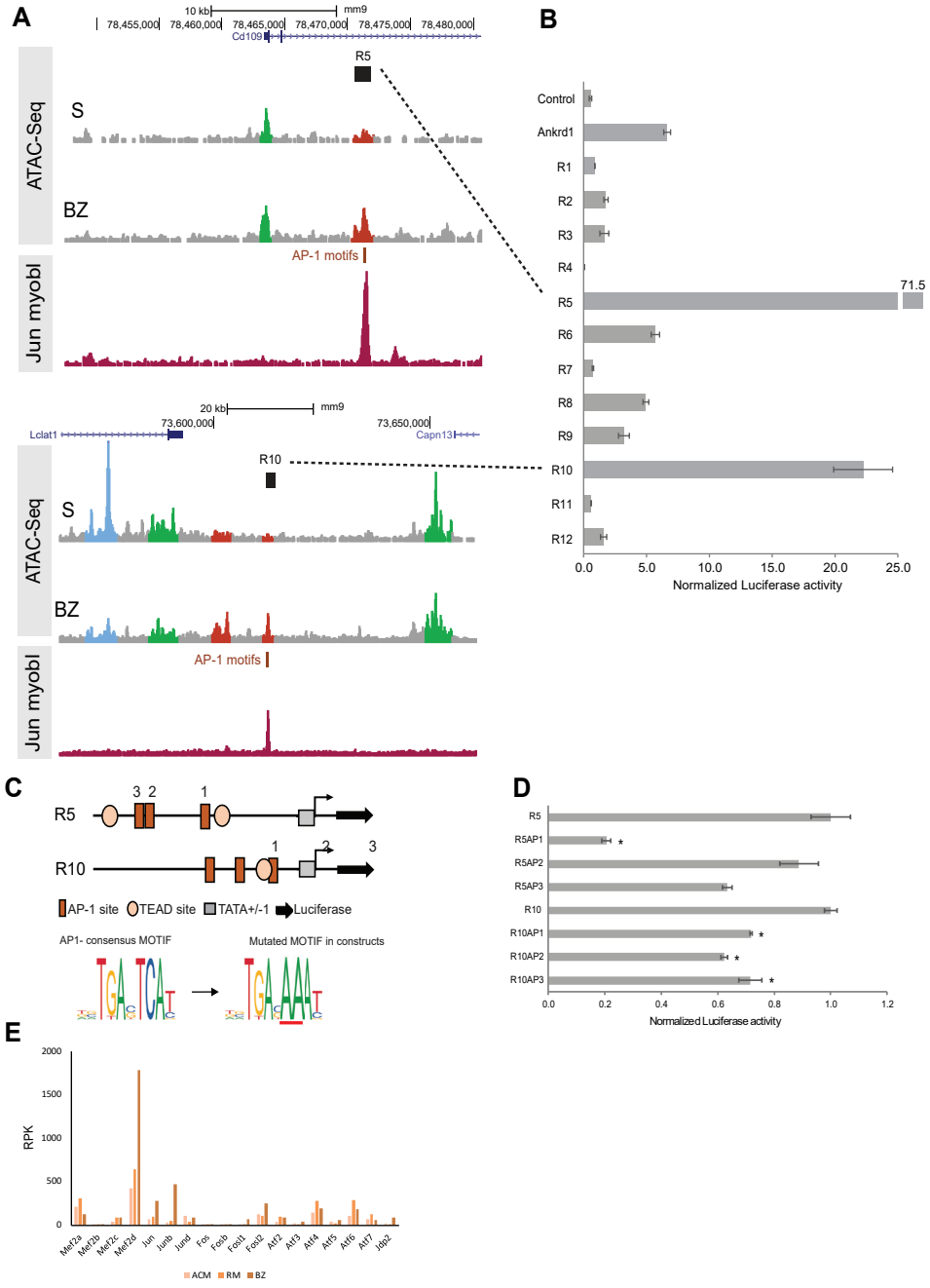

Figure 11. In vitro reporter analysis of putative regulatory regions. (**A**) UCSC browser views of 2 example regions selected on basis of ATAC-seq and ChIP-seq (c-Jun in myoblasts and H3K27ac mouse heart) analysis. Regions chosen for PCR and subsequent cloning to the luciferase reporter vector are marked

by dotted lines and correspond to the regions names in; (**B**) Shows the normalized luciferase activities of the selected putative regulatory regions. Regions 5 and 10, showing the highest fold activations compared to the control vector were selected for AP-1 mutational analysis; (**C**) Relative positions of high scoring predicted AP-1 sites (JASPAR47) and TEAD sites are marked for constructs R5 and R10 respectively. The conserved TC of each of the predicted consensuses was mutated to AA. (**D**) Shows the effect on fold activation of mutating the AP1 consensus in the luciferase reporter assay. Asterisk denotes $p<0.05$ in a student T-test relative to the wild type allele. (**E**) RPKs showing the average expression of Mef2 and AP-1 transcription factors in cardiomyocyte nuclei of adult cardiomyocytes (ACM), border zone (BZ) and remote myocardium (RM).

Supplemental Figure 12

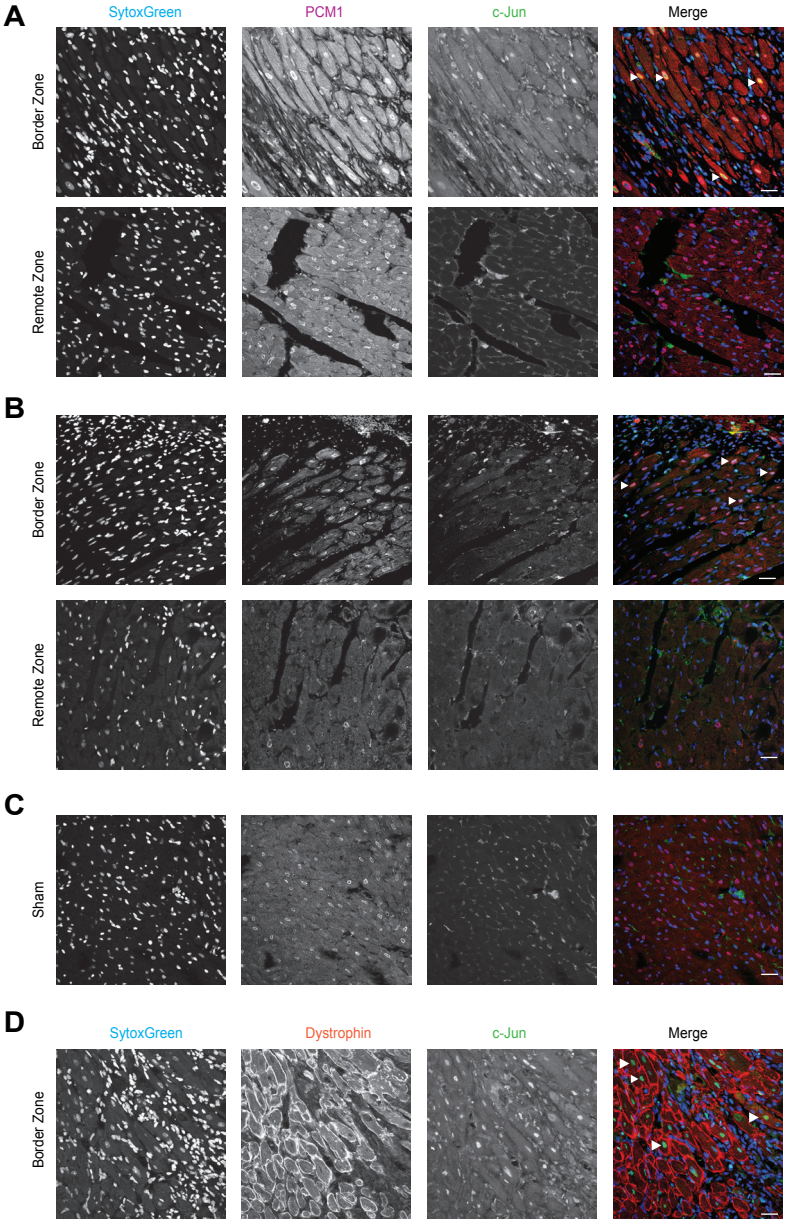

Supplemental Figure 12. Co-localization of c-Jun with border zone (BZ) cardiomyocytes. (**A**) Sham mice do not show c-Jun staining within the cardiomyocytes stained with dystrophin. (**B**) c Jun co-localizes with BZ cardiomyocytes stained with dystrophin at 14 dpi. (**C**) c-Jun co-localizes with cardiomyocytes nuclei stained with PCM-1 at 14 dpi. (**D**) c-Jun in BZ cardiomyocytes stained with dystrophin. Scale bars indicates 10 μm. Arrowheads indicate examples of c-Jun positive cardiomyocytes.

Supplemental Figure 13

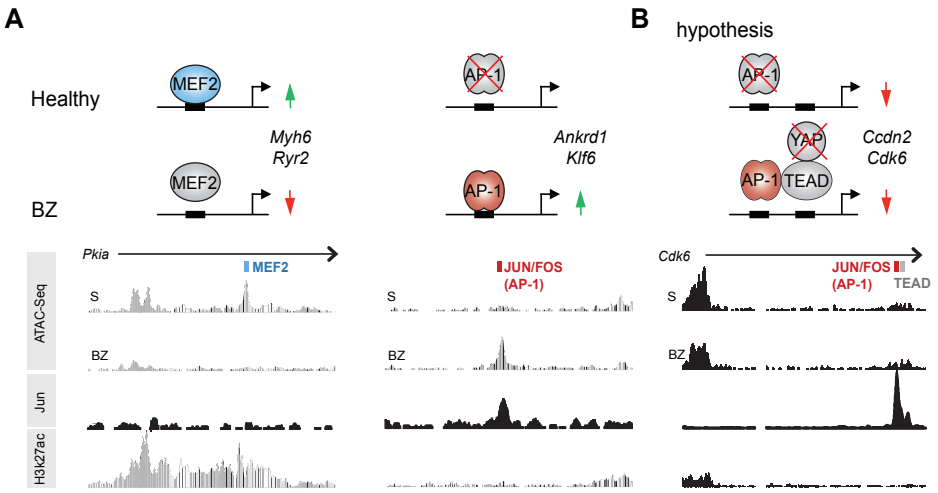

Supplemental Figure 13. A model for the role of AP-1 motif binding in governing cardiomyocyte lineage specificity. Binding of AP-1 motifs overrides homeostatic regulatory elements governing cardiomyocyte lineage specificity. (**A**) Cardiac injury results in the reduction of accessibility of CM lineage-specific transcription binding sites, such as Mef2, whereas accessibility of non-CM lineage typical promoters/genes and enhancers with binding motifs for AP-1 and other stress-responsive transcription factors increases. (**B**) In absence of YAP, the BZ cardiomyocytes increasing AP-1 accessibility does not activate cell cycle genes, but creates a favorable dedifferentiated state poised for proliferation to occur.

SUPPLEMENTAL REFERENCES

1. Ma H, Wang L, Yin C, Liu J and Qian L. In vivo cardiac reprogramming using an optimal single polycistronic construct. Cardiovasc Res. 2015;108:217-219.
2. Liu G, Zhang H, Hao F, Hao J, Pan L, Zhao Q and Wo J. Clusterin Reduces Cold Ischemia-Reperfusion Injury in Heart Transplantation Through Regulation of NF-kB Signaling and Bax/Bcl-xL Expression. Cell Physiol Biochem. 2018;45:1003-1012.
3. Van Dijk A, Vermond RA, Krijnen PA, Juffermans LJ, Hahn NE, Makker SP, Aarden LA, Hack E, Spreeuwenberg M, van Rossum BC, Meischl C, Paulus WJ, Van Milligen FJ and Niessen HW. Intravenous clusterin administration reduces myocardial infarct size in rats. Eur J Clin Invest. 2010;40:893-902.
4. Turkieh A, Fertin M, Bouvet M, Mulder P, Drobecq H, Lemesle G, Lamblin N, de Groote P, Porouchani S, Chwastyniak M, Beseme O, Amouyel P, Mouquet F, Balligand JL, Richard V, Bauters C and Pinet F. Expression and Implication of Clusterin in Left Ventricular Remodeling After Myocardial Infarction. Circ Heart Fail. 2018;11:e004838.
5. Pastori D, Pignatelli P, Farcomeni A, Menichelli D, Nocella C, Carnevale R and Violi F. Aging-RelatedDecline of Glutathione Peroxidase 3 and Risk of Cardiovascular Events in Patients With Atrial Fibrillation. J Am Heart Assoc. 2016;5.
6. Buijsse B, Lee DH, Steffen L, Erickson RR, Luepker RV, Jacobs DR, Jr. and Holtzman JL. Low serum glutathione peroxidase activity is associated with increased cardiovascular mortality in individuals with low HDLc's. PLoS One. 2012;7:e38901.
7. Piccolo S, Dupont S and Cordenonsi M. The biology of YAP/TAZ: hippo signaling and beyond. Physiol Rev. 2014;94:1287-1312.
8. Zanconato F, Forcato M, Battilana G, Azzolin L, Quaranta E, Bodega B, Rosato A, Bicciato S, Cordenonsi M and Piccolo S. Genome-wide association between YAP/TAZ/TEAD and AP-1 at enhancers drives oncogenic growth. Nat Cell Biol. 2015;17:1218-1227.
9. Monroe TO, Hill MC, Morikawa Y, Leach JP, Heallen T, Cao S, Krijger PHL, de Laat W, Wehrens XHT,Rodney GG and Martin JF. YAP Partially Reprograms Chromatin Accessibility to Directly Induce Adult Cardiogenesis In Vivo. Dev Cell. 2019;48(6):765-779.
10. Aihara Y, Kurabayashi M, Saito Y, Ohyama Y, Tanaka T, Takeda S, Tomaru K, Sekiguchi K, Arai M,Nakamura T and Nagai R. Cardiac ankyrin repeat protein is a novel marker of cardiac hypertrophy: role of M-CAT element within the promoter. Hypertension. 2000;36:48-53.
11. Nagueh SF, Shah G, Wu Y, Torre-Amione G, King NM, Lahmers S, Witt CC, Becker K, Labeit S and Granzier HL. Altered titin expression, myocardial stiffness, and left ventricular function in patients with dilated cardiomyopathy. Circulation. 2004;110:155-162.
12. Wei YJ, Cui CJ, Huang YX, Zhang XL, Zhang H and Hu SS. Upregulated expression of cardiac ankyrin repeat protein in human failing hearts due to arrhythmogenic right ventricular cardiomyopathy. European journal of heart failure. 2009;11:559-566.
13. Moulik M, Vatta M, Witt SH, Arola AM, Murphy RT, McKenna WJ, Boriek AM, Oka K, Labeit S,Bowles NE, Arimura T, Kimura A and Towbin JA. ANKRD1, the gene encoding cardiac ankyrin repeat protein, is a novel dilated cardiomyopathy gene. Journal of the American College of Cardiology. 2009;54:325-333.

14. Arimura T, Bos JM, Sato A, Kubo T, Okamoto H, Nishi H, Harada H, Koga Y, Moulik M, Doi YL, Towbin JA, Ackerman MJ and Kimura A. Cardiac ankyrin repeat protein gene (ANKRD1) mutations in hypertrophic cardiomyopathy. Journal of the American College of Cardiology. 2009;54:334-342.
15. Lee MJ, Kwak YK, You KR, Lee BH and Kim DG. Involvement of GADD153 and cardiac ankyrin repeat protein in cardiac ischemia-reperfusion injury. Exp Mol Med. 2009;41:243-252.
16. Han XJ, Chae JK, Lee MJ, You KR, Lee BH and Kim DG. Involvement of GADD153 and cardiac ankyrin repeat protein in hypoxia-induced apoptosis of H9c2 cells. J Biol Chem. 2005;280:23122-23129.
17. Zhang Y, Li S, Yuan L, Tian Y, Weidenfeld J, Yang J, Liu F, Chokas AL and Morrisey EE. Foxp1 coordinates cardiomyocyte proliferation through both cell-autonomous and nonautonomous mechanisms. Genes Dev. 2010;24:1746-1757.
18. Bai S and Kerppola TK. Opposing roles of FoxP1 and Nfat3 in transcriptional control of cardiomyocyte hypertrophy. Mol Cell Biol. 2011;31:3068-3080.
19. Chang SW, Mislankar M, Misra C, Huang N, Dajusta DG, Harrison SM, McBride KL, Baker LA and Garg V. Genetic abnormalities in FOXP1 are associated with congenital heart defects. Human mutation. 2013;34:1226-1230.
20. Wu CC, Kruse F, Vasudevarao MD, Junker JP, Zebrowski DC, Fischer K, Noel ES, Grun D, Berezikov E, Engel FB, van Oudenaarden A, Weidinger G and Bakkers J. Spatially Resolved Genome-wide Transcriptional Profiling Identifies BMP Signaling as Essential Regulator of Zebrafish Cardiomyocyte Regeneration. Dev Cell. 2016;36:36-49.
21. Gupta V, Gemberling M, Karra R, Rosenfeld GE, Evans T and Poss KD. An injury-responsive gata4 program shapes the zebrafish cardiac ventricle. Current biology : CB. 2013;23:1221-1227.
22. Tamura N, Ogawa Y, Chusho H, Nakamura K, Nakao K, Suda M, Kasahara M, Hashimoto R, Katsuura G, Mukoyama M, Itoh H, Saito Y, Tanaka I, Otani H and Katsuki M. Cardiac fibrosis in mice lacking brain natriuretic peptide. Proc Natl Acad Sci U S A. 2000;97:4239-4244.
23. D'Souza SP, Yellon DM, Martin C, Schulz R, Heusch G, Onody A, Ferdinandy P and Baxter GF. B-type natriuretic peptide limits infarct size in rat isolated hearts via KATP channel opening. Am J Physiol Heart Circ Physiol. 2003;284:H1592-1600.
24. Burley DS and Baxter GF. B-type natriuretic peptide at early reperfusion limits infarct size in the
rat isolated heart. Basic research in cardiology. 2007;102:529-541.
25. van den Borne SW, van de Schans VA, Strzelecka AE, Vervoort-Peters HT, Lijnen PM, Cleutjens JP, Smits JF, Daemen MJ, Janssen BJ and Blankesteijn WM. Mouse strain determines the outcome of wound healing after myocardial infarction. Cardiovasc Res. 2009;84:273-282.
26. Sohal DS, Nghiem M, Crackower MA, Witt SA, Kimball TR, Tymitz KM, Penninger JM and Molkentin JD. Temporally regulated and tissue-specific gene manipulations in the adult and embryonic heart using a tamoxifen-inducible Cre protein. CircRes. 2001;89:20-25.
27. Ram R, Mickelsen DM, Theodoropoulos C and Blaxall BC. New approaches in small animal echocardiography: imaging the sounds of silence. Am J Physiol Heart Circ Physiol. 2011;301:H1765-1780.

28. Moorman AFM, Houweling AC, de Boer PAJ and Christoffels VM. Sensitive non-radioactive detection of mRNA in tissue sections: novel application of the whole-mount in situ hybridization protocol. JHistochemCytochem. 2001;49:1-8.
29. Snarr BS, O'Neal JL, Chintalapudi MR, Wirrig EE, Phelps AL, Kubalak SW and Wessels A. Isl1 Expression at the Venous Pole Identifies a Novel Role for the Second Heart Field in Cardiac Development. CircRes. 2007;101:971-974.
30. Sander JD, Maeder ML, Reyon D, Voytas DF, Joung JK and Dobbs D. ZiFiT (Zinc Finger Targeter): an updated zinc finger engineering tool. Nucleic Acids Res. 2010;38:W462-468.
31. Sander JD, Zaback P, Joung JK, Voytas DF and Dobbs D. Zinc Finger Targeter (ZiFiT): an engineered zinc finger/target site design tool. Nucleic Acids Res. 2007;35:W599-605.
32. Hwang WY, Fu Y, Reyon D, Maeder ML, Tsai SQ, Sander JD, Peterson RT, Yeh JR and Joung JK. Efficient genome editing in zebrafish using a CRISPR-Cas system. Nat Biotechnol. 2013;31:227-229.
33. Sergeeva IA, Hooijkaas IB, van der Made I, Jong WM, Creemers EE and Christoffels VM. A transgenic mouse model for the simultaneous monitoring of ANF and BNP gene activity during heart development and disease. CardiovascRes. 2014:78-86.
34. Ruijter JM, Ramakers C, Hoogaars WM, Karlen Y, Bakker O, van den Hoff MJ and Moorman AF. Amplification efficiency: linking baseline and bias in the analysis of quantitative PCR data. Nucleic Acids Res. 2009;37:e45.
35. Gilsbach R, Preissl S, Gruning BA, Schnick T, Burger L, Benes V, Wurch A, Bonisch U, Gunther S, Backofen R, Fleischmann BK, Schubeler D and Hein L. Dynamic DNA methylation orchestrates cardiomyocyte development, maturation and disease. Nature communications. 2014;5:5288.
36. Dobin A, Davis CA, Schlesinger F, Drenkow J, Zaleski C, Jha S, Batut P, Chaisson M and Gingeras TR. STAR: ultrafast universal RNA-seq aligner. Bioinformatics. 2013;29:15-21.
37. Love MI, Huber W and Anders S. Moderated estimation of fold change and dispersion for RNA-seq data with DESeq2. Genome biology. 2014;15:550.
38. Huang dW, Sherman BT and Lempicki RA. Systematic and integrative analysis of large gene lists using DAVID bioinformatics resources. NatProtoc. 2009;4:44-57.
39. Bindea G, Mlecnik B, Hackl H, Charoentong P, Tosolini M, Kirilovsky A, Fridman WH, Pages F, Trajanoski Z and Galon J. ClueGO: a Cytoscape plug-in to decipher functionally grouped gene ontology and pathway annotation networks. Bioinformatics. 2009;25:1091-1093.
40. Lambert SA, Jolma A, Campitelli LF, Das PK, Yin Y, Albu M, Chen X, Taipale J, Hughes TR and Weirauch MT. The Human Transcription Factors. Cell. 2018;172:650-665.
41. Li H and Durbin R. Fast and accurate short read alignment with Burrows-Wheeler transform. Bioinformatics. 2009;25:1754-1760.
42. Quinlan AR and Hall IM. BEDTools: a flexible suite of utilities for comparing genomic features. Bioinformatics. 2010;26:841-842.
43. Ramirez F, Ryan DP, Gruning B, Bhardwaj V, Kilpert F, Richter AS, Heyne S, Dundar F and Manke T. deepTools2: a next generation web server for deep-sequencing data analysis. Nucleic Acids Res. 2016;44:W160-165.
44. Heinz S, Benner C, Spann N, Bertolino E, Lin YC, Laslo P, Cheng JX, Murre C, Singh H and Glass CK. Simple combinations of lineage-determining transcription factors prime cis-regulatory elements required for macrophage and B cell identities. Mol Cell. 2010;38:576-589.

45. Guo A, Wang Y, Chen B, Wang Y, Yuan J, Zhang L, Hall D, Wu J, Shi Y, Zhu Q, Chen C, Thiel WH, Zhan X, Weiss RM, Zhan F, Musselman CA, Pufall M, Zhu W, Au KF, Hong J, Anderson ME, Grueter CE and Song LS. E-C coupling structural protein junctophilin-2 encodes a stress-adaptive transcription regulator. Science. 2018;362:1-9.
46. Umansky KB, Feldmesser E and Groner Y. Genomic-wide transcriptional profiling in primary myoblasts reveals Runx1-regulated genes in muscle regeneration. Genom Data. 2015;6:120-122.
47. Khan A, Fornes O, Stigliani A, Gheorghe M, Castro-Mondragon JA, van der Lee R, Bessy A, Cheneby J, Kulkarni SR, Tan G, Baranasic D, Arenillas DJ, Sandelin A, Vandepoele K, Lenhard B, Ballester B, Wasserman WW, Parcy F and Mathelier A. JASPAR 2018: update of the open-access database of transcription factor binding profiles and its web framework. Nucleic Acids Res. 2018;46:D260-D266.



Chapter 5

Epigenetic State Changes Underlie Metabolic Switch in Mouse Post-Infarction Border Zone Cardiomyocytes

Marie Günthel, Karel van Duijvenboden, Dennis E. M. de Bakker, Ingeborg B. Hooijkaas, Jeroen Bakkers, Phil Barnett and Vincent M. Christoffels

Journal of Cardiovascular Development and Disease. Vol. 8, October 2021: 134

ABSTRACT

Myocardial infarction causes ventricular muscle loss and formation of scar tissue. The surviving myocardium in the border zone, located adjacent to the infarct, undergoes profound changes in function, structure and composition. How and to what extent these changes of border zone cardiomyocytes are regulated epigenetically is not fully understood. Here, we obtained transcriptomes of PCM-1-sorted mouse cardiomyocyte nuclei of healthy left ventricle and 7 days post myocardial infarction border zone tissue. We validated previously observed downregulation of genes involved in fatty acid metabolism, oxidative phosphorylation and mitochondrial function in border zone-derived cardiomyocytes, and observed a modest induction of genes involved in glycolysis, including *Slc2a1* (Glut1) and *Pfkp*. To gain insight into the underlying epi-genetic regulatory mechanisms, we performed H3K27ac profiling of healthy and border zone cardiomyocyte nuclei. We confirmed the switch from Mef2- to AP-1 chromatin association in border zone cardiomyocytes, and observed, in addition, an enrichment of PPAR/RXR binding motifs in the sites with reduced H3K27ac signal. We detected downregulation and accompanying epigenetic state changes at several key PPAR target genes including *Ppargc1a* (PGC-1α), *Cpt2*, *Ech1*, *Fabpc3* and *Vldrl* in border zone cardiomyocytes. These data indicate that changes in epigenetic state and gene regulation underlie the maintained metabolic switch in border zone cardiomyocytes.

Keywords: transcriptome, myocardial infarction, border zone, epigenetics, H3K27ac, nuclear RNA-sequencing

INTRODUCTION

Myocardial infarction (MI) remains one of the leading causes of mortality [1]. The acute cessation of oxygen and metabolite supply causes drastic hypoxia responses and metabolic changes. The oxygen shortage suppresses oxidative fatty acid (FA) metabolism and activates anaerobic glycolysis to reduce the consumption of the limited oxygen [2]. This acute phase is followed by death of irreplaceable cardiomyocytes and other cells in the ischemic region, immune responses and scar formation [3]. The infarct zone (IZ) is highly irregular in shape, consisting of necrotic tissue, infiltrating fibroblasts and immune cells, which will subsequently give rise to fibrous tissue. The remote myocardium (RM), distal from the infarct zone, is less affected by the ischemia. Cardiomyocytes of the border zone (BZ) surrounding the IZ are still viable, but severely affected by the ischemia, infiltrating immune cells and fibroblasts of the neighbouring infarct zone [4]. BZ cardiomyocytes become hypertrophic and show decreased connectivity and interaction with neigh-boring cardiomyocytes and the extracellular matrix [5]. In the BZ, cardiomyocytes appear to undergo a dedifferentiative process, disassembling their sarcomeres, breaking down their sarcoplasmic reticulum and accumulating glycogen. Cardiomyocyte mitochondria also change in volume and shape, a phenotype that is often associated with chronic hibernation [4,6–9].

Recent transcriptome analyses revealed that following MI, gene expression profiles and phenotypes of the different cell types in the BZ region change and become much more heterogeneous [10–18]. The dedifferentiation of BZ cardiomyocytes and their reduction in metabolic activity following MI are seen to be accompanied by profound alterations in the transcriptome and in the epigenetic landscape [13]. When compared to cardiomyocytes from the RM, BZ cardiomyocytes display lower expression of genes involved in contractility, mitochondrial function, oxidative phosphorylation and fatty acid metabolism [13]. These transcriptomic and epigenetic alterations can be observed up to several weeks after MI, indicating the BZ cardiomyocytes are epigenetically maintained in a metabolically inactive and dedifferentiated state. The cardiomyocytes surrounding an injury in the zebrafish heart, which initiate proliferation to regenerate the heart, similarly dedifferentiate and downregulate genes for mitochondrial function and oxidative phosphorylation [19,20]. In addition, these cardiomyocytes increase glucose uptake and induce expression of glycolysis genes, and this metabolic switch was found to be essential for their proliferation during myocardial regeneration [19,21].

Previous studies using ATAC-seq revealed that the accessible chromatin landscape of BZ cardiomyocytes changed dynamically with thousands of chromatin regions gaining or losing accessibility [13]. ATAC-seq defines all classes of regulatory elements, irrespective of their function, including enhancers, promoters, silencers, insulators, boundary elements, etc. On the other hand, acetylation of K27 of histone H3 (H3K27ac) is predominantly enriched at sites flanking active promoters and enhancers [22]. The aim of this study was to

further characterize the epigenetic landscape of BZ cardiomyocytes. We per-formed RNA-sequencing and cleavage under targets and release using nuclease (CUT&RUN)-sequencing [23] for H3K27ac on PCM-1 positive cardiomyocyte nuclei originating from the BZ and the LV. Most of the H3K27ac-marked putative enhancers that in-creased activity in BZ cardiomyocytes compared to controls were enriched for binding sites for AP-1 family of transcription factors, whereas the enhancers with reduced activity were enriched for binding sites for Mef2 transcription factors, validating previous ATAC-seq profiling data. However, enhancers with decreased H3K27ac association were also enriched for motifs recognized by the NR superfamily of transcription factors, including peroxisome proliferator-activated receptors (PPARs) and retinoid X receptor (RXR). RXR forms heterodimers with PPARα to regulate the expression of genes involved in fatty acid oxidation, inflammation and apoptosis [24–26]. We found that RXR/PPARα target genes such as *Cpt2* and *Ech1* are significantly downregulated in BZ cardiomyocytes. Together, our study indicates that changes in epigenetic state and gene regulation underlie the dedifferentiated and metabolically inactive state of border zone cardiomyocytes.

MATERIALS AND METHODS

Myocardial Infarction and Tissue Isolation

Myocardial infarctions were performed as described previously [13]. Male mice of 8 weeks old from the FVB/N background (#001800, Janvier, France) were used to perform myocardial infarctions. Before surgery, mice received 0.075mg/kg buprenofine (Covetrus, Cuijk, The Netherlands) subcutaneously. They were anesthetized with 4% isoflurane in 1L/min oxygen and intubated during surgery. At the site of the chest opening, mice were shaved, and received local analgesia with lidocaine (2 mg/kg) and bupivacaine (3 mg/kg). Left thoracotomy was performed at the fourth intercostal space. An acute myocardial infarction was generated by permanent ligation of the left anterior descending coronary artery (LAD) by surpassing a BV130-5 6.5mm taper point needle with a 8-0 Nylon wired (Ethicon, Johnson & Johnson, Amersfoort, The Netherlands) under the LAD, that was tied with a triple knot. The thoracotomy and skin were closed using a C-1 12mm cutting needle with a 6-0 silicone coated brain silk wire (SOFSLIK, Medtronic, Eindhoven, The Netherlands). During surgery, anesthesia was maintained with the Minivent Mouse ventilator (Hugo Sachs Electronics, Harvard Apparatus) with 2% Isoflurane in 1L/min oxygen. To maintain body temperature, mice were placed on a heating mat. Mice received analgesia up till 2 days by subcutaneous injection of Meloxicam (Covetrus, Cuijk, The Netherlands) at 0.2mg/kg. The hearts were harvested 7 days after infarction. The left ventricle was isolated and dissected to obtain the border zone and remote myocardium. Mice were sacrificed by CO2 and cervical dislocation.

Immunohistochemistry

For immunohistochemistry sections were deparaffinised in xylene, rehydrated through a graded series of ethanol and boiled for 5 min in unmasking solution (H3300, Vector) using a pressure cooker. Sections were stained with antibodies against PCM-1 (diluted 1:400, HPA023370, Atlas Antibodies, Bromma, Sweden, supplied by Bio Connect, Huissen, The Netherlands) and GLUT1 (diluted 1:100, GTX66489, Genetex). SYTOX Green was used (diluted 1:40,000, S7020, Invitrogen, supplied by Fisher Scientific, Landsmeer, The Netherlands) as a nuclear stain. The antibodies were visualized with the secondary antibodies Alexa647 (diluted 1:250, A-31571, Thermo Fisher) and Alexa555 (diluted 1:250, A-31572, Thermo Fisher). Sections were mounted in PBS:Glycerol (v/v). Pictures were taken with the Leica DM6000. Staining for p-PHD was performed using An-ti-phospho-PDHE1-A type I (ser293) (ABS204, Merck, Supplier: Merck, Zwijndrecht, The Netherlands) as described before [19]

In Situ Hybridization

In situ hybridization was performed as described previously [27]. Briefly, sections were de-paraffinized and rehydrated to MilliQ. Sections were treated with Proteinase K (25530031, Invitrogen, Invitrogen, supplied by Fisher Scientific, Landsmeer, The Nether-lands) and were pre-hybridized in hybridization buffer (50% formamide, 20X SSC, blocking reagent, 0.5 M EDTA, 10% CHAPS, heparine solution and 10 mg/ml yeast RNA) at 70 °C. Hybridization was performed overnight with dioxigenin (DIG) labeled probe against *Nppa* (forward: 5'gggcagagacagcaaacatc 3', reverse: 5' cacagtggcaatgtgaccaa 3'), *Hk1* (forward: 5' ggggatttcattgcactgga 3':, reverse: 5' tgtcgcagttcctccatgta 3') and *Pdk2* (forward: 5' accggactctaagccagttc 3', reverse: 5' agatcttcttcaccgagggc). Probes were visualized using alkaline phosphatase-conjugated anti-DIG Fab fragments (11093274910, Roche, Supplier: Merck, Zwijndrecht, The Netherlands) and NBT/BCIP staining reagent (11681451001, Roche, Supplier: Merck, Zwijndrecht, The Netherlands). Sections were de-hydrated and following mounted in Entellan (107961, Sigma Aldrich, Merck, Zwijndrecht, The Netherlands). Images were acquired with the Leica DM5000 microscope.

Isolation of Nuclei from Cardiomyocytes

Nuclei isolation was performed as described previously [13]. All steps were performed on ice. Snap frozen samples of the left ventricle, the micro-dissected border zone and remote myocardium were used. Samples were homogenized with the Ultra-Turrax homogenizer (IKA, Staufen, Germany) in 3 ml lysis buffer (10mM Tris-HCL (pH8.0), 5 mM CaCl2, 2 mM EDTA, 0.5 mM EGTA, 1 mM DTT, 3 mM MgAc). 3 ml of lysis buffer containing 0.4% triton-X was added and the suspension was homogenized 10 times using a large and small pestle (Wheaton, Vancouver, Canada, supplier: Fisher Scientific, Landsmeer, The Netherlands). The solution was filtered through a 100 µm and 30 µm filter (Sysmex, CellTrics, Norderstedt, Germany). The filter were washed with 2 ml lysis buffer containing 0.2% triton-X. The solution was centrifuged for 5 min at 1000g at 4°C. The pellet was

resuspended in 500 µl staining buffer (2.5% BSA in PBS (pH8.0 and 0.2% Igepal CA-630). The solution was incubated with rabbit anti-PCM-1 (diluted 1:1000, HPA023370, Atlas Antibodies) and Alexa 647 (diluted, 1:500, A-31573, Thermo Fisher) for 1h. DAPI was added (0.001 mg/mL, Sigma-Aldrich, D9542, supplier: Merck, Zwijndrecht, The Netherlands). Sorting of PCM-1 positive nuclei was done on the BD Influx cell sorter (BD Bioscience, Vianen, the Netherlands). Nuclei were directly sorted into lysis buffer of the RNeasy plus micro kit (Quiagen) for subsequent RNA isolation or in 500 µl staining buffer for CUT&RUN-sequencing.

RNA-Sequencing

RNA-sequencing from cardiac nuclei was performed as described previously [28]. 500 pg of RNA was used for cDNA preparation with the Ovation RNA-seq V2 kit (7102-08, Tecan, Leek, The Netherlands). Libraries were prepared with the UltraLow V2 kit (0344NB-08, Tecan, Leek, The Netherlands) and sequencing was performed on the HiSeq4000 system (Illumnia, San Diego, USA) with 50 bp single-end reads.

Differential Expression Analysis

Reads were mapped to the mm10 build of the mouse transcriptome using STAR [29]. Differential expression between groups was determined using the DESeq2 packaged based on using the negative binominal distribution [30]. P-values were corrected for multiple testing by using the false discovery rate of Benjamini- Hochberg ($P<0.05$). Principal component analysis was performed with the DESeq2 package, using default parameters. Gene ontology (GO) term analysis was performed using DAVID v6.8 (https://david.ncifcrf.gov/ (accessed on 13-08-2021)). p-values indicated for the GO terms were corrected for multiple testing using Benjamini–Hochberg correction [31,32].

CUT&RUN-Sequencing

Cleavage under targets and release using nuclease (CUT&RUN) sequencing [23] was performed following the protocol from Hainer and Fazzio [33]. Approximately 50.000 nuclei were sorted by flow cytometry. Nuclei were collected in staining buffer and centrifuged for 5 min at 1000g at 4˚C. The supernatant was discarded and the nuclei pellet was resuspended in 600 µl NE buffer (20 mM HEPES-KOH, pH 7.9, 10 mM KCl, 0.5 mM Spermidine, 0.1% Triton X-100, 20% glycerol, freshly added protease inhibitors), according to step 7 of the protocol. Nuclei bound to the Concanavalin A beads (86057-10, Polysciences) were incubated over night at 4˚C with anti- H3K27ac (diluted 1:200, 39133, Active Motif), The pA-MNase (1.75 µl) was diluted in 250 µl wash buffer and samples were incubated for 1h at 4˚C.

For library preparation the NEBNext Ultra 2 – DNA Library Prep Kit for Illumina was used (E7645S, E7335S, NEB), following the protocol according to an input of less than 50 ng DNA. For PCR enrichment of adaptor ligated DNA the protocol in [33] was followed

(98˚C for 45 sec, 14 times 98˚C for 15 sec and 60˚C for 10 sec, finished by 72˚C for 60 sec). Elution of the library was performed in 20µl 10mM Tris-HCl. Samples were sequenced on the Illumnia HiSeq4000 paired-end sequencing 150 bp.

Differential Acetylation Analysis

For differential acetylation analysis the reads were mapped to the mm10 build of the mouse genome using BWA [34]. The signal was distributed into bins of 500 bp using the BEDTools suite [35]. The background read level was determined per sample per 500 bp by taking the average read count in bins with less than 20 tags. The background level of tags was subtracted per bin per sample. To allow for differential peak calling between datasets, quantile normalization was applied using the deepTools2 suite [36]. Differential acetylation was assessed using the DESeq2 package based on a model using the negative binomial distribution [30].P-values were corrected for multiple testing by using the false discovery rate of Benjamini-Hochberg ($P<0.05$). Continuous bins with differential signal were subsequently merged together using the BEDTools suite. For promoter acetylation analysis the H3K27ac signal was distributed into promoter region bins defined as 2000bp up-stream and downstream of the canonical TSS (BioMart, vM3 annotation, mm10 build).

Overlap between H3K27ac and ATAC-Seq and Motif Analysis

H3K27ac data was intersected with ATAC-seq data obtained from 7 dpi FVB wildtype mice [13] using the BEDTools suite (v.2.30.0). To facilitate overlap analysis ATAC-peaks were increased 500 bp downstream and upstream. Motif enrichment analysis was performed on the 200bp ATAC-seq summits using HOMER (v4.11) (http://homer.ucsd.edu/homer/, accessed on 20-04-2020 [37]. Motifs were classified as enriched when $P < 1-10$.

Overlap with ChIP-Seq

Raw ChIP-seq reads for Mef2 [38], c-Jun [39], PPARα [40] and RXR [41] were extracted from the Sequence Read Archives and mapped to the mouse genome (mm10) with BWA [34] as previously described [13].

RESULTS

BZ Cardiomyocytes Downregulate Genes Involved in Lipid Metabolism

We have previously compared the transcriptome of PCM-1-positive cardiomyocyte nuclei isolated from the BZ and RM [13]. To compare the transcriptomes of cardiomyocyte nuclei between cardiomyocytes from the BZ and the healthy left ventricle (LV), myocardial infarction was induced by ligation of the left descending coronary artery on 8-week-old male mice. At 7 days after the infarction, hearts were harvested and microdissected into BZ and RM. We compared the nuclear transcriptome of PCM1+ BZ cardiomyocytes ($n = 5$) with that of cardiomyocytes from the RM ($n = 4$) and the LV of age matched male mice ($n = 3$)

(Table S1, Figure S1). Unsupervised principal component (PC) analysis revealed clustering of samples from the LV and one sample of the RM. Two samples from the BZ cluster together with samples obtained from RM. The remaining three BZ samples do not cluster together and show a high variance along the first and second PC (Figure 1A). Differences between the BZ samples may reflect variability in MI severity or response, and variation in the micro-dissected area, containing different ratios of BZ and RM cardiomyocytes. There are only around a hundred genes differentially expressed between the LV and the RM (Figure 1B). Of the several hundred genes differentially expressed between the BZ and the RM, the established BZ markers *Nppa*, *Acta1*, *Clu*, *Uchl1* and *Serpine1* are all represented as expected (Figure 1C) [13]. When compared to the cardiomyocyte nuclei of the control LV, those of the BZ differentially expressed 2732 genes (p-adj<0.05; Figure 1D). Gene ontology (GO) analysis revealed that genes differentially expressed at higher levels are involved in processes of focal adhesion, cell-cell adherens junctions, as well as receptor interaction with the extracellular matrix.

Genes that are lower expressed in the BZ CM nuclei are mainly involved in mitochondrial processes, lipid metabolism and ion transport. BZ cardiomyocytes also show significantly higher expression of genes known to be expressed by activated fibroblasts such as *Postn* and *Fn1* [12]. An important point to note here is that although sorting of PCM-1 positive nuclei from ventricular tissue highly enriches for cardiomyocyte nuclei [13,42], the very high number of fibroblasts and infiltrating immune cells in the BZ as compared to normal LV tissue may result in contamination of the PCM-1 positive cardiomyocyte nuclei population, causing inflated differences in gene expression between LV and BZ.

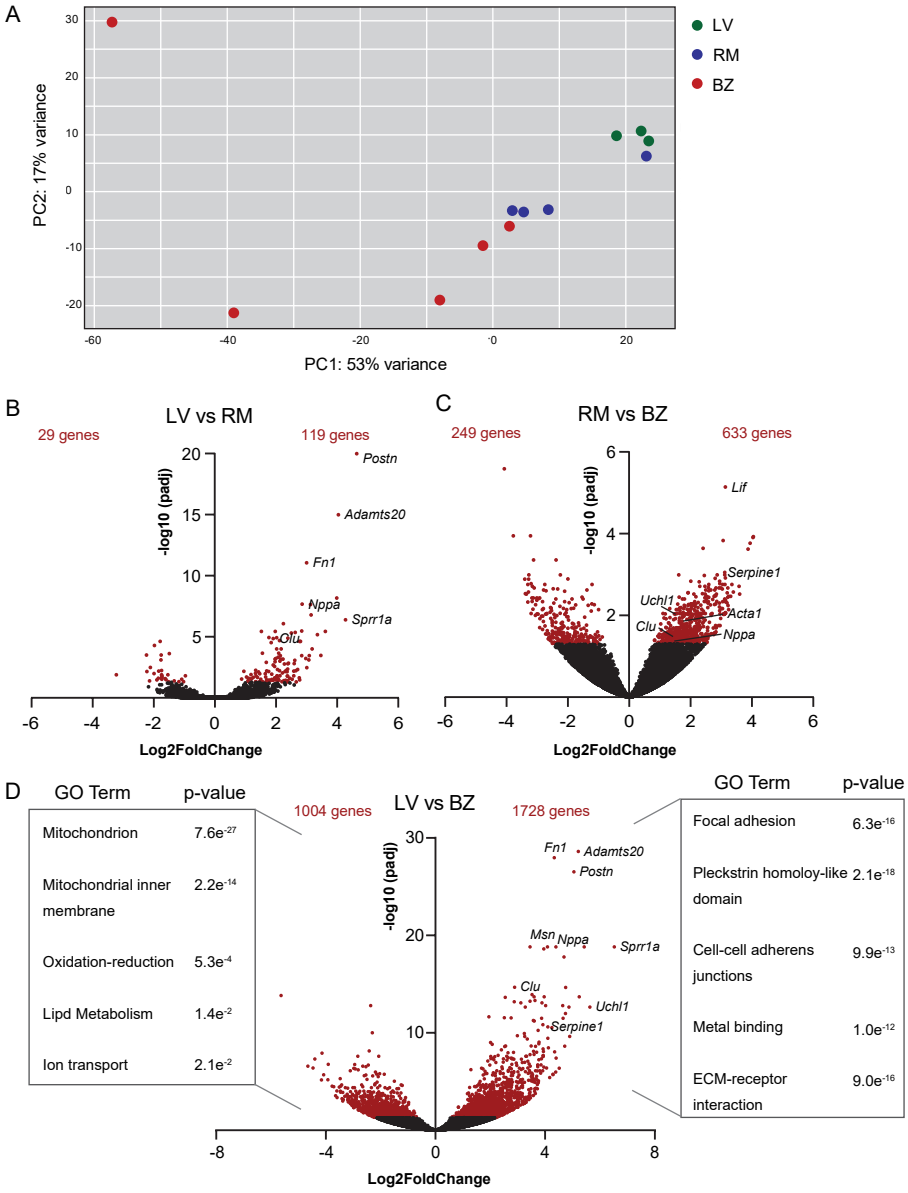

Figure 1. (**A**) Principal component analysis shows that samples from the left ventricle (LV) (n = 3) cluster together. Border zone (BZ) (n = 5) samples partially cluster with samples from the remote myocardium (RM) (n = 4) or do not cluster together. Green: LV, red: BZ, blue: RM. (**B**) Volcano plots showing nuclear transcripts of PCM1-positive cardiomyocytes that are differentially expressed between LV and RM and (**C**) RM and BZ. (**C**) Volcano plots showing nuclear transcripts of PCM1-positive cardiomyocytes that are differentially expressed between RM (n = 4) and BZ (n = 5). Red dots show significantly differentially expressed genes (p adjusted for multiple testing: false discovery date < 0.05). (**D**) Volcano plot shows significantly differentially expressed genes between BZ (n = 5) and LV (n = 3). Gene ontology analysis was performed on significantly higher and lower expressed genes of both groups.

Epigenetic State of Border-Zone Cardiomyocytes

ATAC-sequencing at 7 dpi has shown that the chromatin accessibility of BZ cardiomyocytes changes with thousands of genomic regions gaining or loosing accessibility [13]. Regions gaining accessibility were significantly enriched for motifs recognized by AP-1 transcription factors (i.e. dimers of Jun, Fos, etc.). Less accessible sites were recognized by cardiomyocyte lineage-specific Mef2 transcription factors [13]. ATAC-seq identifies all regions of accessible chromatin, irrespective of the function of those sites. The accessible sites population therefore includes enhancers, promoters, silencers, insulators, boundary elements, etc. On the other hand, H3K27ac is predominantly enriched at sites flanking active promoters and enhancers [22]. We performed H3K27ac profiling of cardiomyocytes by CUT&RUN-sequencing in the BZ (n = 3) and the LV (n = 3) (Table S2). Principal component (PC) analysis shows clustering of the samples originating from the LV with the first component reflecting the origin of the tissue (Figure 2A). We analyzed H3K27ac at transcription start sites of 2663 differentially expressed genes and found that of 1736 genes that lost or gained H3K27ac signal in the BZ, that this directly correlated with the observed change in expression (Figure 2B and Table S2). The known BZ markers *Nppa* and *Nppb* displayed increased expression and increased H3K27ac at their promoters as expected (Figure 2C). We also cross-referenced the H3K27ac data with previously obtained data from ATAC-sequencing of LV and BZ cardiomyocytes [13]. When compared to the LV, 6253 regions showed less H3K27ac signal in BZ (Figure 3A). Of these, almost 3000 overlapped with sites of reduced accessibility. We detected increased BZ H3K27ac signal in 8484 regions. Of these, over 1500 overlapped with chromatin regions being also more accessible (Figure 3B).

We used HOMER to identify enrichment of motifs of transcription factor binding sites at sites of differential accessibility or H3K27ac association (TableS3). Sites with decreased H3K27 acetylation were enriched for motifs recognized by Mef2 transcription factors, in accordance with the decreased accessibility of these motifs seen in the ATAC-seq (Figure 3C). In addition, we observed decreased acetylation of motifs recognized by the nuclear receptor (NR) superfamily of transcription factors, including estrogen related receptor alpha (Erra), retinoid X receptor (RXR) and elements for peroxisome proliferator-activated receptors (PPARs). These transcription factors are involved in the regulation of fatty acid metabolism and oxidative phosphorylation [25,26]. We obtained similar results for the population displaying a decrease in H3K27ac as well as diminished chromatin accessibility (Figure 3D). The population of less accessible chromatin in the ATAC-seq, but with-out a change in H3K27ac, displays mainly motifs recognized by the Mef2 transcription factors. Chromatin regions showing increased accessibility and increased H3K27ac association are enriched for binding sites of transcription factors that form AP-1 (Jun, Fos/Fra, Atf), showing that these putative regulatory elements are likely to be active in BZ cardio-myocytes (Figure 3E,F). The population that is only increased in accessibility as shown by ATAC-seq but does not show increased H3K27ac signal is mainly enriched for binding sites of members of the ETS

(ERG, ETV), SCL, SP and KLF families of transcription factors, and to a lesser extend for binding sites of AP-1 transcription factors.

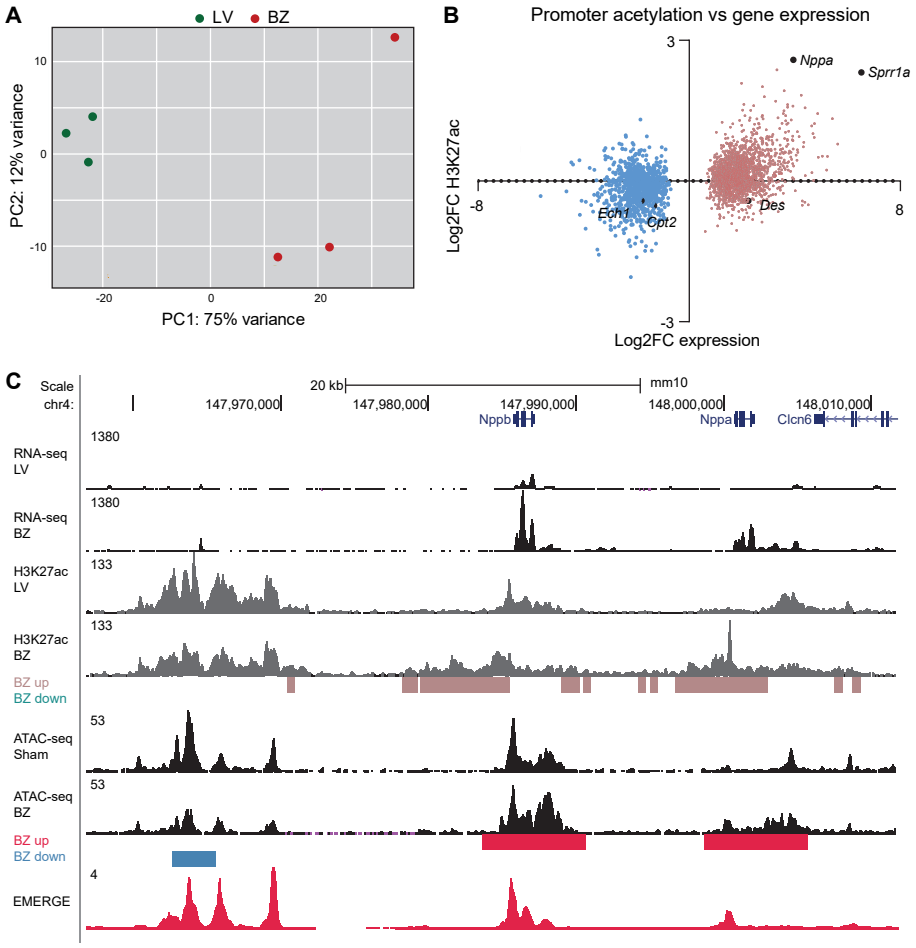

Figure 2. (**A**) Principal component analysis of samples from the left ventricle (LV) (n = 3) and the border zone (BZ) (n = 3) used for H3K27ac profiling by CUT&RUN-sequencing. (**B**) Scatterplot showing the relation between significantly differentially expression of genes between BZ and LV and differential acetylation of the transcription start site (p value adjusted for multiple testing: false discovery rate < 0.05). (**C**) Representative UCSC browser view showing the Nppa and Nppb locus. ATAC-seq, assay for transposase-accessible chromatin using sequencing; CUT&RUN-seq, cleavage under target and release using nuclease -sequencing.

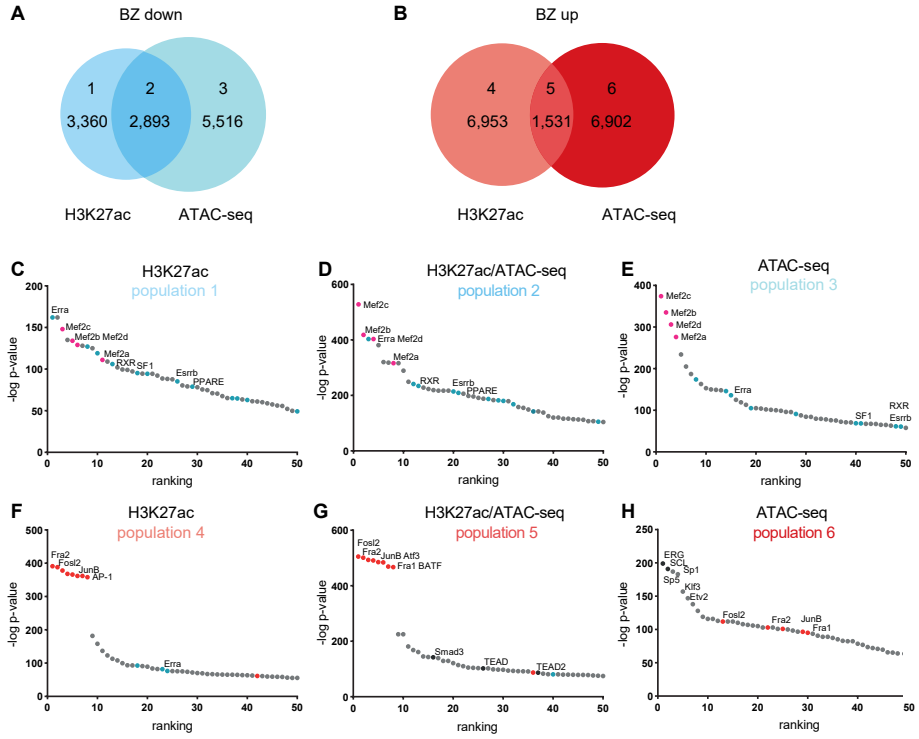

Figure 3. Venn diagram showing overlapping decrease (**A**) and increase (**B**) in H3K27ac and chromatin accessibility by ATAC-seq. Enriched motifs recognized by transcription factors for loci with decreased H3K27ac (**C**), decreased H3K27ac and chromatin accessibility (**D**), or decreased chromatin accessibility only (**E**). Enriched motifs recognized by transcription factors for loci with increased H3K27ac (**F**), increased H3K27ac and chromatin accessibility (**G**), or increased chromatin accessibility only (**H**).

Deregulation of PPAR Target Genes and Glycolysis Genes in BZ Cardiomyocytes

We next further explored the implications of the observation that NR binding sites are enriched in the population of chromatin sites with reduced H3K27ac signal. Expression levels of NR-transcription factors were not significantly changed between BZ and LV, although *Pparg* (encoding PPARα) expression was slightly elevated in BZ cardiomyocytes (Figure 4A). We studied transcription levels of PPARα target genes that were reported to be downregulated in the failing heart and found that *Cpt2*, *Ech1*, *Fabpc3* and *Vldrl* were all significantly reduced in BZ cardiomyocytes [43] (Figure 4B). At the same time, BZ cardiomyocytes showed an increased expression of glycolysis genes *Hk1* (Hexokinase 1), *Pkm* (Pyruvate Kinase M1/2), *Pfkp* (Phosphofructokinase, Platelet) and *Eno2* (Enolase 2) and of *Slc2a1* (Solute Carrier Family 2 Member 1) important in the uptake of glucose into cardiomyocytes (Fig. 4C). However, we did not observe these differences in expression when compared to the RM (Supplemental Figure S3A). Expression of *Hk1*, *Pdk2* and *Slc2a1*

(GLUT1) is induced in Nppa+ BZ cardiomyocytes, *Pdk2* expression is also visible in the RM (Figure 4D, Supplemental Figure S3B). Pyruvate dehydrogenase (PDH) converts pyruvate to Acetyl-CoA, thereby linking glycolysis to the TCA cycle (oxidative phosphorylation of pyruvate). Phosphorylation of PDH inactivates the enzyme complex, causing pyruvate to be diverted away from the TCA cycle, resulting in enhanced lactate production. We observed increased levels of phosphorylated PDH [19] in BZ cardiomyocytes compared to RM cardiomyocytes (Supplemental Figure S3C).

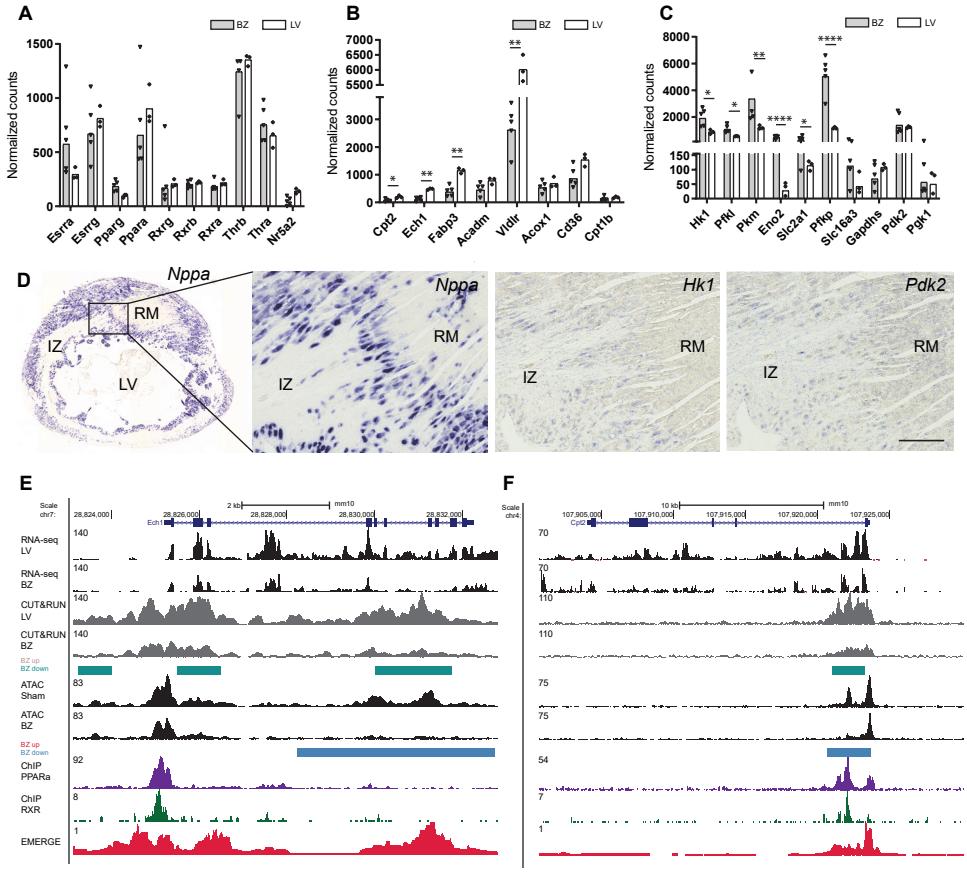

Figure 4. Average expression of NR transcription factors (**A**), PPAR target genes (**B**), and glycolytic genes (**C**) shown as normalized counts in border zone (BZ) samples (n = 5) and samples from the healthy left ventricle (n = 3). (**D**) Expression of *Hk1* and *Pdk1* is induced in *Nppa*+ BZ cardiomyocytes. *Pdk1* expression is also visible in the RM as shown by *in situ* hybridization; scale bar 0.1 mm. UCSC genome browser views of (**E**) *Ech1* and (**F**) *Cpt2*. ATAC-seq, assay for transposase-accessible chromatin using sequencing; CUT&RUN-seq, cleavage under target and release using nuclease-sequencing; ChIP, chromatin immunoprecipitation sequencing; BZ, border zone; RM, remote myocardium; IZ, infarct zone; and LV, left ventricle. * P<0.05, ** P<0.001, **** P<0.0001

To investigate whether the changes in expression were associated with epigenetic state changes, we assessed the distribution of chromatin accessibility as well as H3K27ac signal and compared these with ChIP-seq data for PPARα [40] as well as RXR [41] (Figure 4E,F; Supplemental Figure S1). The *Ech1* gene, encoding the enoyl CoA hydratase 1 (ECH1) is downregulated in BZ cardiomyocytes. The ECH1 enzyme plays a role in the mitochondrial β-oxidation pathway [44] and was previously identified as marker for the remote myocardium [13]. In BZ cardiomyocyte nuclei, H3K27ac association is decreased upstream of the gene locus as well as within the gene body, accompanied by a decrease in chromatin accessibility. ChIP-seq data for RXR and PPARα reveals binding sites for both transcription factors at the *Ech1* promotor (Figure 4E). The gene *Cpt2* encodes the carnitine palmytoiltransferase 2 (CPT2). CPT2 metabolizes acylcarnitines. Decreased levels of CPT2 were detected in ischemic hearts, leading to an increase of fatty acid intermediates and reactive oxygen species and thereby causing mitochondrial damage [45]. We observed a decreased chromatin accessibility overlapping a reduction in H3K27ac levels within the first intron of *Cpt2* (Figure 4F). These regions show binding sites for PPARα as well as RXR. The *Vldlr* gene encodes the very low-density lipoprotein receptor (VLDLR), that mediates the uptake of VLDL [46]. Chromatin accessibility is decreased for the upstream region and the first intron (Supplemental Figure S4A). PPARα is associated with the differential H3K27ac regions including the promoter and first intron.

Fatty acid binding protein 3 (FABP3) binds to long-chain fatty acids to facilitate lipid storage and metabolism, and overexpression of *Fabp3* caused apoptosis of cardiomyocytes after MI [47]. The whole locus of *Fabp3* becomes less accessible in BZ cardiomyocytes, however, H3K27ac signals are not decreased. There are several PPARα binding sites within the gene body and the upstream region flanking *Fabp3*, but no binding sites for RXR (Supplemental Figure S4B). These data indicate that the downregulation of genes involved in fatty acid metabolism is driven by reduced enhancer-promoter activity in BZ cardiomyocytes, and that PPAR-RXR may be involved in this downregulation. In contrast, the induction of *Slc2a1*, *Eno2*, and *Pfkp* is associated with increased H3K27ac and accessibility of promoters and putative enhancers in these loci, suggesting that enhancer activity at these loci is increased (Figure 5A,B; Supplemental Figure S4E). Signal for PPAR or RXR occupation was not detected in these loci. For *Hk1* and *Pkm* the landscape did not change consistently (Figure S4C,D).

In the heart, PPARs form a heterodimeric complex with RXR and recruit co-activators such as the peroxisome proliferator activated receptor alpha and beta (PGC-1α, PGC-1β) [48]. PGC-1α and -β control overlapping gene programs for cellular energy metabolism and are required for postnatal functional and metabolic maturation of the myocardium [48–50]. Target genes regulated by PGC-1 are involved in mitochondrial biogenesis, oxidative phosphorylation and fatty acid metabolism and decreased expression of PGC-1 is associated with a decrease in mitochondrial function [51]. We found that expression of *Ppargc1a*

encoding PGC-1α is significantly reduced in BZ cardiomyocyte nuclei (Figure 5C). Expression of *Ppargc1b* is not significantly altered. In the BZ, the epigenetic state of both *Ppargc1a* and *Ppargc1b* is changed with several chromatin regions within the gene body being less accessible. In addition, several regions at both loci show decreased H3K27ac signal (Figure 5D, Supplemental Figure S4F).

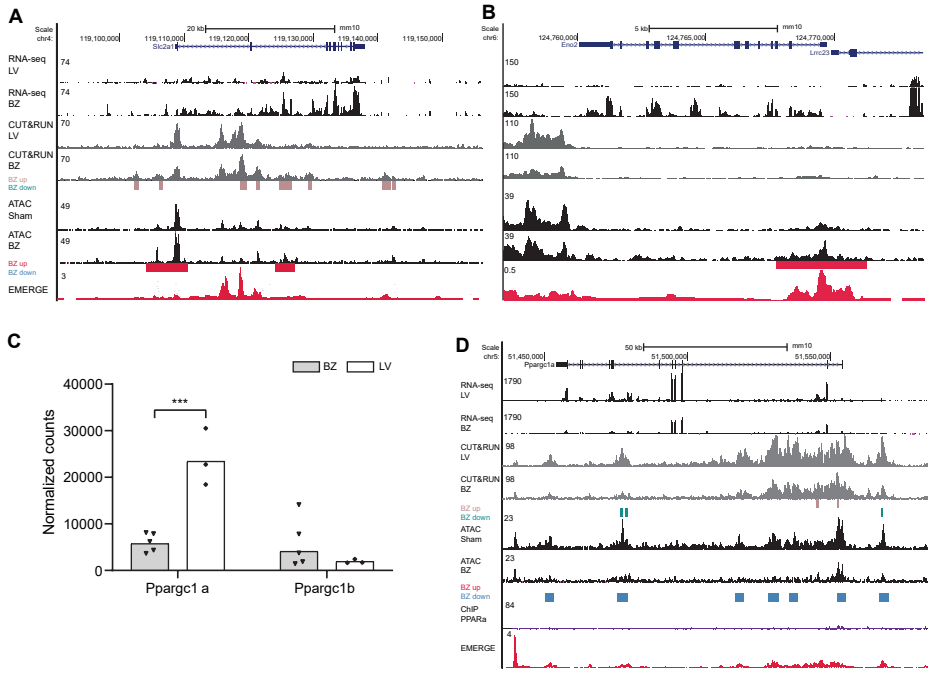

Figure 5. UCSC genome browser views of (**A**) *Slc2a1* and (**B**) *Eno2*. Average expression of *Ppargc1a* and *Ppargc1b* (**C**) shown as normalized counts in border-zone (BZ) samples (n = 5) and samples from the healthy left ventricle (n = 3). UCSC genome browser views of (**D**) *Ppargc1b*. ATAC-seq, assay for transposase-accessible chromatin using sequencing; CUT&RUN-seq, cleavage under target and release using nuclease-sequencing; ChIP, chromatin immunoprecipitation sequencing; BZ, border zone; and LV, left ventricle.*** P<0.001

DISCUSSION

When the coronary occlusion of an MI is not resolved, the myocardium downstream of the occlusion dies and an IZ is formed. The IZ is surrounded by a thin BZ, which contains surviving cardiomyocytes that are highly affected by the physiological condition of the heart and signals from the IZ. The BZ cardiomyocytes themselves are involved in post-MI arrhythmogenesis and play an active role in the healing process [13,52]. The MI BZ of the mammalian (human, mouse) heart shows similarities with the BZ of the injured fish heart [13,19,53]. Fish heart regeneration relies on proliferation of the pre-existing cardiomyocytes

in the BZ [54]. Similarly, in mice with transgenically enhanced cardiac regenerative capacity, cardiomyocyte proliferation occurs mainly in the BZ cardiomyocytes [55–58]. Here, we focused on the transcriptional and epigenetic characterization of the cardiomyocytes in the BZ a week after permanent coronary artery ligation to gain further insight into the properties and potential of these cells. The BZ is comprised of several different cell-types, including endothelial cells, increased numbers of fibroblasts, infiltrating immune cells, and a small number of cardiomyocytes. All these cell types respond to the injury by inducing or repressing injury-responsive gene programs. This, along with the technical challenges of actually separating the different populations of cells, has hampered the characterization of specific cell types such as the cardiomyocytes in the BZ area. Thus far, most transcriptome data and epigenetic state data has been based on whole tis-sue preparations or cryosections of MI hearts, which has limited the detection of cardiomyocyte-specific responses [11,16–18,59]. The use of cell purification approaches or single cell sequencing can overcome these limitations, and have previously been deployed to gain insight into the transcriptomes of BZ cardiomyocytes [13] and cardiomyocytes of the left ventricle after ischemia-reperfusion [10,12]. Here, the purification of PCM-1+ cardio-myocyte nuclei from control left ventricular wall, RM and BZ tissue has allowed us to identify and characterize specifically their transcriptomes and, in addition, their epigenetic H3K27ac profiles. These data sets can be used as a resource and reference data set to explore and study novel aspects specifically relating to BZ cardiomyocytes.

Our current data indicates that the transcriptome of cardiomyocytes of the BZ differs extensively from that of the control LV. The transcriptome of the RM cardiomyocytes was only modestly affected, indicating that the MI responses in RM and BZ cardiomyocytes is comparable but much more extensive in BZ cardiomyocytes. Almost 3 thousand genes were significantly differentially expressed between BZ and LV cardiomyocyte nuclei, and we focused on differential expression of genes involved in energy metabolism. During MI-induced ischemia, reduced oxygen delivery to the myocardium causes mitochondrial metabolic dysfunction and decreased ATP formation by oxidative phosphorylation. This stimulates an increase in glucose uptake and glycolysis, accompanied by lactate accumulation and decreased intracellular pH [60]. While the initial metabolic response to MI occurs at the level of protein activity, genes involved in mitochondrial activity and organization, energy metabolism (oxidative phosphorylation, fatty acid metabolism) were strongly downregulated in the BZ cardiomyocytes, and to a lesser extent in RM. This indicates that 7 and 14 days after MI, the reduction of aerobic energy production and fatty acid consumption have been firmly established in the gene programs in BZ cardiomyocytes [13]. Furthermore, we noted that expression levels of several genes involved in glucose uptake and metabolism are upregulated in BZ cardiomyocytes. This suggests that glucose metabolism preservation at least to some extent is supported by activation of the underlying gene program in BZ cardiomyocytes. In the fish heart, injury BZ cardiomyocytes switch energy metabolism from mitochondrial oxidative phosphorylation to glycolysis and lactate fermentation. This Nrg1/

ErbB2 signaling induced switch is required for the proliferation of the BZ cardiomyocytes to regenerate the cardiac muscle [19]. Also in the mouse heart, activation of ErbB2 signaling caused an increase in cardiac expression of glycolysis genes and suppression of mitochondrial genes in normal and in MI hearts [19]. We also observed increased expression of the glycolysis gene *Pkm*, encoding pyruvate kinase muscle, in BZ cardiomyocytes, and to a lesser extent in RM cardiomyocytes. The M2 isoform of pyruvate kinase (PKM2) catalyzes a rate-limiting reaction in the glycolytic pathway but also modulates gene expression and contributes to tumorigenesis [61]. Intriguingly, a recent study demonstrated that cardiac *Pkm2* overexpression activates two separate and synergistic pathways (increased G6pd and interaction with β-catenin upregulating cell cycle genes) in cardiomyocytes to induce the cardiomyocyte cell cycle and cardiac regeneration after injury [63]. [62]. While the induced expression of native *Pkm* evidently is insufficient to induce proliferation of BZ cardiomyocytes, it may contribute to their predisposition to initiate proliferation after injury when additional cardiomyocyte cell cycle pathways are being activated, such as ERBB, YAP or hypoxia [63].

Previously, we found that the genome-wide chromatin accessibility patterns were changed in BZ cardiomyocytes compared to healthy cardiomyocytes. Accessibility reveals the degree to which nuclear protein complexes have physical access to the chromatinized DNA, irrespective of the function of the accessible site. H3K27ac marks the flanks of active enhancers and promoters [22], and therefore reveals the subpopulation of accessible sites that act as active enhancer or promoter. We assessed the genome-wide patterns of H3K27ac in BZ and control cardiomyocyte nuclei and found that thousands of putative enhancers and promoters gained or lost H3K27ac signal. The reduction in H3K27ac correlated with reduced expression of genes for oxidative phosphorylation and fatty acid metabolism, amongst others, indicating altered enhancer usage and epigenetic status underlies the changes in gene expression in BZ cardiomyocytes 7 days after MI. Accessible genomic sites associated with increased H3K27ac in BZ cardiomyocytes were highly enriched for motifs of binding sites for AP-1 transcription factors. This suggests that the AP-1 mediated transcription regulatory response leads to broad enhancer activation. Interestingly, sites that gained accessibility but not H3K27ac signal were only moderately enriched for AP-1 motifs, but highly enriched for binding sites of members of ERG/ETS, SP, ETV and KLF families of transcription factors. This suggests that these factors gain access to these sites in BZ cardiomyocytes, but that this does not lead to enhancer activation. In this respect, the recently identified function of KLF1 in rewiring of energy metabolism enabling cardiomyocyte proliferation and regeneration may be relevant in mammals [20]. Sites with reduced accessibility, reduced H3K27ac signal, or both, were enriched for MEF2 binding sites, suggesting that loss of MEF2 interaction with DNA occurs, and that this in many cases leads to reduced enhancer activity. Noteworthy, the sites of reduced H3K27ac signal are additionally enriched for motifs of binding sites for nuclear receptors (NRs) PPAR, RXR and ERRA. Previously, we did not detect these motifs as they are not obviously enriched in the population of sites with reduced accessibility [13].

In the heart, fatty acid metabolism is regulated by peroxisome proliferator-activated receptors (PPAR), members of the NR superfamily of transcription factors [26,64–67]. Conditions such as hypoxia were shown to lead to decreased PPARα expression and reduction of PPAR target gene expression causing cardiomyocytes to switch from fatty acid metabolism to glycolysis [67]. However, while we observed significant downregulation of PPARα target genes, we did not observe downregulation of PPAR family members or other NRs in BZ cardiomyocytes. Our data suggest that the reduction of expression of PPAR target genes is mediated by changed DNA binding activity of PPARs (and other involved NRs), leading to decommissioning of PPAR associated enhancers. The function of PPARs as regulators of transcriptional activity is complex and multi layered, and depends on their interaction with co-factors. PGC-1α is a co-factor of both PPARα-RXRα and of ERR (PPAR, RXR and ERR have similar binding motifs), and these complexes bind target gene enhancers and regulate energy metabolism [48–51]. *Ppargc1a*, encoding PGC-1α, is a target of PPAR-RXR and was strongly downregulated in BZ cardiomyocytes. We speculate that reduced concentrations of PGC-1α affects the formation of complexes with PPAR-RXR and ERR, respectively, influencing the association with particular enhancers. Furthermore, in the pathologically hypertrophic heart, PPARα forms a heterodimer with Sirt1 (Silent Information Regulator 1) instead of RXR, leading to altered complex function, altered enhancer usage and suppressed fatty acid metabolism [43,65]. However, while RXRα is downregulated and Sirt1 upregulated in the failing heart, supporting this switch, we did not observe any change in expression of the genes encoding RXR or Sirt family members in BZ cardiomyocytes. Interestingly, treatment of PPAR agonists or PPAR overexpression in the period around experimentally induced ischemia reperfusion or permanent MI shows varying outcomes, with some studies reporting reduced infarct sizes and improved cardiac function, whereas other studies report larger infarct sizes and impaired ventricular function [66]. PPARβ/δ activation has recently been proposed to be cardioprotective after ischemia reperfusion by reducing oxidative stress and maintaining mitochondrial function [68]. While the function of NRs like PPAR and ERR in the BZ cardiomyocytes is not well characterized, we hypothesize that PPAR agonist treatment may induce re-occupation of PPAR-dependent enhancers in BZ cardiomyocytes, which re-activates fatty acid energy metabolism in these cells, influencing their survival and function.

Funding: This research was funded by Netherlands Heart Foundation, grant number COBRA3 (NHS 2013T091) and OUTREACH.

Informed Consent Statement: All animal experiments were performed according to the directive 2010/63/EU of the European Parliament. The protocol was approved by the Animal Experimental Committee of the Amsterdam University Medical Center and was carried out according the guidelines of the Dutch government. Experiments were performed under DAE285.

Data Availability Statement: The RNA-seq data and H3K27ac data has been deposited at the Gene Expression Omnibus under the following accession numbers: GSE183168 and GSE183095.

Conflicts of Interest: The authors declare no conflict of interest.

REFERENCES

1. Mozaffarian, D.; Benjamin, E.J.; Go, A.S.; Arnett, D.K.; Blaha, M.J.; Cushman, M.; Das, S.R.; de Ferranti, S.; Després, J.-P.; Fullerton, H.J.; et al. Heart Disease and Stroke Statistics—2016 Update. Circulation 2016, doi:10.1161/cir.0000000000000350.
2. Zuurbier, C.J.; Bertrand, L.; Beauloye, C.R.; Andreadou, I.; Ruiz-Meana, M.; Jespersen, N.R.; Kula-Alwar, D.; Prag, H.A.; Eric Botker, H.; Dambrova, M.; et al. Cardiac Metabolism as a Driver and Therapeutic Target of Myocardial Infarction. Journal of Cellular and Molecular Medicine 2020, 24, 5937–5954, doi:10.1111/jcmm.15180.
3. Aljakna, A.; Fracasso, T.; Sabatasso, S. Molecular Tissue Changes in Early Myocardial Ischemia: From Pathophysiology to the Identification of New Diagnostic Markers. International Journal of Legal Medicine 2018, 132, 425–438, doi:10.1007/s00414-017-1750-z.
4. Driesen, R.B.; Verheyen, F.K.; Dijkstra, P.; Thoné, F.; Cleutjens, J.P.; Lenders, M.H.; Ramaekers, F.C.S.; Borgers, M. Structural Remodelling of Cardiomyocytes in the Border Zone of Infarcted Rabbit Heart. Molecular and Cellular Biochemistry 2007, 302, 225–232, doi:10.1007/s11010-007-9445-2.
5. Matsushita, T.; Oyamada, M.; Fujimoto, K.; Yasuda, Y.; Masuda, S.; Wada, Y.; Takahiro, O.; Takamatsu, T. Remodeling of Cell-Cell and Cell-Extracellular Matrix Interactions at the Border Zone of Rat Myocardial Infarcts. Circulation Research 1999, 85, 1046–1055, doi:10.1161/01.RES.85.11.1046.
6. Borgers, M.; Thoné, F.; Wouters, L.; Ausma, J.; Shivalkar, B.; Flameng, W. Structural Correlates of Regional Myocardial Dysfunction in Patients with Critical Coronary Artery Stenosis: Chronic Hibernation? Cardiovascular Pathology 1993, 2, 237–245, doi:10.1016/1054-8807(93)90030-6.
7. Wang, W.E.; Li, L.; Xia, X.; Fu, W.; Liao, Q.; Lan, C.; Yang, D.; Chen, H.; Yue, R.; Zeng, C.C.C.C.S.; et al. Dedifferentiation, Proliferation, and Redifferentiation of Adult Mammalian Cardiomyocytes after Ischemic Injury. Circulation 2017, 136, 834–848, doi:10.1161/CIRCULATIONAHA.116.024307.
8. Dispersyn, G.D.; Mesotten, L.; Meuris, B.; Maes, A.; Mortelmans, L.; Flameng, W.; Ramaekers, F.; Borgers, M. Dissociation of Cardiomyocyte Apoptosis and Dedifferentiation in Infarct Border Zones. European Heart Journal 2002, doi:10.1053/euhj.2001.2963.
9. Sharov, V.G.; Sabbah, H.N.; Ali, A.S.; Shimoyama, H.; Lesch, M.; Goldstein, S. Abnormalities of Cardiocytes in Regions Bordering Fibrous Scars of Dogs with Heart Failure. International Journal of Cardiology 1997, doi:10.1016/S0167-5273(97)00117-4.
10. Molenaar, B.; Timmer, L.T.; Droog, M.; Perini, I.; Versteeg, D.; Kooijman, L.; Monshouwer-Kloots, J.; de Ruiter, H.; Gladka, M.M.; van Rooij, E. Single-Cell Transcriptomics Following Ischemic Injury Identifies a Role for B2M in Cardiac Repair. Communications Biology 2021, 4, 1–15, doi:10.1038/s42003-020-01636-3.
11. Lacraz, G.P.A.; Junker, J.P.; Gladka, M.M.; Molenaar, B.; Scholman, K.T.; Vigil-Garcia, M.; Versteeg, D.; De Ruiter, H.; Vermunt, M.W.; Creyghton, M.P.; et al. Tomo-Seq Identifies SOX9 as a Key Regulator of Cardiac Fibrosis during Ischemic Injury. Circulation 2017, doi:10.1161/CIRCULATIONAHA.117.027832.

12. Gladka, M.M.; Molenaar, B.; De Ruiter, H.; Van Der Elst, S.; Tsui, H.; Versteeg, D.; Lacraz, G.P.A.; Huibers, M.M.H.; Van Oudenaarden, A.; Van Rooij, E. Single-Cell Sequencing of the Healthy and Diseased Heart Reveals Cytoskeleton-Associated Protein 4 as a New Modulator of Fibroblasts Activation. Circulation 2018, 138, 166–180, doi:10.1161/CIRCULATIONAHA.117.030742.
13. van Duijvenboden, K.; de Bakker, D.E.M.; Man, J.C.K.; Janssen, R.; Günthel, M.; Hill, M.C.; Hooijkaas, I.B.; van der Made, I.; van der Kraak, P.H.; Vink, A.; et al. Conserved NPPB + Border Zone Switches From MEF2- to AP-1–Driven Gene Program . Circulation 2019, 140, 864–879, doi:10.1161/circulationaha.118.038944.
14. Farbehi, N.; Patrick, R.; Dorison, A.; Xaymardan, M.; Janbandhu, V.; Wystub-Lis, K.; Ho, J.W.K.; Nordon, R.E.; Harvey, R.P. Single-Cell Expression Profiling Reveals Dynamic Flux of Cardiac Stromal, Vascular and Immune Cells in Health and Injury. eLife 2019, doi:10.7554/eLife.43882.
15. Tombor, L.S.; John, D.; Glaser, S.F.; Luxán, G.; Forte, E.; Furtado, M.; Rosenthal, N.; Baumgarten, N.; Schulz, M.H.; Wittig, J.; et al. Single Cell Sequencing Reveals Endothelial Plasticity with Transient Mesenchymal Activation after Myocardial Infarction. Nature Communications 2021, doi:10.1038/s41467-021-20905-1.
16. Kaikkonen, M.U.; Halonen, P.; Liu, O.H.F.; Turunen, T.A.; Pajula, J.; Moreau, P.; Selvarajan, I.; Tuomainen, T.; Aavik, E.; Tavi, P.; et al. Genome-Wide Dynamics of Nascent Noncoding RNA Transcription in Porcine Heart after Myocardial Infarction. Circulation: Cardiovascular Genetics 2017, 10, 1–11, doi:10.1161/CIRCGENETICS.117.001702.
17. Zimmermann, M.; Beer, L.; Ullrich, R.; Lukovic, D.; Simader, E.; Traxler, D.; Wagner, T.; Nemec, L.; Altenburger, L.; Zuckermann, A.; et al. Analysis of Region Specific Gene Expression Patterns in the Heart and Systemic Responses after Experimental Myocardial Ischemia. Oncotarget 2017, doi:10.18632/oncotarget.17955.
18. Li, Y.; Wang, C.; Li, T.; Ma, L.; Fan, F.; Jin, Y.; Shen, J. The Whole Transcriptome and Proteome Changes in the Early Stage of Myocardial Infarction. Cell Death Discovery 2019, doi:10.1038/s41420-019-0152-z.
19. Honkoop, H.; de Bakker, D.E.M.; Aharonov, A.; Kruse, F.; Shakked, A.; Nguyen, P.D.; de Heus, C.; Garric, L.; J Muraro, M.; Shoffner, A.; et al. Single-Cell Analysis Uncovers That Metabolic Reprogramming by ErbB2 Signaling Is Essential for Cardiomyocyte Proliferation in the Regenerating Heart. eLife 2019, doi:10.7554/eLife.50163.
20. Ogawa, M.; Geng, F.-S.; Humphreys, D.T.; Kristianto, E.; Sheng, D.Z.; Hui, S.P.; Zhang, Y.; Sugimoto, K.; Nakayama, M.; Zheng, D.; et al. Krüppel-like Factor 1 Is a Core Cardiomyogenic Trigger in Zebrafish. Science (New York, N.Y.) 2021, 372, 201–205, doi:10.1126/science.abe2762.
21. Fukuda, R.; Marín-Juez, R.; El-Sammak, H.; Beisaw, A.; Ramadass, R.; Kuenne, C.; Guenther, S.; Konzer, A.; Bhagwat, A.M.; Graumann, J.; et al. Stimulation of Glycolysis Promotes Cardiomyocyte Proliferation after Injury in Adult Zebrafish. EMBO reports 2020, 21, e49752, doi:10.15252/embr.201949752.

22. Creyghton, M.P.; Cheng, A.W.; Welstead, G.G.; Kooistra, T.; Carey, B.W.; Steine, E.J.; Hanna, J.; Lodato, M.A.; Frampton, G.M.; Sharp, P.A.; et al. Histone H3K27ac Separates Active from Poised Enhancers and Predicts Developmental State. Proceedings of the National Academy of Sciences of the United States of America 2010, 107, 21931–21936, doi:10.1073/pnas.1016071107.
23. Skene, P.J.; Henikoff, S. An Efficient Targeted Nuclease Strategy for High-Resolution Mapping of DNA Binding Sites. eLife 2017, doi:10.7554/eLife.21856.
24. Belanger, A.J.; Luo, Z.; Vincent, K.A.; Akita, G.Y.; Cheng, S.H.; Gregory, R.J.; Jiang, C. Hypoxia-Inducible Factor 1 Mediates Hypoxia-Induced Cardiomyocyte Lipid Accumulation by Reducing the DNA Binding Activity of Peroxisome Proliferator-Activated Receptor α/Retinoid X Receptor. Biochemical and Biophysical Research Communications 2007, 364, 567–572, doi:10.1016/j.bbrc.2007.10.062.
25. Lee, W.S.; Kim, J. Peroxisome Proliferator-Activated Receptors and the Heart: Lessons from the Past and Future Directions. PPAR Research 2015, 2015, doi:10.1155/2015/271983.
26. Paredes, A.; Santos-clemente, R.; Ricote, M. Untangling the Cooperative Role of Nuclear Receptors in Cardiovascular Physiology and Disease. International Journal of Molecular Sciences 2021.
27. Moorman, A.F.M.; Houweling, A.C.; De Boer, P.A.J.; Christoffels, V.M. Sensitive Nonradioactive Detection of MRNA in Tissue Sections: Novel Application of the Whole-Mount in Situ Hybridization Protocol. Journal of Histochemistry and Cytochemistry 2001, doi:10.1177/002215540104900101.
28. Günthel, M.; van Duijvenboden, K.; Jeremiasse, J.; van den Hoff, M.J.B.; Christoffels, V.M. Early Postnatal Cardiac Stress Does Not Influence Ventricular Cardiomyocyte Cell-Cycle Withdrawal. Journal of Cardiovascular Development and Disease 2021, doi:10.3390/jcdd8040038.
29. Dobin, A.; Davis, C.A.; Schlesinger, F.; Drenkow, J.; Zaleski, C.; Jha, S.; Batut, P.; Chaisson, M.; Gingeras, T.R. STAR: Ultrafast Universal RNA-Seq Aligner. Bioinformatics 2013, doi:10.1093/bioinformatics/bts635.
30. Love, M.I.; Huber, W.; Anders, S. Moderated Estimation of Fold Change and Dispersion for RNA-Seq Data with DESeq2. Genome Biology 2014, doi:10.1186/s13059-014-0550-8.
31. Huang, D.W.; Sherman, B.T.; Lempicki, R.A. Bioinformatics Enrichment Tools: Paths toward the Comprehensive Functional Analysis of Large Gene Lists. Nucleic Acids Research 2009, doi:10.1093/nar/gkn923.
32. Huang, D.W.; Sherman, B.T.; Lempicki, R.A. Systematic and Integrative Analysis of Large Gene Lists Using DAVID Bioinformatics Resources. Nature Protocols 2009, doi:10.1038/nprot.2008.211.
33. Hainer, S.J.; Fazzio, T.G. High-Resolution Chromatin Profiling Using CUT&RUN. Current Protocols in Molecular Biology 2019, 126, 1–22, doi:10.1002/cpmb.85.
34. Li, H.; Durbin, R. Fast and Accurate Short Read Alignment with Burrows-Wheeler Transform. Bioinformatics 2009, doi:10.1093/bioinformatics/btp324.
35. Quinlan, A.R.; Hall, I.M. BEDTools: A Flexible Suite of Utilities for Comparing Genomic Features. Bioinformatics 2010, doi:10.1093/bioinformatics/btq033.
36. Ramírez, F.; Dündar, F.; Diehl, S.; Grüning, B.A.; Manke, T. DeepTools: A Flexible Platform for Exploring Deep-Sequencing Data. Nucleic Acids Research 2014, doi:10.1093/nar/gku365.

37. Benner, C.; Heinz, S.; Glass, C.K. HOMER - Software for Motif Discovery and next Generation Sequencing Analysis. http://homer.ucsd.edu/homer/motif/, accessed 20-04-2020.
38. Guo, A.; Wang, Y.Y.; Chen, B.; Wang, Y.Y.; Yuan, J.; Zhang, L.; Hall, D.; Wu, J.; Shi, Y.; Zhu, Q.; et al. E-C Coupling Structural Protein Junctophilin-2 Encodes a Stress-Adaptive Transcription Regulator. Science 2018, doi:10.1126/science.aan3303.
39. Umansky, K.B.; Feldmesser, E.; Groner, Y. Genomic-Wide Transcriptional Profiling in Primary Myoblasts Reveals Runx1-Regulated Genes in Muscle Regeneration. Genomics Data 2015, doi:10.1016/j.gdata.2015.08.030.
40. Shen, Y.; Su, Y.; Silva, F.J.; Weller, A.H.; Sostre-Colón, J.; Titchenell, P.M.; Steger, D.J.; Seale, P.; Soccio, R.E. Shared PPARα/γ Target Genes Regulate Brown Adipocyte Thermogenic Function. Cell Reports 2020, 30, 3079-3091.e5, doi:10.1016/j.celrep.2020.02.032.
41. Simandi, Z.; Horvath, A.; Cuaranta-Monroy, I.; Sauer, S.; Deleuze, J.F.; Nagy, L. RXR Heterodimers Orchestrate Transcriptional Control of Neurogenesis and Cell Fate Specification. Molecular and Cellular Endocrinology 2018, 471, 51–62, doi:10.1016/j.mce.2017.07.033.
42. Bergmann, O.; Zdunek, S.; Alkass, K.; Druid, H.; Bernard, S.; Frisén, J. Identification of Cardiomyocyte Nuclei and Assessment of Ploidy for the Analysis of Cell Turnover. Experimental Cell Research 2011, 317, 188–194, doi:10.1016/j.yexcr.2010.08.017.
43. Oka, S.I.; Zhai, P.; Yamamoto, T.; Ikeda, Y.; Byun, J.; Hsu, C.P.; Sadoshima, J. Peroxisome Proliferator Activated Receptor-α Association With Silent Information Regulator 1 Suppresses Cardiac Fatty Acid Metabolism in the Failing Heart. Circulation: Heart Failure 2015, 8, 1123–1132, doi:10.1161/CIRCHEARTFAILURE.115.002216.
44. Patkar, R.N. Mitochondrial β-Oxidation Regulates Organellar Integrity and Is Necessary for Conidial Germination and Invasive Growth in Magnaporthe Oryzae. Molecular Microbiology 2012, 86, 1345–1363, doi:10.1111/mmi.12060.
45. Liepinsh, E.; Makrecka-Kuka, M.; Volska, K.; Kuka, J.; Makarova, E.; Antone, U.; Sevostjanovs, E.; Vilskersts, R.; Strods, A.; Tars, K.; et al. Long-Chain Acylcarnitines Determine Ischaemia/Reperfusion-Induced Damage in Heart Mitochondria. Biochemical Journal 2016, 473, 1191–1202, doi:10.1042/BCJ20160164.
46. Gao, Y.; Shen, W.; Lu, B.; Zhang, Q.; Hu, Y.; Chen, Y. Upregulation of Hepatic VLDLR via PPARα Is Required for the Triglyceride-Lowering Effect of Fenofibrate. Journal of Lipid Research 2014, 55, 1622–1633, doi:10.1194/jlr.M041988.
47. Zhuang, L.; Li, C.; Chen, Q.; Jin, Q.; Wu, L.; Lu, L.; Yan, X.; Chen, K. Fatty Acid-Binding Protein 3 Contributes to Ischemic Heart Injury by Regulating Cardiac Myocyte Apoptosis and MAPK Pathways. American Journal of Physiology - Heart and Circulatory Physiology 2019, 316, H971–H984, doi:10.1152/ajpheart.00360.2018.
48. Finck, B.N.; Kelly, D.P. Peroxisome Proliferator-Activated Receptor Gamma Coactivator-1 (PGC-1) Regulatory Cascade in Cardiac Physiology and Disease. Circulation 2007, 115, 2540–8, doi:10.1161/CIRCULATIONAHA.107.670588.
49. Lai, L.; Leone, T.C.; Zechner, C.; Schaeffer, P.J.; Kelly, S.M.; Flanagan, D.P.; Medeiros, D.M.; Kovacs, A.; Kelly, D.P. Transcriptional Coactivators PGC-Lα and PGC-Lβ Control Overlapping Programs Required for Perinatal Maturation of the Heart. Genes and Development 2008, 22, 1948–1961, doi:10.1101/gad.1661708.

50. Murphy, S.A.; Miyamoto, M.; Kervadec, A.; Kannan, S.; Tampakakis, E.; Kambhampati, S.; Lin, B.L.; Paek, S.; Andersen, P.; Lee, D.-I.; et al. PGC1/PPAR Drive Cardiomyocyte Maturation at Single Cell Level via YAP1 and SF3B2. Nature communications 2021, 12, 1648, doi:10.1038/s41467-021-21957-z.
51. Zhu, X.; Shen, W.; Yao, K.; Wang, H.; Liu, B.; Li, T.; Song, L.; Diao, D.; Mao, G.; Huang, P.; et al. Fine-Tuning of PGC1α Expression Regulates Cardiac Function and Longevity. Circulation Research 2020, 707–719, doi:10.1161/CIRCRESAHA.119.315529.
52. Lörchner, H.; Pöling, J.; Gajawada, P.; Hou, Y.; Polyakova, V.; Kostin, S.; Adrian-Segarra, J.M.; Boettger, T.; Wietelmann, A.; Warnecke, H.; et al. Myocardial Healing Requires Reg3β-Dependent Accumulation of Macrophages in the Ischemic Heart. Nature Medicine 2015, 21, 353–362, doi:10.1038/nm.3816.
53. Beisaw, A.; Kuenne, C.; Guenther, S.; Dallmann, J.; Wu, C.-C.; Bentsen, M.; Looso, M.; Stainier, D.Y.R. AP-1 Contributes to Chromatin Accessibility to Promote Sarcomere Disassembly and Cardiomyocyte Protrusion During Zebrafish Heart Regeneration. Circulation research 2020, 126, 1760–1778, doi:10.1161/CIRCRESAHA.119.316167.
54. Nguyen, P.D.; de Bakker, D.E.M.; Bakkers, J. Cardiac Regenerative Capacity: An Evolutionary Afterthought? Cellular and Molecular Life Sciences 2021.
55. Pasumarthi, K.B.S.S.; Nakajima, H.H.O.; Nakajima, H.H.O.; Soonpaa, M.H.; Field, L.J. Targeted Expression of Cyclin D2 Results in Cardiomyocyte DNA Synthesis and Infarct Regression in Transgenic Mice. Circulation Research 2005, 96, 110–118, doi:10.1161/01.RES.0000152326.91223.4F.
56. Leach, J.P.; Heallen, T.; Zhang, M.; Rahmani, M.; Morikawa, Y.; Hill, M.C.; Segura, A.; Willerson, J.T.; Martin, J.F. Hippo Pathway Deficiency Reverses Systolic Heart Failure after Infarction. Nature 2017, doi:10.1038/nature24045.
57. Xiang, F.L.; Guo, M.; Yutzey, K.E. Overexpression of Tbx20 in Adult Cardiomyocytes Promotes Proliferation and Improves Cardiac Function after Myocardial Infarction. Circulation 2016, 133, 1081–1092, doi:10.1161/CIRCULATIONAHA.115.019357.
58. Lin, Z.; Von Gise, A.; Zhou, P.; Gu, F.; Ma, Q.; Jiang, J.; Yau, A.L.; Buck, J.N.; Gouin, K.A.; Van Gorp, P.R.R.; et al. Cardiac-Specific YAP Activation Improves Cardiac Function and Survival in an Experimental Murine MI Model. Circulation Research 2014, doi:10.1161/CIRCRESAHA.115.303632.
59. Meng, Q.; Sun, Z.; Gu, H.; Luo, J.; Wang, J.; Wang, C.; Han, S. Expression Profiles of Long Noncoding RNAs and Messenger RNAs in the Border Zone of Myocardial Infarction in Rats. Cellular and Molecular Biology Letters 2019, doi:10.1186/s11658-019-0185-6.
60. Stanley, W.C.; Lopaschuk, G.D.; Hall, J.L.; McCormack, J.G. Regulation of Myocardial Carbohydrate Metabolism under Normal and Ischaemic Conditions. Potential for Pharmacological Interventions. Cardiovascular research 1997, 33, 243–57, doi:10.1016/s0008-6363(96)00245-3.
61. Dayton, T.L.; Jacks, T.; Vander Heiden, M.G. PKM2, Cancer Metabolism, and the Road Ahead. EMBO reports 2016, 17, 1721–1730, doi:10.15252/embr.201643300.

62. Magadum, A.; Singh, N.; Kurian, A.A.; Munir, I.; Mehmood, T.; Brown, K.; Sharkar, M.T.K.; Chepurko, E.; Sassi, Y.; Oh, J.G.; et al. Pkm2 Regulates Cardiomyocyte Cell Cycle and Promotes Cardiac Regeneration. Circulation 2020, 141, 1249–1265, doi:10.1161/CIRCULATIONAHA.119.043067.
63. Leach, J.P.; Martin, J.F. Cardiomyocyte Proliferation for Therapeutic Regeneration. Current cardiology reports 2018, 20, 63, doi:10.1007/s11886-018-1011-x.
64. Ravingerova, T.; Adameova, A.; Carnicka, S.; Nemcekova, M.; Kelly, T.; Matejikova, J.; Galatou, E.; Barlaka, E.; Lazou, A. The Role of PPAR in Myocardial Response to Ischemia in Normal and Diseased Heart. General Physiology and Biophysics 2011.
65. Warren, J.S.; Oka, S.I.; Zablocki, D.; Sadoshima, J. Metabolic Reprogramming via PPARα Signaling in Cardiac Hypertrophy and Failure: From Metabolomics to Epigenetics. American Journal of Physiology - Heart and Circulatory Physiology 2017, 313, H584–H596, doi:10.1152/ajpheart.00103.2017.
66. Wagner, K.D.; Wagner, N. PPARs and Myocardial Infarction. International Journal of Molecular Sciences 2020.
67. Barger, P.M.; Kelly, D.P. PPAR Signaling in the Control of Cardiac Energy Metabolism. Trends in Cardiovascular Medicine 2000.
68. Papatheodorou, I.; Galatou, E.; Panagiotidis, G.-D.; Ravingerová, T.; Lazou, A. Cardioprotective Effects of PPARβ/δ Activation against Ischemia/Reperfusion Injury in Rat Heart Are Associated with ALDH2 Upregulation, Amelioration of Oxidative Stress and Preservation of Mitochondrial Energy Production. International journal of molecular sciences 2021, 22, doi:10.3390/ijms22126399.

SUPPLEMENTAL MATERIAL

Supplementary Materials: The following are available online at www.mdpi.com/xxx/s1, Supplementary Tables S1, S2, S3 (Excel files).

Supplemental Figure 1

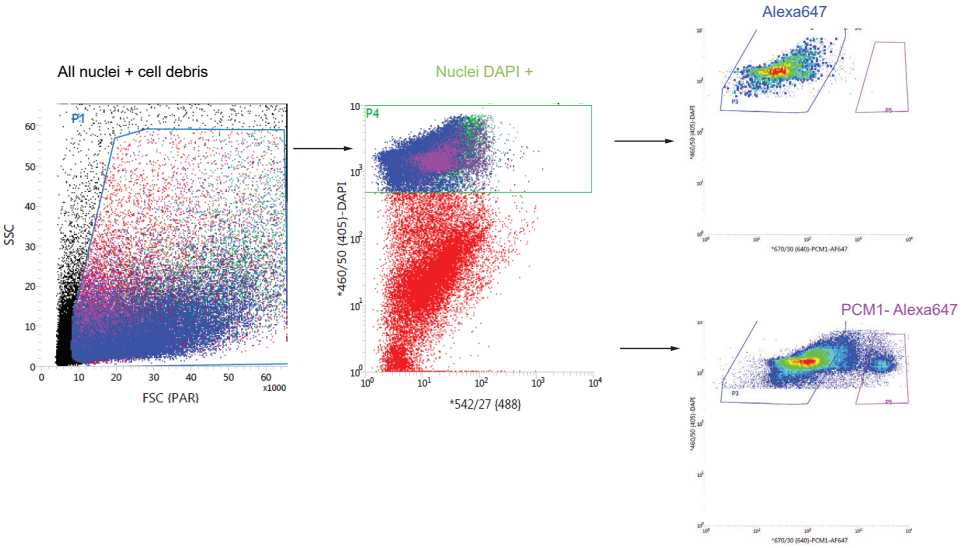

Figure S1. Flow cytometry dot plot showing nuclei isolated from BZ tissue stained with DAPI and a secondary AB (Alexa647). Cardiomyocyte nuclei were identified by staining with anti-PCM-1 antibody bound by the secondary antibody Alexa-647.

Supplemental Figure 2

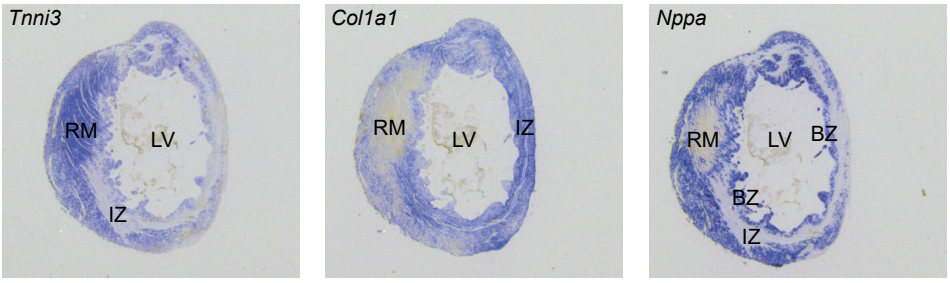

Figure S2. *In situ* hybridization at 7 dpi showing the expression of the cardiac marker *Tnni3*, the BZ marker *Nppa*, and *Col1a1*, marking the IZ. Scale bar, 1mm. Dpi, days post infarction; BZ, border zone, IZ, infarct zone; LV, left ventricle; RM, remote myocardium.

Supplemental Figure 3

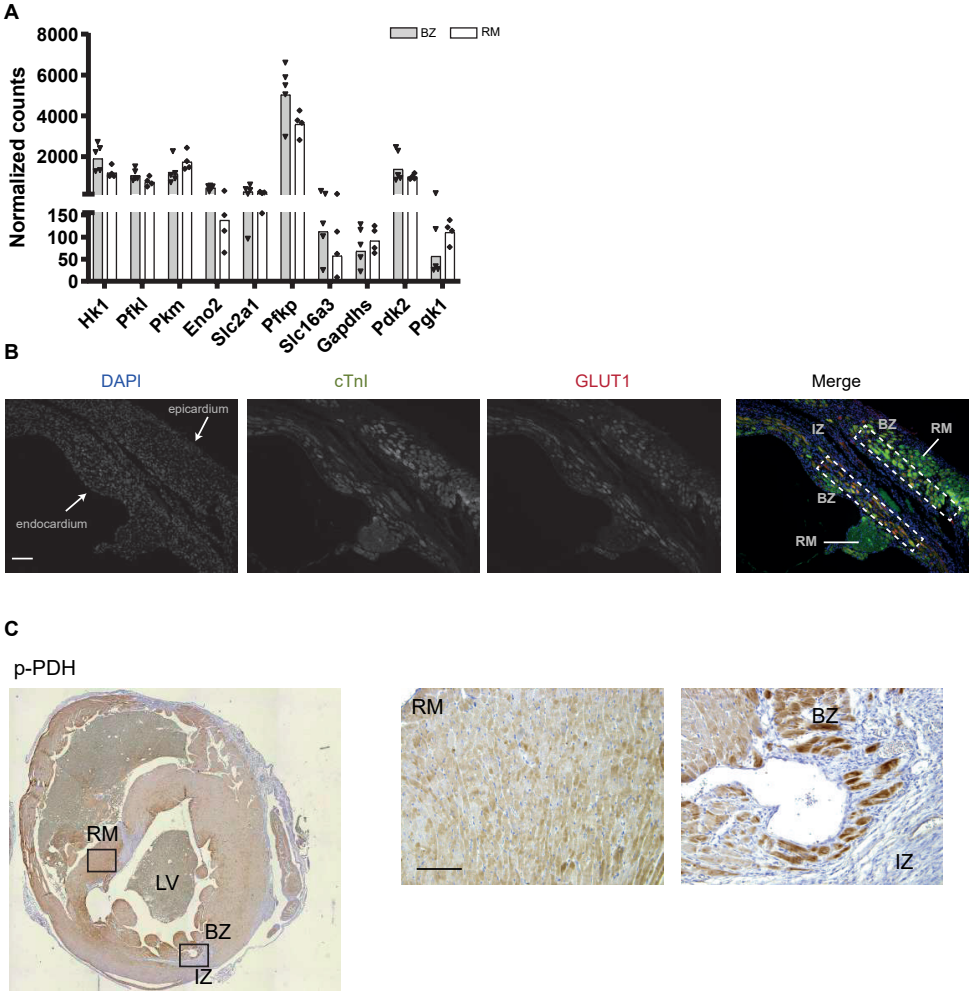

Figure S3. (**A**) Average expression glycolytic genes shown as normalized counts in border-zone (BZ) samples (n = 5) and samples from the remote myocardium (RM) (n = 4). (**B**) Immunohistochemical staining of cTnI, GLUT1, and Sytox Green at 7 dpi. BZ, border zone; RM, remote myocardium; IZ, infarct zone. (**C**) Immunohistochemical staining of p-PDH at 7 dpi in RM and BZ. Scale bar, 10 μm. Dpi, days post infarction; RM, remote myocardium; BZ, border zone.

Supplemental Figure 4

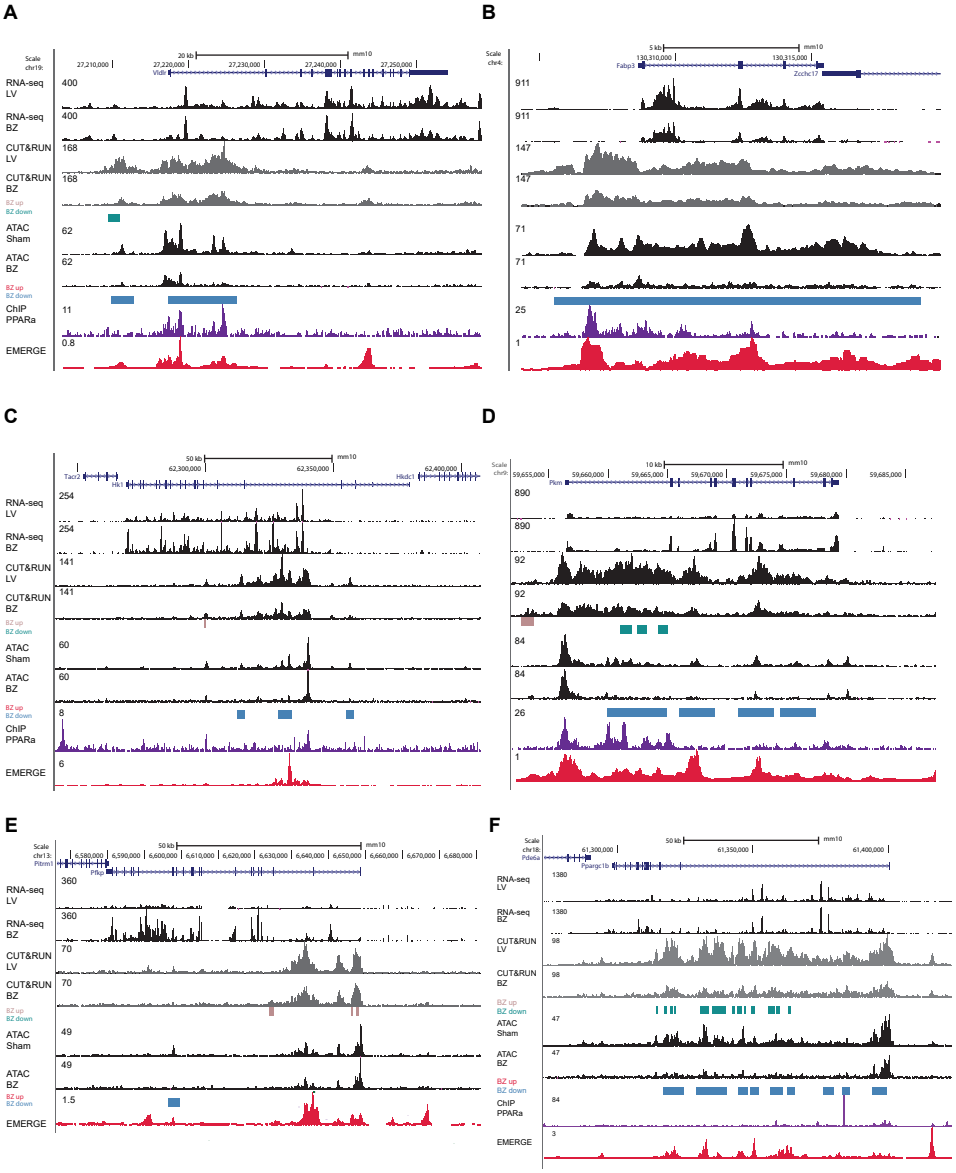

Figure S4. UCSC genome browser views of (**A**) Vldlr, (**B**) Fabp3, (**C**) Hk1, (**D**) Pfkm, (**E**) Pfkp, and (**E**) Ppargc1b.

6

Chapter 6

General Discussion and Future Perspectives

In this chapter, we summarize current strategies for cardiac regeneration and their limitations, and discuss how our findings contribute to the ultimate goal of restoring lost cardiomyocytes.

Cardiovascular diseases, and in particular heart failure, remain the leading cause of death worldwide [1]. Heart failure is the consequence of the chronic inability of the cardiac pump to meet the circulatory requirements of the body. It is accompanied by pathological remodelling of the myocardium, which includes fibrosis, inflammation, hypertrophic growth and death of cardiomyocytes, as well as changes of the electrophysiological properties of the heart [2]. Heart failure is a common consequence of cardiac damage caused by (1) congenital heart defects, during which post-surgery residual structural problems (e.g., valvar insufficiency) can lead to chronic volume or pressure overload of the heart [3,4], and (2) acute myocardial infarction, during which up to a billion cardiomyocytes are lost and replaced by a fibrotic scar [5,6].

Numerous therapies have been developed to prevent heart failure. However, existing approaches only delay the progression of the disease, because they fail to renew poorly-functioning cardiomyocytes or restore the lost myocardium [7]. After myocardial infarction, revascularization of the infarcted tissue has been the standard of care for many years. It includes enzymatic fibrinolysis/thrombolysis, coronary artery bypass graft, and percutaneous coronary intervention [7]. While reperfusion after myocardial infarction saves more than half of the myocardium that would otherwise be damaged, it also causes additional injury by the increase of oxidative stress and intracellular calcium levels, and leukocyte invasion [8,9]. In addition, this approach does not prevent the formation of a fibrotic scar and consequently ventricular dysfunction.

New therapies to restore function of the injured or diseased heart involve stimulation of the formation of novel functionally mature cardiomyocytes and vascular tissue, elimination of the fibrotic scar and safeguarding the electromechanical properties of the heart [10]. Currently, new therapies that are being developed either aim to replenish (*i.e.*, transplantation of *ex vivo* generated cardiomyocytes) or regenerate (*i.e., in vivo* generation of new cardiomyocytes) the injured myocardium. These strategies include **(1)** direct reprogramming of the resident cardiac fibroblasts into cardiomyocytes, **(2)** transplantation of stem/progenitor cells, **(3)** transplantation of cardiomyocytes derived from stem cells, **(4)** induction of proliferation of the remaining cardiomyocytes, and **(5)** initiation of cardiomyocyte re-differentiation.

(1) Direct reprogramming of the resident cardiac fibroblasts into cardiomyocytes. Cardiac fibroblasts account for about two-thirds of the cells of the heart [11]. During myocardial infarction, activated fibroblasts migrate to the injury zone, where they secrete extracellular matrix proteins to form a fibrotic scar which, although being initially beneficial by preventing cardiac rupture, finally compromises cardiac function [12]. Due to their proliferative potential and high concentration in the infarcted myocardium, cardiac fibroblasts offer the most suitable target for *in vivo* reprogramming into cardiomyocyte-like cells [13]. This method has been proven to reduce the fibrotic scar and partially restore the heart function [14].

Current limitations of this approach: Although reprogramming fibroblasts in animal models has been successful, it is still challenging to obtain sufficient rates of differentiation of human fibroblasts [7]. Since insufficient maturation of cardiomyocyte-like cells poses a risk for the development of cardiac arrhythmias, it will be important to determine the optimal efficiency and stage of maturation before findings can be translated safely into the clinic[15].

(2) Transplantation of stem/progenitor cells. Another attempt to restore the heart function, is by using stem-cell based therapy. Both exogenous and resident stem cells were believed to be able to differentiate to cardiomyocytes and restore heart muscle [16]. Since resident c-kit+ stem-cells in the adult heart rarely transdifferentiate into cardiomyocytes after myocardial injury [17] it is now explored if the lost myocardium can be replenished through the transplantation of stem/progenitor cells.

Current limitations of this approach: It has become clear that neither resident nor other stem cells contributes to new myocardium and any beneficial outcomes of stem-cell therapies are mainly achieved by paracrine effects and immune regulation, and not by the differentiation of stem-cells into new cardiomyocytes [18].

(3) Transplantation of cardiomyocytes derived from stem cells. Another strategy has been the direct transplantation of cardiomyocytes derived from pluripotent stem cells. These can be delivered by intramyocardial injection or engineered epicardial patches [19]. The latter provide mechanical support and function as a scaffold for interactions with the extracellular matrix, and thereby promote higher cardiomyocyte engraftment rates when compared to injected cardiomyocytes [19].

Current limitations of this approach: Challenges linked to this method include (1) immune rejection of the patch [20], (2) low cell survival and retention of the transplanted cells [21] (3) inadequate electromechanical integration of new cardiomyocytes [22], and (4) insufficient maturation of the transplanted cardiomyocytes [19]. Before translation into the clinic is possible, the long term effects and optimal time point for transplantation will need to be determined. For example, while cardiomyocyte transplantation two weeks after myocardial infarction improved cardiac function in rats [23] the transplantation four weeks after myocardial infarction did not lead to the same result [24]. In addition, most studies have used small patches that will not be suitable to be transplanted into human patients. The development of thicker patches needs to overcome the limitation of low diffusion for oxygen, nutrients and biological materials [25].

(4) Induction of proliferation of the remaining cardiomyocytes. One appealing possibility to achieve cardiac regeneration is to stimulate the proliferation of endogenous cardiomyocytes. For a long time, the heart was thought to be a post-mitotic organ. However, it has become evident that there is a very low amount of cardiomyocyte renewal in the adult heart [26]. Furthermore, insights from highly regenerative species such as the zebrafish [27–29] and neonatal rodents [30], proved that after cardiac injury, newly regenerated cardiomyocytes are derived from pre-existing cardiomyocytes. In adult mice, exposed to hypoxemia after myocardial infarction, newly formed myocardium was derived from pre-existing cardiomyocytes[31]. This

has led to the assumption that cardiomyocytes harbour a latent proliferative capacity, which can be targeted to induce heart regeneration.
Current limitations of this approach: To be able to replenish the lost cardiomyocytes, it is important to fully understand the molecular mechanisms that hinder cardiomyocytes to proliferate after injury. In addition, if successful, mechanisms to control uncontrolled cardiomyocyte proliferation need to be explored.
(5) Initiation of cardiomyocyte re-differentiation: While increasing the quantity of cardiomyocytes is crucial, the regulation and subsequent redifferentiation into mature cardiomyocytes, as well as the incorporation of these newly formed cardiomyocytes into the existing heart, are of equal significance[32]. Throughout the maturation process, cardiomyocytes undergo a sequence of transcriptional, structural, metabolic, and functional alterations, enabling them to effectively fulfil their contractile function[32]. A recent study in zebrafish revealed that cardiomyocyte re-differentiation after cardiac injury is an active process [33]. The cardiac dyad, a structure crucial for regulating calcium handling and excitation-contraction coupling, played a fundamental role in the redifferentiation process, by negatively regulating cardiomyocyte proliferation, while promoting redifferentiation. This articles highlights that the interplay between calcium signalling and sarcomeres during the maturation of cardiomyocytes in the context of regeneration emerges as crucial factors influencing the success of cardiomyocyte re-differentiation during regeneration.
Current limitations of this approach: Limitations to optimize strategies for enhancing cardiac regeneration by promoting maturation arise from the complexity of these interactions, requiring further exploration.

In this section, we discuss our findings on the epigenetic and transcriptional changes in cardiomyocytes during cardiac perturbations (i.e., ventricular loading abnormalities and acute myocardial infarction).

In **Chapter 1**, we review current knowledge about molecules and pathways that guide cardiomyocyte proliferation during heart development, postnatal growth and regeneration. During heart development the heart grows first by differentiation of cardiac progenitor cells, and after by proliferation of the already differentiated cardiomyocytes[34]. After birth, the rate of cardiomyocyte proliferation drastically decreases to less than 1% annually[26]. For these adult cardiomyocytes to proliferate, they need to dedifferentiate, causing a disassembly of the sarcomeres, a metabolic switch from oxidative phosphorylation to glycolysis and re-expression of genes that are expressed during heart development [35].

In neonatal mice, cardiomyocyte proliferation is completed one week after birth [36] and the time in which the murine neonatal heart can respond to injury by cardiomyocyte proliferation is restricted to the first 3 days after birth [37]. During the first two weeks after birth, cardiomyocytes will mainly undergo incomplete cell cycles and become polyploid and bi-nuclear [36]. A general consensus is that only mononuclear and diploid cardiomyocytes are

able to proliferate [38]. Whereas cardiomyocytes in the zebrafish heart stay mononucleated and diploid during their whole life [39], the majority of cardiomyocytes of the adult human heart are polyploid [40] and in the mouse heart binucleated [36]. Hence, to achieve heart regeneration, therapies either need to overcome these intrinsic hurdles, or target the small fraction of cardiomyocytes that remain mononuclear and diploid throughout life.

Cardiac loading abnormalities do not induce cardiomyocyte proliferation in neonatal mice and rats.

Studies have indicated that the process of postnatal cardiomyocyte maturation and cell-cycle regulation is highly susceptible to external factors [41,42]. For example, postnatal hypoxemia can prolong the period of cardiomyocyte proliferation in mice [43]. Therefore, we hypothesized that early postnatal cardiac perturbations in the form of volume and pressure overload, which are complications commonly observed in children with congenital heart disease [44], may influence cardiac maturation events.

In **Chapter 2** we discovered that volume overload during the juvenile period (mouse heart 10 to 14 days after birth) had only a slight influence on the transcriptome of cardiomyocytes. Although it caused an increase in expression of several genes involved in cell-cycle regulation, this did not lead to changes in cardiomyocyte cell-cycle activity. In **Chapter 3**, juvenile rats were exposed to chronic pressure overload of the right ventricle and followed into adulthood. Here, we observed an increase of cardiomyocyte cell-cycle activity, which were likely the result of cardiomyocytes undergoing incomplete cell-cycles, leading to an increase in polyploidy or nucleation. At the same time, pressure overload caused a decreased expression of genes involved in fatty-acid metabolism and oxidative phosphorylation, which could indicate a delay in metabolic cardiomyocyte maturation. It has previously been shown that stimulating cardiomyocyte proliferation via ErbB2/Neuregulin-1 enhances cardiac regeneration by promoting cardiomyocyte proliferation [45,46].

When these rats were treated with Neuregulin-1, we observed increasing cell-cycle activity, improved cardiac function and delayed fibrosis. However, also here we could not detect an induction of cardiomyocyte proliferation.

The different findings in Chapter 2 and Chapter 3 on cardiomyocyte cell-cycle activity upon cardiac stress could be explained by the use of different models (mouse vs rat), loading abnormalities (volume overload vs pressure overload) and time points (10 days vs 3 weeks postnatal). In general, it will remain challenging to translate the results of these studies to the human situation, because cardiac maturation events are also influenced by other factors such as differences between mammalian species in physiology, gestation time and intrauterine environment[32]. Nevertheless, the insights from both chapters will help us to gain a better understanding of how cardiomyocytes adapt to abnormal cardiac loading conditions in paediatric patients with congenital heart disease. Such knowledge will help to

define optimal stages for corrective surgery (e.g., surgical repair of the pulmonary stenosis or pulmonary valve replacement in patients with Tetralogy of Fallot)[47].

Cardiomyocytes of the infarct border zone are primed to re-enter the cell cycle.

Heart regeneration in zebrafish is achieved by proliferating cardiomyocytes located next to the injury, the border zone (BZ) [48]. Also in transgenic mouse models of regeneration, cardiomyocytes respond to cell-cycle induction mainly in the BZ and achieving transient cardiomyocyte proliferation in the post-infarction BZ preserved cardiac function and reduced scar size in a porcine model [49–52].

In **Chapter 4** and **Chapter 5** we studied how the transcriptional and regulatory properties of BZ cardiomyocytes differ from cardiomyocytes from the remote and healthy myocardium. BZ cardiomyocytes are characterized by dedifferentiation and sarcomere depletion, and a decrease in their mitochondrial volume [53,54]. We observed that these changes are caused by profound changes of the transcriptome and epigenome. After acute myocardial infarction, BZ cardiomyocytes showed reduced chromatin accessibility of elements that are bound by the MEF2 family of transcription factors. These transcription factors are involved in maintaining the cardiomyocyte lineage by activating genes that regulate mitochondrial oxidative phosphorylation, fatty acid metabolism, calcium handling, and sarcomere function. The downregulation of the MEF2-driven gene expression program is in line with the observed reduction of the mature state and mitochondrial activity of BZ cardiomyocytes. Downregulation of the fatty-acid metabolism and switch to glycolysis is also observed in cardiomyocytes from the zebrafish BZ, and is a pre-requisite for cardiomyocyte proliferation. In zebrafish, metabolic reprogramming is marked by the upregulation of genes involved in glycolysis, changes in the morphology of mitochondria and decrease in the rates of oxidative phosphorylation [55]. In line with this, overexpression of the glycolytic enzyme Pkm2 has been shown to activate cardiomyocyte cell-division in the murine BZ [56]. Moreover, inhibition of fatty acid oxidation in the mouse heart improves resistance to hypoxia, stimulates cardiomyocyte proliferation and allows regeneration after ischemia-reperfusion injury. The underlying mechanism involves activation of KDM5, demethylation of H3K4me3 at genes involved in maturation, shifting cardiomyocytes to a less mature state, thus promoting proliferation. We demonstrated that murine BZ cardiomyocytes de-maturate but only slightly upregulated genes involved in glycolysis and failed to induce genes involved in cell-cycle regulation, suggesting the BZ cardiomyocytes face additional obstacles or lack essential stimuli to proliferate.

Sites that gained chromatin accessibility in the BZ where enriched for motifs bound by the AP-1 (activator protein 1) family of transcription factors, which induce a stress-responsive gene expression program. We specifically detected the AP-1 family member c-Jun in in nuclei of border zone cardiomyocytes, which is known to maintain the sarcomeric structure

of cardiomyocytes during hypertrophy [57]. The switch to an AP-1 responsive-gene program also plays an important role during heart regeneration in zebrafish, where it activates cardiomyocyte dedifferentiation, proliferation, and consequently their protrusion into the injured myocardium [58]. In line with this, blocking the function of AP-1 decreased the regenerative capacity of the zebrafish heart. Compared with the mouse heart, however, cardiomyocytes of the zebrafish BZ express different AP-1 family members that likely regulate different target genes [58]. For future studies, it will be important to elucidate these differences between the mouse and zebrafish response, and to study if manipulation of the AP-1 responsive gene program is the key to promoting heart regeneration in humans.

Taken together, the results described in Chapter 4 and Chapter 5 demonstrate that BZ cardiomyocytes are likely to be primed for proliferation to occur and remain promising targets for cardiac regeneration.

Overall, our findings provide new insights for translational research aimed at stimulating cardiac survival and regeneration after myocardial infarction. However, the transcriptional and epigenetic changes that we observed may form only a small part of the complex regulatory system that needs to be manipulated to achieve cardiomyocyte proliferation in humans. To realize the ultimate goal of cardiac regeneration, it will be necessary to take a holistic approach that takes into account the immune response, neovascularization, epicardial and endocardial regeneration, as well as fibroblast inactivation. In addition, there are still significant knowledge gaps that need to be addressed before therapies can be applied in clinical practice: **(1)** How can we achieve sufficient cardiomyocyte proliferation and does the human diseased heart have sufficient suitable cardiomyocytes in which this can be induced? **(2)** How do we control transient cardiomyocyte proliferation and what is the perfect timing? Notably, long-term proliferation of cardiomyocytes can lead to cardiomyocyte hyperplasia, sudden arrhythmic death, and cancer [59,60]. **(3)** How do dedifferentiated cardiomyocytes re-differentiate to form functionally integrated and mature myocardium that adequately performs? This aspect is currently being addressed in several studies where the degree of maturation, memory of the de-differentiated state and requirements for re-maturation are being addressed [33,61] **(4)** How are other cell types in the heart affected? And **(5)** what are the long-term consequences?

REFERENCES

1. WHO. *Cardiovascular diseases. 06/2023* (2023).
2. Burchfield, J. S., Xie, M. & Hill, J. A. Pathological ventricular remodeling: Mechanisms: Part 1 of 2. *Circulation* **128**, 388–400 (2013).
3. Maximilian Buja, L. & Vela, D. Cardiomyocyte death and renewal in the normal and diseased heart. *Cardiovascular Pathology* **17**, 349–374 (2008).
4. Zomer, A. C. *et al.* Circumstances of death in adult congenital heart disease. *International Journal of Cardiology* **154**, 168–172 (2012).
5. Jenča, D. *et al.* Heart failure after myocardial infarction: incidence and predictors. *ESC Heart Failure* (2021). doi:10.1002/ehf2.13144
6. Lin, Z. & Pu, W. T. Strategies for cardiac regeneration and repair. *Science Translational Medicine* **6**, 1–23 (2014).
7. Riching, A. S. & Song, K. Cardiac Regeneration: New Insights Into the Frontier of Ischemic Heart Failure Therapy. *Frontiers in Bioengineering and Biotechnology* **8**, (2021).
8. Fröhlich, G. M., Meier, P., White, S. K., Yellon, D. M. & Hausenloy, D. J. Myocardial reperfusion injury: Looking beyond primary PCI. *European Heart Journal* (2013). doi:10.1093/eurheartj/eht090
9. Yellon, D. M. & Hausenloy, D. J. Myocardial Reperfusion Injury. *New England Journal of Medicine* (2007). doi:10.1056/nejmra071667
10. Farache Trajano, L. & Smart, N. Immunomodulation for optimal cardiac regeneration: insights from comparative analyses. *npj Regenerative Medicine* **6**, 1–11 (2021).
11. Fan, D., Takawale, A., Lee, J. & Kassiri, Z. Cardiac fibroblasts, fibrosis and extracellular matrix remodeling in heart disease. *Fibrogenesis and Tissue Repair* (2012). doi:10.1186/1755-1536-5-15
12. Humeres, C. & Frangogiannis, N. G. Fibroblasts in the Infarcted, Remodeling, and Failing Heart. *JACC: Basic to Translational Science* (2019). doi:10.1016/j.jacbts.2019.02.006
13. Perveen, S., Vanni, R., Lo Iacono, M., Rastaldo, R. & Giachino, C. Direct Reprogramming of Resident Non-Myocyte Cells and Its Potential for In Vivo Cardiac Regeneration. *Cells* **12**, (2023).
14. Qian, L. *et al.* In vivo reprogramming of murine cardiac fibroblasts into induced cardiomyocytes. *Nature* (2012). doi:10.1038/nature11044
15. Garry, G. A. & Olson, E. N. Reprogramming of cardiac cell fate as a therapeutic strategy for ischemic heart disease. *Journal of Molecular and Cellular Cardiology* **179**, 2–6 (2023).
16. Sturzu, A. C. & Wu, S. M. Developmental and regenerative biology of multipotent cardiovascular progenitor cells. *Circ Res* **108**, 353–364 (2011).
17. Maliken, B. D. *et al.* Gata4-dependent differentiation of c-Kit+-derived endothelial cells underlies artefactual cardiomyocyte regeneration in the heart. *Circulation* (2018). doi:10.1161/CIRCULATIONAHA.118.033703
18. Liu, C., Han, D., Liang, P., Li, Y. & Cao, F. The Current Dilemma and Breakthrough of Stem Cell Therapy in Ischemic Heart Disease. *Frontiers in Cell and Developmental Biology* (2021). doi:10.3389/fcell.2021.636136
19. Silver, S. E., Barrs, R. W. & Mei, Y. Transplantation of Human Pluripotent Stem Cell-Derived Cardiomyocytes for Cardiac Regenerative Therapy. *Frontiers in Cardiovascular Medicine* (2021). doi:10.3389/fcvm.2021.707890
20. Neofytou, E., O'Brien, C. G., Couture, L. A. & Wu, J. C. Hurdles to clinical translation of human induced pluripotent stem cells. *Journal of Clinical Investigation* (2015). doi:10.1172/jci80575

21. Wu, K. H., Mo, X. M., Han, Z. C. & Zhou, B. Stem cell engraftment and survival in the ischemic heart. *Annals of Thoracic Surgery* (2011). doi:10.1016/j.athoracsur.2011.07.012
22. Huang, N. F. *et al.* Big bottlenecks in cardiovascular tissue engineering. *Communications Biology* (2018). doi:10.1038/s42003-018-0202-8
23. Miki, K. *et al.* Bioengineered Myocardium Derived from Induced Pluripotent Stem Cells Improves Cardiac Function and Attenuates Cardiac Remodeling Following Chronic Myocardial Infarction in Rats. *Stem Cells Translational Medicine* (2012). doi:10.5966/sctm.2011-0038
24. Fernandes, S. *et al.* Human embryonic stem cell-derived cardiomyocytes engraft but do not alter cardiac remodeling after chronic infarction in rats. *Journal of Molecular and Cellular Cardiology* (2010). doi:10.1016/j.yjmcc.2010.09.008
25. Pretorius, D. *et al.* Layer-By-Layer Fabrication of Large and Thick Human Cardiac Muscle Patch Constructs With Superior Electrophysiological Properties. *Frontiers in Cell and Developmental Biology* (2021). doi:10.3389/fcell.2021.670504
26. Bergmann, O. *et al.* Evidence for cardiomyocyte renewal in humans. *Science* **324**, 98–102 (2009).
27. Jopling, C. *et al.* Zebrafish heart regeneration occurs by cardiomyocyte dedifferentiation and proliferation. *Nature* **464**, 606–609 (2010).
28. Kikuchi, K. *et al.* Primary contribution to zebrafish heart regeneration by gata4+ cardiomyocytes. *Nature* **464**, 601–605 (2010).
29. Wang, J. *et al.* The regenerative capacity of zebrafish reverses cardiac failure caused by genetic cardiomyocyte depletion. *Development* (2011). doi:10.1242/dev.068601
30. Lam, N. T. & Sadek, H. A. Neonatal heart regeneration comprehensive literature review. *Circulation* **138**, 421–423 (2018).
31. Nakada, Y. *et al.* Hypoxia induces heart regeneration in adult mice. *Nature* **541**, 222–227 (2017).
32. Beisaw, A. & Wu, C. C. Cardiomyocyte maturation and its reversal during cardiac regeneration. *Developmental Dynamics* (2022). doi:10.1002/dvdy.557
33. Nguyen, P. D. *et al.* Interplay between calcium and sarcomeres directs cardiomyocyte maturation during regeneration. *Science* (2023). doi:10.1126/SCIENCE.ABO6718
34. Kelly, R. G., Buckingham, M. E. & Moorman, A. F. Heart fields and cardiac morphogenesis. *Cold Spring Harb Perspect Med* **4**, 1–10 (2014).
35. Günthel, M., Barnett, P. & Christoffels, V. M. Development, Proliferation, and Growth of the Mammalian Heart. *Molecular Therapy* **26**, (2018).
36. Alkass, K. *et al.* No evidence for cardiomyocyte number expansion in preadolescent mice. *Cell* **163**, 1026–1036 (2015).
37. Porrello, E. R. *et al.* Transient regenerative potential of the neonatal mouse heart. *Science (New York, N.Y.)* **331**, 1078–80 (2011).
38. González-Rosa, J. M. *et al.* Myocardial Polyploidization Creates a Barrier to Heart Regeneration in Zebrafish. *Developmental Cell* **44**, 433-446.e7 (2018).
39. Poss, K. D., Wilson, L. G. & Keating, M. T. Heart Regeneration in Zebrafish. *Science* **298**, 2188–2190 (2002).
40. Bergmann, O. & Jovinge, S. Isolation of Cardiomyocyte Nuclei from Post-mortem Tissue. *Journal of visualized experiments : JoVE* 4–9 (2012). doi:10.3791/4205
41. Ding, X. *et al.* Neonatal Heart Responds to Pressure Overload With Differential Alterations in Various Cardiomyocyte Maturation Programs That Accommodate Simultaneous Hypertrophy and Hyperplasia. *Frontiers in Cell and Developmental Biology* **8**, 1–12 (2020).
42. Kannan, S. & Kwon, C. Regulation of cardiomyocyte maturation during critical perinatal window. *Journal of Physiology* **598**, 2941–2956 (2020).

43. Puente, B. N. *et al.* The oxygen-rich postnatal environment induces cardiomyocyte cell-cycle arrest through DNA damage response. *Cell* **157**, 565–79 (2014).
44. Schwerzmann, M. *et al.* Challenges of congenital heart disease in grown-up patients. *Swiss medical weekly* **147**, w14495 (2017).
45. D'Uva, G. *et al.* ERBB2 triggers mammalian heart regeneration by promoting cardiomyocyte dedifferentiation and proliferation. *Nat Cell Biol* **17**, 627–638 (2015).
46. Aharonov, A. *et al.* ERBB2 drives YAP activation and EMT-like processes during cardiac regeneration. *Nature Cell Biology* (2020). doi:10.1038/s41556-020-00588-4
47. Van Der Ven, J. P. G. *et al.* Ventricular function and biomarkers in relation to repair and pulmonary valve replacement for tetralogy of Fallot. *Open Heart* (2023). doi:10.1136/openhrt-2022-002238
48. Wu, C. C. *et al.* Spatially resolved genome-wide transcriptional profiling identifies BMP signaling as essential regulator of zebrafish cardiomyocyte regeneration. *Dev Cell* **36**, 36–49 (2016).
49. Pasumarthi, K. B. S., Nakajima, H. H. O., Nakajima, H. H. O., Soonpaa, M. H. & Field, L. J. Targeted expression of cyclin D2 results in cardiomyocyte DNA synthesis and infarct regression in transgenic mice. *Circ Res* **96**, 110–118 (2005).
50. Leach, J. P. *et al.* Hippo pathway deficiency reverses systolic heart failure after infarction. *Nature* (2017). doi:10.1038/nature24045
51. Xiang, F. L., Guo, M. & Yutzey, K. E. Overexpression of Tbx20 in adult cardiomyocytes promotes proliferation and improves cardiac function after myocardial infarction. *Circulation* **133**, 1081–1092 (2016).
52. Abouleisa, R. R. E. *et al.* Transient Cell Cycle Induction in Cardiomyocytes to Treat Subacute Ischemic Heart Failure. *Circulation* **145**, 1339–1355 (2022).
53. Dispersyn, G. D. *et al.* Dissociation of cardiomyocyte apoptosis and dedifferentiation in infarct border zones. *European Heart Journal* (2002). doi:10.1053/euhj.2001.2963
54. Sharov, V. G. *et al.* Abnormalities of cardiocytes in regions bordering fibrous scars of dogs with heart failure. *International Journal of Cardiology* (1997). doi:10.1016/S0167-5273(97)00117-4
55. Honkoop, H. *et al.* Single-cell analysis uncovers that metabolic reprogramming by ErbB2 signaling is essential for cardiomyocyte proliferation in the regenerating heart. *eLife* (2019). doi:10.7554/eLife.50163
56. Magadum, A. *et al.* Pkm2 regulates cardiomyocyte cell cycle and promotes cardiac regeneration. *Circulation* (2020). doi:10.1161/CIRCULATIONAHA.119.043067
57. Windak, R. *et al.* The AP-1 Transcription Factor c-Jun Prevents Stress-Imposed Maladaptive Remodeling of the Heart. *PLoS ONE* **8**, 1–11 (2013).
58. Beisaw, A. *et al.* AP-1 Contributes to Chromatin Accessibility to Promote Sarcomere Disassembly and Cardiomyocyte Protrusion during Zebrafish Heart Regeneration. *Circulation Research* (2020). doi:10.1161/CIRCRESAHA.119.316167
59. Gabisonia, K. *et al.* MicroRNA therapy stimulates uncontrolled cardiac repair after myocardial infarction in pigs. *Nature* **569**, 418–422 (2019).
60. Monroe, T. O. *et al.* YAP Partially Reprograms Chromatin Accessibility to Directly Induce Adult Cardiogenesis In Vivo. *Developmental Cell* **48**, 765-779.e7 (2019).
61. Shakked, A. *et al.* Redifferentiated cardiomyocytes retain residual dedifferentiation signatures and are protected against ischemic injury. *Nature Cardiovascular Research* (2023). doi:10.1038/s44161-023-00250-w

7

Chapter 7

Summary

SUMMARY

Transcriptomic and epigenetic response to cardiac injury

In this thesis, we characterize the response of cardiomyocytes to early abnormal cardiac loading conditions, as found in patients with certain types of congenital heart defects, and after myocardial infarction. Here, I summarize the findings of the individual chapters.

In **Chapter 1**, we summarized recent insights into the mechanisms that govern cardiomyocyte proliferation during development and regeneration in mice and humans.

In **Chapter 2** and **Chapter 3**, we studied how cardiomyocytes adapt to abnormal cardiac loading conditions during early postnatal development of the heart. In **Chapter 2**, we investigated how early postnatal cardiac volume overload changes gene expression of cardiomyocytes and whether the overload-induced changes impact postnatal cardiomyocyte cell-cycle withdrawal. To this end, we used a mouse model that develops left ventricular volume overload, due to mitral regurgitation within the first two weeks after birth. Our results show that cardiomyocytes from the murine neonatal heart respond to volume overload with only minor changes in the transcriptome. Although the expression of cell-cycle genes was affected in mice experiencing cardiac stress, cardiomyocyte cell-cycle activity was unchanged. In **Chapter 3**, we investigated how pressure overload of the right ventricle influences cell-cycle activity and cardiac function. We induced right ventricular pressure overload in weaning rats by pulmonary artery banding and followed these rats into adulthood. RNA-sequencing revealed differential expression of genes involved in metabolic maturation. Cardiomyocytes were found to respond to pressure overload with an increase in cell-cycle activity. Whether this increase also resulted in an increase in cardiomyocyte proliferation could not be determined. Staining of cardiomyocytes for H3P, a marker for mitosis, showed no differences between both groups. Stimulation with neuregulin-1, a signalling molecule previously implicated in stimulation of postnatal cardiomyocyte proliferation, improved the adaptation to pressure overload and delayed the onset of fibrosis in the right ventricle of the pressure overload rats.

In **Chapter 4** and **Chapter 5,** we characterize the mammalian post-infarction border zone. In **Chapter 4**, we studied the border zone in mice using RNA-sequencing and ATAC-sequencing. We identified the border zone as a transcriptionally discrete compartment in which cardiomyocytes downregulate mature cardiomyocyte lineage-specific genes, including genes involved in the contractile apparatus, in fatty acid oxidation, and in calcium handling, but fail to activate programs for proliferation. We showed that the transcriptional processes of the border zone are conserved between mouse and human and include the upregulation of *Nppb*, which we demonstrated to be necessary to prevent acute heart failure after myocardial infarction. ATAC-sequencing revealed that the epigenetic landscape of border zone cardiomyocytes changed significantly, with thousands of chromatin regions gaining

or losing accessibility. We demonstrated that cardiomyocytes switch from a MEF2-driven homeostatic lineage specific to an AP-1-driven gene program. However, ATAC-sequencing identifies all classes of regulatory elements including enhancers, promoters, silencer *etc* and does not distinguish active enhancers and promoters. Therefore, in **Chapter 5**, we further characterized the transcriptome and epigenome of isolated cardiomyocyte nuclei from the murine border zone. We performed RNA-sequencing and studied the profiles of H3K27ac, which is flanking active promoters and enhancers. In this study, we validated the in Chapter 4 observed downregulation of genes involved in fatty acid metabolism and oxidative phosphorylation and detected a slight induction of genes involved in glycolysis. We further confirmed the switch from MEF2 to AP-1 chromatin association in border zone cardiomyocytes. In addition, we also observed enrichment of PPAR/RXR binding motifs at genomic sites with decreased H3K27ac signal together with a reduced expression of PPAR target genes. These genes are responsible for regulating the fatty acid metabolism in the heart.

In **Chapter 6**, we present the different strategies that are currently explored to regenerate the mammalian heart. In addition, we discuss the findings presented in this thesis in the context of current literature and share our outlook on the field of heart regeneration.

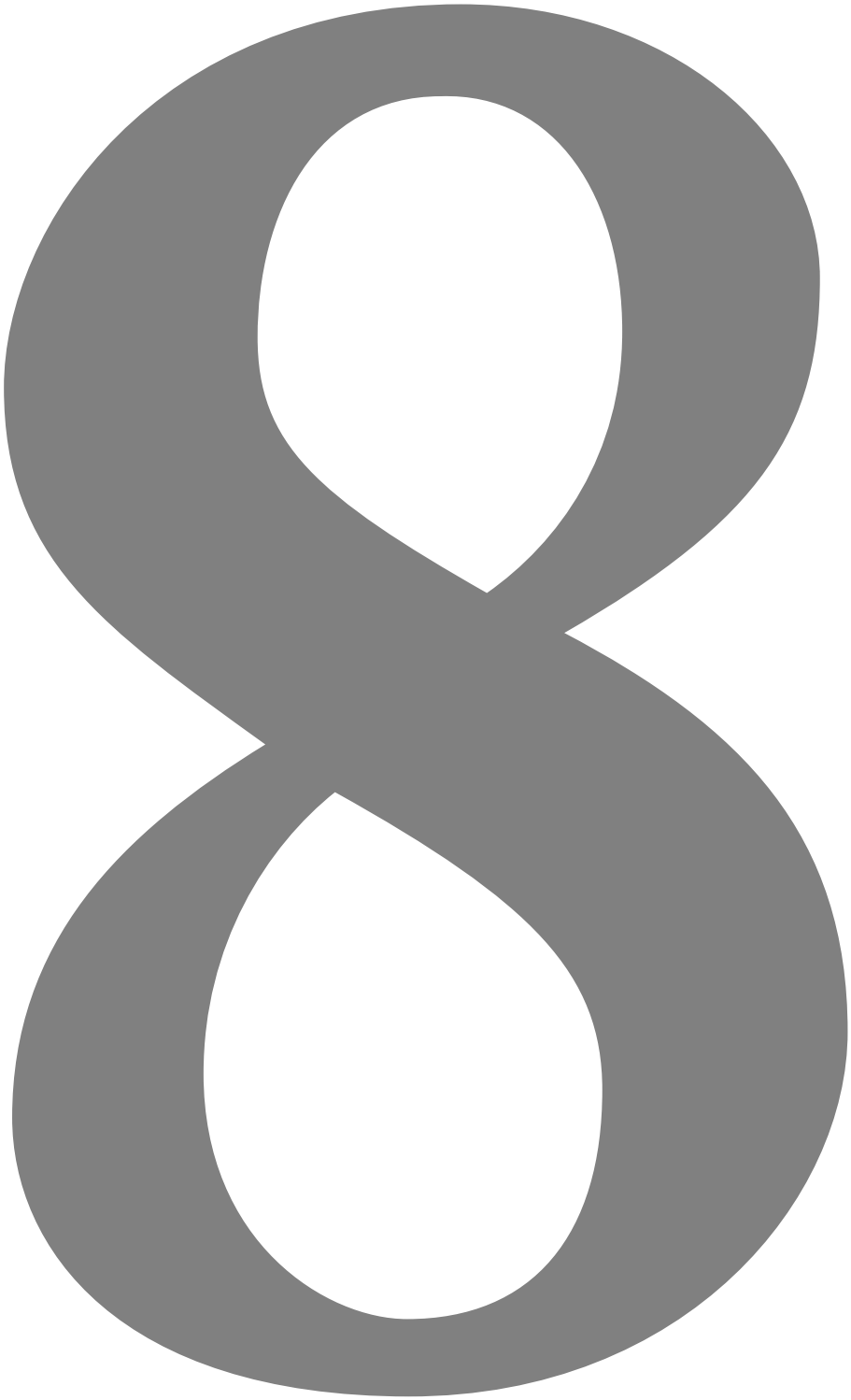

Chapter 8

Samenvatting

SAMENVATTING

Transcriptomische en epigenetische respons op hartschade

In dit proefschrift karakteriseren we de respons van cardiomyocyten op vroege abnormale cardiale belastingstoestanden, zoals gevonden bij patiënten met bepaalde soorten aangeboren hartafwijkingen en na een myocardinfarct. Hier vat ik de bevindingen van de afzonderlijke hoofdstukken samen.

In **Hoofdstuk 1** hebben we recente inzichten samengevat in de mechanismen die de proliferatie van cardiomyocyten tijdens ontwikkeling en regeneratie bij muizen en mensen beheersen.

In **Hoofdstuk 2** en **Hoofdstuk 3** hebben we onderzocht hoe cardiomyocyten zich aanpassen aan abnormale cardiale belastingstoestanden tijdens de vroege postnatale ontwikkeling van het hart. In **Hoofdstuk 2** hebben we onderzocht hoe vroege postnatale cardiale volume-overbelasting de genexpressie van cardiomyocyten verandert en of de door overbelasting geïnduceerde veranderingen invloed hebben op de postnatale terugtrekking van de celcyclus van cardiomyocyten. Hiervoor gebruikten we een muismodel dat linkerventrikel-volume-overbelasting ontwikkelt als gevolg van mitralisklepregurgitatie binnen de eerste twee weken na de geboorte. Onze resultaten tonen aan dat cardiomyocyten van het neonatale hart van de muis reageren op volume-overbelasting met slechts kleine veranderingen in het transcriptoom. Hoewel de expressie van celcyclusgenen werd beïnvloed bij muizen die cardiale stress ervoeren, bleef de celcyclusactiviteit van cardiomyocyten onveranderd. In **Hoofdstuk 3** hebben we onderzocht hoe drukoverbelasting van het rechterventrikel de celcyclusactiviteit en cardiale functie beïnvloedt. We induceerden drukoverbelasting van het rechterventrikel bij gespeende ratten door banding van de longslagader en volgden deze ratten tot in de volwassenheid. RNA-sequencing onthulde differentiële expressie van genen die betrokken zijn bij metabole rijping. We ontdekten dat cardiomyocyten reageerden op drukoverbelasting met een toename in celcyclusactiviteit. Of deze toename ook resulteerde in een toename van cardiomyocytproliferatie kon niet worden bepaald. Kleuring van cardiomyocyten voor H3P, een marker voor mitose, toonde geen verschillen tussen beide groepen. Stimulatie met neureguline-1, een signaalmolecuul dat eerder werd geïmpliceerd in de stimulatie van postnatale cardiomyocytproliferatie, verbeterde de aanpassing aan drukoverbelasting en vertraagde het begin van fibrose in het rechterventrikel van de ratten met drukoverbelasting.

In **Hoofdstuk 4** en **Hoofdstuk 5** karakteriseren we de post-infarctgrenszone bij zoogdieren. In **Hoofdstuk 4** hebben we de grenszone bij muizen bestudeerd met RNA-sequencing en ATAC-sequencing. We identificeerden de grenszone als een transcriptioneel discreet compartiment waarin cardiomyocyten volwassen cardiomyocytlijnspecifieke genen, waaronder genen betrokken bij het contractiele apparaat, vetzuuroxidatie en

calciumhuishouding, downreguleren, maar er niet in slagen proliferatieprogramma's te activeren. We toonden aan dat de transcriptionele processen van de grenszone geconserveerd zijn tussen muis en mens en de opregulatie van *Nppb* omvatten, waarvan we aantoonden dat het noodzakelijk is om acuut hartfalen na een myocardinfarct te voorkomen. ATAC-sequencing onthulde dat het epigenetische landschap van grenszone cardiomyocyten significant veranderde, met duizenden chromatinedomeinen die toegankelijkheid winnen of verliezen. We toonden aan dat cardiomyocyten overschakelen van een MEF2-gedreven homeostatische lijnspecifieke naar een AP-1-gedreven genprogramma. Echter, ATAC-sequencing identificeert alle klassen van regulerende elementen, inclusief enhancers, promoters, silencers enz., en maakt geen onderscheid tussen actieve enhancers en promoters. Daarom hebben we in **Hoofdstuk 5** het transcriptoom en epigenoom van geïsoleerde cardiomyocytenkernen uit de grenszone van muizen verder gekarakteriseerd. We voerden RNA-sequencing uit en bestudeerden de profielen van H3K27ac, die actieve promoters en enhancers flankeert. In deze studie valideerden we de in Hoofdstuk 4 waargenomen downregulatie van genen betrokken bij vetzuurmetabolisme en oxidatieve fosforylering en detecteerden een lichte inductie van genen betrokken bij glycolyse. We bevestigden verder de switch van MEF2 naar AP-1 chromatine associatie in grenszone cardiomyocyten. Daarnaast observeerden we ook verrijking van PPAR/RXR bindingsmotieven op genomische locaties met een verminderde H3K27ac signaal, samen met een verminderde expressie van PPAR-doelgenen. Deze genen zijn verantwoordelijk voor de regulering van het vetzuurmetabolisme in het hart.

In **Hoofdstuk 6** presenteren we de verschillende strategieën die momenteel worden verkend om het zoogdierhart te regenereren. Daarnaast bespreken we onze bevindingen gepresenteerd in dit proefschrift in de context van de huidige literatuur en delen we onze vooruitzichten op het gebied van hartregeneratie.

Appendix

PHD PORTFOLIO

PhD student: Marie Günthel
PhD period: 2016-2026
Supervisor: prof. dr. Vincent M. Christoffels
Co-supervisor: dr. Phil Barnett

PhD courses		**ECTS**
2016	The AMC World of Science	0.7
2016	Advanced qPCR	0.7
2016	Laboratory animal science (article 9 certified)	3.9
2017	Project Management	0.6
2018	Species-specific fish course (article 9 certified)	0.6
2019	Practical Biostatistics	1.4
2019	Career Development	0.8
2019	From Pixel to Publication	0.8
2019	Famelab	1.0
2020	Bioinformatics	1.1

Seminars and Workshops		**ECTS**
2016-2021	Weekly department meetings, Department of Medical Biology	11
2016-2021	Weekly progress reports, Heart Failure Research Center	11
2016-2020	Quarterly COBRA3 meetings	1.6

Presentations		**ECTS**
2018	Annual Meeting of the Association for European Paediatric and Congenital Cardiology (AEPC), Athens, Greece, *(oral presentation)*	1
2019	3rd, DCVA Translational Cardiovascular Research Meeting, Utrecht, the Netherlands, *(oral presentation)*	0.2
2019	1st Amsterdam Cardiovascular Sciences PhD Retreat, Soesterberg, the Netherlands *(oral presentation)*	1
2019	ESC Cardiovascular Development Meeting, Marseille, France *(poster presentation)*	1
2019	Masterclass with dr. Gabriele D'Uva and prof. dr. Mark Friedberg *(oral presentation)*	0.2

Teaching		**ECTS**
2016- 2020	Practical assistant Embryology course (Bachelor Biomedical Sciences, Biology and Psychobiology)	3
2017	Supervisor HLO internship: Jorn Jeremiasse, Hogeschool Inholland Amsterdam. Project: Growth of the congenitally malformed heart (5 months)	2

Parameters of Esteem

2018	Invited Speaker for the Annual Meeting of the Association for European Paediatric and Congenital Cardiology
2019	Best Presentation within the Amsterdam UMC: British council FameLab science communication
2019	Best Presentation during the Amsterdam Cardiovascular Science PhD retreat

PUBLICATIONS

Giovou AE, Mulleners OJ, **Günthel M**, Man JCK, Jensen B, Gladka MM, Christoffels VM. *Nppa and Nppb Deficiency Drives Ventricular Hypertrophy and Subendocardial Gene Deregulation in the Mouse Heart*. International Journal of Molecular Sciences. 2026 Mar 6;27(5):2450.

Bouwman M, de Bakker DEM, Honkoop H, Giovou AE, Versteeg D, Boender AR, Nguyen PD, Slotboom M, Colquhoun D, Vigil-Garcia M, Kooijman L, Janssen R, Hooijkaas IB, **Günthel M**, Visser KJ, Klerk M, Zentilin L, Giacca M, Kaslin J, Boink GJJ, van Rooij E, Christoffels VM, Bakkers J. *Cross-species comparison reveals that Hmga1 reduces H3K27me3 levels to promote cardiomyocyte proliferation and cardiac regeneration.* Nature Cardiovascular Research. 2025 Jan;4(1):64-82.

van der Ven JPG, **Günthel M**, van den Bosch E, Kamphuis VP, 1 Blom NA, Breur J, Berger RFM, Bogers AJJC, Koopman L, Ten Harkel ADJ, Christoffels V, Helbing WA. *Ventricular function and biomarkers in relation to repair and pulmonary valve replacement for tetralogy of Fallot.* Open Heart; 2023, Apr;10(1):e002238

Günthel M, van Duijvenboden K, de Bakker DEM, Hooijkaas IB, Bakkers J, Barnett P, Christoffels VM. *Epigenetic State Changes Underlie Metabolic Switch in Mouse Post-Infarction Border Zone Cardiomyocytes*. Journal of Cardiovascular Development and Disease; 2021, 8, 134.

Günthel M, van Duijvenboden K, Jeremiasse J, van den Hoff MJB, Christoffels VM. *Early Postnatal Cardiac Stress Does Not Influence Ventricular Cardiomyocyte Cell-Cycle Withdrawal.* Journal of Cardiovascular Development and Disease. 2021, 8, 38.

Bossers GPL, **Günthel M**, van der Feen DE, Hagdorn QJA, Koop AC, van Duijvenboden K, Barnett P, Borgdorff MAJ, Christoffels VM, Herman H. W. Silljé HHW, Berger RMF, Bartelds B. *Neuregulin-1 enhances cell-cycle activity, delays cardiac fibrosis, and improves cardiac performance in rat pups with right ventricular pressure load.* 2021; 164(6): e493-e510.

van Duijvenboden K*, de Bakker DEM*, Man JCK*, Janssen R*, **Günthel M***, Hill MC, Hooijkaas IB, van der Made I, van der Kraak PH, Vink A, Creemers EE, Martin JF, Barnett P, Bakkers J, Christoffels VM. *Conserved NPPB+ Border Zone Switches From MEF2- to AP-1–Driven Gene Program.* Circulation. 2019; 140(10):864-879.

Günthel M, Barnett P, Christoffels VM. *Development, Proliferation, and Growth of the Mammalian Heart.* Molecular Therapy. 2018; 26(7):1599-1609.

* these authors contributed equally

LIST OF CONTRIBUTING AUTHORS

(in alphabetical order)

Bakkers, J., PhD
Hubrecht institute, KNAW, University Medical Center Utrecht, Utrecht, The Netherlands

de Bakker, D.E.M., PhD
Hubrecht institute, KNAW, University Medical Center Utrecht, Utrecht, The Netherlands

Barnett, P., PhD
Department of Medical Biology, Amsterdam UMC, Amsterdam, The Netherlands

Bartels, B,. MD, PhD
Department of Pediatrics, Division of Cardiology, Erasmus University Medical Centre-Sophia Children's Hospital, Rotterdam, The Netherlands.

Berger, R.M.F., MD, PhD
Center for Congenital Heart Diseases, Department of Pediatric Cardiology, University of Groningen, University Medical Center Groningen, Groningen, The Netherlands

Borgdorff, M.A. J., MD, PhD
Center for Congenital Heart Diseases, Department of Pediatric Cardiology, University of Groningen, University Medical Center Groningen, Groningen, The Netherlands

Bossers, G.P.L., MD
Center for Congenital Heart Diseases, Department of Pediatric Cardiology, University of Groningen, University Medical Center Groningen, Groningen, The Netherlands

Christoffels, V.M., PhD
Department of Medical Biology, Amsterdam UMC, Amsterdam, The Netherlands

Creemers, E.E., PhD
Department of Experimental Cardiology, Amsterdam UMC, Amsterdam, The Netherlands

van Duijvenboden, K., PhD
Department of Medical Biology, Amsterdam UMC, Amsterdam, The Netherlands

van der Feen, D.E., MD
Center for Congenital Heart Diseases, Department of Pediatric Cardiology, University of Groningen, University Medical Center Groningen, Groningen, The Netherlands

Hagdorn, Q.A.J., MD, PhD
Center for Congenital Heart Diseases, Department of Pediatric Cardiology, University of Groningen, University Medical Center Groningen, Groningen, The Netherlands

Hill, M.C., PhD
Program in Developmental Biology, Baylor College of Medicine, Houston, Texas, The United States

van den Hoff, M.J.B., PhD
Department of Medical Biology, Amsterdam UMC, Amsterdam, The Netherlands

Hooijkaas, I.B., MSc
Department of Medical Biology, Amsterdam UMC, Amsterdam, The Netherlands

Jeremiasse, J., BSc
Department of Medical Biology, Amsterdam UMC, Amsterdam, The Netherlands

Janssen, R., PhD
Department of Medical Biology, Amsterdam UMC, Amsterdam, The Netherlands

Koop, A.C., MD, PhD
Center for Congenital Heart Diseases, Department of Pediatric Cardiology, University of Groningen, University Medical Center Groningen, Groningen, The Netherlands

van der Kraak, P.H., BSc
Department of Pathology, University Medical Center Utrecht, Utrecht, The Netherlands

van der Made, I., MSc
Department of Experimental Cardiology, Amsterdam UMC, Amsterdam, The Netherlands

Man, J.C.K., PhD
Department of Medical Biology, Amsterdam UMC, Amsterdam, The Netherlands

Martin, J.F., MD, PhD
Program in Developmental Biology, Baylor College of Medicine, Houston, Texas, The United States

Silljé, H.H.W., PhD
Department of Cardiology, University of Groningen, University Medical Center Groningen, Groningen, The Netherlands

Vink, A., MD, PhD
Department of Pathology, University Medical Center Utrecht, Utrecht, The Netherlands

AUTHOR CONTRIBUTIONS

Chapter 1: Development, Proliferation and Growth of the Mammalian heart

Marie Günthel, Phil Barnett, Vincent M. Christoffels

Molecular Therapy Vol. 26 No 7, July 2018: 1599

Conceptualization and writing-original draft, M.G, V.M.C and P.B.

Chapter 2: Early Postnatal Cardiac Stress Does Not Influence Ventricular Cardiomyocyte Cell-Cycle Withdrawal

Marie Günthel, Karel van Duijvenboden, Jorn Jeremiasse, Maurice J. B. van den Hoff, Vincent M. Christoffels

Journal of Cardiovascular Development and Disease. Vol. 8, April 2021: 38

Conceptualization, M.G., M.J.B.v.d.H. and V.M.C.; data curation, K.v.D.; formal analysis, M.G., K.v.D. and V.M.C.; funding acquisition, V.M.C.; investigation, M.G., K.v.D. and J.J.; methodology, K.v.D.; project administration, M.G. and V.M.C.; resources, M.J.B.v.d.H.; supervision, V.M.C.; writing: M.G., M.J.B.v.d.H. and V.M.C.

Chapter 3: Neuregulin-1 enhances cell-cycle activity, delays cardiac fibrosis, and improves cardiac performance in rat pups with right ventricular pressure load

Guido P L Bossers , Marie Günthel, Diederik E van der Feen , Quint A J Hagdorn , Anne-Marie C Koop , Karel van Duijvenboden , Phil Barnett , Marinus A J Borgdorff , Vincent M Christoffels , Herman H W Silljé , Rolf M F Berger , Beatrijs Bartelds

The Journal of Thoracic and Cardiovascular Surgery. Vol. 164, Issue 6, December 2022: E493-E510

Conceptualization: G.P.B, M.G, V.M.C., H.H.W.S, R.M.F.B, B.B.; data analysis: G.P.B, M.G, K.v.D, P.B, B.B.; writing G.P.B, M.G, V.M.C., B.B.; supervision: V.M.C., P.B., R.M.F.B, B.B.; funding acquisition: V.M.C., B.B, R.M.F.B; methodology and data curation: D.E.V.D.F., Q.A.J.H., A.M.C.K., M.A.J.B., G.P.B, M.G.

Chapter 4: Conserved NPPB+ Border Zone Switches From MEF2- to AP-1–Driven Gene Program

Karel van Duijvenboden*, Dennis E.M. de Bakker*, Joyce C.K. Man*, Rob Janssen*, Marie Günthel*,Matthew C. Hill, Ingeborg B. Hooijkaas, Ingeborg van der Made, Petra H. van der Kraak, Aryan Vink, Esther E. Creemers, James F. Martin, Phil Barnett, Jeroen Bakkers, Vincent M. Christoffels

*these authors contributed equally.

Circulation. 2019;140:864-879.

Conceptualization, K.v.D , D.E.M.d.B, J.C.K.M., M.G., R.J., V.M.C., J.B.; methodology and data curation: K.v.D , D.E.M.d.B, J.C.K.M., M.G., R.J., I.B.H., J.B., I.v.d.M., P.H.v.d.K., A.V., M.C.H., E.E.C.; data analysis: K.v.D , D.E.M.d.B, J.C.K.M., M.G., R.J.; writing—original draft preparation: K.v.D, J.C.K.M., M.G., R.J., V.M.C.; writing—review and editing, P.B., J.B., J.F.M.; supervision, V.M.C., P.B. and J.B.; funding acquisition, V.M.C. and J.B.

Chapter 5: Epigenetic State Changes Underlie Metabolic Switch in Mouse Post-Infarction Border Zone Cardiomyocytes

Marie Günthel, Karel van Duijvenboden, Dennis Eduard Maria de Bakker, Ingeborg Brigitta Hooijkaas, Jeroen Bakkers, Phil Barnett and Vincent M. Christoffels

Journal of Cardiovascular Development and Disease. Vol. 8, October 2021: 134

Conceptualization, M.G. and V.M.C.; methodology, M.G., K.v.D., D.E.M.d.B. and I.B.H.; data analysis and curation, M.G., K.v.D., D.E.M.d.B., I.B.H., J.B., P.B. and V.M.C.; writing—original draft preparation, M.G. and V.M.C.; writing—review and editing, P.B., J.B., K.v.D. and V.M.C.; supervision, V.M.C., P.B. and J.B.; funding acquisition, V.M.C. and J.B.

ACKNOWLEDGEMENTS

De tijd vliegt. Hoewel het inmiddels alweer meer dan vijf jaar geleden is dat ik voor het laatst een pipet heb opgepakt, heeft dit boek toch iets langer op zich laten wachten dan gedacht. Maar het is gelukt. Daarom wil ik hier graag iedereen bedanken die dit traject mogelijk heeft gemaakt, een bijdrage heeft geleverd aan dit proefschrift en mij tijdens en na mijn tijd bij het AUMC heeft bijgestaan om dit boek tot stand te brengen.

Mijn promotor, **prof. dr. Vincent Christoffels**. Beste Vincent, allereerst wil ik je bedanken voor de kans om mijn promotieonderzoek binnen jouw onderzoeksgroep uit te voeren. Dank voor je begeleiding, je kritische vragen en waardevolle input, en voor de manier waarop je me steeds weer in de juiste richting wist te sturen. Ook ben ik je dankbaar voor de kansen en uitdagingen die ik tijdens mijn onderzoek heb gekregen. Je hebt me geleerd om meer in mezelf te geloven, dat er in korte tijd vaak meer mogelijk is dan ik vooraf denk, en om vooral in mogelijkheden in plaats van beperkingen te denken. Dat is iets wat ik heb meegenomen en waar ik ook in mijn huidige carrière nog veel aan heb.

Mijn co-promotor: **dr. Phil Barnett**: Beste Phil, dankjewel voor je hulp en je luisterend oor tijdens mijn promotietraject. Ik kon altijd bij je terecht met mijn vragen of voor advies. Ook op het lab kon ik op je rekenen en stond je klaar om te helpen wanneer dat nodig was. Heel erg bedankt voor je betrokkenheid en voor alle hulp door de jaren heen.

Ook wil ik graag de **leden van mijn promotiecommissie prof. dr. C.J.M. de Vries, dr. ir. C.J. Zuurbier, prof. dr. P.L. Hordijk, prof. dr. F. van Leeuwen, dr. M.M. Gladka en prof. dr. N.A. Blom** bedanken voor de tijd en moeite die jullie hebben genomen om mijn proefschrift te lezen en te beoordelen, en voor jullie aanwezigheid bij mijn verdediging.

Fern, mijn paranimf: Dear Fern, I could not be happier to have you as my paranimf, my former colleague and, most importantly, my friend. My PhD years simply would not have been the same without you. Thank you for all the laughter, the great conversations, your encouragement, and of course all the scientific advice and guidance in the lab. I will never forget our shared love for *Frozen* and the Backstreet Boys, and I still treasure all the little drawings and notes you left on my desk. And, of course, most importantly, my molecular biologist card, which finally feels well deserved now that this book is finished. I am so grateful to have had you by my side throughout this journey.

Het COBRA3-consortium: prof. dr. Wim Helbing, prof. dr. Nico Blom, prof. dr. Rolf Berger, dr. Beatrijs Bartelds, prof. dr. Jeroen Bakkers, prof. dr. Vincent Christoffels en alle andere betrokkenen, dank voor jullie inzet en bijdrage aan het onderzoek in al deze jaren. **Eva, Vivian, Dennis, Guido en Jelle**, bedankt voor de gezellige tijd tijdens, maar zeker ook na onze consortiummeetings, met Marseille als absoluut hoogtepunt. Ik vond het ontzettend

inspirerend om van dichtbij mee te maken hoe klinisch en fundamenteel onderzoek binnen het consortium samenkwamen en elkaar versterkten. Dat onze samenwerking ook wetenschappelijk succesvol was, blijkt wel uit de mooie publicaties die we samen tot stand hebben gebracht. **Jelle**, jij kwam er wat later bij, maar toch is het ons gelukt om samen het Fallot-artikel tot een mooi einde te brengen. Je hebt me enorm geholpen om de klinische data beter te begrijpen. Bedankt voor al je uitleg, je hulp en de leuke samenwerking! **Guido**, het was ontzettend leuk om met je samen te werken. Ik ben blij dat onze samenwerking heeft geleid tot een mooie gezamenlijke publicatie en dat dit werk nu ook onderdeel is van dit proefschrift. Bedankt voor de prettige samenwerking en al je hulp. **Dennis**, ook met jou heb ik aan meerdere publicaties mogen werken. Bedankt voor al je hulp met de zebravissen en de border zone-data. **Beatrijs Bartels**, bedankt voor de kans om tijdens het AEPC-congres in Athene te mogen presenteren. Het was een mooie uitdaging en een bijzondere ervaring waar ik met veel plezier op terugkijk.

Mijn kamergenoten: **Fern, Koen, Jaeike, Antoinette en Rob**. Ik denk dat we onszelf destijds hebben uitgeroepen tot een van de gezelligste kamers van de afdeling Medische Biologie. Elke ochtend werden de gebeurtenissen van de afgelopen dagen uitgebreid besproken, werden er avocadobomen gekweekt en varens in leven gehouden, en ieder jaar met kerst zetten we traditiegetrouw onze kleine kerstboom neer. Niet te vergeten is ook onze Halloween-reproductie van het schilderij uit de koffiekamer. Het was altijd gezellig en jullie waren een grote steun voor me! **Jaeike**, bedankt voor je nuchtere en directe blik op de dingen, je advies en alle goede gesprekken. En natuurlijk voor je tip om af en toe gewoon happy hardcore te luisteren als alles even tegenzit. Daar moet ik nog regelmatig aan denken. **Antoinette**, jouw discipline op het werk en je energie om je ook buiten het lab met zoveel leuke dingen bezig te houden, heb ik altijd bewonderd. Dankjewel voor alle leuke momenten die we samen hebben gehad, in het bijzonder tijdens onze vrijdagmiddagborrels. **Koen**, we hebben het echt heel leuk gehad, zeker in onze tijd als bier-AIO's. Ik denk dat we toen wel onze roeping hadden gevonden. Bedankt voor de gezelligheid en alle gesprekken die we hebben gevoerd, zowel op kantoor als in de trein terug van werk. **Rob**, ook al waren we maar kort kamergenoten, ik wil je bedanken voor de leuke tijd. Je hebt me aan het begin van mijn PhD goed op weg geholpen en ik ben blij dat ik je project na je vertrek mocht overnemen. Het was een mooie start van mijn eigen onderzoek en ik heb er met veel plezier aan verder gewerkt.

Jettie, je had altijd een luisterend oor en ik kon met al mijn vragen en problemen bij je terecht. Het was altijd fijn om even bij je binnen te lopen en bij te kletsen. Ik zal met veel plezier terugdenken aan onze afdelingsfeestjes en uitjes, zoals die keer dat we met de hele afdeling bij 36 graden verkoeling zochten in de Loosdrechtse Plassen. Ook tijdens de laatste loodjes van mijn PhD kon ik op je rekenen. Bedankt voor al je steun, hulp en betrokkenheid!

Karel, bedankt voor het verwerken van al mijn sequencingdata en voor je hulp met de bio-informatica! De keren dat ik achter je bureau stond, ongeduldig af te wachten tot we eindelijk meer zouden weten, of om te vragen hoe het nou écht zat met de data en natuurlijk: "...is het nou significant?", zijn niet te tellen. Je bijdrage aan dit boek is dan ook onmisbaar geweest! En niet alleen op het gebied van sequencingdata: tussendoor wist je me ook steeds weer van goede Stephen King-boekenaanbevelingen te voorzien. **Ingeborg**, vooral tijdens de laatste twee jaar van mijn PhD hebben we veel samengewerkt. Bedankt voor al je hulp met de werkprotocollen en de muis- en zebravisexperimenten. Maar vooral ook bedankt voor alle leuke gesprekken en de gezellige tijd samen, in het lab, in het ARIA, tijdens borrels en buiten het werk. Je was een collega op wie ik altijd kon rekenen. **Quinn,** wat hebben wij veel plezier gehad op het lab! Je was altijd in voor een grapje en stond altijd klaar om te helpen als ik voor de zoveelste keer moest vragen hoe de instellingen van de microscoop ook alweer werkten. Ik zal met heel veel plezier terugdenken aan onze tijd samen op het lab. En ik hoop natuurlijk dat je bij de eerste klanken van *Achy Breaky Heart* nog af en toe aan mij moet denken. **Corrie,** bedankt voor al je hulp bij het inbedden, snijden en kleuren van mijn coupes. Je stond altijd voor me klaar en dacht met me mee als dat nodig was. Ik heb met ontzettend veel van je geleerd en met plezier met je samengewerkt. **Joyce**, je doorzettingsvermogen en discipline waren altijd een inspiratie voor mij en het is leuk om te zien dat je verder bent gegaan met een carrière in de wetenschap! Je stond altijd klaar om te helpen. Bedankt daarvoor! **Andrea,** you always made time for your colleagues. Whether it was to share a joke or to take another look at an experiment, you were always there to help. I really appreciated that!

Vincent Wakker en **Aho**, bedankt dat ik met mijn vragen op het lab altijd bij jullie terechtkon. **Vincent van Eif, Rajiv en Henk**, met jullie was er altijd een leuke en luchtige sfeer, of dat nou op het lab was of tijdens de borrels. Bedankt voor de gezellige tijd!

Maurice, bedankt voor al je hulp en advies bij de Follistatin-experimenten, maar ook voor je humor en positiviteit door de jaren heen. **Bas, Bjarke en Alex,** bedankt voor jullie kritische vragen tijdens de presentaties. Ze zorgden er altijd voor dat ik weer net even anders of verder over mijn onderzoek nadacht. **Jaco,** bedankt dat ik altijd bij je terechtkon met al mijn computervragen en voor alle hulp daarbij!

Een speciale dank gaat ook uit naar **Berend Hooibrink**, voor de ontelbare keren dat we samen cardiomyocytkernen hebben gesorteerd, wat toch iedere keer weer even puzzelen was. Mijn student **Jorn Jeremiasse**, bedankt voor je bijdrage aan dit boek door urenlang cardiomyocyten te tellen! Ook wil ik alle **medewerkers van het ARIA** bedanken. Zonder jullie goede en zorgvuldige verzorging van alle muislijnen was dit onderzoek nooit mogelijk geweest.

Uiteraard gaat mijn dank ook uit naar **Jianan, Alexandra, Harsha, Berend, Mischa, Lianne, Arnie, Max, en Geert Boink**, evenals naar alle collega's van **Experimentele Cardiologie**.

Bedankt voor jullie input en feedback tijdens de werkbesprekingen, maar zeker ook voor de gezelligheid tijdens de borrels en eindejaarsfeesten. Ook wil ik alle collega's bedanken die ik hier niet bij naam heb genoemd. Dank voor jullie bijdrage aan mijn onderzoek en voor alle mooie herinneringen.

Familie, vrienden en nieuwe collega's

Bedankt aan al mijn vrienden en familie die mij tijdens dit traject hebben gemotiveerd en gesteund en altijd een luisterend oor voor me hadden. Ook aan alle vrienden die ik hier niet bij naam heb genoemd, maar die er voor me waren en direct of indirect hebben bijgedragen aan de totstandkoming van dit proefschrift: bedankt voor alles!

Lisanne, mijn eerste lab-buddy in Leiden! Bedankt voor onze tijd samen en voor het begin van mijn avontuur in het lab. **Und an meine treuen Freunde Jule, Lisa, Carina, Buschtel und Milena.** Vielen Dank, dass ihr mir immer mit Rat und Tat zur Seite steht und mich über all die Jahre begleitet und unterstützt habt!

Vielen Dank auch an meine Eltern. Ohne eure Unterstützung wären mein ganzes Studium, meine Auslandsjahre und letztendlich auch diese Position nie möglich gewesen. Danke, dass ihr mich immer unterstützt und an mich geglaubt habt! Mijn dank gaat ook uit naar mijn schoonfamilie, **Wiel en Marij**, en **Bram en Marlaine**. Bedankt voor jullie steun, interesse en betrokkenheid door de jaren heen.

Na het stoppen met mijn onderzoek en het beginnen aan een nieuwe baan, was het soms best moeilijk om toch nog door te zetten en dit proefschrift af te maken. Dit was niet mogelijk geweest zonder de steun en continue motivatie van de mensen om mij heen. Daarom ook bedankt aan mijn collega's van **PNO**, vooral **Marc, Stefanie, Simona, Rilana en Christy**, voor het toch af en toe stellen van de vraag: "Hoe staat het nou met de promotie?" Dat duwtje had ik soms precies nodig om toch weer verder te gaan. En ook veel dank aan mijn nieuwe collega's bij **Avans Hogeschool** voor het bijstaan tijdens de allerlaatste loodjes!

En dan als allerlaatste mijn beste vriend, echtgenoot en nu dus eindelijk ook mijn paranimf, **Koen**. Bedankt voor al je steun door de jaren heen. Je wist me altijd weer te motiveren als ik het even niet meer zag zitten, hielp me door de moeilijke momenten en lange avonden heen en bleef in mij geloven toen ik zelf dacht dat dit promotietraject misschien wel nooit tot een einde zou komen. Je nam dingen van me over als ik toch weer langer moest werken en gaf me de ruimte om dit boek uiteindelijk af te maken. Je zei dat het dankwoord vooral niet te *cringy* moest worden, dus ik hoop dat ik bij deze de juiste grens heb gevonden ;)

En uiteraard gaat mijn dank ook naar mijn lieve dochters, **Lotta en Linnea**. Jullie waren een enorme motivatie voor mij om mijn promotietraject af te ronden.